Univerzita Karlova v Praze

Přírodovědecká fakulta

Charles University in Prague

Faculty of Science

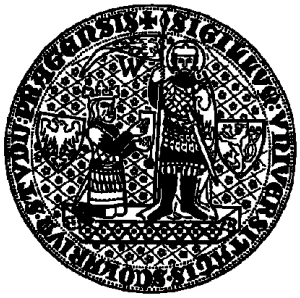

Czech Academy of Sciences

Institute of Physiology, v.v.i

Změny energetického metabolizmu spojené s obezitou: metabolická flexibilita a úloha tuku v dietě

Energy Metabolism in Obesity: Metabolic Flexibility and Dietary Fat

Disertační práce / Ph.D. thesis

Mgr. Kristina Bardová

Školitel / Supervisor: MUDr. Jan Kopecký, DrSc.

Praha 2016

Prohlášení:

Prohlašuji, že jsem závěrečnou práci zpracovala samostatně a že jsem uvedla všechny použité informační zdroje a literaturu. Tato práce ani její podstatná část nebyla předložena k získání jiného nebo stejného akademického titulu.

Statement of authorship

I certify that the thesis represents valid work elaborated under the supervision of MUDr. Jan Kopecký, DrSc., and that neither this manuscript nor one with substantially similar content under my authorship has been submitted in support of an application for any other academical degree. My participation in the published papers is specified in the text, and summarized in the list of Publications on the page 121-122.

16.3. 2016 in Prague

Mgr. Kristina Bardová

Statement of co-authors

I certify that Kristina Bardová substantially contributed to the formation of the papers used as a basis of this thesis, and that her participation specified in the text of the thesis is correct.

16.3. 2016 in Prague

MUDr. Jan Kopecký, DrSc.

Acknowledgement

I would like to express my sincere thanks to my supervisor and head of the department MUDr. Jan Kopecký, DrSc., for his scientific and financial support during my Ph.D. studies. I also want to acknowledge all the co-authors of publications summarized in this thesis. I thank all my colleagues, and my family and friends.

Abstrakt

Tuková tkáň hraje v těle důležitou homeostatickou funkci. Nejenom že vyrovnává hladiny mastných kyselin v krvi, ale také uvolňuje důležité autokrinní, parakrinní a endokrinní faktory, ktere mají vliv na metabolizmus celého těla. Biologie tukové tkáně má úzký vztah k metabolickým důsledkům obezity, zejména k diabetu II. typu. Obezita a diabetes II. typu způsobuje a nebo naopak může být zapříčiněna metabolickou inflexibilitou, která je definovaná jako neschopnost organismu adaptovat oxidaci substrátů k jejich dostupnosti. Tato dizertační práce je postavena na průsečíku důležitých témat na poli živočišné fyziologie, jakými jsou biologie tukové tkáně, obezita a její metabolické důsledky a teorie metabolické flexibility. V práci je zahrnuto pět publikací, které se věnují výše zmíněným tématům.

Hlavním cílem práce je porovnání několika postupů pro určení metabolické flexibility; zejména těch, které se věnují energetické homeostázi celého organizmu. Specifické cíle, zdůrazněné zahrnutými publikacemi, (i) jsou vyhodnocení vlivu *n*-3 dlouhých mastných kyselin, rosiglitazonu a jejich kombinace, na metabolickou flexibilitu jak na úrovni celého organizmu, tak i na buněčné úrovni; (ii) vyhodnocení důsledku podávání diety s vysokým obsahem tuků na metabolickou flexibilitu obou pohlaví laboratorních myší; (iii) vyhodnocení vlivu chenodeoxycholové kyseliny na celotělovou homeostázu; (iv) analyzování několika typů testů pro stanovení metabolické flexibility a (v) vyhodnocení vlivu krátkodobé chladové expozice na metabolizmus tukové tkáně.

Metabolické inflexibilita, chápaná jako snížená schopnost organismu měnit preference oxidace jednotlivých substrátů podle aktuální dostupnosti, může být stanovena různými metodami. V této Ph.D. práci jsou shrnuta využití jak konvenční zátěže organismu po aplikaci konkrétní dávky glukózy, tak pozorované změny při přechodu mezi hladovým a sytým stavem a dále pak testy na měření metabolické flexibility pomocí nepřímé kalorimetrie. Stanovení metabolické flexibility je velmi důležité pro vyhodnocení vlivu dietních intervencí, a tedy je významnou součástí fyziologických experimentů na laboratorních zvířatech i klinického výzkumu.

Abstract

Adipose tissue is an important homeostatic tissue within the body. It not only buffers FA availability in the organism, but also releases important autocrine, paracrine or endocrine factors influencing energy metabolism. The biology of adipose tissue is closely related and underlies whole-body metabolic consequences of obesity, such as type II. diabetes. Obesity and type II. diabetes causes and maybe are caused by metabolic inflexibility, the inability of organism to adapt fuel oxidation to fuel availability. The intersection of adipose tissue biology, obesity and its metabolic consequences and theory of metabolic flexibility is discussed in this PhD. thesis. Five articles dealing with above mentioned topics are included.

The general goal of this study was to compare several approaches for metabolic flexibility assessment with respect to overall energy homeostasis. The specific goals, delineated by included articles, were (i) to evaluate the influence of *n-3* long chain fatty acids (*n-3* LC-PUFA), rosiglitazone, and their combination, on metabolic flexibility at a whole-body and cellular level; (ii) to evaluate impact of high-fat feeding on metabolic flexibility of male and female mice; (iii) to evaluate the impact of chenodeoxycholic acid (CDCA) on whole body homeostasis; (iv) to analyze several types of metabolic flexibility tests and (v) to evaluate the effect of short-term cold exposure on metabolism of adipose tissue.

Metabolic inflexibility as a theory of diminished ability to switch between metabolic substrates may be determined by several methodological approaches. We employed either conventional application of a glucose load; or the switch between fasted and refed state in several assessments or an indirect calorimetry - derived tests. Assessment of metabolic flexibility is important for evaluation of dietary influences, and as such, deserves attention in physiological experiments as well as in clinical research.

Contents

1 List of abbreviations

AR	adrenergic receptor
ATGL	adipose triacylglycerol lipase
AUC	area under the curve
BAT	brown adipose tissue
BCAA	branched-chain amino acids
BMI	body mass index
BrDU	bromodeoxyuridine
cAMP	cyclic adenosine monophosphate
CD36	fatty acid translocase
CDCA	chenodeoxycholic acid
cHF	composite high-fat diet
cHF+F	composite high-fat diet supplemented with ω-3 concentrate from fish oil
CLS	crown-like structure
C/EBPβ	CCAAT-enhancer-binding protein β
CREB	cAMP response element-binding protein
DGAT	diacylglycerol acyltransferase
EE	energy expenditure
ERK	extracellular-signal-regulated kinase
FA	fatty acid
FFA	free fatty acid
FABP	fatty acid binding protein
FATP1	fatty acid transport protein 1
FM	fat mass

FQ	food quotient
HIF1-α,β	hypoxia-inducible factor 1 – alpha and beta
HSL	hormone sensitive lipase
IPGGT	intraperitoneal glucose tolerance test
LBM	lean body mass
LPL	lipoprotein lipase
MAG	monoacylglycerol
MAP kinase	p38 mitogen-activated protein kinase
MGAT	monoacylglycerol acyltransferase
MGL	monoacylglycerol lipase
NEFA	non-esterified fatty acid
n-3 LC-PUFA	*n-3* long chain fatty acids
OGTT	oral glucose tolerance test
PDGFRa	alpha-type platelet-derived growth factor receptor
PF	pair-fed
PEPC-K	phosphoenolpyruvate carboxykinase
PET	positron emission tomography
PGC1	PPARγ coactivator 1
PKA	cAMP activated protein kinase
PPAR	peroxisome proliferator-activated receptor
PRCF	percent cumulative frequency
PRDM16	PR domain containing 16
RER	respiratory exchange ratio
RQ	respiratory quotient
STD	standard chow diet
TAG	triacylglycerol

T2D	type II. diabetes
UCP1	uncoupling protein 1
VEGF-A	vascular endothelial growth factor
WAT	white adipose tissue

2 Introduction

The ability to manage energy input and output differentiates life from unliving things. Every organism needs to manage its energetic intake, expenditure and storage to be able to survive. Imbalance between these processes is also a basement of oncoming epidemic of obesity; and as such, the need to precisely specify all three aspects of energy homeostasis is increasing. Whereas the methods for energy intake and storage assessment are widely used and validated, the methods for assessment of energy expenditure are not such frequently employed and above all correctly interpreted.

A promising strategy to characterize whole body energy metabolism and substrate partitioning represents indirect calorimetry (INCA). This technique is able to determine not only longer-period whole-body energy homeostasis, but also using challenge tests detect small differences in metabolic flexibility that we would not be able to detect by other techniques. In this thesis, I will focus on specific tests used in our experiments dealing with the topic of energy homeostasis and obesity and on the usefulness of these approaches.

As was previously mentioned, energy homeostasis has a very tight relationship to obesity. Obesity may be caused by several possible mechanisms, with the imbalance between energy intake and energy expenditure beeing probably the most influential. Genetic background, endocrine disorders, pharmaceuticals, sleep deprivation, circadian desynchronisation, composition of microbiota in our gastrointestinal tract and many other reasons have probably also bigger or smaller impact on obesity development. Among others, there is a popular scientific theory that declares that metabolic inflexibility, discovered as a consequence of obesity and type II. diabetes (T2D), is more a cause that a consequence of obesity. We tried to explore this theory in several articles, with two of them being the basis of this thesis. Another important aspect of obesity is the gender-different impact on metabolism, a topic adressed by another of the articles, that forms the basis of this PhD Thesis.

Obesity is connected to several metabolic consequences, which are more deleterious than obesity per se. Treatments of obesity and connected metabolic disorders include interference with many metabolic pathways, tissues and organs. A very promising new target for obesity and/or T2D treatment emerged several years ago, when the presence of brown adipose tissue in adult humans was revealed by positron-emission tomography (PET). The presence of functional brown (or more probably brite) adipose cells in humans provided opportunity to deal with negative consequences of obesity by transforming energy reserves in the form of TAG into heat. This new possibility attracted a lot of attention and two articles dealing with induction of brite cells by chemical compound and by cold exposure, and its impact on whole-body and white adipose cell metabolism, will be also discussed in this thesis.

To sum up, I will discuss in this PhD. thesis the intersection of possibly interacting fields: adipose tissue biology and its connection to obesity and metabolic health, energy homeostasis assessed by INCA, and metabolic flexibility.

2.1 Adipose organ

Adipose tissue is present in many locations over the human or animal body. It forms many depots, which together are sometimes called adipose organ. Nevertheless, the adipose tissue is interconnected in the organism and all attempts to divide it into separate parts are artefitial, but technically necessary. The parts deposited subcutaneously differ metabolically from the visceral ones. There are two large subcutaneous, located in the upper part of the thorax and neck and in the lower part of the abdomen, and numerous visceral depots in laboratory mice; whereas in humans, subcutaneous adipose tissue is not confined to specific areas but forms a continuous layer beneath the skin. Subcutaneous adipose tissue store more than 80% of body fat in humans, whereas the intraabdominal depots associated with internal organs represent 5-20% of total body fat (Lee, Wu et al. 2012). The human visceral depots correspond to those of rodents by its localisation, but the omental depot is much more developed in humans and, on the other hand, mouse epididymal depot frequently used for scientific analyses and considered as a visceral depot, is not found in humans (Cinti 2009). Nomenclature of adipose organ in mice is unsteady, thus the same depot may bear different names in different sources. We to some extent adhere to

the nomenclature of Professor Cinti (Vitali, Murano et al. 2012) (Fig. 1), and use the names subcutaneous posterior (referred as subcutaneous), mesenteric and abdominopelvic (referred as epididymal) fat depot.

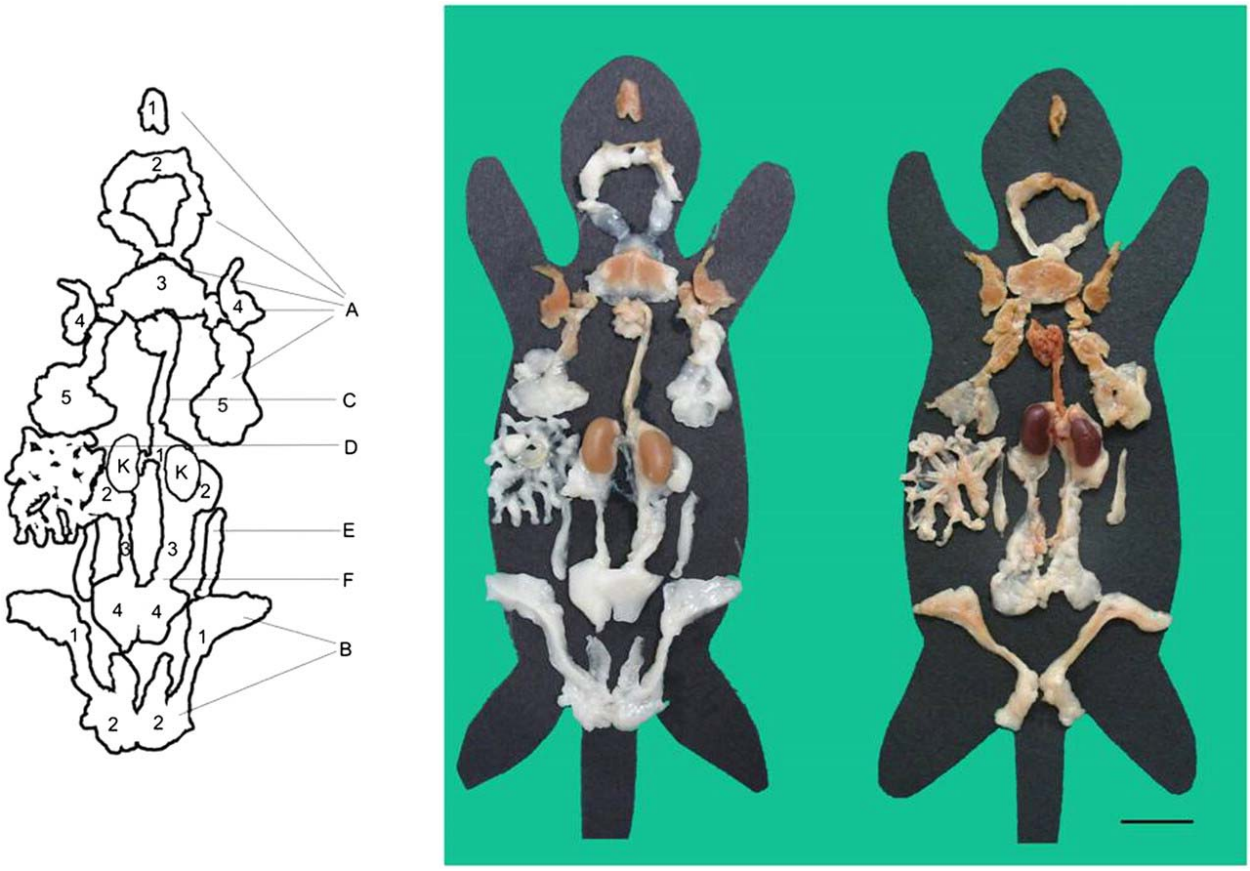

Fig.1*: Multidepot adipose organ of adult C57BL/6J female mice kept at 28°C (left) or 6°C (right) for 10 days. The organ is made up of the two subcutaneous depots (A) anterior and (B) posterior, and the visceral depots (C) mediastinial, (D) mesenteric, (E) retroperitoneal, and (F) abdominopelvic. Reprint from (Vitali, Murano et al. 2012).*

Adipose tissue is formed by adipose cells (adipocytes) and stromal vascular fraction. When comparing two types of adipocytes (white and brown) at a cellular level, in white unilocular adipocytes about 90% of cell volume represents a single large lipid droplet, whereas nucleus and cytoplasm forms a thin rim. Mitochondria are small, elongated and have short, randomly organized cristae. On the other hand, cytoplasm of brown multilocular adipocytes contain several to many small lipid droplets and numerous, large and spherical mitochondria with laminar cristae.

These mitochondria contain uncoupling protein 1 (UCP1) conducting thermogenic function (Fig. 2).

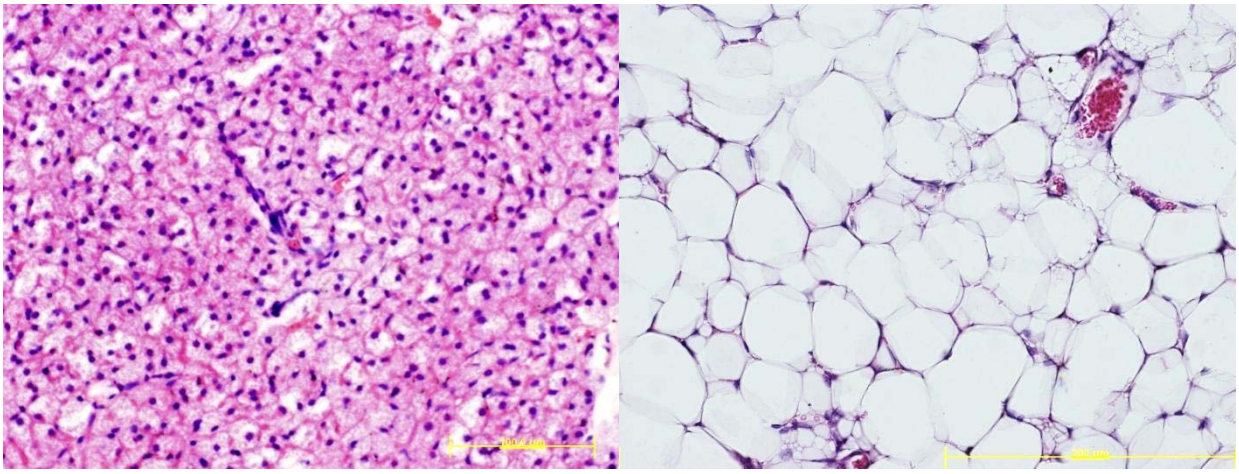

***Fig. 2**: Brown and white mouse adipose tissue (hematoxylin and eosin staining) (unpublished results).*

Metabolism, role and appearance of adipose depots in mice differ with ambient temperature, at thermoneutrality it is predominantly white with several brown areas, located mainly in the thoracic subcutaneous region, whereas after cold acclimatisation, many depots acquire brown appearance. This transition is related to increased function and appearance of brown at the expense of white adipocytes. Thus, the relative ratio between white and brown adipocytes differ with ambient temperature; and also with age and diet (Smorlesi, Frontini et al. 2012).

2.1.1 Adipose tissue metabolism

Adipose tissue was regarded to be only a site for storage of energy-rich triacylglycerols and steryl esters. Only lately, adipose tissue was discovered as an important adipokine secreting organ. Adipocytes also function as highly dynamic regulators of non-esterified fatty acid (NEFA) and triacylglycerol (TAG) whole-body metabolism.

Adipocytes are able to release fatty acids (FA) and glycerol arised by the breakdown of TAG. Stored TAG are hydrolysed by several intracellular lipases, each of them usually removes a single FA – adipose triglyceride lipase (ATGL), hormone-sensitive lipase (HSL) and monoglyceride lipase (MGL). TAG is thus converted to diacylglycerol (DAG) and FA by ATGL, than to

monoacylglycerol (MAG) and FA by HSL, and finally to free glycerol and FA by MAG. The rate-limiting enzyme of TAG hydrolysis is ATGL. HSL has affinity to TAG, DAG and MAG molecules, even though its affinity for TAG is much smaller than that of ATGL, and is responsive to various hormones, such as catecholamines and insulin. After complete hydrolysis of TAG molecule, glycerol is released by adipocytes and utilised in hepatic lipogenesis or gluconeogenesis (Viscarra and Ortiz 2013). In liver, glycerol is phosphorylated by glycerol kinase and subsequently transformed into glycolytic intermediate dihydroxyacetone phosphate (Voet and Voetov 1994). Lipolysis in WAT is on a systhemic level regulated among others by adrenaline and noradrenaline as initiators of lipolysis, and insulin as inhibitor of this process (Bartness, Shrestha et al. 2010).

Reverse metabolic pathway, synthesis of neutral lipids, forms lipid droplets and also detoxify FA in cases of oversupply of FA inside the cell. Adipocytes are able to uptake FA from blood through the action of fatty acid translocase (CD36), fatty acid binding protein (FABP), and fatty acid transport protein 1 (FATP1). FA are used for TAG synthesis after the activation by coenzyme A at the expense of ATP, together with glycerol-3-phosphate, a backbone of newly arising TAG. Adipocytes can re-create glycerol-3-phosphate from glycerol only in a limited amount due to very low levels of glycerol-kinase activity in white adipose tissue, in contrast to brown adipose tissue, where glycerol-kinase activity is high (Reshef, Olswang et al. 2003); and have to synthesize glycerol-3-phosphate for TAG synthesis through glyceroneogenic pathway from pyruvate, alanine, glutamine or intermediates of TCA cycle. A marker and a rate limiting enzyme of this metabolic pathway is phosphoenolpyruvate carboxykinase (PEPC-K) (Viscarra and Ortiz 2013).

Generally, FA are incorporated into newly arising TAG by two major biochemical pathways for TAG synthesis in adipose tissue. The MAG pathway begins with the acylation of MAG with a fatty acyl-CoA by monoacylglycerol acyltransferase (MGAT) to form DAG. A second pathway begins with acylation of glycerol-3-phosphate with a fatty acyl-CoA, producing lysophosphatidic acid, followed by further acylation and dephosphorylation to yield DAG. In both pathways, DAG is than converted to TAG, by diacylglycerol acyltransferases (DGATs). DGATs also recognize MAG as substrate in the synthesis of TAG. MGAT and DGAT acyltransferase activities are localized to endoplasmic reticulum and in the case of DGAT enzymes also to lipid droplets (Shi and Cheng

2009). Two mammalian DGAT enzymes, DGAT1 and 2 account for the vast majority of TAG synthesis in mice, and their function is required for lipid droplet´s formation in adipocytes, but not in other cell types (Harris, Haas et al. 2011). DGAT1 and 2 catalyse the same reaction and are expressed in most cells, but they are not redundant. DGAT2 largely determines the rate of *de-novo* synthesis of TAG (Wurie, Buckett et al. 2012). In hepatocytes, TAG synthesis depends on FA *de novo* synthesis, even though newly synthetized TAG accounts only for less than 5% of secreted TAG (Zammit 2013), but this phenomenon has not been investigated in adipocytes. Also the specificities of discrete enzymes to specific FA types are not known and may play an important role in the process of reesterification.

Reesterification is a futile cycle, in which TAG are hydrolysed and again re-synthetised. This cycle is energy-consuming due to consumption of ATP in FA activation and synthesis of glycerol-3-phosphate. This futile cycle permits a fast reaction to metabolic disturbances in organism, much faster than would be through the synthesis of proteins of respective metabolic pathways. This cycle is involved in a fine regulation of FA release into blood or incorporation into TAG, may be involved in non-shivering thermogenesis and in regulation of enhanced surface of lipid droplets in adipocytes, mainly under high-lipolytic circumstances. Intracellular recycling is a metabolically important pathway, in white adipose tissue represents approximately 20-30% of the whole-body reesterification (Reshef, Olswang et al. 2003). Wang et al. descibe that in normal fed animals 49,5% of endogeneous FA are reesterified (Wang, Zang et al. 2003).

2.1.2 Development of adipocytes and adipose tissue

Adipose depots in mice emerge during embryonic and early postnatal period. Using model of adipogenesis monitoring by inducible and permanent labeling of mature adipocytes (AdipoChaser mouse), Wang et al. showed that epididymal fat depot develops postnatally, whereas subcutaneous depot develops between embryonic days 14 and 18 (Wang, Tao et al. 2013). During early postnatal development white adipose depots, mainly retroperitoneal and inguinal, display a transient emergence of multilocular UCP1 expressing adipocytes (Lasar, Julius et al. 2013)(Fig. 3). The emergence of these adipocytes do not influence later ability of mice to induce brite cells within white adipose depots, because Kozak et al. documented that in

undernutritioned mouse pups, that do not develop transitial browning of white depots, the ability of britening after cold exposure is not altered (Kozak, Koza et al. 2012).

In adulthood, adipose depots can after stimulation by excessive energy intake increase volume by increasing the volume of adipocytes (hypertrophy) or increasing the number of adipocytes (hyperplasia). During hyperplasia, adipogenesis involve a two-step process – genesis of preadipocytes from multipotent fibroblast-like mesenchymal stem cells, and a differentiation step, when preadipocytes acquire the features of mature adipocytes. Mature adipocytes in adults arise from a pool of preadipocytes, ready for differenciation and included within the population of adipose stromal vascular fraction (Ma, Lee et al. 2015). The amount of pre-prepared adipogenic progenitors differ in various fat depots – in subcutaneous depots they are eightfold more abundant than in visceral ones (Joe, Yi et al. 2009). Both morphological and genetic tracing methods located the origin of adipocytes to a perivascular niche. Tran et al. were able to show that murine endothelial cells of adipose depots share ultrastructural characteristics with pericytes, which are pluripotent and can give rise to preadipocytes, and that capillary growth is related to adipocyte differentiation during embryogenesis and adulthood (Tran, Gealekman et al. 2012), (Frontini, Giordano et al. 2012). Similarly, Tang et al. used PPARγ-GFP marked mice for studying perivascular adipogenesis and discovered by this approach progenitors residing in the mural cell compartment of the adipose vasculature (Tang, Zeve et al. 2008). Thus, adipose vasculature probably functions as a niche for progenitors and provide signals for adipocyte development.

The ability to renew adipocytes in adulhood is rather a controversial topic. Spalding et al. (Spalding, Arner et al. 2008) evaluated dynamic of fat cells on a human model by analysing the integration of ^{14}C derived from nuclear bomb tests into genomic DNA. They found that annualy 10% of fat cells are renewed irrespective of age and BMI. The number of fat cells stays constant in both lean and obese adults, indicating that the number of adipocytes is set during childhood and adolescence. On a murine model, Wang et al. discovered in a previously mentioned AdipoChaser mouse that after high-fat feeding, epididymal fat initiate adipogenesis after 4 weeks, while subcutaneous fat increases its amount only by hypertrophy up to 12 weeks. (Wang, Tao et al. 2013). Thus, dynamic of fat cell proliferation in human and murine models is probably different

and is probably based on different pattern of feeding and restricted feeding periods during a longer human or shorted murine life.

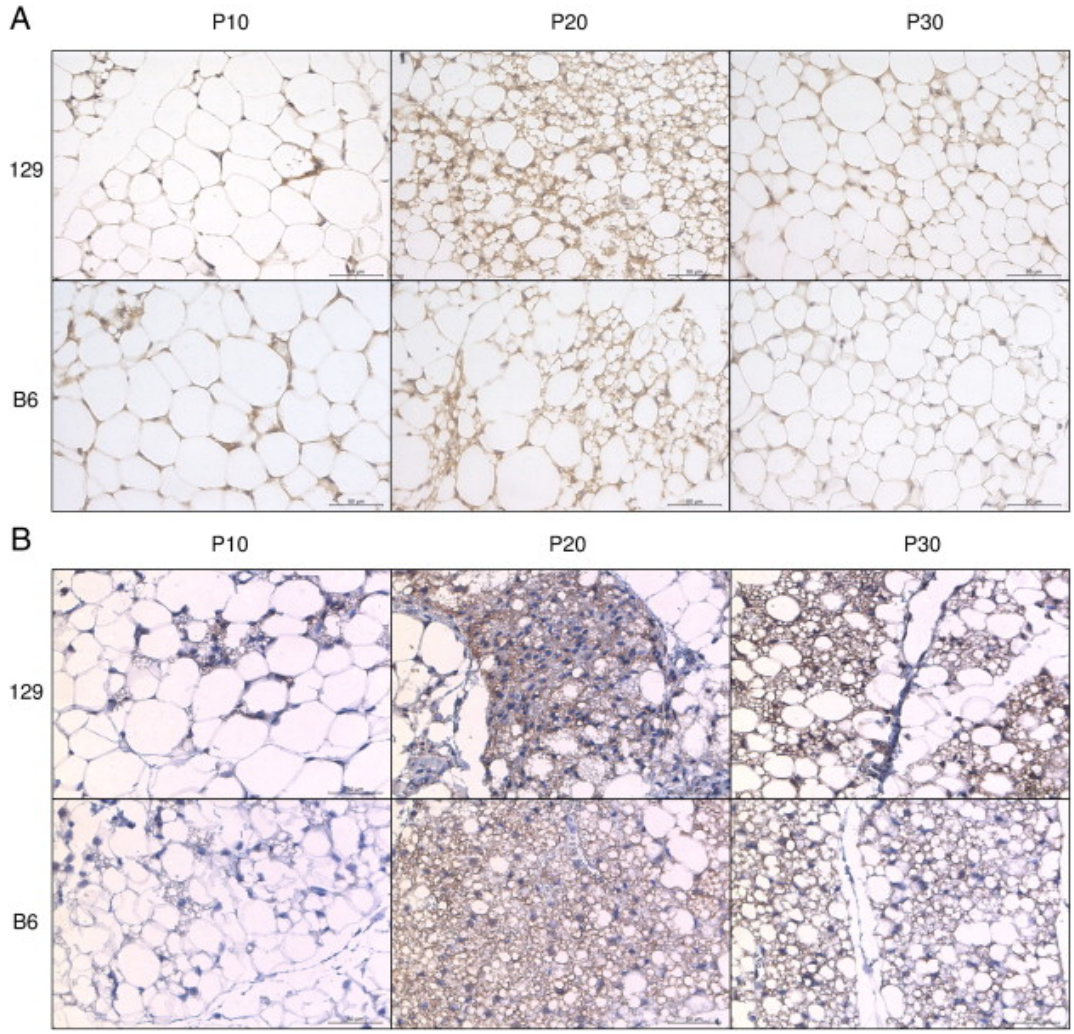

Fig. 3 : *Immunohistochemical detection of UCP1-positive adipocytes in retroperitoneal WAT and inguinal WAT of C57BL6/N and 129S6sv/ev mice. Morphologic change and IHC detection of UCP1-positive multilocular cells in retroperitoneal WAT (**A**) and inguinal WAT (**B**) at the indicated time points, abbreviated P10, P20 and P30, indicating the respective postnatal day of life; nuclei stain hematoxylin. Magnification × 40; Scale bars: 50 µm. Reprint from (Lasar, Julius et al. 2013).*

2.1.3 Adipose tissue vascularisation

Sufficient vascularisation of adipose tissue is pivotal both for white and brown adipose tissue. In WAT it enables sufficient blood flow for bringing and taking away TAG and FA, helping adipose tissue to play a role in buffering accessibility of energy substrates in the bloodstream (Fig.

4). In BAT it helps in conditions of stimulated non-shivering thermogenesis to bring sufficient amount of metabolic substrates as well as oxygene for heat generation.

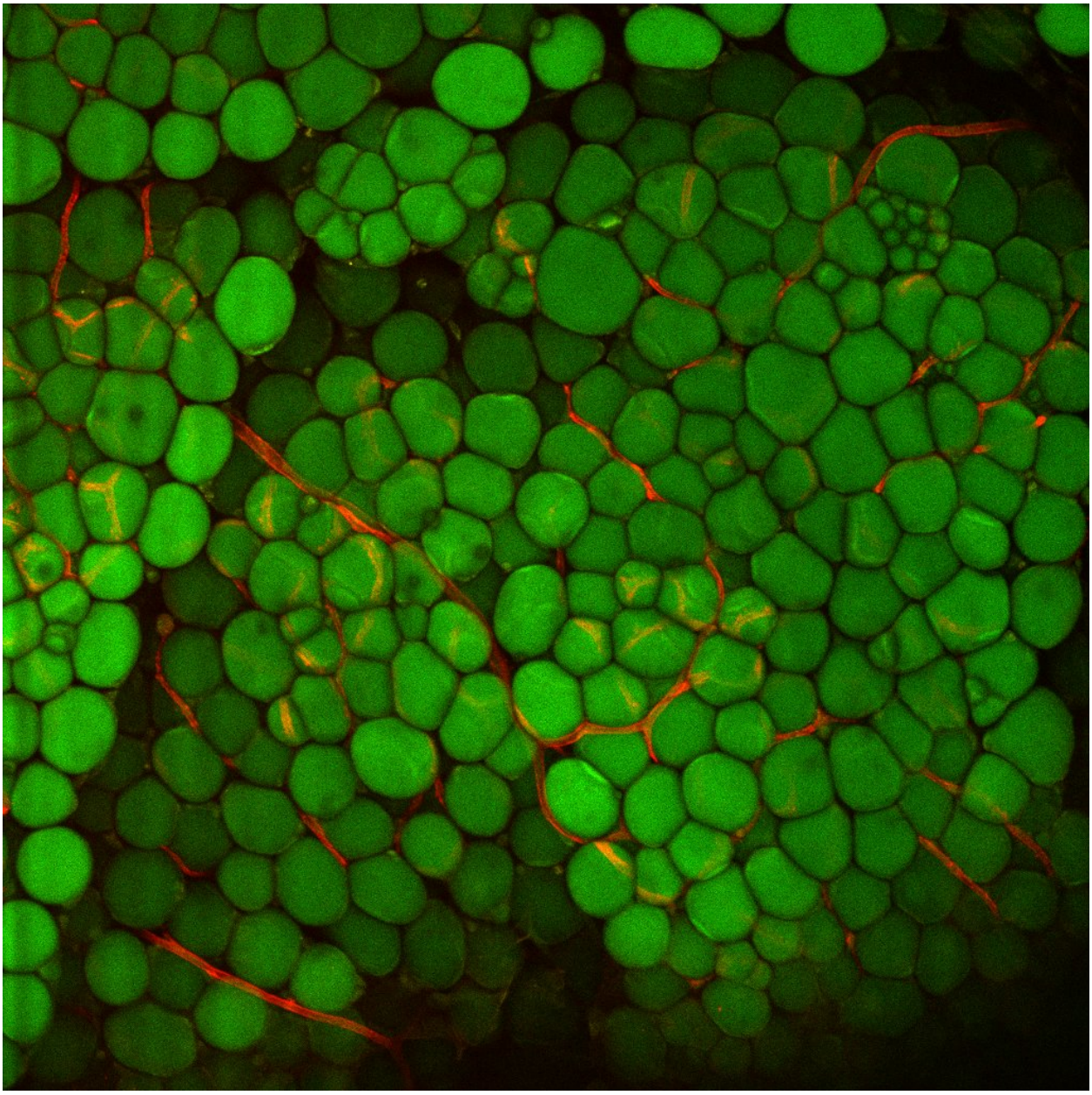

Fig. 4*: Lipid droplets (green, BODIPY FL) and capillaries (red, isolectin) in epididymal adipose tissue of C57BL/6J mouse acclimated in 4^{o}C for 7 days (K. Bardova, O. Chernyavskiy unpublished results).*

Generally, there are two models of possible connection of capillary network growth and adipocyte hyperplasia and/or differentiation. The first one based on embryogenic morphological analyses states that establishment of capillary network precedes the emergence of adipocytes

during development of embryonal tissues and maybe also in adulthood and is driven by metabolic stimulus. The second one based on tumor growth studies states that the growth of capillaries answers to hypoxia of surrounding cells, reflected in HIF-1α and HIF1-β tissue levels. The function of HIF-1α has been revealed by genetic approaches and the most probable model says that adipose tissue hypoxia induces HIF-1α, which induces a fibrotic and inflammatory response rather than a compensatory pro-angiogenic response. There is also another member of hypoxia-induced cascade, vascular endothelial growth factor (VEGF). In tumors, HIF1 is stabilized by hypoxia and activates VEGF transcription and secretion, and VEGF consequently stimulates angiogenesis. In human and mouse models, increased levels of VEGF-A allow for healthy expansion of adipose tissue and protect from lipotoxicity (Corvera and Gealekman 2014). Using a three-dimensional visualisation of intact adipose tissue Nishimura et al. demonstrated that adipocyte differentiation in adult mice takes place in adipogenic/angiopoietic cell clusters and that new blood vessels formation is coupled with adipocyte differentiation. They also defined VEGF as a key mediator of that process (Nishimura, Manabe et al. 2007).

The densitiy of capillary network differs in different adipose depots; it is much denser around multilocular than unilocular adipocytes and therefore in brown than white parts of adipose tissue (Cinti 2009). Cold exposure leads to activation of angiogenesis in both white and brown tissues (Xue, Petrovic et al. 2009). The regulation of blood flow through BAT is crutial for provision of both oxygene and substrates to brown adipocytes at times when non-shivering thermogenesis is ongoing. Noradrenaline increases blood flow through BAT in a dose-dependent manner. Interestingly, UCP1-KO mice have fully preserved BAT blood flow response to noradrenaline (Abreu-Vieira, Hagberg et al. 2015).

Vasculogenesis is also seen in the adipose tissue of fasted animals. In this state, adipocytes needs to have a sufficient capillary network to fit their increased lipolytic function, as evidenced by thin cytoplasmic projections of the slimmed adipocytes visible on electron microscopy (Giordano, Frontini et al. 2005).

To sum up, the density of capillary network answers to metabolic demands of whole-body metabolism and metabolism of discrete cells within adipose depots. The mechanism of

recruitment of vascular growth is still not completely understood; nevertheless, it probably involves VEGF and HIF-1α pathways.

2.1.4 Adipose tissue innervation

The nerve supply is, in the same way as vasculature, connected to multilocular and unilocular areas, in the way that it is denser around the brown/brite adipocytes (Cinti 2009). The density of noradrenergic parenchymal fibers increases in BAT after cold exposure (Murano, Barbatelli et al. 2009) and in WAT during fasting (Giordano, Frontini et al. 2005). Prevalent type of parenchymal nerve fiber in adipose tissue is noradrenergic, with tyrosine hydroxylase (TH) immunostaining used as a widely acknowledged marker of noradrenergic fibers (Vitali, Murano et al. 2012).

Adrenaline (ephinephrine) and noradrenaline (norepinephrine) are secreted from sympathetic nerve fibres and adrenal medulla. Adrenaline can be bound by all adrenergic receptors (AR), while noradrenaline binds to β2-adrenergic receptors with a low affinity. Noradrenaline influences many physiological targets, like heart, amygdala in the brain; it increases glucose release from glycogen and increases blood flow through muscles. In the adipose tissue, the sympathetic nervous system controls not only the hydrolysis of TAG, but also adaptive thermogenesis through the activation of β-AR. All types of adrenergic receptors are localised in adipose tissue (α1, α2, β1, β2 and β3) and on adipocytes (mainly β1 and β3) (Murano, Barbatelli et al. 2009). β3-adrenoreceptors are highly expressed in rodent WAT and BAT and are relatively specific to this tissues, but they are not present in humans. They increase heat production in brown adipose tissue, stimulate lipolysis and expression of lipoprotein lipase and UCP1.

β-AR are coupled to heterotrimeric G-protein G_s and to adenylyl cyclase. There are several possible pathways of intracellular signalling following G protein activation, with the most well-described acting through the elevated levels of intracellular cAMP and activation of cAMP-dependent protein kinase (PKA). Additional signaling pathways may be incorporated in a wide spectrum of effects of adrenergic receptor´s activation including the ERK and p38 mitogen-activated protein (MAP) kinase pathways, with roles in regulating fuel mobilisation and thermogenesis (Collins, Yehuda-Shnaidman et al. 2010).

α2 AR, contrary to β-AR, inhibit BAT function in the presence of noradrenaline. They are coupled to G_i and their stimulation lowers intracellular cAMP (Virtue and Vidal-Puig 2013).

2.1.5 White adipose tissue

White adipose tissue serves as an energy storing organ and also as an organ that secretes a wide variety of cytokines influencing whole-body homeostasis and insulin sensitivity. White adipose tissue constists of unilocular adipocytes and stromal vascular fraction (see also 2.1 Adipose Organ). It can by distributed either in subcutaneous or visceral localisation. In humans, visceral depots are related to increased risk of metabolic complications of obesity, maybe due to the fact that visceral fat releases FA to portal vein and by this way influence hepatic function, whereas the subcutaneous depots are protective in their respect (Lee, Wu et al. 2012). In rodent models, visceral adipose depots contain homogeneously distributed cells according to size and probability of cell death (Mirka Matejkova, Thesis). Murine subcutaneous depots, on the other hand, display a very heterogeneous pattern of discrete layers of cells, that differ in their size, probability of induction of multilocularity after cold adaptation and density of capillary network and innervation (unpublished results).

After the induction of obesity by high-fat diet in both human and rodent models the size of adipocytes and the level of local inflammation increase (Haase, Weyer et al. 2014), (Strissel, Stancheva et al. 2007). Local inflammation includes increased amount of adipose tissue macrophages, which are both attracted from blood in the form of bone-marrow-derived monocytes and also proliferates within the tissue (Amano, Cohen et al. 2014). There is a whole spectrum of macrophages present within adipose tissue, with extremes distinguished as pro-inflammatory M1, associated with insulin resistance (Fujisaka, Usui et al. 2009) and anti-inflammatory M2 subtypes. Macrophages furthemore function as antigen-presenting cells and regulate CD4+ T cells in adipose tissue (Morris, Cho et al. 2013). Inside the tissue, macrophages surround dying adipocytes and form immunohistochemically visualised crown-like structure (CLS) (Cinti, Mitchell et al. 2005), (Cinti 2006). The adipocytes in CLS die probably of necrosis, as evidenced by ultrastructural features (Cinti, Mitchell et al. 2005), but the role of possible apoptotic death has also been questioned (Murano, Rutkowski et al. 2013). Chronic inflammation in obese

humans is documented for example in a study by Naukkarinen et al., who phenotyped adult obesity-discordant monozygotic twins. Obese co-twins formed two distinct groups, being either metabolically healthy, or metabolically disturbed having higher liver fat, impaired glucose tolerance and upregulated genes for chronic inflammation (Naukkarinen, Heinonen et al. 2014).

The generally accepted opinion is that the bigger is the adipocyte size, the higher is the probability of cell death. In a study by Strissel et al. (Strissel, Stancheva et al. 2007), the incidence of adipocyte death increased during time-course of high-fat feeding, leading after 16 weeks to a marked inflammation of up to 80% adipocytes. The tissue than underwent hyperplasia and new smaller adipocytes emerged. Hepatic steatosis increased together with adipocyte depot inflammation. Nevertheless, from experiments by Jo et al. emerges that hyperplasia is enhanced by high-fat diet in a strain-dependent way (Jo, Gavrilova et al. 2009). The process of hyperplasia-connected adipocyte death may be driven by a stressfull influence of tight extracellular scaffold, because in a genetic model of absence of collagen VI, the expansion of adipocytes in a weakened extracellular scaffold was associated with improvements of whole-body homeostasis (Khan, Muise et al. 2009). On the other hand, in a human study by McLaughlin et al. (McLaughlin, Deng et al. 2010), the size of adipocytes in subcutaneous tissue was associated with inflammation in a reverse way; it was associated with an increased proportion of smaller adipose cells.

Adipocytes from obese mice, that are close to necrotic cellular death exhibit ultrastructural abnormalities, such as calcium accumulation and cholesterol crystals deposition; and these changes are more common in visceral than subcutaneous depots. Ultrastructural changes may be accompanied by oxidative stress, a possible reason of cell death (Giordano, Murano et al. 2013).

To sum up, these data suggest that adipocytes after the induction by a high-fat diet feeding increase at first their size and ultrastructural features of oxidative stress, than after remodelling of adipose tissue due to necrotic death of adipocytes and infiltration of macrophages and other immune cells, the number of smaller adipocytes increase and tissue growth is ensured by hyperplasia. Inflammation of adipose tissue through different pathways directly influences whole body metabolism.

2.1.6 Brown adipose tissue

Brown adipose tissue (BAT) consists of predominantly multilocular adipocytes and stromal vascular fraction. BAT merges with white adipose tissue in a transitional zone of mixed isles of white and brown adipocytes.

BAT reacts to cold exposure by increased proliferation of endothelial cells and interstitial cells expressing platelet-derived growth factor receptor alpha (PDGFRα), located to the dorsal edge of interscapular BAT. This process can be reverted by surgical denervation of interscapular BAT that reduces cold-induced adipogenesis by more than 85% and stimulated by the infusion of noradrenaline that increases proliferation in warm adapted animals to levels observed in cold-exposed ones (Lee, Petkova et al. 2015).

Brown adipose tissue is in warm-adapted animals present mainly in thoracic subcutaneous (interscapular), perirenal and periaortic region, but after cold adaptation multilocular (brite) adipocytes appear in most of the adipose depots, except for several abdominal ones.

Multilocular adipocytes contain uncoupling protein 1 (UCP1), a key component of β-adrenergically controlled non-shivering thermogenesis in BAT. Generally, UCP1 decreases proton gradient generated by oxidative phosphorylation and increases permeability of inner mitochondrial membrane, so that protons can return back to mitochondrial matrix at the expense of heat production. BAT function is activated by noradrenaline, that acts through β3-adrenergic receptors (AR) on adenylyl cyclase creating cAMP. cAMP activates protein kinase A, which phosphorylates perilipin and, subsequently through release of Comparative Gene Identification-58 (CGI58) activates ATGL and HSL, with ATGL being more important for BAT function, as was assessed by evaluation of ATGL and HSL KO mice temperature sensitivity (Virtue and Vidal-Puig 2013). Protein kinase A also phosphorylates transcription factor cAMP response element-binding protein (CREB) involved in activation of UCP1 expression, activates HSL and deactivates perilipin covering lipid droplets. This leads to increase in intracellular FA and glycerol concentrations. Most FA are channelled into mitochondria, where they serve as substrates for thermogenesis and are most likely involved in the regulation of function of UCP1 (Cannon and Nedergaard 2004). BAT has a very high uptake of glucose per gram of tissue; however, glucose probably forms only 5-15%

of oxidative substrate of BAT and it is only converted to pyruvate and lactate and exported from adipocytes or used to increase the capacity of TCA cycle. Uptake of glucose is stimulated during thermogenesis after cold exposure and during anabolic processes stimulated by insulin. Glucose uptake is also influenced by denervation (decreases glucose uptake) and noradrenaline (increases glucose uptake) (Cannon and Nedergaard 2004).

Function of BAT and UCP1 is frequently studied on a model of cold-exposed or cold-adapted animals, a physiologicaly relevant model of metabolic stress. Cold exposure is defined as an acute change in temperature lasting up to 72 hours, while cold acclimation refers to a period of time between 7 days and 3 months. After a period of acclimation BAT function reaches a steady state with respect to its level of thermogenic capacity (Virtue and Vidal-Puig 2013). Cold exposure *per se* is an exposure to temperatures below thermoneutral zone. Thermoneural zone is an ambient temperature, at which an organism does not have to employ active heat production nor evaporate heat dissipation to maintain its core body temperature and the lowest metabolic rate is observed (Virtue and Vidal-Puig 2013). Laboratory mice are usually kept below their thermoneutral zone (28-35^{o}C, depending on a strain, gender and age) and must expend energy to generate heat even in laboratory conditions, but in the literature, the term cold exposure or adaptation generally refers to temperatures lower than 15^{o}C. Energy expenditure increases below thermoneutral zone in C57BL/6 mice by 8% per 1^{o}C of ambient temperature and this increase is probably linear (Virtue, Even et al. 2012). Animals exposed to cold at first try to preserve their body temperature by vasoconstriction and piloerection and than increase their body temperature by shivering or non-shivering thermogenesis. Under the conditions of ongoing non-shivering thermogenesis, nutrient oxidation in BAT can account for over 60% of the total energy expenditure of the mouse and the whole-body metabolic rate increases up to 2.5 fold (Virtue, Even et al. 2012). Cold nor only activates UCP1-mediated non-shivering thermogenesis (Heldmaier 1975), but also increases the recruitment of thermogenic capacity in BAT (Cannon and Nedergaard 2011). UCP1 synthesis increases with lowering ambient temperature and duration of exposure (Fromme and Klingenspor 2011) and UCP1 ablated animals are cold-sensitive (Enerback, Jacobsson et al. 1997). However, the activity of sympathetic nervous system is not demanded for activation of thermogenic gene program (including PGC1α, UCP1 and DIO2) because white and

brite, but not brown, adipocytes respond to low temperatures in a cell-autonomous manner (Ye, Wu et al. 2013). Cold exposure influences not only BAT function, but also influences other organs, like increasing the heart weight and cardiac output (Virtue and Vidal-Puig 2013).

Noradrenaline is a hormone with important impact on BAT function (see also 2.1.4 Adipose Tissue Innervation). Noradrenaline test is commonly employed for estimation of non-shivering thermogenesis (Fig. 5). In this test noradrenaline is injected to anesthetized animals at thermoneutral temperature. Injection of noradrenaline simulates the sympathetic system stimulation of BAT. Nevertheless, noradrenaline activates also other adrenergic receptors in the body, leading to over-estimation of BAT non-shivering thermogenic capacity. This problem can be overcome by using proper controls in laboratory experiments, such as comparing warm and cold acclimated animals and subtracting the effect of noradrenaline on warm acclimated animals from the cold acclimated ones. Noradrenaline test in combination with UCP1 KO mice disclosed a UCP1 independent (increased muscle metabolism) and dependent component of response to noradrenaline. (Cannon and Nedergaard 2011), (Golozoubova, Cannon et al. 2006), (Cannon and Nedergaard 2004).

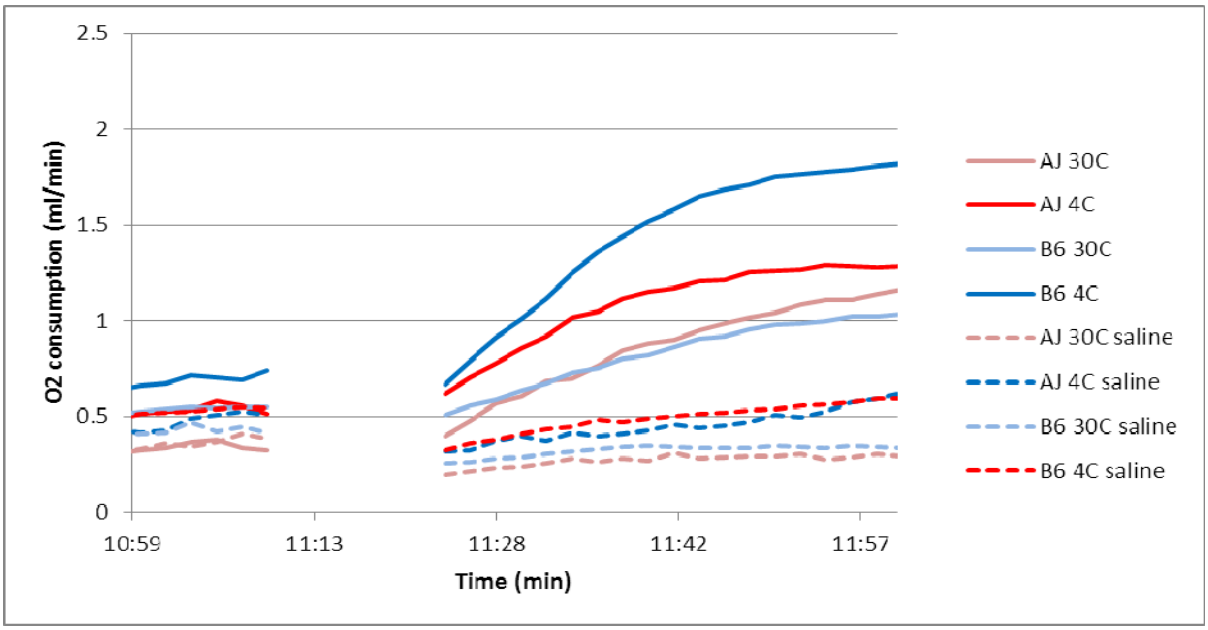

Fig.5: *Noradrenaline test on A/J and C57BL/6J mice acclimated in 30°C or 4°C for 7 days (unpublished results).*

It was believed that BAT is present only in small mammals and in newborn humans in relation to their need to preserve temperature homeostasis. Nevertheless, recently many publications referred about functional BAT in adult humans. Using positron emission tomography (PET), Virtanen et al. found that cold-induced glucose uptake was increased in paracervical and supraclavicular adipose tissue. The finding of BAT in adult humans was confirmed by both the UCP1 immunostaining and UCP1 mRNA levels (Virtanen, Lidell et al. 2009). Another study found in a larger cohort that probability of BAT detection was conversely correlated with age and outdoor temperature at the time of the PET scan. Women were also refered to have a greated mass of BAT (Cypess, Lehman et al. 2009). Activity of BAT in humans correlates with BMI and energy expenditure during rest (Celi 2009). Nevertheless, the functionality of BAT in humans has been questioned because BAT activity in humans was not activated during β-adrenergic stimulation (Vosselman, van der Lans et al. 2012).

2.1.7 Brown-in-white - „brite“ or „beige“ cells

After cold exposition or using chemical compounds, a specific cell type can be induced within white adipose depots. Brown-in-white or brite or beige adipocytes are morphologically brown adipocytes expressing among others UCP1 as a marker of brown cells. Besides brite cells also intermediate type named paucilocular cells appear after cold exposition or using chemical stimuli, containing several smaller lipid droplets and being either UCP1 positive or negative (Giordano, Smorlesi et al. 2014). Paucilocular cells have mixed mitochondria with classic brown and white features (Barbatelli, Murano et al. 2010). Classical white fat depots are prone to britening to a different degree, with inguinal and retroperitoneal depots being the most prone. The degree of britening also differs in different murine inbred strains (Vitali, Murano et al. 2012).

There is a need to precisely specify and distinguish brown and brite cells; therefore, specific markers of each type has been proposed. Nevertheless, some of them were later uncovered as rather positionally based than cell type defining. Among those generally accepted for brite cells is PR domain containing 16 (PRDM16), a zinc-finger protein that induces britening. It forms a transcriptional complex with the active form of CCAAT-enhancer-binding protein β (C/EBPβ) (Kajimura, Seale et al. 2009). Fibroblastic cells with a forced expression of PRDM16

induce a fully functional brown fat program. When injected into mice, these fibroblasts give rise to an ectopic fat pad with the morphological and biochemical characteristics of brown fat (Kajimura, Seale et al. 2009).

There are two main theories of brite cells origin. The first one assumes bidirectional interconversion between unilocular white and multilocular brown adipocytes. The second one states that brite cells arise *de novo* from a unique preadipocyte lineage.

2.1.7.1 Transdifferentiation

Transdifferentiation theory is based on the fact that adipocytes can acquire either unilocular, paucilocular or multilocular appearance based on metabolic and thermoregulatory demands and that interconversion between them is possible. This theory is mainly based on a histological point of view, with no signs of necrosis or apoptosis of vanishing white adipocytes nor proliferation of newly arising brown adipocytes visible during the process of increased britening. Transdifferentiation of white adipocytes is physiologically relevant on itself, because in pregnant and lactating mice adipocytes turn into cells producing and secreting milk (mammary gland) and back again (Giordano, Smorlesi et al. 2014). Transdifferentiation theory is further supported by the fact that after bromodeoxyuridine (BrDU) treatment of proliferating cells combined with β3-agonist treatment inducing britening of white adipose depots, 80-95% of newly established brown adipocytes are BrDU negative and so not originated from proliferation (Cinti 2009). BrDU is a commonly used analogue of nucleoside thymidine used for detection of proliferating cells in living tissues, and is frequently applied in experiments, where proliferation of cells is followed for a longer period of days to weeks.

Another confirmation of transdifferentiation theory brought a work by Vitali et al. (Vitali, Murano et al. 2012), who calculated that cold-induced increase of multilocular adipocytes was almost as big as cold-induced decrease in unilocular adipocytes, and there were no significant differences in adipocyte total number or any signs of apoptosis, that would had to accompany disappearance of white adipocytes.

Further approach to study appearance of brite cells are genetic tracing methods. Rosenwald et al. were able to show in a very convincing experiment that cold-induced brite

adipocytes can be reverted to morphologically and transcriptionally defined white adipocytes by 5 weeks of warm adaptation. These white adipocytes can be than further re-reverted to brite ones after additional cold stimulation (Rosenwald, Perdikari et al. 2013).

2.1.7.2 Newly formed cells of BAT/muscle origin

There are efforts to trace the origin of mature adipocytes to their procursors and embryonic ancestors. There is a theory based on genetic-tracing models saying that brown adipocytes originate from a precursor shared with a skeletal muscle cells expressing Myf5 and all white adipocytes arise form a Myf5 negative lineage. This seems to be logical because of metabolic similarities between BAT and muscle (such as high mitochondrial content and increased energy expenditure). However, by precisely quantifying the ratio between Myf5 positive and negative adipocyte cells, a changeable ratio was found in specific adipose depots (varying from 95% positive and 5% negative in interscapular BAT to 1% positive and 99% negative in intramyocellular WAT). Based on these data, there are two proposed models of adipocyte origin: Myf5 positive adipocytes originate from central dermomyotome and mix with Myf5 negative lineages in the adipocyte precursor cell compartment of each depot or Myf5 expression is or is not induced during determination or adipocyte differentiation in adipose depots. White adipocytes arising from Myf5 positive cells may have metabolic advantage(s) and metabolic variations between distinct lineages could affect depot-specific fat growth, and also endocrine activity may be different between lineages. On the other hand, Myf5 also can have no metabolic impact on white adipocytes (Sanchez-Gurmaches and Guertin 2014).

Supporting the theory of *de novo* brite cells emergence, using controversial inducible and permanent labeling model of mature adipocytes, Wang et al. suggested that during cold-induced browning of subcutaneous fat, most brite cells are newly formed (Wang, Tao et al. 2013).

2.1.7.3 Induction of brite cells by chemical compounds

There are several chemical compounds used for brite cell induction within white adipose depots. Among the most popular is β3-AR agonist CL 316.243 and promising information on metabolite lactate causing britening has also emerged.

β3-AR influence on britening of white adipose depots has been shown by Frontini et al. (Frontini, Vitali et al. 2013), who explored biopsies of white omental fat from patients affected by the catecholamine-secreting tumor pheocytochroma. Half of the samples contained multilocular UCP1 and PRDM16 positive clusters of cells with a dense capillary network and noradrenergic innervation. Immunohistochemistry for Ki67, a proliferative marker, suggested an unlikely contribution of proliferation to this phenomenon.

Simulating the effect of catecholamines on β3-AR, a selective agonist CL 316.243 has been used in several experiments. Administration of CL 316.243 and stimulation of β3-AR induces the occurrence of brite adipocytes also in murine white adipose depots (Barbatelli, Murano et al. 2010). Induction of multilocular cells derives from cells already present in the WAT, as was shown by using BrDU treatment (Himms-Hagen, Melnyk et al. 2000). Chronic treatment by CL 316.243 increases *de novo* lipogenesis and TAG turnover in all adipose depots, despite differences in UCP1 abundance (Mottillo, Balasubramanian et al. 2014). Chronic stimulation by CL 316.243 also induces expression of PPARα and several of its target genes (Li, Zhu et al. 2005). In mice knock-outed for β-3 AR specifically in adipose tissue, the transdifferentiation is blunted probably due to a mediation of this process by sympathetic nervous system (Smorlesi, Frontini et al. 2012).

Process of brightening may be also driven by the presence of metabolite lactate. Lactate induced browning of murine adipose cells with expression of functional UCP1 in a study by Carriere et al. (Carriere, Jeanson et al. 2014). Lactate effect on UCP1 was mediated by intracellular redox modifications as a result of lactate transport through monocarboxylate transporters. According to this study, browning may be an adaptive mechanism to alleviate redox pressure.

2.2 Indirect calorimetry

Indirect calorimetry uses the first principle of thermodynamics – energy cannot be created or destroyed, but can be exchanged between the body and its environment. The term indirect calorimetry (INCA) comes from the fact that it measures respiratory gas exchanges and allows for indirect estimation of energy expenditure. INCA measures O_2 consumption and CO_2 production of an organism, and assumes that they both come from the oxidation of energetic substrates. Through the oxidation of substrates the chemical energy stored in carbo-hydrogen bounds of

carbohydrates, lipids and proteins is released as heat, or used to create chemical bonds of high-energy compounds. The main INCA outcomes are a relative decrease in O_2 and a relative increase in CO_2 volume caused by animal metabolism together with the measurement of the air flow through the chamber.

Although the operating principle of INCA is relatively simple, the accuracy and long-term stability is highly dependent on calibration, amount of humidity in the measured air and the atmospheric pressure. While CO_2 analysers are usually highly stabile and require monthly or even yearly calibration, O_2 analysers are much more prone to measuring artifacts and must be calibrated before every measurement (Even, Mokhtarian et al. 1994), (Ferrannini 1988).

The principle of indirect calorimetry is often compared with direct calorimetry. Direct calorimetry is a standard method for accurate quantification of animal heat production and thus metabolic rate (Kaiyala and Ramsay 2011). When directly comparing the function of direct and indirect calorimetry in different dietary set-ups, the outcomes are slightly different (up to 2%), but the overall ability to detect changes of energy expenditure in different dietary set-ups is preserved (Burnett and Grobe 2014).

2.2.1 Methods for energy metabolism assessment

Energy expenditure calculation is based on several equations derived from comparison of indirect and direct calorimetry with regard to respiratory gasses and heat loss. There are several equations used for energy expenditure calculation, such as

EE (kcal) = 3.77 x VO_2 (l) + 1.41 x VCO_2 (l) (Lusk),

EE (kcal) = 3.90 x VO_2 (l) + 1.09 x VCO_2 (l) (Weir), in (Weir 1949),

EE (kcal) = 3.78 x VO_2 (l) + 1.24 x VCO_2 (l) (Elia)

EE (kcal) = 3.84 x VO_2 (l) + 1.12 x VCO_2 (l) (Brouwer)

When directly compared, all equations give approximately the same (up to 1% of difference in a situation, when RQ is close to 0.7) estimate of energy expenditure based on changes in concentration of respiratory gasses (Even and Nadkarni 2012).

The important question is how to compare lean and obese mice with respect to energy expenditure. Each cell of the body contributes to the whole-body energy expenditure to a different extent, with some of them being extremely metabolicaly active (such as hepatocytes) and some of them being extremely metabolically inactive (such as adipocytes). Lean and obese mice usually differ not in their metabolically active lean body mass, but in the metabolicaly inactive fat mass, that means in the amount of adipose tissue present in the body. Hence, the topic of normalisation of energy expenditure to the relative size of an animal has aroused a lot of attention.

The easiest and the most misleading option is to normalize energy expenditure to body weight of the measured animal. This approach assumes that all tissues contribute equally to VO_2, but the contribution of adipose tissue to a whole-body energy expenditure is not the same as the contribution of lean body mass. This type of normalisation often leads in genetically modified animals to a false conclusion that an obese (geneticaly modified) animal has lower energy expenditure than their lean controls and that the lower energy expenditure is the cause of obesity in a mentioned genetic model (Butler and Kozak 2010).

Because heat loss is more connected to body surface than to body weight, more logical would be to normalize energy expenditure to a surface area. This scales in relation to body weight raised to the power of 0.66 – 0.75. By comparing several animal models regarding their energy expenditure, an ideal relationship between metabolic rate and body weight in mammals is along linear regression with a slope of 0.75. Smaller animals have higher per-kg rates of EE than bigger ones, partly because their larger surface area relative to volume increases heat loss. The problem of this attitude is that this relationship was defined on lean and healthy animals of different species, and it is of course different to compare lean animals in between species and lean and obese animals within species, differing in their relative fat mass abundance (Even and Nadkarni 2012).

There is also the possibility to normalize energy expenditure to lean body mass and dismiss the influence of fat mass, but by this method, the contribution of fat mass, although small, is

neglected and also the contribution of adipokines to regulation of whole-body energy homeostasis is not implied (reviewed in (Alberts, Johansson et al. 2005), (Arch, Hislop et al. 2006).

Another approach to normalisation of energy expenditure represent regression models. The amount of lean body mass and fat mass are evaluated with respect to their relative contribution to energy expenditure. Using them, a relatively small contribution of fat mass of 15-20% of the contribution of the same mass of lean tissue (reviewed in (Arch, Hislop et al. 2006) or a relatively high contribution of 53% (Kaiyala, Morton et al. 2010), (Kaiyala, Morton et al. 2010), (Kaiyala and Schwartz 2011) may be observed . The method of regression analysis can be used in humans; nevertheless, it is not very practical for laboratory animals, for a relatively low number of animals per group is frequently used in laboratory experiments (Butler and Kozak 2010).

Up to date, the best statistical approach is to use the analysis of covariance ANCOVA. It makes no prior assumptions about scaling relationships between lean body mass, fat mass and metabolism, but rather derives them empirically using actual data (Arch, Hislop et al. 2006).

Important topic regarding energy expenditure of laboratory animals is the relationship between activity and energy expenditure. While Van Klinken et al. published that physical activity is a main determinant of total energy expenditure in freely moving mice and were able to mathematically describe participation of activity-related energy expenditure and resting metabolic rate (Van Klinken, van den Berg et al. 2012); Virtue et al. stated that activity contributes for 26,6% of total energy expenditure at thermoneutrality, but below thermoneutral zone despite a substantial amount of energy spend on activity, no independent effect of energy expenditure from activity on total daily energy expenditure is found (Virtue, Even et al. 2012).

Estimation of energy expenditure is imporatant for assessment of thermoneutral zone, i.g. an ambient temperature, at which an organism does not have to employ active heat production nor evaporate heat dissipation to maintain its core body temperature (Virtue and Vidal-Puig 2013). The assessment of thermoneutral zone involves comparison of resting metabolic rate of animals measured under defined ambient temperatures. The thermoneutral zone reaches 28-35^{o}C and is different for different mouse strains, gender and age of animals (Fig. 6).

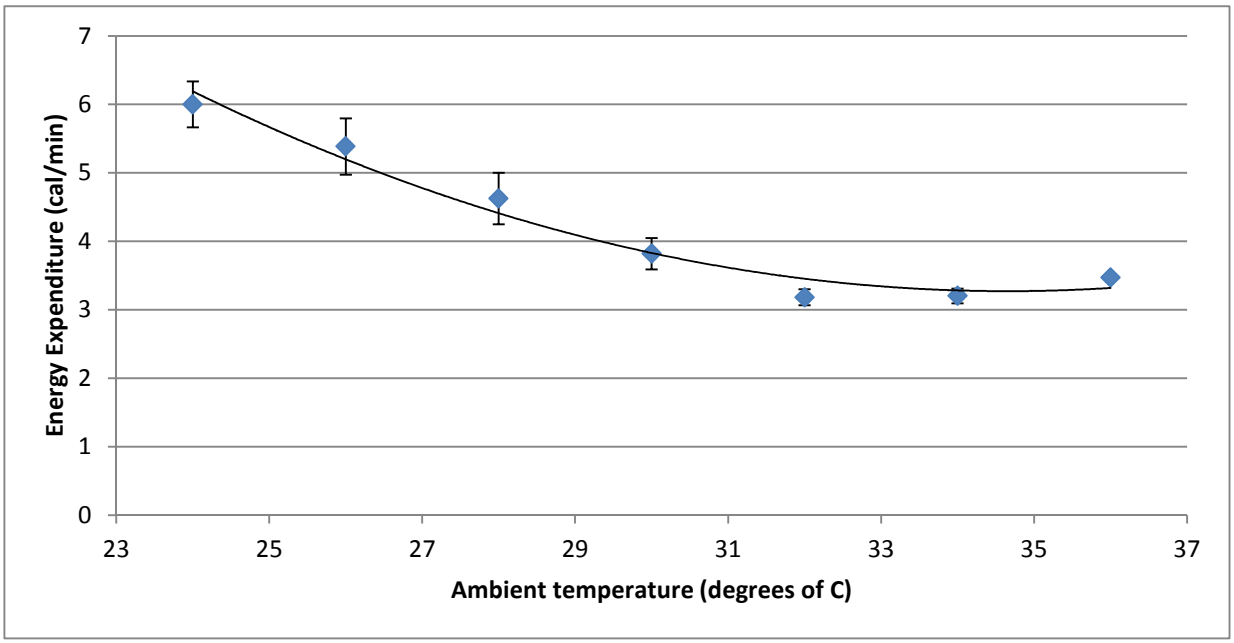

Fig.6: *Assessment of thermoneutral zone of mouse pups of the strain C57BL/6J at a time of weaning, e. g. at 30 days of age (unpublished results).*

2.2.2 Respiratory Quotient

Respiratory Quotient (RQ) or Respiratory Exchange Ratio (RER) is an important INCA outcome. It is calculated as

$RQ = VCO_2/VO_2$

RQ defines whole-body substrate oxidation. When it is close to 1, 0.8 or 0.7, it implies oxidation of carbohydrates, proteins or fatty acids, respectively. These ratios can by derived from a universal equation of carbohydrate oxidation

$HCOH + O_2 \rightarrow CO_2 + H_2O,$

where 1 CO_2 is produced per 1 O_2 consumed,

and lipid oxidation

$CH_2 + O_2 \rightarrow CO_2 + H_2O,$

where 1 CO_2 requires 1.5 O_2 consumed (this equation also includes oxygenes on the carboxy end of fatty acids, and, as a consequence, gives a ratio of 0.7). There are specific conditions, when RQ differs from the range 0.7-1. RQ of liponeogenesis is 5, hence a relatively small proportion of liponeogenesis from glucose increases RQ above 1 (Elia and Livesey 1988). In the presence of severe metabolic derangements, such as lactic acidosis, diabetic ketoacidosis or ethanol ingestion RQ also differs. RQ of lactate oxidation is 1, whereas RQ of β-hydroxybutyrate is 0.89 and of ethanol oxidation is 0.67. In case ketones are secreted by urine or accumulated within the body, RQ decrease (Ferrannini 1988).

RQ can be directly compared to food quotient of a respective diet FQ = (0.855 x % protein) + (1 x % carbohydrate) + (0.71 x % fat). During a defined period of 24 hours, where both energy saving period during the night and energy consuming period during the day are included, the RQ has to equal to FQ, otherwise a disequilibrium in body weight of an animal is implied (Longo, Charoenthongtrakul et al. 2010).

RQ can be either evaluated as a mean across a defined period of time, or can be arranged using relative percent cumulative frequency (PRCF) curves to detect even small differences in the distribution of measured RQ data. This method involves sorting data in an ascending order, calculating their cumulative frequency and expressing the frequencies in the form of percentile curves. This approach is most frequently used for RQ data (Longo, Charoenthongtrakul et al. 2010), but can be also applied on VO_2 data (Riachi, Himms-Hagen et al. 2004). The greater slope of PRCF curve implies a relative loss of substrate flexibility, whereas a relatively shallower curve means greater flexibility to oxidized substrates.

2.2.3 Calculation of substrate oxidation

It is possible to estimate rates of substrate oxidations from INCA data. For oxidation of carbohydrates, an equation:

GLUOX (g) = 4.57 x VCO_2 (l) – 3.23 x VO_2 (l) – 2.60 x N (g) (Even, Mokhtarian et al. 1994), if the nitrogene detection in urine is possible, or

GLUOX (g) = 4.55 x VCO_2 (l) – 3.21 VO_2 (l) (Ferrannini 1988), if the nitrogene detection in urine is impossible,

are used. For oxidation of lipids, equations:

LIPOX (g) = 1.69 VO_2 (l) – 1.69 VCO_2 (l) – 2.03 x N (g) (Even, Mokhtarian et al. 1994), if the nitrogene detection in urine is possible; a positive solution expresses the rate of lipid oxidation or

LIPOX (g) = 1.67 (VCO_2 (l) - VO_2 (l)) (Ferrannini 1988), if the nitrogene detection in urine is impossible; a negative solution expresses the rate of lipid oxidation

are used. These equations can nevertheless be used only in situations, when interconversion processes, such as ketogenesis, *de-novo* lipogenesis and gluconeogenesis are negligible (Even, Mokhtarian et al. 1994). The only solvable situation is when liponeogenesis is ongoing, e.g. in a situation, when the solution of the equation for lipid oxidation published by Ferranini is positive and it quantify liponeogenesis, than the rate of carbohydrate oxidation is overestimated and an equation GLUOX (g) = 1.34 x VCO_2 (l) must be used (Ferrannini 1988). However, it is important to note that estimates of fuel utilisation or synthesis is 10 to 12-fold more sensitive to errors in the RQ than energy expenditure (Livesey and Elia 1988), (Ferrannini 1988).

The most important feature of substrate oxidation derived from INCA data is that it provides a net disappearance rate of a substrate regardless of the metabolic interconversions that the substrate may undergo before its disappearance from its metabolic pool (Simonson and DeFronzo 1990). Direct oxidation usually is the main metabolic route of substrate disappearance, but the possible interconversion of metabolic substrates do not affect the rate of substrate oxidation or RQ and can, on the other side, be detected only by energy expenditure increased by futile cycles. In the presence of interconversion processes, errors up to 30% can occur in the calculation of oxidation of carbohydrates or lipids (Even, Mokhtarian et al. 1994).

Composition of oxidized proteins reflects rather diet composition than the composition of animal muscle. Nitrogen liberated during protein oxidation can be measured during long-term

measurements by urinary nitrogen excretion rate, while it is not possible to assess protein oxidation by this way during short-time measurements. The influence of protein oxidation on energy expenditure may be totally ignored, because the contribution of protein disappearance to energy production cause an error smaller than 2%, which is below the detection limit of any INCA device. Above mentioned equations for substrate oxidation either includes protein oxidation assessed as urinary nitrogen secretion or not, but those ones not including nitrogen oxidation are more widely used. While protein oxidation do not excesivelly influence energy production, the contribution to substrate oxidation is the smallest when RQ is close to 0.8 and correspondingly increases as the RQ values deviates from this value (Simonson and DeFronzo 1990).

Calculation of substrate oxidation can be biased by several metabolic processes. Important condition is that there should be no retention or release of CO_2 in the blood to regulate pH (Even, Mokhtarian et al. 1994). It can be influenced by processess such as postexcercise excess oxygen consumption, and a shift in acidobasic equilibrium, such as acidosis, alkalosis, hyper- or hypoventilation. While the O_2 consumption is relatively quickly mirrored in measured values, CO_2 enters blood bicarbonate pool with complete kinetics, so the changes in metabolic CO_2 production give rise to changes in expired CO_2 with some delay (Ferrannini 1988).

The possibility to calculate substrate oxidation can nevertheless lead to an impressive results, such as in the work of Bruss et al. (Bruss, Khambatta et al. 2010), where a pronounced cycle of liponeogenesis and lipid oxidation in calorie-restricted animals in comparison with their ad-libitum fed controls was revealed.

To sum up, INCA data allows for assessment of RQ as a measure of metabolic partitioning and for indirect estimation of energy expenditure and substrate oxidation.

2.3 Metabolic flexibility

Theory of metabolic flexibility was for the first time mentioned by Kelley et al. (Kelley, Goodpaster et al. 1999), (Kelley and Mandarino 2000), (Kelley, He et al. 2002), as the ability of metabolism to switch between insulin stimulated and unstimulated state. The precise definition

according to Galgani et al. (Galgani, Moro et al. 2008), is that metabolic flexibility is the capacity of the organism to adapt fuel oxidation to fuel availability.

The most classical way to assess metabolic flexibility is simultaneous measurement of the switch between insulin unstimulated and stimulated conditions during euglycemic-hyperinsulinemic clamp combined with indirect calorimetry assessment of substrate oxidation in both states. The increase in RQ above fasting levels after meal test challenge or re-feeding, called ΔRQ, is also the original approach to evaluate the metabolic flexibility to carbohydrates, used in laboratory animals. The metabolic flexibility, defined on healthy, lean individuals, is disturbed in obese, pre-diabetic and diabetic patients. Metabolic inflexibility includes many possible metabolic manifestations, such as the failure of skeletal muscle to appropriately switch between the use of lipids in the fasting state and the use of carbohydrates in the insulin-stimulated state, impaired transition from FA efflux from adipose tissue in the fasting state and storage in insulin-stimulated conditions, and also the ability to minimize glucose levels after insulin stimulation. All of these functions requires coordinated regulation of the major organs involved in carbohydrate and lipid metabolism – pancreas, liver, skeletal muscle and adipose tissue. Involvement of skeletal muscle in the whole-body energy homeostasis is important, as it contributes approximately by 20% to the total energy expenditure and is the major site of insulin stimulated glucose uptake and glucose storage (Storlien, Oakes et al. 2004).

Kelley and his co-workers (Kelley, Goodpaster et al. 1999), (Kelley and Mandarino 2000), (Kelley, He et al. 2002) defined that the glucose uptake in basal fasting conditions is normal or even increased in obese vs. lean humans, and that fatty acid uptake in obese is normal, while fatty acid oxidation is lower and its storage elevated. In insulin stimulated conditions, glucose uptake in lean controls increase approximately 10-fold and fatty acid uptake is dramatically decreased, while in obese subjects the changes in skeletal muscle metabolism are suppressed and glucose uptake, oxidation and storage are relatively reduced. On the other hand, the oxidation of fatty acids remains on relatively high levels. These changes are mirrored in RQ values across the leg, which changes from 0.82 to 1 in lean controls and stays at 0.9 in both conditions in obese humans (reviewed in (Storlien, Oakes et al. 2004)). Inability of muscle cells from obese patients to switch

to glucose oxidation is not bound to the ability of muscle cells to oxidize glucose, but rather is caused by a decrease of insulin-stimulated glucose disposal rate, because after controlling for this variable, metabolic flexibility is not altered in obesity or T2D. The lowered capacity to regulate muscle lipid oxidation may lead to increased accumulation of lipids and their intermediates, such as ceramides and diacylglycerols and to insulin resistance of muscle cells of obese patients (Galgani, Moro et al. 2008).

Besides skeletal muscle, other tissues are involved in the metabolic flexibility regulation. Adipose tissue plays a crucial role in buffering the flux of NEFA in the blood between insulin stimulated and unstimulated state (reviewed in (Storlien, Oakes et al. 2004)). NEFA can mediate many adverse metabolic effects, such as insulin resistance. Process of mobilization of FA from adipose tissue is normally suppressed by insulin, but in obesity becomes insulin resistant and lipolysis is increased (reviewed in (Karpe, Dickmann et al. 2011)). NEFA turnover in plasma is relatively high, with plasma half-life around 2-4 min. NEFA in the fasting state come almost entirely from hydrolysis of TAG in adipose tissue. However, post absorptive NEFA plasma levels comes from 40-50% from a spillover of FA released from TAG-rich lipoprotein particles through the action of lipoprotein lipase (LPL) in the capillaries of adipose tissue. The contribution of spillover in obese individuals is relatively lower than in lean individuals because of a relatively low LPL rate of action per unit of fat tissue. This lower activity allows more TAG-rich lipoproteins to escape hydrolysis in adipose tissue and they are in the end taken up by the liver. As a result of fat mobilization suppressed by insulin, NEFA plasma concentrations in humans have a circadian rhythm showing the highest concentration after an overnight fast, with suppression after each meal (reviewed in (Karpe, Dickmann et al. 2011)).

2.3.1 Metabolic flexibility and mitochondria

The basic interaction between substrates at a cellular level has been described by Randle et al. in 1963 (reviewed in (Hue and Taegtmeyer 2009)). The metabolic cycle suggested by Randle includes the fact that increased fat oxidation in muscle cells inhibits both pyruvate kinase and phosphofructokinase by accumulation of acetyl-CoA and citrate. The blocked glycolytic pathway leads to increased glucose-6-phosphate concentration, which inhibits hexokinase and by this way reduces glucose uptake and oxidation by muscle cells. This cycle is able to explain competition

between glucose and fatty acids both in muscle and adipose tissue cells, it controls fuel uptake and oxidation in response to demand in normal tissues in coordination with hormones involved in substrate utilization pathways.

Obesity and T2D are connected to increased content of TAG within muscle fibers. Increased intramuscular lipids are related to the development of insulin resistance and its severity, but are also observed in muscle cells of highly trained athletes, who have normal or enhanced insulin sensitivity. This discrepancy between intramuscular lipid content being associated both with the unhealthy and super healthy state is called athlete´s paradox. In obese humans the failure to adapt lipid oxidation to energy demand is the mechanism leading to lipid accumulation within skeletal muscle (Kelley and Mandarino 2000).

Relationship of mitochondria to metabolic flexibility has been confirmed by several studies. De Weijer et al. (van de Weijer, Sparks et al. 2013), who compared type 2 diabetics with controls, found that the intramyocellular lipid content was not different, as was also confirmed in a study by Van Herpen (van Herpen, Schrauwen-Hinderling et al. 2011), but in this study the mitochondrial function was lowered by 12.5%, whole body glucose disposal as a determinant of substrate utilization to insulin was higher at baseline and lower after insulin stimulation. As a result, the mitochondrial reduction was accompanied by lower metabolic flexibility.

Kelley et al. (Kelley, He et al. 2002) also confirmed that type 2 diabetics as compared to lean controls exhibit not only decreased metabolic flexibility, but also decreased mitochondrial function assessed as citrate synthase activity and decreased mitochondrial size assessed by electron microscopy. He suggested that impaired mitochondrial function could directly contribute to insulin-resistant glucose metabolism due to inefficient provision of ATP for hexokinase and other energy-requiring pathways. Chomentowski et al. (Chomentowski, Coen et al. 2011) clarified the topic of mitochondria contribution to metabolic flexibility topic. They divided population of mitochondria into intermyofibrilar and subsarcolemmal subpopulations by using electron microscopy, with the decrease of the former associated with obesity, T2D, fasting RQ and metabolic flexibility.

The important question whether mitochondrial inflexibility is rather a cause or a consequence of obesity and T2D was addressed by Ukropcova et al. (Ukropcova, Sereda et al. 2007). They found that in subjects with a family history of diabetes, metabolic inflexibility and lower ability to adapt to high-fat diet are connected to decreased muscle mitochondrial content.

2.3.2 Assessment of metabolic flexibility

The original way to assess metabolic flexibility is RQ measurement during euglycemic-hyperinsulinemic clamp. It is still the most commonly used method for establishment of metabolic flexibility in humans; nevertheless, metabolic flexibility can be also assessed as the difference between fasting and post absorptive RQ in response to meal. The important topic is the stability of fasting RQ as a baseline for metabolic flexibility assessment, which is highly related to dietary history and in humans it takes 7-10 days to fully adapt RQ to a newly established diet.

In rodents, alternative ways of metabolic flexibility assessment are rare. Duivenvoorde et al. published three alternative ways for metabolic flexibility assessment using INCA (Duivenvoorde, van Schothorst et al. 2015). The first test included INCA measurement throughout the whole day period, reflecting increased activity and feeding behavior during nights and decreased physical activity and increased resting behavior during days. In this test, the difference between day and night RQ is compared. The second approach was an INCA reaction to a challenge in the form of glucose bolus of 2 mg of glucose per gram of body weight. Compared adult and old mice nevertheless did not differ in answer to those two tests. The third test, the most successful in detection of expected differences between adult and old mice, included adaptation to a challenge of oxygen restriction. Old mice were not able to maintain reduced oxygen consumption following challenge conditions.

Important question of different metabolic flexibility together with metabolic improvements in young healthy women and men was addressed in the work of Sparks et al. (Sparks, Pasarica et al. 2009). They found that women are metabolically more flexible than men and that this difference is driven more by an increase of insulin-stimulated glucose oxidation than differences in fasting fat oxidation. Women also display greater capacity for insulin suppression of

fatty acid release from adipose tissue despite their similar chemokine and macrophage content in WAT.

Glucose tolerance tests (GTT) are used for evaluation of diabetes, insulin resistance and metabolic flexibility of carbohydrate metabolism. They determine blood glucose levels after glucose load given either by an intraperitoneal injection or by an oral gavage. The oral route is more physiological, but there may be an increased variability associated with inconsistent rates of gastric emptying. Furthermore, glucose tolerance following an oral glucose loading is influenced by the effect of incretins, which have an impact on insulin secretion from pancreas. These effects are not present in the case of intraperitoneal GTT. When directly comparing them, glucose and insulin increase after glucose load is reported to be lower in the case of oral GTT on adult mice (Andrikopoulos, Blair et al. 2008).

GTT is usually performed on fasted mice. Overnight fasting before GTT is a significant metabolic stress even for adult mice, as mice eat the majority of food at night. To avoid this stress GTT can be performed after 6 hours of fasting (6:00 a.m. till 12:00 a.m.), recommended by (Andrikopoulos, Blair et al. 2008) as the test with the best response and most physiological conditions.

Another important issue to address is the glucose dose. Glucose can be administered either in a form of a fixed amount and volume (usually used in the oral GTT in the human studies) or at a dose of 1 to 3 mg of glucose per g of body weight (usually used in the intraperitoneal GTT on mice). Moreover, glucose dose is routinely adjusted to body weight of the animal, despite the fact that lean and fat tissue contribute to glucose metabolism differently and a normalization on lean body mass would be more precise.

Application of glucose during OGTT in humans has surprisingly large effects on whole-body metabolism delineated in plasma metabolome. The effects were in the work of Shaham et al. mainly on metabolites connected to proteolysis, lipolysis, ketogenesis and glycolysis, known targets of insulin actions (Shaham, Wei et al. 2008). Shaham et al. detected mainly changes in concentrations of bile acids, urea cycle intermediates and purine degradation products. Zhao et

al. (Zhao, Peter et al. 2009) found as discriminating OGTT biomarkers FA, acylcarnitines, bile acids and lysophosphatidylcholines.

To sum up, metabolic flexibility is the ability to efficiently switch between metabolic substrates and can be assessed either by INCA combined with a challenge test or by glucose tolerance tests.

3 Aims of the thesis

The general goal of this study was to compare several approaches for metabolic flexibility assessment with respect to overall energy homeostasis. Specific goals were as follows:

1. to evaluate influence of *n-3* long chain fatty acids (*n-3* LC-PUFA) and rosiglitazone, a drug from thiazolidinedione group, and their combination on metabolic flexibility in dietary obese mice, both at a whole-body and cellular level.
2. to evaluate metabolic flexibility in both genders of C57BL/6N mice challenged by high-fat diet.
3. to evaluate whole body energy homeostasis challenged by chenodeoxycholic acid, with respect to BAT and WAT metabolism.
4. to evaluate several aspects of metabolic flexibility by using intraperitoneal and oral glucose tolerance tests, INCA tests using glucose bolus and fasted-re-feeding setup.
5. to evaluate metabolic flexibility as a reaction metabolism to short-term cold exposure.

4 Methods

4.1 General description of conducted experiments

All the presented studies are based on animal experiments performed in the Department of Adipose Tissue Biology. Experiments were performed using either C57BL/6N male mice from Charles River Laboratories, Germany (publication A), C57BL/6N male and female mice, parental generation from Charles River Laboratories, Germany (publication B), C57BL/6J male mice bred in our laboratory since 1993 (publication C), C57BL/6J and A/J mice of both genders bred in our laboratory since 1993 or 1997, respectively (publication D) or C57BL/6JBomTac male mice form Taconic, Denmark and A/JOlaHsd mice from Harlan, UK (publication E). The mice bred in our laboratory were weaned onto standard laboratory chow diet (**STD**; energy density 13.0 $kJ.g^{-1}$, ~35.2% $wt.wt^{-1}$ of lipids, extruded R/M-H diet, Ssniff Spezialdiäten, Soest, Germany). With the exception of publication E, animals were maintained at 20°C on a 12:12-hr light-dark cycle with free access to water and food. Mice were single-caged during the experiments. Body weight and food intake were monitored weekly. All the experiments were conducted according to the guidelines for the use and care of laboratory animals of the Institute of Physiology AS CR, v. v. i., the directive of the European Communities Council (86/609/EEC), and the Principles of Laboratory Animal Care (NIH Publication no. 85-23, revised 1985).

4.1.1 Publication A

Three-months-old mice were randomly assigned to STD diet (energy density 13.0 kJ/g, ~35.2% wt/wt of lipids, extruded R/M-H diet, Ssniff Spezialdiäten, Soest, Germany), cHF diet (lipid content 35% wt/wt, mainly corn oil, carbohydrate content 35.4%, protein content 20.5%) or to a cHF derived intervention diets as follows: cHF+F - cHF based diet supplemented with *n-3* LC-PUFA concentrate (product EPAX 1050 TG, EPAX a.s., Aalesund, Norway, containing 46% DHA, 14% EPA in the form of TAG) replacing 15% of dietary lipids; cHF+ROSI - cHF diet supplemented with 10 mg rosiglitazone per kg of diet (Avandia, GlaxoSmithKline, USA); and cHF+F+ROSI - cHF based diet supplemented with both *n-3* LC-PUFA concentrate and rosiglitazone. Diet intervention lasted 8

weeks, when diet was distributed daily and food consumption and body weight were monitored weekly.

Animals were killed by cervical dislocation under pentobarbital anesthesia. One group of animals had free access to experimental diets (n=8), the other group underwent diet-switch protocol. They were fasted since 8:00 a.m. till 6:00 p.m., then since 6:00 p.m. refed STD diet and killed the next morning (n=10). Glycaemia was measured and EDTA-plasma was collected either before the period of fasting in the fed state or before the killing in the STD diet-refed state.

INCA was performed during the 6^{th} week of the experiment for evaluation of energy expenditure and metabolic flexibility to high-carbohydrate meal during diet-switch protocol. Metabolic flexibility was assessed as the change of RQ between fasting and refed state and visualized as PRCF curves. NEFA, TAG, β-hydroxybutyrate and glycaemia were evaluated from EDTA-plasma; and targeted metabolomics analysis from extracts of skeletal muscle and gene expression and western blot analysis were performed.

4.1.2 Publication B

In this experiment F1 generation of mice was used. Parental male and female C57BL/6N mice were supplied by the Charles River Laboratories, Germany. Mice pups were 4 weeks after birth randomly assigned either to STD diet (energy density 13.0 kJ/g, ~35.2% wt/wt of lipids, extruded R/M-H diet, Ssniff Spezialdiäten, Soest, Germany) or cHF diet (lipid content 35% wt/wt, mainly corn oil, carbohydrate content 35.4%, protein content 20.5%). Fresh diet was supplied three times a week, body weight was recorded weekly and food intake was recorded either weekly (between week 4 and 14) or fortnightly (between week 17 and 30). Glucose tolerance tests were performed at week 10, 25 and 33. The experiment lasted either 15 or 35 weeks, when 10 animals from each gender and diet were killed by cervical dislocation under dietylether anesthesia. EDTA-plasma was collected for NEFA, TAG, glucose and adiponectin evaluation; liver samples were collected for tissue TAG content evaluation and histological staining on cryosections; epididymal (eWAT) and subcutaneous (scWAT) adipose tissue samples were collected for DNA content

evaluation, RNA analysis and immunohistochemical assessment of CLS on formaldehyde-fixed samples.

4.1.3 Publication C

Mice used in two experiments in this publication were before the start of the experiment allowed since 2 till 6 months of age a free access to cHF diet (lipid content 35% wt/wt, mainly corn oil, carbohydrate content 35.4%, protein content 20.5%) for induction of obesity and connected metabolic disturbances. After this period, two experiments were performed – 8 and 3 weeks reversions.

In the 8-week reversion experiment, 10-12 mice per group were fed either cHF diet (cHF) or cHF diet supplemented by 0.5 % CDCA (0.5 % CDCA, wt/wt) or cHF diet supplemented by 1% CDCA (1% CDCA, wt/wt, Sigma-Aldrich, USA, 95% pure). Body weight and food intake were monitored weekly. In the 6^{th} week of the experiment, 5 mice per group were subjected to oral glucose tolerance test. Mice were killed at week 8 in a random-fed state. Blood was collected for TAG, NEFA, cholesterol, glucose, insulin, adiponectin and hepatic enzymes evaluation; and liver, eWAT, scWAT, BAT and gastrocnemius muscle were collected for RNA isolation. Moreover, feces were collected for TAG and cholesterol content evaluation.

In the 3-week reversion experiment, 8 mice per group were randomly assigned either to cHF diet (cHF) or to cHF diet supplemented by 1% CDCA (1% CDCA) or to a group that received cHF diet to the amount consumed by 1% CDCA group (PF). Animals fed STD diet since weaning were also included. Body weight and food intake was monitored 4 times a week. During the day 15-17 INCA was measured. Animals were dissected in a random-fed state and the same samples were taken as in the previous experiment.

4.1.4 Publication D

In this publication, mice pups of C57BL/6J and A/J mice kept in our laboratory since 1993 and 1997, respectively, were used. Pups were weaned at 30 days of age onto STD diet (energy density 13.0 kJ/g, ~35.2% wt/wt of lipids, extruded R/M-H diet, Ssniff Spezialdiäten, Soest, Germany). The next morning, diet was removed until the following experiments were performed (except for the fasted/refed protocol, in which pups had free access to diet till 1:00 p.m.). Firstly, we performed

intraperitoneal glucose tolerance test (IPGTT) using a dose of 1 mg of glucose/g of body weight. Next, on a separate group of mice, we performed oral glucose tolerance test (OGTT) using a dose of either 1 or 3 mg of glucose/g of body weight. In all experiments, separate groups were treated by 0.9% NaCl solution to reveal possible effects of handling, injection or gavage on glycaemia. Afterwards we performed INCA in an OGTT setting with a dose of 1 mg of glucose/g of body weight at 22°C, a dose 7.5 mg of glucose/g of body weight at 22°C and the same dose but measured at 34°C (within a previously defined thermoneutral zone for mouse pups of this age, see also Fig. 6). The last experiment included INCA measurement of fasted/refed switch protocol. Pups fasted since the start of measurement at 1:00 p.m. till 6:00 p.m. when a pre-weighted diet was given and EDTA-plasma in the fasted state was collected. The experiment terminated the next morning, when EDTA-plasma was collected in the refed state. In a separate experiment we evaluated effect of stress on indirect calorimetry outcomes by measuring corticosterone levels in plasma and feces collected after the INCA measurement.

4.1.5 Publication E

In publication E, C57BL/6JBomTac male mice form Taconic, Denmark and A/JOlaHsd mice from Harlan, UK were since the age of 6 weeks kept at least for 7 days at thermoneutrality (30°C). Afterwards, mice were randomly assigned to a group kept at thermoneutrality (n=9) or to groups kept at 6°C for 2 or 7 days (n=9). Food intake and body weight were periodically recorded. Mice were killed in a random-fed state under diethylether anesthesia and EDTA-plasma samples were collected for NEFA, TAG, β-Hydroxybutyrate, cholesterol, glucose, insulin, leptin, adiponectin and FGF21 plasma level evaluation. Samples of BAT, eWAT and scWAT were collected both for RNA isolation and histological and immunohistochemical evaluations. In a separate group of animals (n=6) kept either at thermoneutrality or at 6°C for 7 days.

4.2 *In vivo* tests of glucose tolerance

In publication B and C, IPGTT was performed after an overnight fasting (15-16h). A dose of 1 mg of glucose / gram of body weight was used. Glycaemia was assessed before glucose injection in the fasted state and then at 15, 30, 60, 120 and 180 min after the glucose application. Glycaemia was measured using a glucometer (LifeScan, USA). Results were expressed as an area

under the glucose curve. Moreover, to assess changes in glycaemia in response to fasted/refed transition in the experiment B, mice scheduled for killing at week 35 were either fasted between 8:00 a.m. and 10:00 p.m. or fasted between 8:00 a.m. and 6:00 p.m. and then were given diet *ad libitum* for the next 3 hours. In each mouse, blood glucose was randomly assessed in both the fasted and refed state in two subsequent days.

In publication D, both IPGTT and OGTT were performed on 6-hours-fasted mice (6 a.m. till 12 a.m.). IPGTT was performed using a dose of 1 mg of glucose / g of body weight in the form of 10% D-glucose. OGTT was performed using a dose of 1 or 3 mg of glucose / g of body weight in the form on either 10% or 50% D-glucose. Blood glycaemia was assessed in the fasted state before glucose injection and then 15, 30, 60, and 120 min after glucose application. Glycaemia was measured using a glucometer (LifeScan, USA). All GTT tests were performed at 20^{o}C.

4.3 Evaluation of plasma parameters

In EDTA-plasma samples, several parameters were evaluated. NEFA levels in publication A, B, C and D were evaluated using NEFA C kit (Wako Chemicals, Germany). TAG levels in publication A, B, C and D were evaluated by Triacylglycerols Liquid (Erba-Lachema Diagnostika, Brno, Czech Republic). Cholesterol levels in publication C and D were evaluated by Cholesterol Liquid (Erba-Lachema Diagnostika, Brno, Czech Republic). Insulin levels in publication A, B and C were evaluated using the Sensitive Rat Insulin RIA Kit (LINCO Research, USA). β-hydroxybutyrate levels in publication A were evaluated using Autokit 3-HB (Wako Chemicals, Germany). Aspartate transaminase and alanine transaminase in publication C were evaluated by enzymatic kits (Roche Diagnostics, Germany). Leptin levels in publication B were evaluated by Mouse Leptin RIA Kit (LINCO Research, USA), in publication D (by E. van Schothorst, F Hoevenaars) measured by mouse serum adipokine milliplex multianalyte kit (Millipore Corporation, USA) and analyzed using BioPlex200 system (Bio-Rad, The Netherlands).

Multimeric forms of adiponectin were determined in publication B (by D. Medrikova) and in publication C and D (by P. Janovska) using western blotting and primary rabbit anti-mouse polyclonal antibodies (BioVendor, Brno, Czech Republic), followed by secondary donkey anti-rabbit IgG infrared dye conjugated antibodies (IR Dye 800, Rockland, USA). Membranes were scanned using Odyssey IR Imager (Li-Cor Biosciences, USA).

4.4 Corticosterone levels

Corticosterone levels in publication D (by M. Uil) were evaluated either in plasma or in extracts (Wasser, Monfort et al. 1994) from feces collected after INCA measurement using ImmuChem soluble antibody corticosterone 125I RIA kit (MP Biomedicals, USA) and 1:200 dilution of the samples.

4.5 Metabolomic Analysis

Targeted metabolomics analysis was performed in publication A (by O. Kuda) using extracts from skeletal muscle. Kit AbsoluteIDQTM p150 (Biocrates Life Sciences, Austria) based on FIA-MS was used for evaluation of 163 metabolites, such as amino acids, hexoses, acylcarnitines, sphingomyelins, hydroxysphingomyelins, diacyl-phosphatidylcholines, acyl-alkyl-phosphatidylcholines and lysophosphatidylcholines.

4.6 RNA Isolation and Gene Expression

Total RNA was in publication A and B isolated from tissue samples stored in RNA *later* (Ambion, USA) at -20^{o}C using TRI Reagent (Sigma-Aldrich, USA). RNA was purified by RNeasy columns after isolation (Qiagen, The Netherlands). In publication C RNA was isolated from frozen tissues using kit from Qiagen GmbH (Germany). RNA yields were quantified by Nanodrop instrument (Thermo Scientific, USA). Complementary DNA was produced using 1 μg of RNA with a Bio-Rad iScript cDNA synthesis kit (Bio-Rad, USA). Gene expression was evaluated by real-time PCR, LightCycler (Roche Diagnostics, Germany) and MiniOpticon (Bio-Rad, USA) equipment. Primer sequences are included in Table S5 in publication A, on page 264 in publication B, and in Table S1 in publication C. Gene expression analysis in publication A was performed by O. Horakova, in publication B by D. Medrikova, and in publication C by P. Zouhar.

4.7 Western Blot Analysis

In publication A, O. Horakova performed western blot analysis of PDK4. Tissue lysates from frozen muscle samples were separated on 10% sodium dodecylsuphate-polyacrylamide gel electrophoresis. Primary rabbit antibody against PDK4 (1:200, Abgent, USA) and secondary antibody conjugated to IRDye 800CW (Li-COR, USA) were used for detection.

In publication C, P. Zouhar performed western blot analysis of UCP1 in BAT. Membranous fractions were separated on 10% polyacrylamide gel electrophoresis. Primary rabbit antibody against UCP1 (raised by J. Kopecky, 1:500) and secondary infrared dye-conjugated antibody (1:5000) were used for detection.

4.8 Tissue TAG Content

In publication B, fragments of tissues were digested in 0.15 ml of 3M alcoholic KOH (70^{o}C, 2h) and the concentration of glycerol in the solubilisate was assessed by Triacylglycerols Liquid (Erba-Lachema Diagnostika, Czech Republic (by D. Medrikova).

4.9 Adipose Tissue TAG Content

In publication B, the DNA content was measured fluorometrically after overnight digestion of the tissue using proteinase K (by D. Medrikova).

4.10 Light Microscopy and Immunohistochemical Analysis

Liver lipids were in publication B detected on cryosections. 8 μm sections were fixed in 10% neutral buffered formalin (Sigma-Aldrich, Switzerland) and after a wash in 50% ethanol stained with a saturated solution of Oil red O (Sigma-Aldrich, Switzerland) in 70% ethanol. After a wash in 50% ethanol, counterstaining by hematoxylin (Gill III Hematoxylin, VWR Chemicals, France) was performed and slides were mounted to aqueous mounting medium VectaMount AQ (Vector Laboratories, USA).

Generally, tissue samples of BAT, eWAT and scWAT determined for histology and immunohistochemistry were fixed for 24 hours in 10% neutral buffered formalin (Sigma-Aldrich) and then replaced to 70% ethanol until tissue processing. Tissues were dehydrated, cleared and embedded in paraffin. 5μm thick sections were stained by hematoxylin and eosin (Gill III Hematoxylin, VWR Chemicals, France, Eosin Y in aqueous solution 0.5%, Labonord SAS, France).

Morphometric analysis in publication B (by Z. M. Jilkova, K Bardova), C and E on hematoxylin and eosin stained slides were performed using thresholding instrument in Imaging Software NIS-Elements AR3.0 (Laboratory Imaging, Czech Republic). The morphometry data are based on measurements of ~ 800 cells taken randomly from two to three different sections per animal.

Immunohistochemical staining was generally performed as follows, with modifications needed for specific antibodies mentioned bellow. After deparafination and hydratation, endogenous peroxidase activity was blocked by incubation with 1% H_2O_2 in methanol. After PBS wash (2 x 15min), a non-specific binding was prevented by incubation with solution of specific serum 1:50 in PBS. Primary antibody was applied overnight. The next day, after a PBS wash (2 x 15min), secondary antibody in a dilution 1:200 in PBS was applied for 1 hour. After PBS wash (2 x 15min), Vectastain ABC kit (Vector Laboratories, USA) was applied for 1 hour. After PBS wash (2 x 15min), incubation with SIGMA*FAST* 3,3´- diaminobenzidine (Sigma-Aldrich, Switzerland) diluted in H_2O was used for visualization of immunohistochemical staining. Slides were washed by H_2O and

counterstained in hematoxylin (Gill III Hematoxylin, VWR Chemicals, France). Slides were embedded after dehydration in hardening mounting medium Eukitt (Sigma-Aldrich, Switzerland). For each treatment, a positive control with known positivity for specific antibody and a negative control with omitted primary antibody were included. Digital images were captured using an Olympus AX70 light microscope and a DP 70 camera (Olympus, Japan).

In publication B, activated macrophages were detected in eWAT (by ZM Jilkova) using MAC-2/galectin antibody (Cedarlane Laboratories, USA). In this protocol, Normal Horse Serum (Vector Laboratories, USA), primary antibody in a concentration 1:3000 and Horse Anti-mouse IgG biotinylated secondary antibody (Vector Laboratories, USA) were used. Quantitative morphology on MAC2/galectin positive CLS vs. all adipocytes was performed. Data are expressed in % and based on 8 microphotos per sample taken in 200x magnification.

In publication C, UCP1 positive brite cells were detected in scWAT using UCP1 antibody raised in rabbit against recombinant UCP1 by P. Flachs. In this protocol, an antigen retrieval step was performed after deparafination using Citrate buffer, pH6, 2x15min in 95^{o}C. We used Goat Serum in 1:10 dilution (Vector Laboratories, USA), primary antibody in a concentration 1:4000 and anti-rabbit IgG biotinylated secondary antibody (Vector Laboratories, USA). Quantitative morphology on UCP1 positive multilocular cells vs. all adipocytes was performed and data were expressed in %. Data are based on 8 microphotos per sample taken in 200x magnification.

In publication E, immunohistochemistry for ATGL (Cell Signaling, USA) was performed according to general protocol. Antigen retrieval step was performed after hydratation in DakoCytomation Target retrieval Solution (Dako, USA). Normal goat serum, anti-mouse primary antibody made in rabbit (Cell Signaling, USA) in a concentration 1:800 and anti-rabbit IgG biotinylated secondary antibody (see above) were used. Immunostaining for diacylglycerol acyltransferase 1 (DGAT1) was performed according to general protocol. Antigen retrieval step was performed after hydratation in DakoCytomation Target retrieval Solution (Dako, USA). Normal horse serum, primary anti-mouse and human antibody made in goat (Abcam, USA) in a concentration 1:1000 and anti-goat IgG biotinylated secondary antibody (see above) were used.

4.11 Indirect Calorimetry

Indirect calorimetry was performed in a system INCA Somedic (Somedic, Sweden). The system allows for 8 individually caged mice to be monitored simultaneously (Eurostandard type II mouse plastic cages, 6000 ml, Techniplast, Italy). The cages are placed in sealed measuring chambers equipped with thermostatically controlled heat exchangers. Measurements were performed under a constant airflow rate (1000 ml/min). Oxygen consumption VO_2 and carbon dioxide production VCO_2 were recorded every 2 min. Calibration of oxygen sensors was performed before each experiment. To assess fuel partitioning, RQ was calculated (RQ= VCO_2/ VO_2). Energy expenditure (EE, cal) eas calculated using the equation 3,9* VO_2 (ml) + 1,1* VCO_2 (ml).

To compare subtle differences between groups, the percent cumulative frequency (PRCF) curves were calculated in publication A and C, based on RQ values pooled from all animals in a group.

4.12 Statistical Analysis

All values are presented as means±SE. Comparisons were judged to be significant at $p<0.05$. In publication A, ANOVA was used for analysis of results. Correlation matrices were computed using MS Excel. Gene array data were processed with MetaCore Pathway analysis software (GeneGo, USA). PLS-DA was performed using Umetrics SIMCA-P+12 statistical software (Umetrics

AB, Sweden). The PRCF curves in publication A were analyzed using nonlinear regression using SigmaPlot (Systat Software, USA). In publication B data were analyzed using two-way ANOVA in SigmaStat (SSI, USA) statistical software. Some data were evaluated by repeated measures ANOVA. In publication C, one-way ANOVA with a Holm-Sidak correction in SigmaPlot 10 software (Systat Software, USA) was used for data evaluation. In publication D and E, two-way and three-way ANOVA with post-hoc Holm-Sidak method were employed using SigmaStat statistical software (SSI, USA). Heterogeneous data were log-transformed.

5 Results

5.1 Publication A

Horakova O, Medrikova D, van Schothorst EM, Bunschoten A, Flachs P, Kus V, Kuda O, **Bardova K**, Janovska P, Hensler M, Rossmeisl M, Wang-Sattler R, Prehn C, Adamski J, Illig T, Keijer J, Kopecky J. *Preservation of metabolic flexibility in skeletal muscle by a combined use of n-3 PUFA and rosiglitazone in dietary obese mice.*

The aim of this study was to evaluate influence of *n-3* long chain fatty acids (*n-3* LC-PUFA) and rosiglitazone, a drug from thiazolidinedione group, and their combination on metabolic flexibility in dietary obese mice, both at a whole-body and cellular level.

We compared mice fed either STD diet, or cHF diet or diets based on cHF combined with *n-3* LC-PUFA concentrate, rosiglitazone, or combined both treatments. The intervention lasted 8 weeks. During this time, only combined intervention prevented induction of diet-induced obesity (Table 5-1-1).

Assessment of metabolic flexibility by indirect calorimetry included diet-switch protocol; mice had since the start of the measurement at 6:00 p.m. *ad libitum* access to water and their respective diets (for experimental setup see Fig. 5-1-1). At 8:00 a.m. the following morning, the diets were removed and animals fasted till 6:00 p.m.. At 6:00 p.m. mice were offered STD diet and the measurement continued for another 20 hours.

Overall parameters from INCA are shown in Table 5-1-2. INCA data were separately evaluated in distinctive time periods, e.g. on original diets (0:00 p.m. to 8:00 a.m.), during fasting (9:00 a.m. to 5:00 p.m.) and re-feeding STD diet (0:00 p.m. to 8:00 a.m.). *V*O2 as an approximate marker of energy expenditure was significantly lower during fasting period in combined cHF+F+ROSI group. This relative decline may mirror lower body weight of measured animals, as compared to other cHF-based experimental groups.

RQ switch between fasting and re-feeding carbohydrate-rich STD diet mirror metabolic flexibility to carbohydrates at a whole-body level. ΔRQ of average values was significantly higher

in combined cHF+F+ROSI group, cHF+F group displayed lower increase in RQ, and cHF and cHF+ROSI mice increased RQ in response to diet challenge only indistinctively.

RQ curves from STD re-feeding period (Fig. 5-1-2) reflected RQ increase of average values after diet delivery. This increase peaked after midnight with a slow decline after the start of light period at 6:00 a.m.. As was already mentioned, mice from combined cHF+F+ROSI group were able to switch more efficiently onto carbohydrates than other groups (Fig. 5-1-2 B) and it was not accompanied by a relative difference in $\dot{V}O_2$ between groups as a measure of energy expenditure (Fig. 5-1-2 A). When expressed as PRCF curves of all RQ values measured within a given period, cHF+F+ROSI group displayed highest metabolic flexibility, e.g. highest difference between fasted and STD re-fed values (Fig. 5-1-2 C).

Another approach to measure metabolic flexibility represents diet switch protocol employed before dissection at week 8 of the experiment. Mice were either killed by cervical dislocation when allowed free access to cHF-based diets (n=8), or after a period of fasting (8:00 a.m. and 6:00 p.m.) and re-feeding STD diet (6:00 p.m. and 8:00 a.m.) (n=10). Various parameters were evaluated in plasma samples taken at 7:00 a.m. either before fasting period (e.g. on respective cHF-based diets) or before dissection (re-fed STD diet).

In plasma samples taken after free access to cHF-based diets, TAG levels were the lowest in cHF+F+ROSI group, and NEFA levels decreased significantly in both cHF+F and cHF+F+ROSI groups. Insulin in cHF+F+ROSI group significantly decreased almost to a STD group levels.

After re-feeding STD diet, the hypolipidemic effect of *n-3* LC-PUFA diminished and insulin, as well as glucose, levels did not display any differences between groups, as were visible in measurement in cHF-based diets. β-hydroxybutyrate levels were the highest in cHF and the lowest in the cHF+F+ROSI group.

Metabolic flexibility differences observed at a whole-body level may correspond to metabolic flexibility on a cellular level. We explored this topic by targetted metabolomic analysis in the skeletal muscle cells from mice re-fed STD diet. We generated heatmaps of the correlation matrices of all pairwise correlations of muscle acylcarnitines (Fig. 5-1-3). As associations between acylcarnitine levels show complete β-oxidation of fatty acids and acetylcarnitine (C2) can be used as a marker of acetyl-CoA levels and pripionyl-L-carnitine (C3 and isovalerylcarnitine (C5) are primarily derived from catabolism of branched-chain amino acids, we were able to show that *n-3*

LC-PUFA improved efficiency of β-oxidation, while rosiglitazone had negligible effect. cHF+F+ROSI group also exhibited regulation of C3 and C5 metabolism. *n-3* LC-PUFA probably ameliorate lipid-induced mitochondrial stress and *n-3* LC-PUFA in combination with rosiglitazone modulate branched-chain amino acid metabolism.

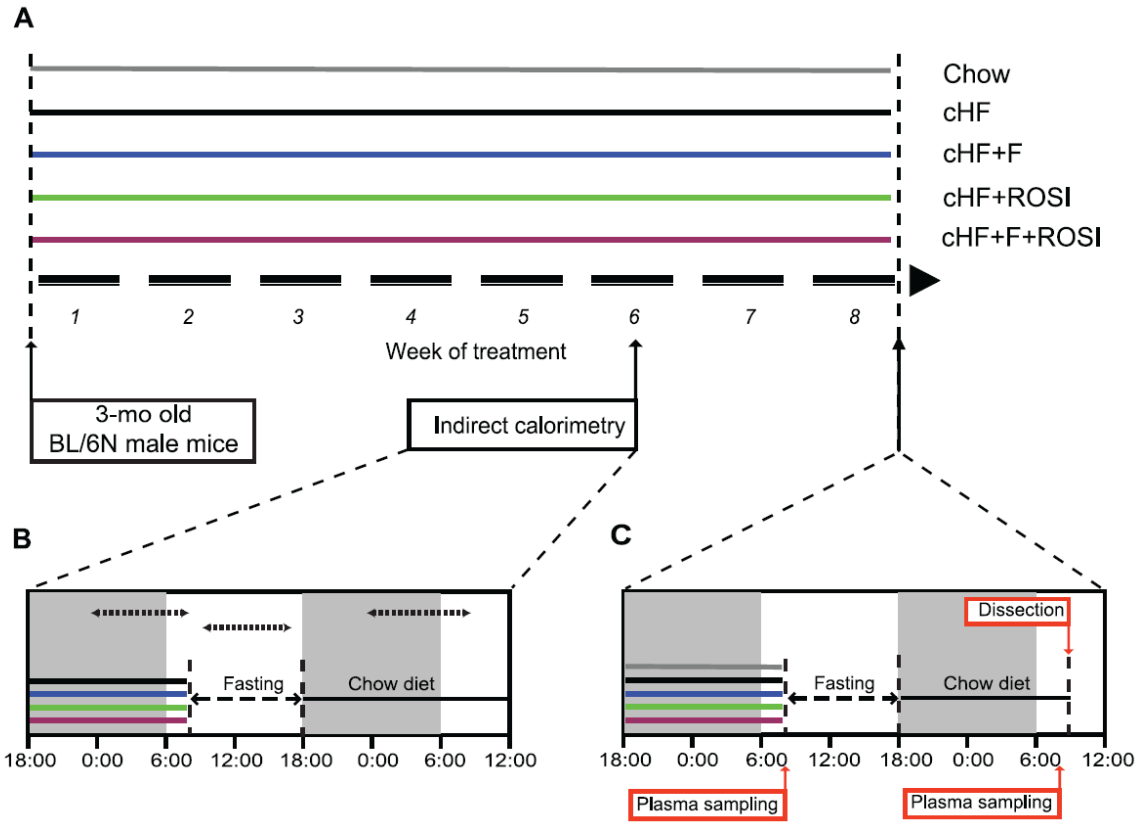

Fig. 5-1-1: *Overview on experimental setup (**A**): From 3 months of age, mice were fed STD or cHF, cHF+F, cHF+ROSI or cHF+F+ROSI diets. During week 6 of the experiment, INCA was performed using fasted/re-fed transition (**B**). At week 8, mice were dissected either without any manipulation or in the re-fed STD diet state (**C**). Dotted arrow lines, periods of data collection for calculation of the mean values of VO_2, RQ and PRCF.*

	Chow	cHF	cHF+F	cHF+ROSI	cHF+F+ROSI
Body weight (g)					
Initial	24.7±0.8	25.9±0.5	26.2±0.5	25.1±0.3	25.5±0.4
Final	31.4±1.0	37.6±1.1[f]	34.8±1.1	37.4±1.2[f]	32.3±0.8[a,c]
Body weight gain	5.7±0.5	11.7±1.3[f]	8.6±1.0	12.2±1.1[f]	6.8±0.9[a,c]
Plasma parameters					
cHF-based diets					
Triglycerides (mmol/l)	0.70±0.05	0.90±0.11	0.55±0.06	0.55±0.04[f]	0.46±0.03[a,f]
NEFA (mmol/l)	0.56±0.06	0.48±0.08	0.30±0.03[f]	0.44±0.05	0.33±0.05[f]
Glucose (mmol/l)	15.1±0.6	14.6±0.4	14.1±0.3	14.6±0.6	14.1±0.4
Insulin (nmol/l)	0.13±0.01	0.38±0.07[f]	0.24±0.03	0.30±0.03	0.19±0.05[a]
Re-fed Chow					
Triglycerides (mmol/l)	0.69±0.13	0.84±0.17	0.63±0.06	0.47±0.06	0.56±0.10
NEFA (mmol/l)	0.39±0.11	0.33±0.03	0.46±0.06	0.35±0.04	0.27±0.07
Glucose (mmol/l)	18.3±1.11	15.5±1.1	13.4±0.8[f]	16.2±0.7	15.2±0.5[f]
Insulin (nmol/l)	0.11±0.02	0.15±0.02	0.12±0.03	0.16±0.03	0.09±0.01
β-HB (μmol/l)	46.0±7.5	95.4±18.1[f]	68.1±6.9[f]	94.3±11.1[f]	35.2±6.4[a,c]
n	6	8–10	8–10	8–10	8–10

Table 5-1-1: *Growth characteristics and plasma parameters: [a] significantly different from cHF; [b] significantly different from cHF+F; [c] significantly different from cHF+ROSI; [d] significantly different from cHF+F+ROSI (ANOVA); [f] significantly different form STD (t-test).*

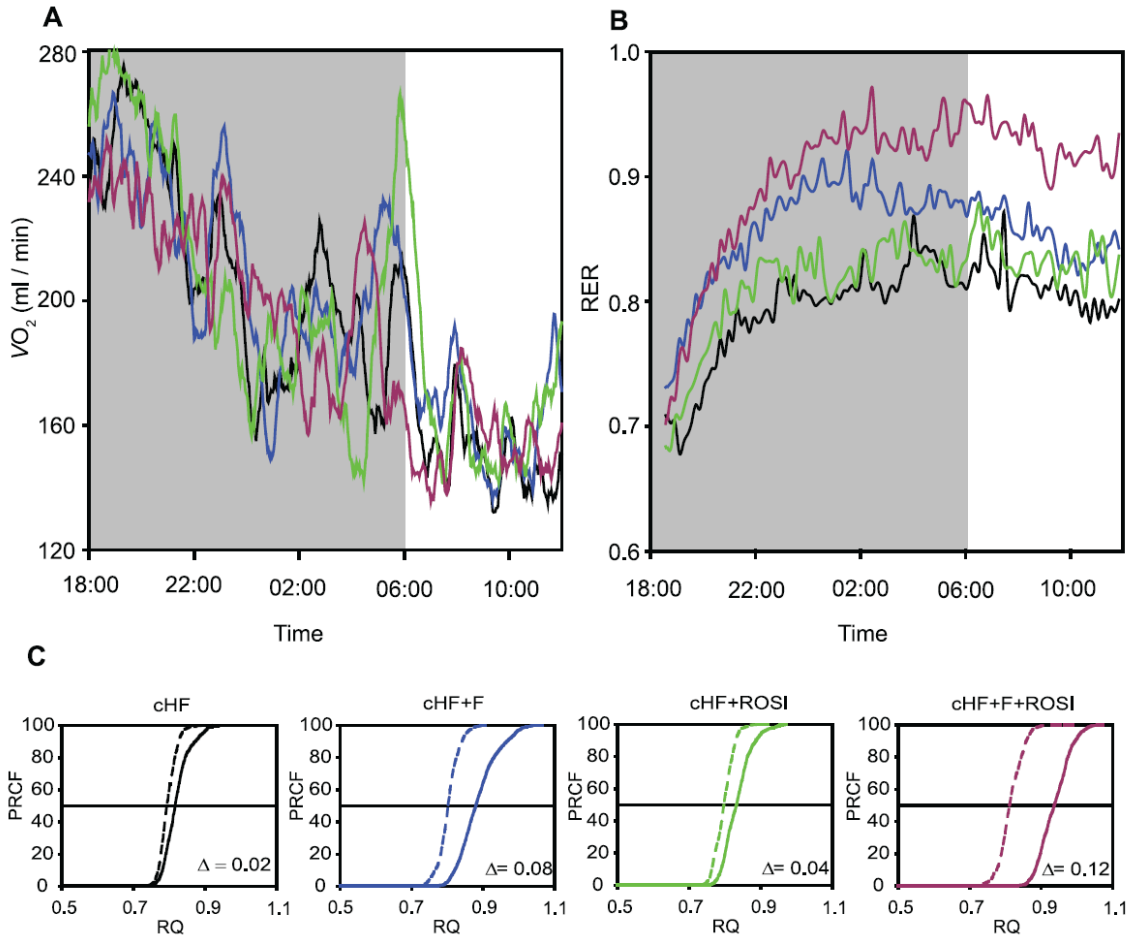

Fig. 5-1-2: *On mice randomly chosen from each dietary group INCA was performed using the diet-switch protocol. Since the start of the measurement at 6:00 p.m. mice had ad libitum access to water and cHF-based diets. At 8:00 a.m. the following morning, the diets were removed and the animals fasted for 10 hours, until 6:00 p.m.. At the beginning of the second dark phase of the measurement, mice were offered STD diet and the measurement continued for another 20 hours. (**A**) oxygen consumption and (**B**) RQ values during re-feeding STD diet, (**C**) PRCF curves of RQ values during the period of fasting (broken lines, data collected between 9:00 a.m. and 5:00 p.m.) and re-feeding STD diet (solid lines, data collected between 0:00 p.m. and 8:00 a.m.). Each curve represents the data pooled from 5 mice within a given group.*

	cHF	cHF+F	cHF+ROSI	cHF+F+ROSI
VO_2 (ml/min)				
Original diets	2.00±0.04	1.99±0.09	1.97±0.04	1.97±0.06
Fasting	1.83±0.06	1.83±0.03	1.94±0.08	1.69±0.04[b]
Re-feeding Chow	1.85±0.06	1.90±0.06	1.86±0.06	1.81±0.04
RER				
Original diets	0.84±0.01	0.84±0.01	0.83±0.01	0.87±0.01
Fasting	0.80±0.01	0.80±0.01	0.80±0.01	0.81±0.01
Re-feeding Chow	0.85±0.03	0.89±0.02	0.84±0.02	0.94±0.02[ab]
ΔRER	0.05±0.02	0.08±0.01	0.04±0.01	0.12±0.01[ab]

Table 5-1-2: *INCA outcomes: VO2 and RQ values from time periods: original diets (0:00 p.m. to 8:00 a.m.), fasting (9:00 a.m. to 5:00 p.m.) and re-feeding STD diet (0:00 p.m. to 8:00 a.m.). For experimental setup see also Fig. 5-1-2.* [a] *significantly different from cHF diet,* [b] *significantly different from cHF+ROSI (ANOVA).*

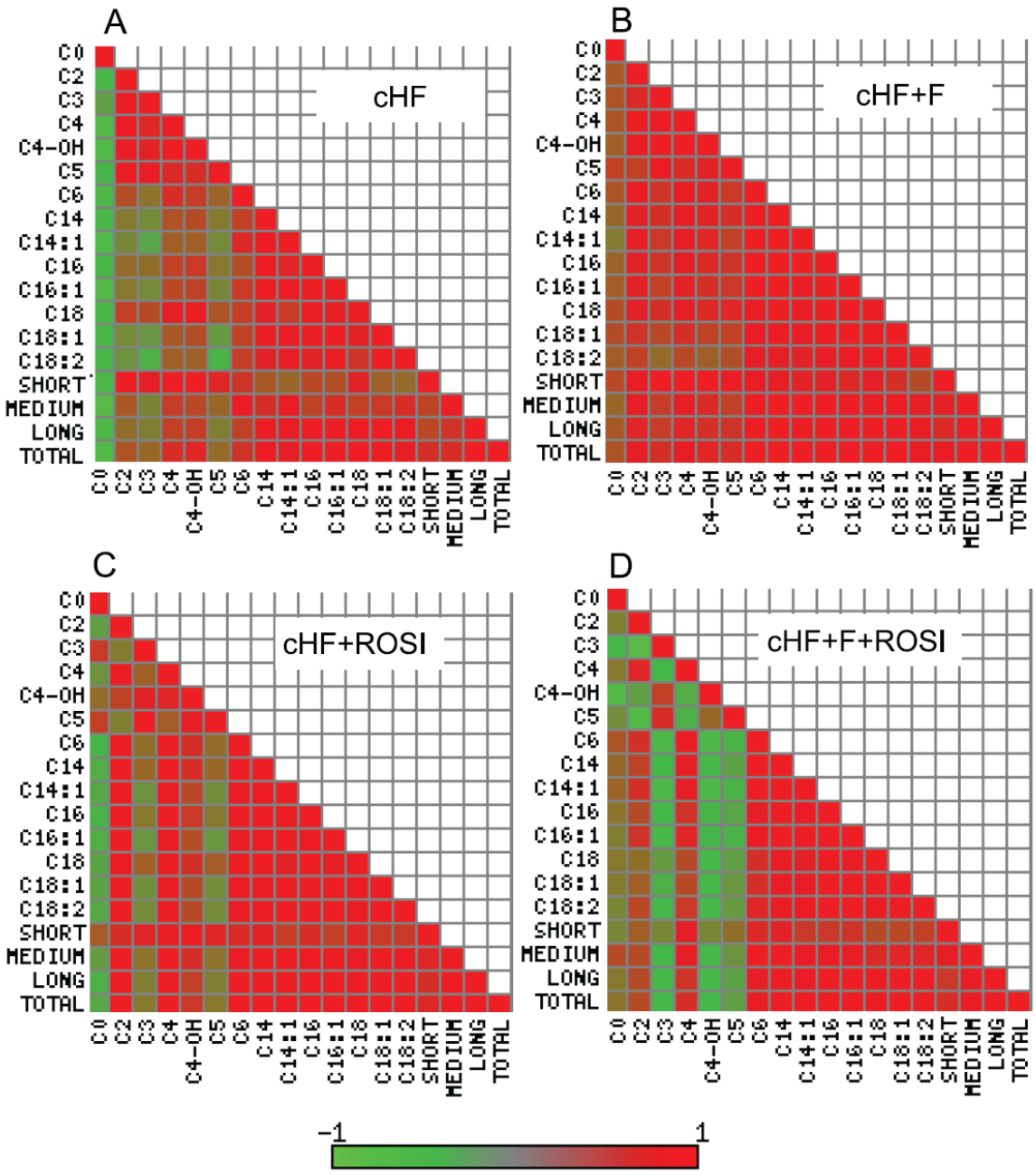

Fig. 5-1-3: *Heatmap analysis of pairwise correlation matrix of acylcarnitine levels in the muscle. Metabolites from mice fed cHF (**A**), cHF+F (**B**), cHF+ROSI (**C**), cHF+F+ROSI (**D**) diets. Each square represents Pearson correlation coefficient between the metabolite in the row and that in the column. The strength of correlation (Red, positive; green, negative) is expressed as a color intensity. SHORT sum of C3-C7 acylcarnitines; MEDIUM, sum of C8-C13 acylcarnitines; LONG, sum of C14-C18 acylcarnitines; Total, sum of all acylcarnitines.*

To sum up, combination of n-3 LC-PUFA and rosiglitazone is able to preserve metabolic flexibility on a whole-body level, as defined by using INCA. Targetted metabolomics from skeletal muscle extracts support this statement.

5.2 Publication B

Medrikova D, Jilkova ZM, **Bardova K**, Janovska P, Rossmeisl M, Kopecky J. *Sex differences during the course of diet-induced obesity in mice: adipose tissue expandability and glycemic control.*

The aim of this study to evaluate metabolic flexibility in both genders of C57BL/6N mice challenged by high-fat diet.

Growth characteristics

All experiments were performed using F1 generation of C57BL/6N mice imported from Charles River Laboratories. Male and female mice were followed since 4 weeks of age, when they were weaned onto STD or cHF (addressed as ST and HF in the original article) diet (week 0). 10 mice of each gender and diet group were killed at week 15 and 35, respectively.

Female mice displayed lower body weight at a time of weaning and this phenomenon persisted on mice fed STD diet up till 35 weeks (Fig. 4-2-1). In mice fed cHF diet body weight curves increased steeply between weeks 0 and 20, as compared to STD diet-fed mice. In cHF fed animals, up till the week 20, there was a significant difference between male and female mice, with female mice having lower body weight. Since week 20, the body weight gain was more rapid in female mice, so that at the end of this study at week 35 female mice body weights tended to be even higher than that of male mice.

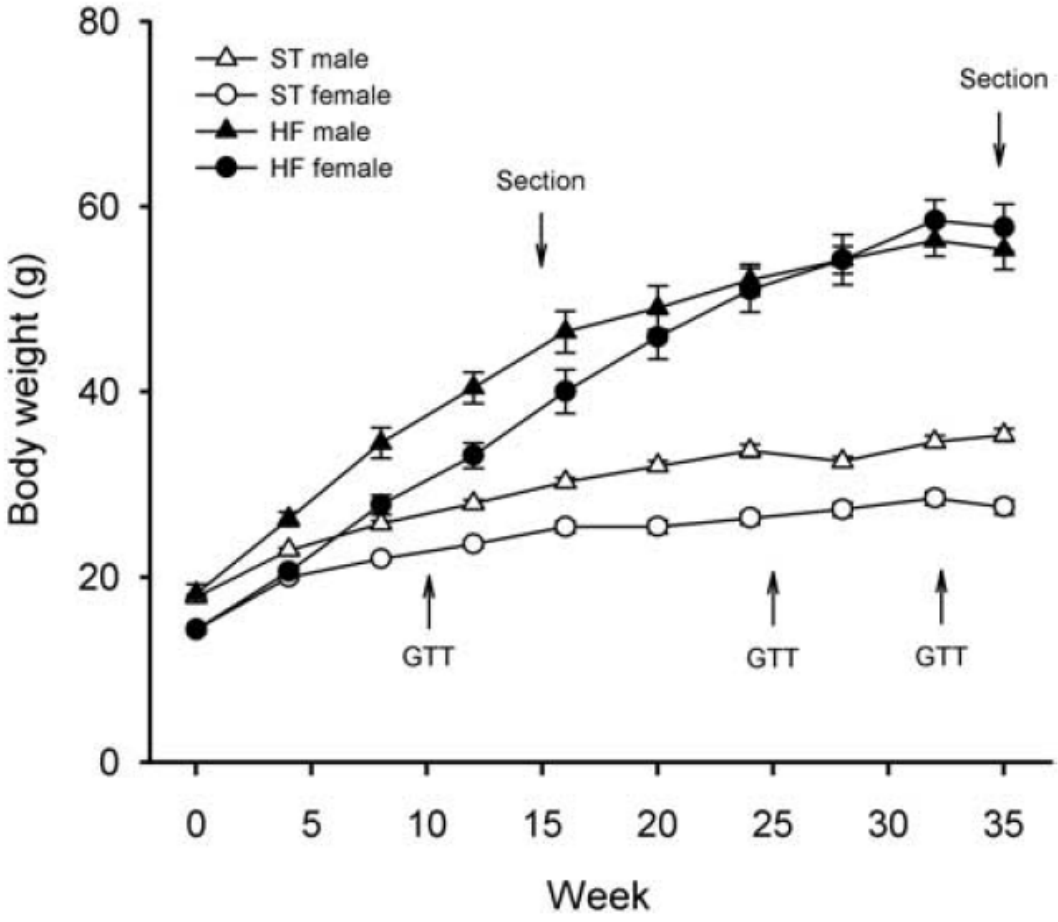

Fig. 4-2-1: *Growth curves of male and female mice of C57BL/6N mice weaned at 4 weeks of age onto STD or cHF diet (week 0). n=20 in each gender and dietary group between week 0 and 15. At week 15, n=10 mice from each group were killed; after week 15 n=10 mice remained per group. Data are shown as means±SEM. Intraperitoneal glucose tolerance tests were performed at week 10, 25, and 33.*

Food consumption (Table 4-2-1) differed in the period of week 4-14 between both sexes on STD diet, while it was not significantly different on a cHF diet. This difference did not persist between weeks 17 and 30, when there were no differences between genders on both diet groups. On the other hand, in both time periods, there was a significant difference between food intake of female mice on a STD and cHF diet.

Weights of subcutaneous and gonadal WAT (Table 4-2-1) were significantly higher between STD and cHF fed animals of both sexes both at week 15 and 35, and this relationship persisted

even after normalization per body weight. At week 35, weights of both adipose depots differed significantly between sexes on cHF diet, with female mice having more fat tissue.

Liver weight (Table 4-2-1) increased significantly after high-fat feeding as compared to controls, and male mice on cHF diet displayed heavier liver than female mice. This phenomenon was statistically significant at both time points. Most of these differences remained valid even after normalization per body weight and were mirrored in higher accumulation of liver TAG in cHF-fed animals than in their STD-fed controls. The amount of liver TAG induced by cHF diet was gender dependent, with male mice displaying higher liver lipids than female mice on cHF diet. This observation was confirmed at a histological level by staining of liver lipids by Oil red O (Fig 4-2-2).

Table 1 Growth characteristics, adiposity, and liver weight and TAG content

	ST		HF	
	Male	*Female*	*Male*	*Female*
BW (g)				
Week 0	17.8 ± 0.2	14.3 ± 0.3[a]	18.2 ± 1.0	14.3 ± 0.3[a]
Week 15	28.5 ± 0.4	24.1 ± 0.4[a]	43.6 ± 1.9[b]	36.4 ± 1.7[a,b]
Week 35	35.3 ± 0.7	27.6 ± 0.8[a]	55.4 ± 2.2[b]	57.7 ± 2.6[b]
BWG (g)				
Week 15	11.6 ± 0.6	10.6 ± 0.5	27.2 ± 1.4[b]	23.1 ± 2.3[a,b]
Week 35	17.5 ± 0.6	13.2 ± 0.6	37.2 ± 1.8[b]	43.4 ± 2.4[b]
FC (kJ per day)				
Week 4–14	66.3 ± 0.7	56.2 ± 1.4[a]	69.5 ± 2.4	68.5 ± 3.6[b]
Week 17–30	64.8 ± 1.1	61.1 ± 2.3	66.7 ± 4.1	70.6 ± 2.0[b]
gWAT (mg)				
Week 15	484 ± 31	364 ± 26	1881 ± 158[b]	2147 ± 301[b]
Week 35	1032 ± 107	711 ± 97	1565 ± 95	5989 ± 470[a,b]
gWAT (% of BW)				
Week 15	1.8 ± 0.1	1.62 ± 0.1	4.8 ± 0.4[b]	5.87 ± 0.5[a,b]
Week 35	2.9 ± 0.3	2.5 ± 0.3	2.8 ± 02	10.2 ± 0.5[a,b]
scWAT (mg)				
Week 15	217 ± 14	195 ± 11	797 ± 95[b]	873 ± 117[b]
Week 35	312 ± 35	271 ± 24	1297 ± 113[b]	1590 ± 133[a,b]
scWAT (% of BW)				
Week 15	0.8 ± 0.0	0.8 ± 0.1	2.0 ± 0.2[b]	2.4 ± 0.2[b]
Week 35	0.9 ± 01	1.0 ± 0.1	2.3 ± 0.2[b]	2.7 ± 0.2[a,b]
Liver (mg)				
Week 15	1247 ± 55	1144 ± 29	1606 ± 130[b]	1236 ± 56[a]
Week 35	1544 ± 51	1160 ± 56[a]	2541 ± 231[b]	1806 ± 111[a,b]
Liver (% of BW)				
Week 15	4.6 ± 0.2	4.9 ± 0.1	4.0 ± 0.1[b]	3.6 ± 0.1[a,b]
Week 35	4.4 ± 0.1	4.2 ± 0.1	4.5 ± 0.3	3.1 ± 0.1[a,b]
Liver TAG (mg/g of tissue)				
Week 15	28 ± 1	32 ± 3	109 ± 20[b]	72 ± 6[a,b]
Week 35	34 ± 3	38 ± 3	197 ± 27[b]	121 ± 8[a,b]

Table 4-2-1: *Abbreviations: BW, body weight; BWG, body weight gain since week 0; FC, mean food consumption;* [a] *Significant differences between sexes within diet;* [b] *significant differences between diets within sex (ANOVA). Data are shown as means±SEM.*

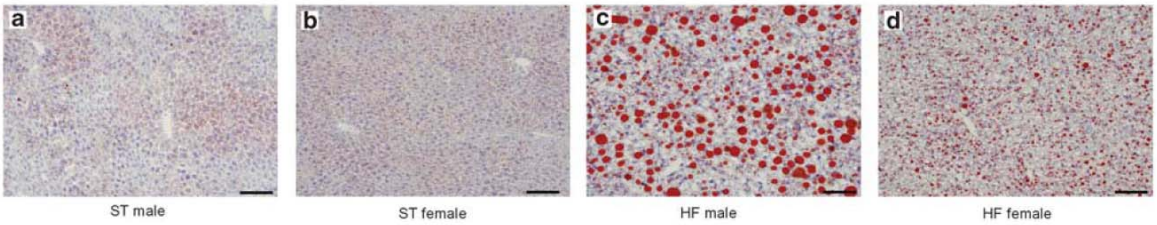

Fig 4-2-2: *Staining of liver sections. TAG are visualized in red (Oil Red O), nuclei are blue (hematoxylin). Scale bar 0.1 mm.*

Plasma markers

Plasma markers were evaluated from *ad libitum* – fed mice at dissection at week 15 and 35 of the study (Table 4-2-2). Levels of TAG in plasma were increased in male mice on cHF diet at week 15 as compared to male mice on STD diet and female mice of cHF diet. At week 35, female mice on STD diet displayed lower TAG levels than male mice of STD diet and female mice on cHF diet.

Insulin levels were higher in male mice, irrespective of the diet and the length of treatment, and its levels increased during the duration of this experiment. cHF diet feeding increased leptin levels in both genders and time points. At week 35, females on cHF diet had higher plasma leptin levels than male and a reverse relationship was observed in STD fed mice. Adiponectin (total, high, medium and low molecular weight), on the other hand, was higher in female as compared to male in both time-points and some forms were higher in STD than in cHF diet – fed animals.

Metabolic flexibility was tested in this experiment by two challenge tests – intraperitoneal GTT and fasted/re-fed transition (Fig 4-2-3).

In the fasted/re-fed protocol, mice were fasted either fasted between 8:00 a.m. and 10:00 p.m. or fasted between 8:00 a.m. and 6:00 p.m. and then were given diet ad libitum for the next 3 hours. In each mouse, blood glucose was randomly assessed in both the fasted and refed state in two subsequent days. Whereas there were not statistically significant differences in glucose plasma levels in the fasting state, there was a pronounced difference between fasting levels and in the ability to withdraw glucose from plasma mirrored in their flexibility to fasted and refed

states. Hence, female mice at week 15 displayed preserved glucose sensitivity at both diets, with mice on STD diet more sensitive; while male mice on cHF diet were nearly metabolically inflexible.

Intraperitoneal GTT were performed at week 10, 25, and 33 after an overnight fast with a glucose bolus of 1 mg of glucose per g of body weight. The fact, that male mice on cHF diet are metabolically inflexible, was repeated at a level of fasting plasma glucose during IPGTT setup at week 25 and 33, when male mice displayed higher plasma glucose levels, irrespective of dietary intervence. Even though the two tests for metabolic flexibility used differed in the time period of fasting (14 hours during the day in the case of fasted/refed protocol and 14 hours overnight in the case of IPGTT) and in the length of diet intervention (15 weeks in the case of fasted/refed protocol and 25 and 33 weeks in the case of IPGTT), the differences in fasting plasma glucose levels remained similar. AUC of the glucose curve followed development of fasting glucose levels. During the IPGTT performed at week 33, plasma insulin levels were assessed. Both at a baseline and 30 min after glucose load the insulin levels were significantly higher in male mice, irrespective of diet intervention.

Table 2 Plasma lipids and hormones

	ST		*HF*	
	Male	*Female*	*Male*	*Female*
TAG (mmol l^{-1})				
Week 15	1.20 ± 0.12	1.01 ± 0.05	1.66 ± 0.21[a]	1.21 ± 0.14[b]
Week 35	0.97 ± 0.11	0.61 ± 0.04[b]	0.96 ± 0.03	0.92 ± 0.06[a]
NEFA (mmol l^{-1})				
Week 15	0.51 ± 0.04	0.48 ± 0.03	0.59 ± 0.06	0.62 ± 0.06
Week 35	0.40 ± 0.05	0.39 ± 0.03	0.41 ± 0.06	0.46 ± 0.03
Cholesterol (mmol l^{-1})				
Week 15	1.77 ± 0.11	1.54 ± 0.10	4.08 ± 0.30[a]	3.55 ± 0.20[a]
Week 35	1.96 ± 0.10	1.47 ± 0.06	4.78 ± 0.38[a]	4.08 ± 0.25[a,b]
Insulin (ng ml^{-1})				
Week 15	0.88 ± 0.21	0.38 ± 0.04[b]	2.71 ± 0.54[a]	1.15 ± 0.23[a,b]
Week 35	0.97 ± 0.16	0.21 ± 0.03[b]	4.68 ± 0.45[a]	2.30 ± 0.46[a,b]
Leptin (ng ml^{-1})				
Week 15	6.2 ± 0.7	8.8 ± 0.8	45.5 ± 7.6[a]	41.7 ± 8.0[a]
Week 35	17.7 ± 2.0	9.1 ± 1.7[b]	71.9 ± 4.7[a]	89.6 ± 2.8[a,b]
Adiponectin (AU)				
Week 15				
HMW	0.45 ± 0.03	0.62 ± 0.05[b]	0.33 ± 0.02[a]	0.63 ± 0.03[b]
MMW	0.46 ± 0.02	0.65 ± 0.04[b]	0.44 ± 0.02	0.60 ± 0.03[b]
LMW	0.02 ± 0.00	0.02 ± 0.00	0.01 ± 0.00	0.02 ± 0.00[b]
Total	0.94 ± 0.05	1.29 ± 0.08[b]	0.78 ± 0.03[a]	1.25 ± 0.05[b]
Week 35				
HMW	0.46 ± 0.04	0.86 ± 0.10[b]	0.40 ± 0.06	0.63 ± 0.07[a,b]
MMW	0.55 ± 0.03	0.80 ± 0.06[b]	0.50 ± 0.02	0.78 ± 0.07[b]
LMW	0.04 ± 0.01	0.03 ± 0.00	0.02 ± 0.00[a]	0.03 ± 0.00
Total	1.06 ± 0.06	1.69 ± 0.15[b]	0.92 ± 0.07	1.44 ± 0.13[b]

***Table 4-2-2**: Abbreviations: AU, arbitrary units; HMW, high-molecular-weight adiponectin; LMW, low-molecular-weight adiponectin; MMW, medium-molecular-weight adiponectin; [a] Significant differences between sexes within diet; [b] significant differences between diets within sex (ANOVA). Data are shown as means±SEM.*

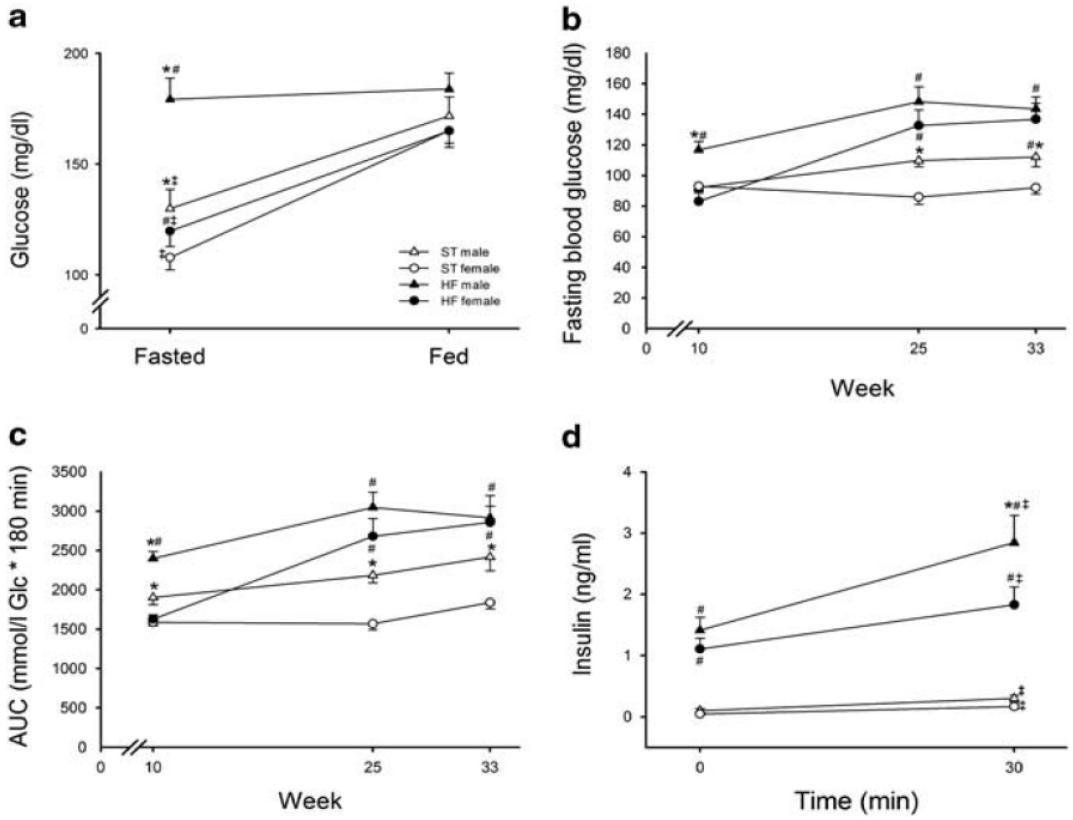

Fig 4-2-3: *Glucose homeostasis assessment: (**A**) plasma glucose in fasted and fed mice at week 15, (**B-D**) IPGTT performed at week 10, 25 and 33, (**B**) fasting blood glucose, (**C**) AUC of the glucose curve, (**D**) plasma insulin levels before and 30 min after glucose application. Data are shown as means±SEM, n=10 in each group. * Significant difference between the sexes within the same diet; # significant difference between the diets within the same sex (ANOVA); ‡ significant difference before and after the respective treatment (RM ANOVA).*

Adipose tissue morphology and inflammation

The possible connection between metabolic flexibility and adipose tissue was explored (Fig. 4-2-4). While mice on STD diet did not show higher inflammation of adipose tissue, female mice on cHF diet displayed markedly lowered level of inflammation of adipose tissue expressed as % of dying cells than male mice. This fact we were not able to clarify by the expected relationship between the adipocyte size and level of inflammation, because adipocyte area, an indirect

measure of adipocyte size, did not differ between genders on both diets at week 15 and was even higher in female mice at week 35. This pattern was clearly visible in both adipose depots explored (eWAT and scWAT) and in both time-points; nevertheless, it did not reach statistical significance in scWAT at week 15.

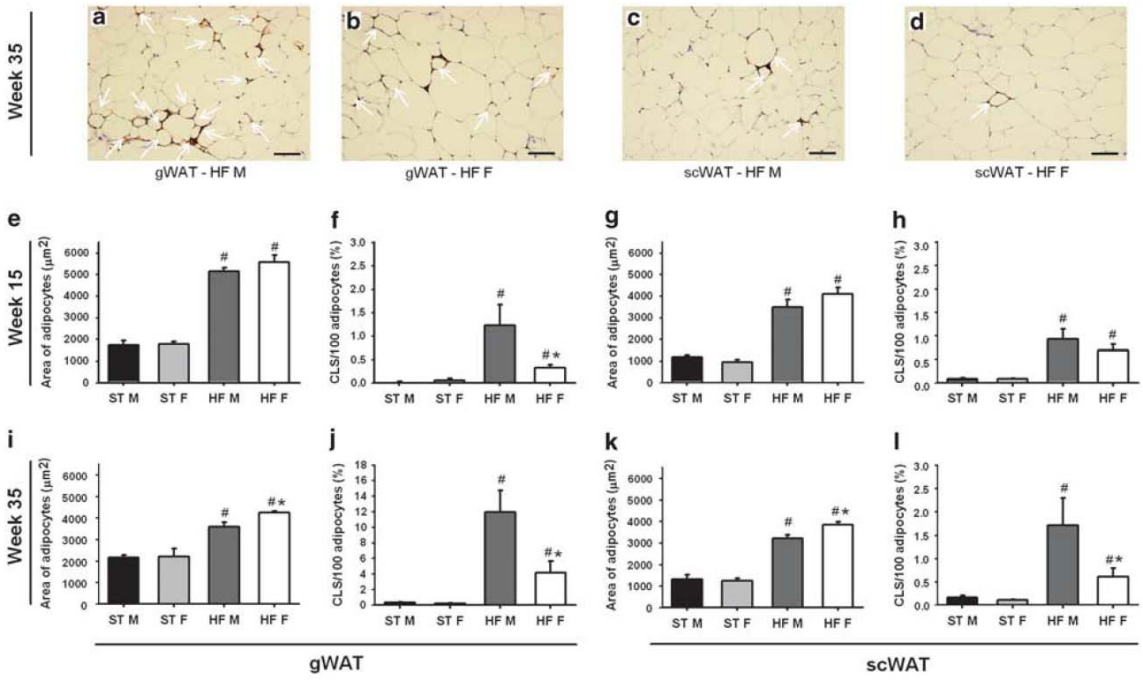

Fig. 4-2-4: *Evaluation of adipose tissue histological parameters: (**A-D**) immunodetection of MAC-2-positive macrophages aggregated in CLS in eWAT and scWAT of male (M) and female (F) mice at 35 weeks of diet intervention. Sections were counterstained with hematoxylin. Scale bar 0.1 mm. At week 15 (**E-H**) and week 35 (**I-L**), size of adipocytes was evaluated by morphometric analysis in hematoxylin-eosin stained sections of eWAT (**E** and **I**) and scWAT (**G** and **K**) in both sexes. Frequency of CLS in eWAT (**F** and **J**) and scWAT (**H** and **I**) in both sexes was evaluated. Data are shown as means±SEM (n=8 in each group). * Significant difference between the sexes within the same diet; # significant difference between the diets within the same sex (ANOVA).*

To sum up, metabolic flexibility in mice challenged by high-fat diet was tested using two independent tests. It is in females connected to adipocyte size, inflammation of adipose tissue, leptin and adiponectin levels in plasma and to insulin resistance.

5.3 Publication C

Teodoro JS, Zouhar P, Flachs P, **Bardova K**, Janovska P, Gomes AP, Duarte FV, Varela AT, Rolo AP, Palmeira CM, Kopecký J. *Enhancement of brown fat thermogenesis using chenodeoxycholic acid in mice.*

Publication C focused on the relationship between BAT and WAT metabolism and whole-body energy homeostasis using chenodeoxycholic acid (CDCA). Mice were allowed for 4 months a free access to cHF diet to develop obesity. In the 8-week reversion, 10-12 mice per group received either cHF or cHF diet supplemented with 0.5 % CDCA (0.5 % CDCA, wt/wt) or cHF diet supplemented by 1% CDCA (1% CDCA, wt/wt, Sigma-Aldrich, USA, 95% pure). In the 3-week reversion experiment, 8 mice per group were randomly assigned either to cHF diet (cHF) or to cHF diet supplemented by 1% CDCA (1% CDCA, wt/wt) or to a group that received cHF diet to the amount consumed by 1% CDCA group (PF). In some analyses, a group of mice fed STD diet since weaning was included.

Reversal of dietary obesity

We performed 2 experiments to reveal the possible effect of CDCA. In the first experiment, 8-week reversion was performed on dietary obese mice. CDCA had clear effect on body weight, and this effect was dose dependent on 0.5% and 1% group (Fig. 4-3-1 B). However, this effect may be accounted to severe decrease in caloric intake during the first two weeks of dietary intervention (Fig. 4-3-1 A), hence in a period, when the body weight lowered in a dose-dependent manner. Surprisingly, in spite of a similar caloric intake between week 3 and 8 of intervention, the body weight in CDCA groups remained on a relatively low levels till the end of the study.

To reveal the influence of transient drop in food intake during the first two weeks of dietary intervention, we performed second experiment. In a 3-week reversion we included control cHF, 1% CDCA and PF group. We aimed to follow decreased caloric intake and by comparing CDCA and PF group to distinguish observed effects to food-intake- and CDCA-caused. During a 3-week reversion, there was again a transient decrease in food intake observed (Fig. 4-3-1 C), and a consequent depression in body weight curves in both 1% CDCA and PF group (Fig. 4-3-1 D).

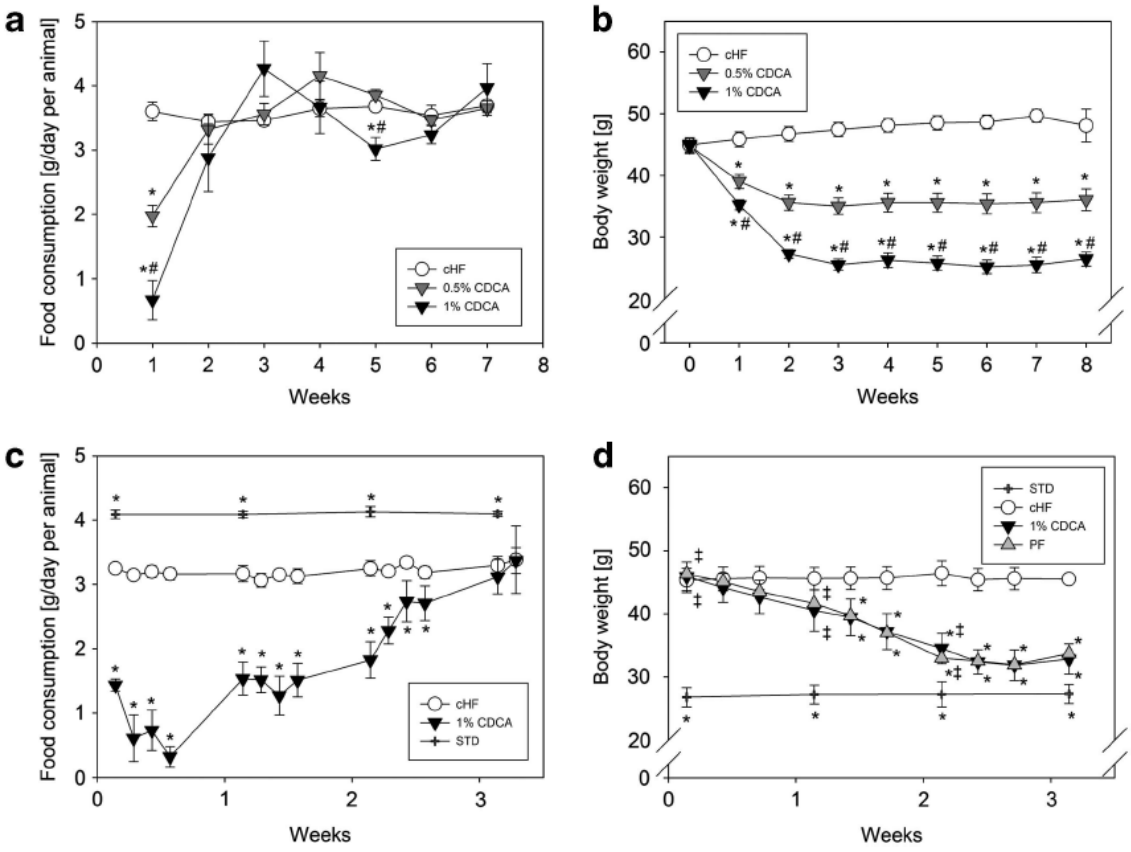

Fig 4-3-1: *Growth curves and food intake: food intake (**A**) and growth curve (**B**) during the 8-week reversion experiment (n=10-12); food intake (**C**) and growth curve (**D**) during the 3-week reversion experiment (n=8, except for STD, where n=4). Data are means±SEM. * Significantly different in comparison to the cHF group; # significantly different in comparison to the 0.5% CDCA group (only in a and b); ‡ significantly different in comparison to the STD group (only in d).*

Effects on BAT and WAT depots

Decrease in BW in 1% CDCA and PF group caused a reduction in eWAT and scWAT depot weights and this effect was not dependent on CDCA, but was rather body-weight-dependent. Morphometry of adipocytes in scWAT indicated that the differences in adiposity were reflected in adipocyte size (Fig. 4-3-3 A). Morphological assessment of BAT appearance indicated higher accumulation of lipid droplets in the case of cHF as compared to STD group (Fig. 4-3-2). Body weight reduction in both the 1% CDCA and PF group induced elimination of lipids in BAT. The reduction of body weight and adiposity published by Watanabe et al. (Watanabe, Houten et al. 2006) in a similar model using cholic acid was attributed to an induction of UCP1-mediated

thermogenesis. Hence, we explored this topic by measuring UCP1 mRNA (Fig. 4-3-2 B) and UCP1 protein content in the whole interscapular BAT (Fig. 4-3-2 C). UCP1 mRNA normalized using 18S RNA was significantly higher in 1% CDCA as compared to cHF and no such induction was visible in the case of PF group. The amount of UCP1 protein in the whole depot reflected these differences.

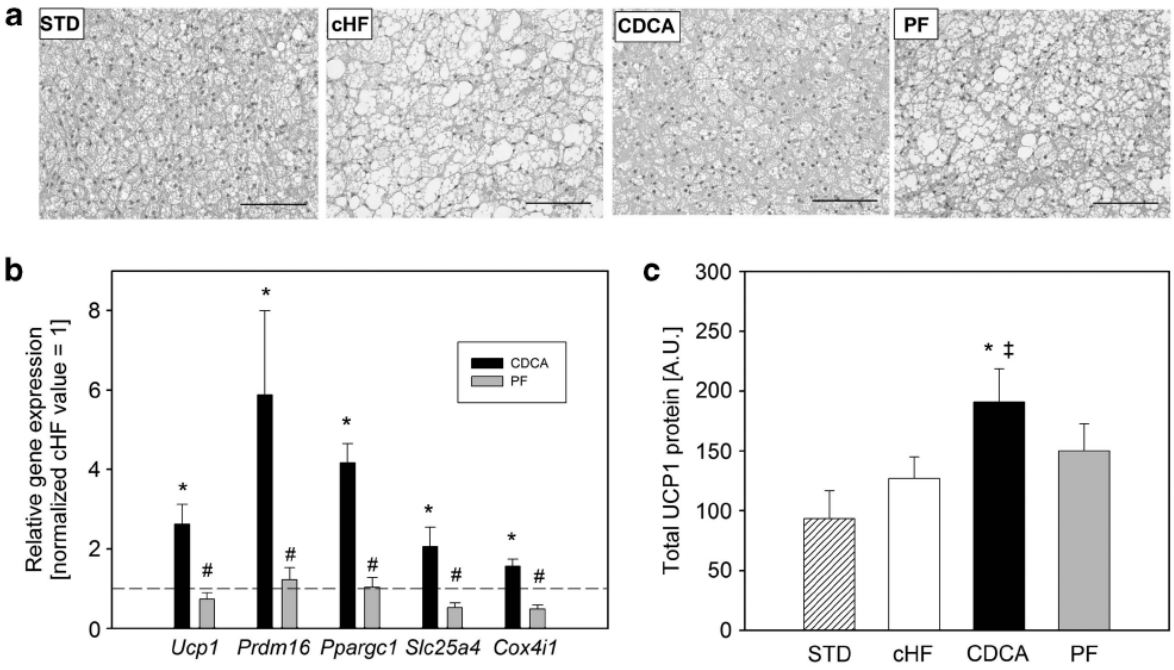

Fig. 4-3-2: *Interscapular BAT parameters in the 3-week reversion experiment: (**A**) representative images of BAT, (**B**) relative gene expression (cHF%1, dashed line); data are normalized using 18S RNA as a housekeeping gene, (**C**) content of UCP1 protein in whole interscapular BAT. Scale bar 0.1mm.* Significantly different in comparison to the STD group. Data are means±SEM.(n=8, except fro STD, where n=4).*

Together with increased BAT function, also the induction of brite cells within WAT can potentially have an impact on whole-body energy homeostasis. We immunohistochemically quantified brite cells as the proportion of UCP1-positive brite cells within the scWAT (Fig. 4-3-3 D and E). Brite cells were induced both by CDCA treatment and body weight loss in PF group; nevertheless, the induction was statistically higher in the case of 1%CDCA mice. On the other hand, the relative proportion of brite cells was so low that it cannot have any whole-body effects on energy homeostasis.

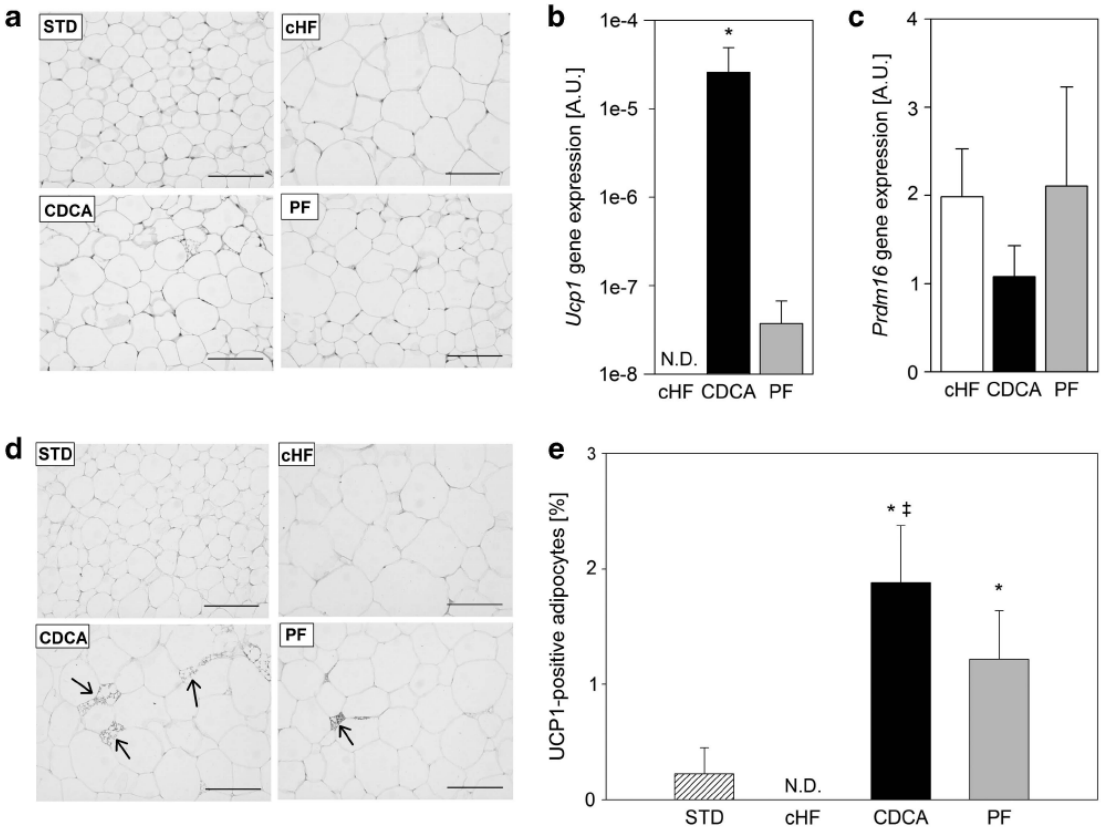

Fig. 4-3-3: *scWAT parameters in the 3-week reversion experiment: (**A**) representative images of WAT; (**B** and **C**) Ucp1 and Prdm16 gene expression; data are normalized using 18S RNA as a housekeeping gene; (**D**) representative images of immunostaining for UCP1 possitive cells are indicated by arrows; (**E**) graphical representation of the percentage of UCP1-positive cells relative to all adipocytes visualized. * Significantly different in comparison to the cHF group; ‡ significantly different in comparison to the STD group. Data are means±SEM. (n=8, except for STD, where n=4). (a and b) Scale bar 0.1 mm.*

Indirect calorimetry

Indirect calorimetry was performed during the third week of 3-week reversion experiment. All groups were measured on their respective diets and dietary set-ups during 24h INCA. Time-course of RQ values (Fig. 4-3-4 B) reflects indistinctive circadian rhythm of cHF group with a poor metabolic flexibility. 1%CDCA mice in addition to poor metabolic flexibility displayed lower RQ values during the night phase of the measurement, indicating preferential lipid oxidation even in the presence of consumed carbohydrates. RQ data from PF group, on the other hand, reflected preserved metabolic flexibility, that means higher difference between the highest and lowest RQ

values. However, PF group was given diet in the morning and mice with restricted accessibility to food consumed most of their food immediately after delivery, that means during the day, as compared to normal circadian rhythm of murine feeding, when diet is consumed during the night. Thus, RQ values reflecting consumption and oxidation of dietary carbohydrates peaked during the day and displayed lowest values during the night, when fasting mice had to rely up to lipid oxidation. Metabolic flexibility was further assessed by PRCF evaluation of RQ values (Fig. 4-3-4 C). The slopes of PRCF curves were not different in dietary groups, indicating similar metabolic flexibility of all groups. cHF mice displayed the highest and CDCA the lowest RQ values during the 24h-measurement, indicating differences in reliance on lipid vs. carbohydrate metabolism. This was further quantified as mean RQ values during 24h measurement (Fig. 4-3-4 F) and as EC_{50} of PRCF curves (Fig. 4-3-4 G), as a more sensitive approach to detect differences between RQ distribution. Neither of these approaches were able to detect differences between 1% CDCA and PF groups.

Time-course of energy expenditure indicated a clear pattern of increased EE immediatelly after the start of the measurement and during the night. When assessed as mean values either with (Fig. 4-3-4 E) or without (Fig. 4-3-4 D) normalization per body weight, there were no differences between 1% CDCA and PF groups, that would evidence metabolic effect of CDCA on a whole-body metabolism.

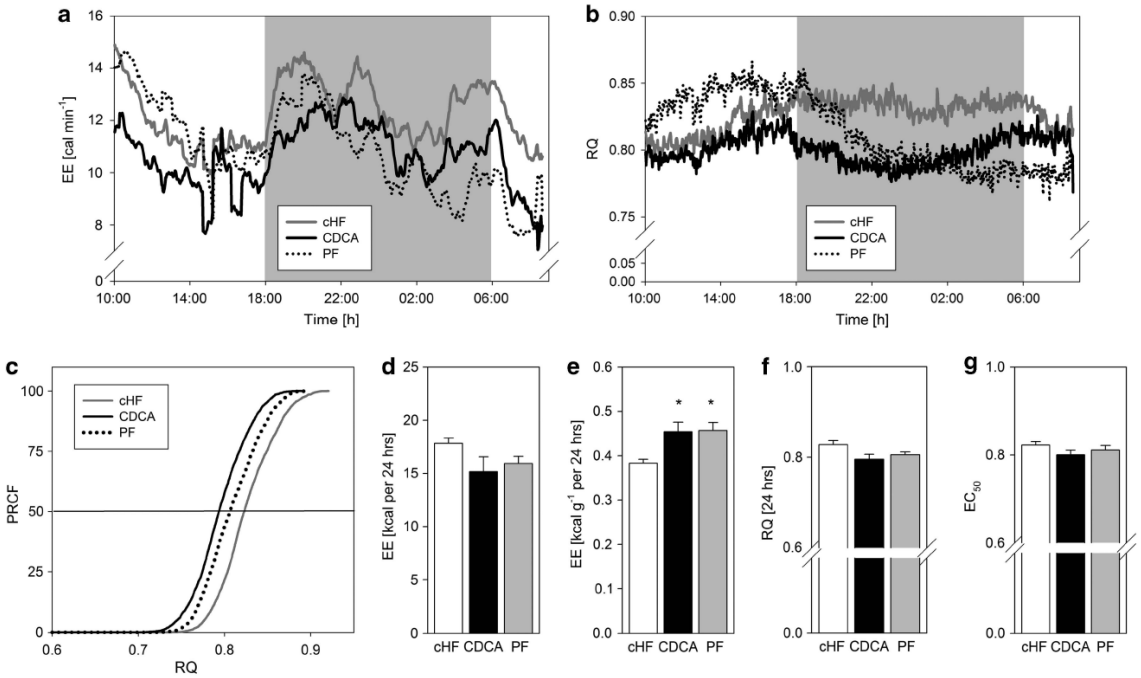

Fig. 4-3-4: *INCA measurement between day 15 and 17 of the 3-week reversion experiment: (**A**) time-course of the EE measurements; (**B**) time-course of the RQ measurements; grey area in a and b represents the dark phase of the day; (**C**) plot of PRCF of RQ values during 24h period; (**D**) total EE per mouse for 24h; (**E**) total EE normalized per body weight; (**F**) mean 24h RQ; (**G**) 50th percentile value of PRCF derived from (**C**). * Significantly different in comparison to the cHF group.*

To sum up, CDCA causes changes in whole-body metabolism which are mostly affected by lowered food intake, as was revealed by pair-feeding experiment. Energy homeostasis assessed by INCA was not influenced by CDCA as compared to pair-fed group. The detected differences in induction of brown adipocyte´s abundance and function probably do not have major impact on whole-body metabolism.

5.4 Publication D

Bardova K, Horakova O, Janovska P, Hansikova J, Kus V, van Schothorst EM, Hoevenaars F, Uil M, Hensler M, Keijer J, Kopecky J. *Early differences in metabolic flexibility between obesity-resistant and obesity-prone mice.*

The aim of tis study was to introduce several tests for metabolic flexibility assessment and by using them to compare metabolic flexibility of A/J and C57BL/6J mice of both genders.

Experiment 1: comparison of IPGTT and OGTT at a dose 1 mg of glucose per g of body weight

An intraperitoneal GTT on mice pups one day after weaning using a dose of 1 mg of glucose per g of body weight was performed. As illustrated in Fig. 4-4-1 A, C57BL/6J mice increased their blood glucose levels more than A/J mice after glucose load. To avoid the confounding effect of different baseline glucose levels, incremental AUC was evaluated (Fig. 4-4-1 B). Using two-way ANOVA, only the effect of strain on incremental AUC was statistically significant (p=0,002). During a GTT, mice are under significant stress from fasting, handling and glucose delivery. The solely effect of stress was evaluated in a separate test where saline solution was injected in the same amount as during GTT. Blood glucose levels after injection increased only slightly and this effect was negligible when an incremental AUC was calculated (data not shown).

Next an oral GTT on mice one day after weaning using the same dose of 1 mg of glucose per g of body weight administered by an oral gavage was performed. C57BL/6J mice again increased their blood glucose levels more than A/J mice (Fig. 4-4-1 C). Using two-way ANOVA, only the effect of strain on incremental AUC (Fig. 4-4-1 D) was statistically significant (p=0,039). The single effect of stress was again evaluated in a separate test where saline solution was orally administered in the same amount as during GTT. Glucose levels after oral gavage of saline increased only slightly and this effect was negligible when an incremental AUC was calculated (data not shown). The difference between intraperitoneal and oral form of GTT on mouse pups was detected mainly in lower glucose levels 30 min after glucose administration in the case of the oral GTT. This could be accounted to incretin production after oral glucose administration and their effect on glucose uptake into cells 6943 (Baggio and Drucker 2007). Although during the intraperitoneal GTT blood glucose levels increased more than during the oral one, this difference between two forms of GTT was not as big as in the case of adult mice (Andrikopoulos, Blair et al. 2008).

Experiment 2: comparison of OGTT at a dose 1 or 3 mg of glucose per g of body weight

To compare the effect of different glucose doses, Experiment 2 was performed using a dose of 3mg of glucose per g of body weight orally administered (Fig. 4-4-1 E). In this setup, the difference between strains was not high enough to reach statistical significance when expressed as incremental AUC (Fig. 4-4-1 F). The glucose dose was probably so high, that even in the case of A/J mice, which during the GTT with lower glucose dose eliminated glucose from blood much faster than C57BL/6J mice; glucose in the blood remained relatively high.

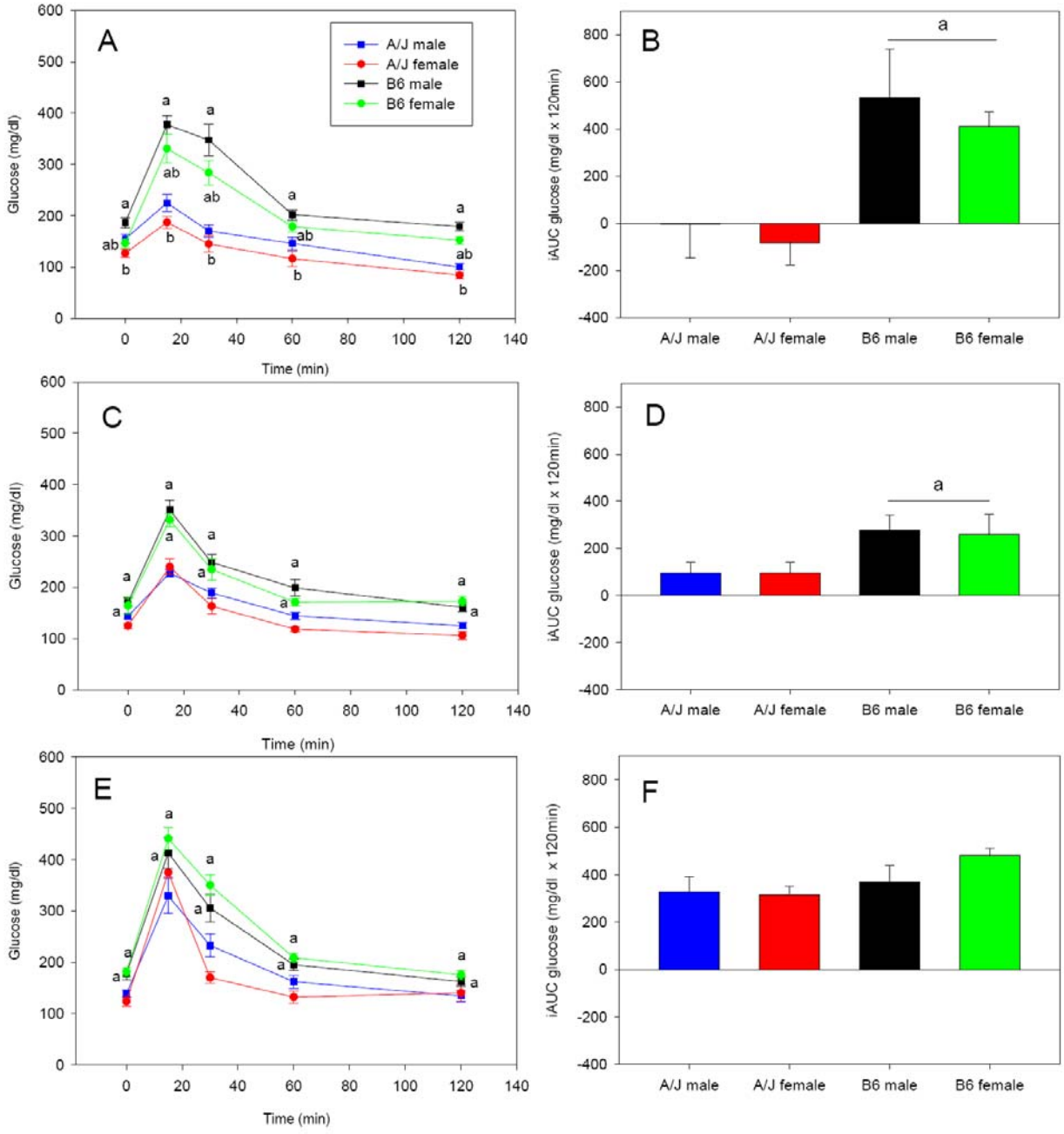

Fig. 4-4-1: *IPGTT (**A-B**) or OGTT (**C-F**) performed using either 1 mg glucose/g BW (**A-D**) or 3 mg glucose/g BW (**E-F**) at 20°C. Left panels, glycemia during the time course of the test; right panels, incremental AUC. Data are mean ± SEM; n = 6-11. a, different from A/J strain; b, different from male mice.*

Experiment 3: indirect calorimetry equivalent of OGTT at a dose 1 mg of glucose per g of body weight at a room temperature

While using indirect calorimetry measurement as a marker of whole body substrate oxidation we applied glucose in the form of intragastric gavage. This form of glucose application is more physiological and, as described in previous experiments, there is not any adverse effect of this form of application on GTT outcomes in the form of higher variability of obtained data as compared with intraperitoneal application. Intragastric gavage also allows physiological incretin´s effect to be employed. We firstly followed GTT experimental setup concerning glucose dose (1 mg of glucose per g of body weight) and then maximized the indirect calorimetry outputs by applying the maximal possible dose of 7.5 mg of glucose per gram of body weight, which is approximately 1/8 of the daily energy consumption of mice.

In Experiment 3, metabolic reaction to glucose bolus administered by intragastric gavage was followed during indirect calorimetry measurement. The measurement started at 9:00 a.m. after 3h fast. Mice were fasted till 11:00 a.m., when measurement was interrupted and glucose bolus of 1 mg per g of body weight was administered by intragastric gavage. Mice exhibited low RQ values during an initial fasting phase of experiment, corresponding to a high lipid or protein oxidation in a fasting state (Fig. 2A). After intragastric gavage of glucose, the RQ increased. So a glucose bolus frequently used during GTT is sufficient to increase blood glucose levels; however, it is not so high to affect RQ values substantially. Higher RQ increase after glucose bolus in the case of A/J mice corresponds to lower blood glucose detected during GTT; therefore higher oxidation of carbohydrates corresponds to higher ability of glucose withdrawal from blood in the case of A/J mice.

Experiment 4: indirect calorimetry equivalent of OGTT at a dose 7.5 mg of glucose per g of body weight at a room temperature

In Experiment 4 we addressed the question of maximal response of whole body metabolism to glucose load. Hence, we used a maximal dose of glucose that is possible to deliver by intragastric gavage due to a limited volume of stomach; that means 7.5 mg of glucose per g of body weight. Indirect calorimetry measurement was performed as previously at a room

temperature and started at 9:00 a.m. after 3h fast. Mice fasted till 11:00 a.m., when measurement was interrupted and glucose bolus was administered by intragastric gavage. In this setup, we observed an increase from fasting RQ values around 0.85 to values around 1 after glucose load (Fig.4-4-2 B). This rapid increase was followed by slowly decrease back to fasting values.

Experiment 5: indirect calorimetry equivalent of OGTT at a dose 7.5 mg of glucose per g of body weight at thermoneutral temperature

Experiment 5 was performed in thermoneutral temperature to avoid the confounding effect of heat production. A high glucose dose 7.5 mg of glucose per g of body weight administered by intragastric gavage was used to highlight the metabolic reaction to glucose. The measurement started at 9:00 a.m. after 3h fast. Mice were given water and fasted till 11:00 a.m., when measurement was interrupted and glucose bolus of 7.5 mg per g of body weight was administered by intragastric gavage. Mice exhibited respiratory quotient (RQ) values around 0.85 during initial phase of experiment, corresponding to a high lipid or protein oxidation in fasting state. After intragastric gavage of glucose, RQ rose to values close to 1, meaning higher carbohydrate oxidation (Fig. 4-4-2 C). An increase in RQ values caused by intragastric gavage was quantified as HillSlope parameter of curve fitted into individual RQ data from each mouse. Fast response to glucose gavage has a shape of sigmoidal curve, and can be described by the same equation as enzymatic activity as it is simply an enzymatic response of the whole organism to the preferential substrate. HillSlope parameter was higher in the case of A/J when compared with C57BL/6J mice (Table 1B), corresponding to faster response to substrate change and so higher metabolic flexibility.

As can be seen in Fig. 4-4-2 C, the peak of RQ values after glucose administration was higher in A/J mice as compared with C57BL/6J mice, irrespective of gender. However, this difference did not reach statistical significance, when evaluated as the highest value of smoothed RQ curves from individual mice ($p=0.091$ for strain, two-way ANOVA). Subsequent return to basal fasting RQ values after glucose administration was faster in female than male mice, irrespective of strain, and this aspect of metabolic flexibility, e.g. the ability to return back to lipid oxidation, was faster in the case of female mice when compared to male, irrespective of strain.

Experiment 6: indirect calorimetry measurement of fasted-refed transition in a thermoneutral temperature

In Experiment 6 we introduced the most physiological test, e.g. the transition from fasted to refed state, as an equivalent of meal tests frequently employed in human experiments (Table 4-4-2). The goal of this experiment was to compare GTTs, indirect calorimetry tests using glucose dose challenge and the most physiological fasted-refed transition originating in circadian rhythms of mice. In this experiment indirect calorimetry measurement started at 1:00 p.m., mice fasted till 6:00 p.m., when blood samples for EDTA-plasma isolation were taken (fasted state) and pre-weighted diet was released. Measurement was terminated at 8:00 a.m. the next day and blood samples for EDTA-plasma isolation were taken (re-fed state).

Mice displayed RQ values around 0.8 during initial phase of experiment, corresponding to a high lipid or protein oxidation in a fasting state. After re-feeding, RQ rose to values close to 0.9 – 1, corresponding to higher carbohydrate oxidation. In some cases, RQ rose even to values higher than 1, probably due to expected increased lipogenesis (Fig.4-4-2 D).

RQ values in the steady state of measurement (0:00-2:00 a.m.) were higher in A/J mice than in C57BL/6J mice (Table 4-4-2). This was probably a consequence of slightly increased caloric intake in A/J mice; nevertheless, the RQ value remained higher in A/J mice even after the adjustment to the caloric intake (not shown).

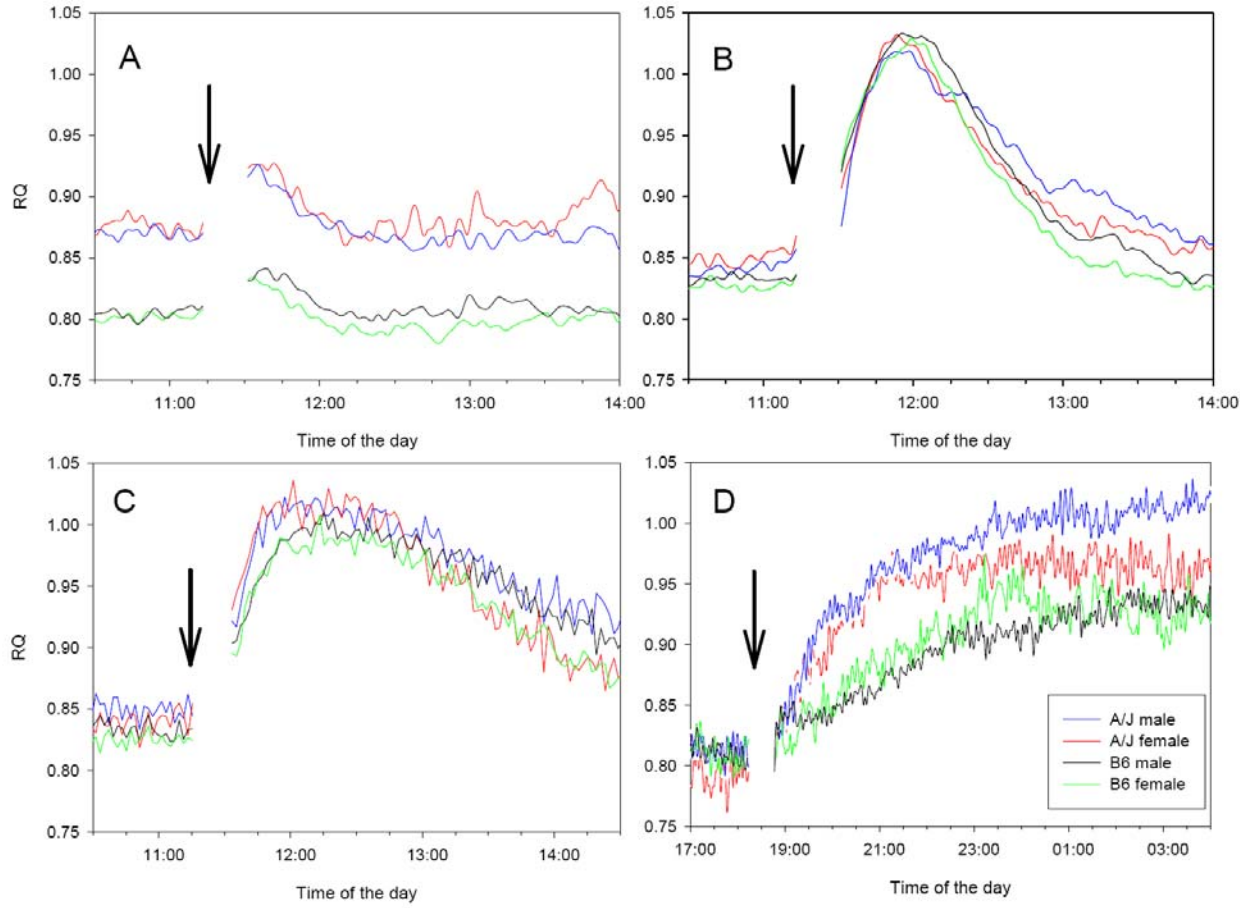

Fig. 4-4-2: *INCA performed using either an intragastric gavage of glucose (arrow;* ***A-C****) in mice fasted for 5 hours before the bolus or during fasting/re-feeding transition (****D;*** *food was removed for 5 hours before it was offered again at 6.00 p.m.; arrow). Measurements were performed either at 20°C (****A-B****) or 34°C (****C-D****).* ***A****, 1 mg glucose/g BW;* ***B,C****, 7.5 mg glucose/g BW. Each line represents an averaged signal from several mice:* ***A,*** *n = 12 - 22;* ***B****, n = 15 - 41;* ***C,*** *n = 13 - 22;* ***D****, n = 13 - 18.*

	A/J male			A/J female			C57BL/6J male			C57BL/6J female			Strain	Gender
n	86			81			121			124				
BW (g)	14.5	±	0.2	13.2	±	0.3	15.5	±	0.2	14.0	±	0.2	<0.01	<0.01

***Table 4-4-1**: Body weight of mice at weaning: Pooled data from various experiments in this study. Data are mean ± SEM. Data are evaluated using two-way ANOVA for influence of strain and gender, respectively.*

	A/J male			A/J female			C57BL/6J male			C57BL/6J female			Strain	Gender
Caloric intake (kcal)	7.04	±	0.78	5.85	±	1.13	5.22	±	0.28	4.74	±	0.67	0.04	0.22
Indirect calorimetry parameters														
EE														
Fasted	2.77	±	0.12	2.74	±	0.18	3.13	±	0.11	3.21	±	0.15	<0.01	0.87
Re-fed	4.84	±	0.26	4.91	±	0.39	4.48	±	0.20	4.29	±	0.19	0.06	0.81
Delta EE	2.07	±	0.24	2.17	±	0.27	1.35	±	0.17	1.00	±	0.23	<0.01	5.59
RQ														
Fasted	0.81	±	0.01	0.79	±	0.01	0.81	±	0.02	0.82	±	0.01	0.34	0.71
Re-fed	1.00	±	0.03	0.97	±	0.02	0.92	±	0.02	0.93	±	0.02	0.01	0.51
Delta RQ	0.20	±	0.03	0.18	±	0.02	0.13	±	0.02	0.13	±	0.03	0.02	0.85
Plasma parameters														
Glucose (mg/dl)														
Fasted	119	±	8	102	±	17	103	±	10	106	±	6	0.55	0.48
Re-fed	135	±	9	138	±	18	195	±	11	187	±	17	<0.01	0.85
Delta glucose	16	±	12	36	±	21	92	±	8	82	±	17	<0.01	0.73
NEFA (mmol/l)														
Fasted	0.62	±	0.04	0.61	±	0.07	0.53	±	0.03	0.65	±	0.04	0.67	0.26
Re-fed	0.75	±	0.13	0.69	±	0.14	0.39	±	0.03	0.53	±	0.09	<0.01	0.70
Delta NEFA	0.14	±	0.12	0.08	±	0.15	-0.14	±	0.04	-0.18	±	0.10	0.01	0.63
TAG (mg/dl)														
Fasted	46	±	5	48	±	3	56	±	9	52	±	6	0.33	0.91
Re-fed	103	±	12	105	±	14	90	±	9	104	±	19	0.38	0.36
Delta TAG	57	±	12	56	±	11	30	±	10	53	±	16	0.25	0.42

Table 4-4-2: *Caloric intake during 6:00 p.m. and 8:00 p.m. the following morning INCA; fasted EE and RQ were evaluated during 90 min before re-feeding (between 4:30 p.m. and 6:00 p.m.), while EE in re-fed state were evaluated during 6 hours after re-feeding and RQ between 0:00 a.m. and 2:00 a.m.. Plasma parameters: fasted, at 6:00 p.m.; re-fed, at 8:00 a.m. the next day after re-feeding, respectively, using tail-blood samples. Delta, difference between fasted and re-fed state. See Fig. 2D for INCA time-courses and Fig. 3 for leptin and adiponectin data. Data are mean ± SEM; n =13-18. Data are evaluated using two-way ANOVA for influence of strain and gender, respectively.*

Differences found in mouse pups measured at thermoneutral temperature might have been caused by different stress response to high ambient temperatures. We have addressed this question by measuring corticosterone as a marker of stress (Turner, Vaughn et al. 2012) in plasma and feces of mice at the end of 24h indirect calorimetry. While plasma corticosterone levels reflect immediate stress level, corticosterone in feces represents stress levels during the last 6-8 hours (Turner, Vaughn et al. 2012). One day after weaning a 24 h indirect calorimetry measurement with free access to water and diet was performed at 30^{o}C on male mice of A/J and C57BL/6J strain. Immediately after the end of measurement, plasma and 24h feces were collected and corticosterone levels were measured. There was not a significant difference in plasma corticosterone levels between A/J and C57BL/6J male mice (83.64±23.75 and 89.43±26,62 ng/ml) nor in 24h feces corticosterone levels (14.9±7.1 and 21.1±11.2 ng/24h feces.

Plasma samples collected during experiment were analyzed as follows. Glucose levels in the evening fasted samples were similar in all groups; while morning re-fed glucose levels were higher in C57BL/6J mice (Table 4-4-2). Non-esterified fatty acids (NEFA) levels in the evening fasted samples were also similar in all groups, while morning NEFA levels were lower in C57BL/6J mice (Table 4-4-2). TAG (Table 4-4-2) and also cholesterol (not shown) levels in the evening fasted and in the morning re-fed samples were similar in all groups. Triacylglycerol levels in the morning re-fed samples were almost twice as high as in the evening fasted samples. Leptin levels were higher in A/J mice both in evening and in morning samples irrespective of gender (Fig 4-4-3). HMW as well as MMW and total adiponectin levels in plasma were higher in C57 BL/6J mice both in the evening fasted samples and in the morning re-fed samples (Fig 4-4-3).

Data from Experiment 6 suggest higher metabolic flexibility of A/J mice and higher RQ values in a stable phase of measurement together with higher ability to maintain stable glucose plasma level despite a higher caloric intake.

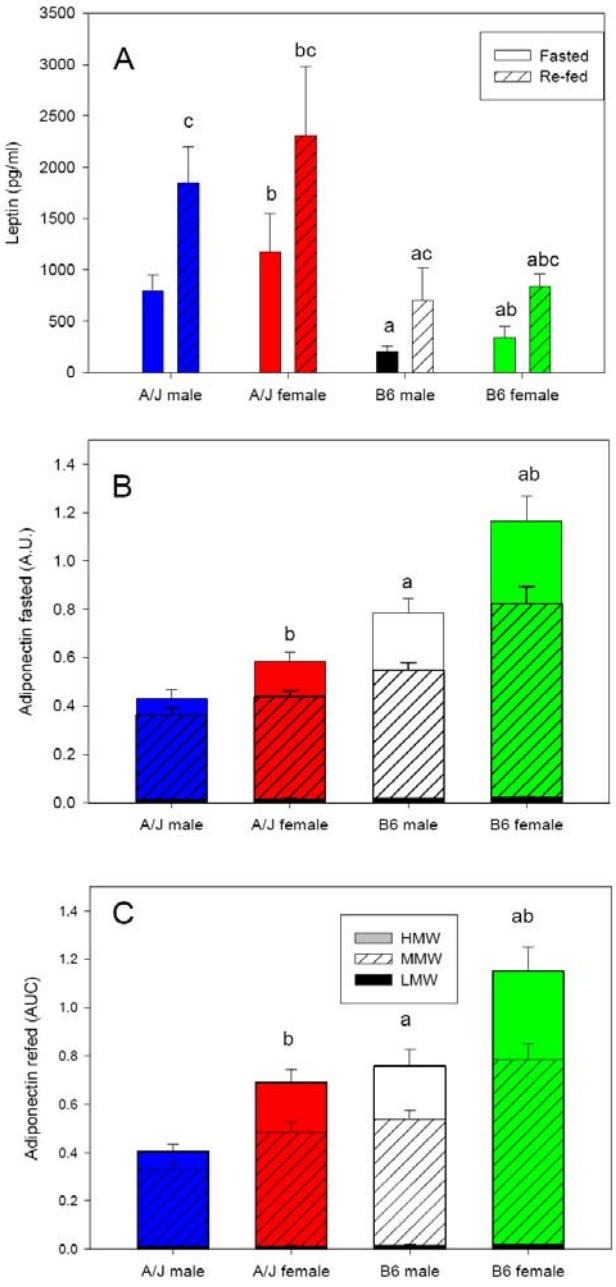

Fig. 4-4-3: *Leptin and adiponectin plasma levels during INCA at thermoneutral temperature. The re-feeding protocol was used. Plasma adipokine´s levels were measured in a fasted (at 6:00 p.m.) and re-fed (at 8:00 a.m., the next day after re-feeding) state, respectively, using tail-blood samples. (**A**) leptin plasma levels in the fasted and re-fed state, respectively. The effect of strain, gender, and nutritional status were determined using three-way ANOVA. Adiponectin plasma levels in the fasted (**B**) and re-fed (**C**) state. The effect of strain and gender on total adiponectin were determined using two-way ANOVA. See also Fig. 2D and Table 2. Data are mean ± SEM; n = 13 - 18. a, different from A/J strain; b, different from male mice; c, different from fasted state.*

To sum up, metabolic flexibility of murine strains that differ in their propensity to obesity was assessed by many experimental setups. Fasting/re-feeding transition and GTT, either in the connection with INCA or performed as a classical GTT, were able to detect metabolic differences between A/J and C57BL/6J mice.

5.5 Publication E

Flachs P, Jones JG, Zouhar P, Adamcova K, Svobodova M, **Bardova K**, Janovska P, Hansikova J, Liisberg U, Keenan A, Madsen L, Kristiansen K and Kopecky J, *Induction of triacylglycerol/fatty acid futile cycling in white adipose tissue during cold exposure is linked to obesity-resistance in mice*

The aim of this study was to evaluate metabolic flexibility as a reaction metabolism to short-term cold exposure. A/J and C57BL/6J mice were compared in this respect.

Mice of A/J and C57BL/6J (B6) strain pre-acclimated to thermoneutral temperature were exposed either to 6^{o}C for 2 or 7 days or remained at 30^{o}C. Generally, food intake increased approximately 2-times in both strains in response to cold exposure, while body weights did not change (Table 5-5-1). Nevertheless, weights of both epididymal and inguinal WAT markedly decreased, and this effect was more pronounced in A/J mice (Table 5-5-1). BAT weight decreased dramatically after two days of cold exposure and morphologically lost almost all stored lipid droplets and increased its weight again after 7 days of cold exposure as BAT re-developed fully it´s morphological appearance with accentuated fat deposition in the multilocular form (Table 5-5-1).

Physiological parameters

Plasma concentrations of TAG and NEFA decreased after 2 days of cold exposure in both strains. This effect was partially rescued in A/J mice after 7 days of cold exposure, when plasma levels of TAG and NEFA partially returned to basal levels (Table 5-5-1). β-hydroxybutyrate as a measure of liver ketogenesis was at thermoneutrality higher in A/J as compared to B6 mice. It gradually increased after cold stimulus, and this increase was more pronounced in A/J as compared to B6 mice (Table 5-5-1). Plasma cholesterol and glucose levels did not change in response to cold stimulus and were higher in B6 than A/J mice, irrespective of ambient temperature (Table 5-5-1). Plasma insulin levels were higher in B6 as compared to A/J mice and except for B6 6^{o}C – 2d mice did not change in response to cold stimulus (Table 5-5-1). Plasma leptin levels increased after 7 days at 6^{o}C in B6 mice and decreased in A/J mice after 2 and 7

days at 6^{o}C, while plasma FGF21 levels decreased in both strains in response to cold (Table 5-5-1).

	B6			A/J		
	30°C	**6°C – 2d**	**6°C – 7d**	**30°C**	**6°C – 2d**	**6°C – 7d**
Food consumption (g per day)	3.07 ± 0.07	5.16 ± 0.25	6.64 ± 0.30	3.09 ± 0.09	4.48 ± 0.14	6.67 ± 0.19
Body weight (g)	27.4 ± 0.5	26.4 ± 0.5	27.1 ±0.7	21.5 ± 0.4[c]	21.1 ± 0.3[c]	21.5 ± 0.5[c]
Weight of tissues						
eWAT (mg)	383.3 ± 27.7	350.5 ± 16.3	286.3 ± 16.3[a]	448.2 ± 30.2[c]	286.4 ± 78.6[a,c]	179.1 ± 11.2[a,b,c]
scWAT (mg)	299.8 ± 23.9	231.10 ± 13.4[a]	267.66 ± 12.3	388.0 ± 31.4[c]	259.4 ± 20.4[a]	233.3 ± 11.0[a,c]
iBAT (mg)	100.8 ± 4.5	54.7 ± 2.2[a]	104.47 ± 2.62[b]	69.1 ± 3.7[c]	47.4 ± 3.1[a]	72. 0 ± 1.7[b,c]
Plasma levels						
TAG (mmol l^{-1})	0.83 ± 0.18	0.41 ± 0.10[a]	0.45 ± 0.04[a]	1.31 ± 0.21[c]	0.27 ± 0.04[a,c]	0.78 ± 0.15[a,b,c]
NEFA (mmol l^{-1})	0.44 ± 0.06	0.26 ± 0.09[a]	0.30 ± 0.03[a]	0.71 ± 0.05	0.24 ± 0.05[a]	0.55 ± 0.08[a,b,c]
β-Hydroxybutyrate (nmol μl^{-1})	0.27 ± 0.04	0.48 ± 0.06[a]	0.56 ± 0.10[a]	0.44 ± 0.04[c]	0.59 ± 0.08[a]	0.83 ± 0.27[a,b,c]
Cholesterol (mmol l^{-1})	2.07 ± 0.09	2.32 ± 0.19	2.29 ± 0.17	1.30 ± 0.11[c]	1.31 ± 0.05[c]	1.33 ± 0.06[c]
Glucose (mg dl^{-1})	240.3 ± 8.5	232.2 ± 9.9	N.E.	203.8 ± 9.04[c]	194.9 ± 7.6[c]	N.E.
Insulin (ng ml^{-1})	0.934 ± 0.09	0.721 ± 0.108[a]	0.897 ± 0.100	0.585 ± 0.065[c]	0.677 ± 0.112	0.614 ± 0.011[c]
Leptin (pg ml^{-1})	1683 ± 395	1764 ± 193	2434 ± 246[a,b]	3390 ± 583 [c]	1571 ± 193[a]	1526 ± 149[a,c]
FGF21 (pg ml^{-1}]	271.7 ± 75.5	103.6 ± 7.9[a]	49.0 ± 11.8[a,b]	258.4 ± 41.9	154.4 ± 29.9[a,c]	147.6 ± 18.3[a,c]

Table 5-5-1: *Food consumption, body weight and tissue weight characterisation and plasma parameters. Mice pre-acclimated at thermoneutrality and fed standard diet were either exposed to 6°C for 2 or 7 days, or remained at thermoneutral zone. Tissue dissection and plasma collection were performed in a random-fed state (between 08:00 a.m. and 10:00 a.m.). Data are mean ± SEM. a, different from 30°C within the strain; b, different from 6°C – 2d within the strain; c, different between strains within the treatment.*

Re-esterification in Epididymal White Adipose Tissue

Cold exposure leads to increased energy expenditure in the form of shivering and non-shivering thermogenesis. These processes require considerable amount of energy input, either from increased food intake (see Food consumption; Table 5-5-1) or from intracellular energy reserves. Thus, adrenergically stimulated lipolysis of TAG in WAT increases in response to cold (see Weights of tissues; Table 5-5-1). The ability of adipose tissue to react adequately and promptly to energy demands in the form of released FA may be enabled by futile TAG/FA cycling. This process of TAG lipolysis and FA re-esterification is regulated by allosteric regulations of discrete enzymes and as such reacts immediately to metabolic demands. Moreover, futile cycling protects adipose cells from possible toxic effects of released FA through the formation of micro lipid droplets. Re-esterification of FA into lipid droplets is also essential for the rate of lipolysis, at least in *in vitro* conditions (Hashimoto, Segawa et al. 2012). Therefore, we analyzed the rate of TAG/FA cycling using deuterium labeling and ^{2}H-NMR technique in eWAT. Two days prior to dissection, mice were injected with a bolus of $^{2}H_2O$ and also 5% of drinking water was replaced by $^{2}H_2O$. ^{2}H labeling of the glyceryl moiety of isolated TAG from eWAT was checked by NMR spectroscopy to estimate the rate of TAG synthesis and FA *de novo* synthesis in this depot (Figure 5-5-1). NMR data clearly show higher activity of FA synthesis and re-esterification of FA in A/J as compared to B6 mice.

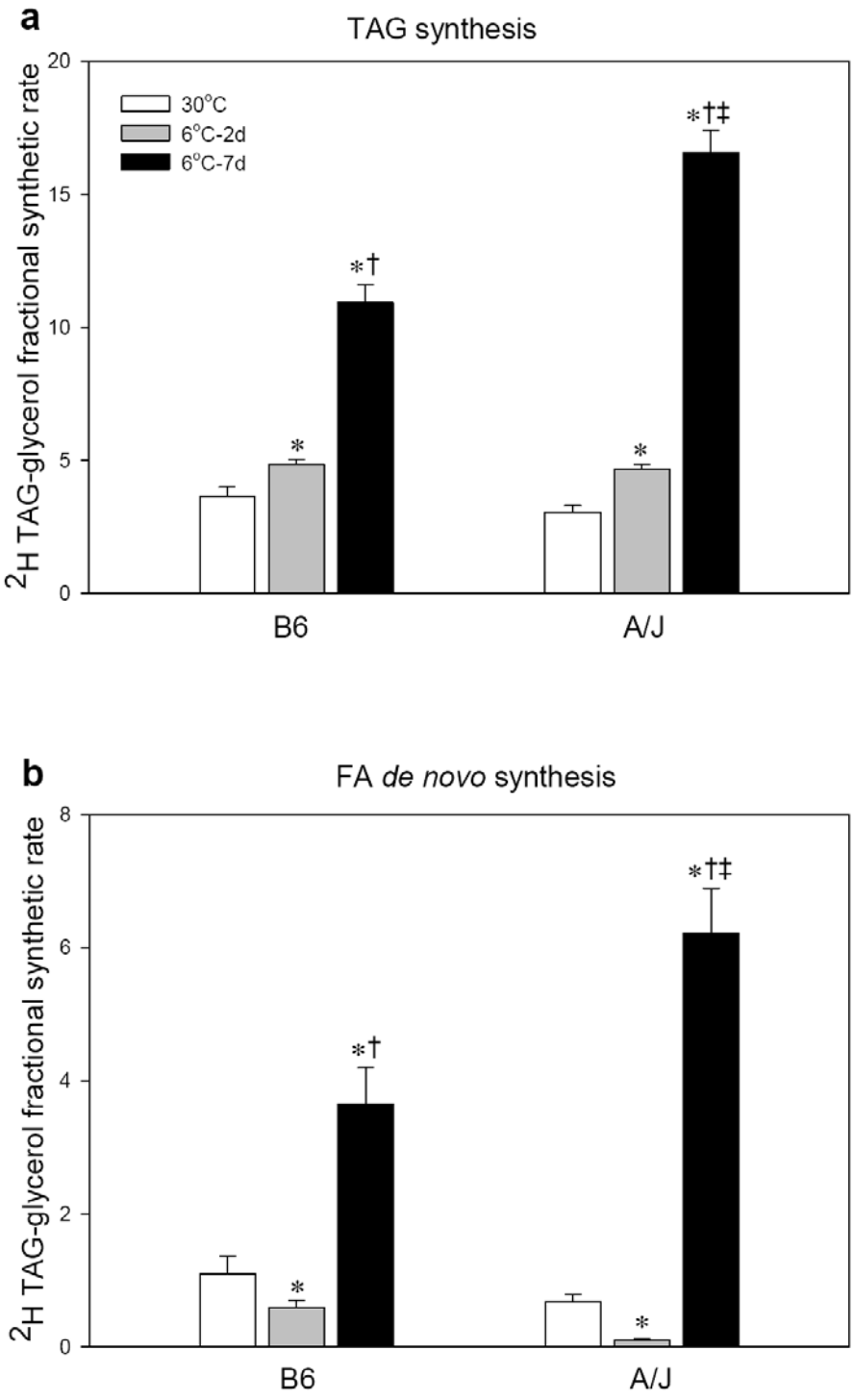

Fig. 5-5-1: *Measurement of TAG synthesis (**A**) and de novo FA synthesis (**B**) in eWAT by ^2H_2O incorporation in vivo. Data are mean ± SEM. *, different from 30°C within the strain; †, different from 6°C – 2d within the strain;‡, different between strains within the treatment.*

FA re-esterification was confirmed by ex vivo analysis of isoproterenol induced lipolysis in epididymal adipocytes. Re-esterification, expressed as released NEFA/glycerol ratio, was negligible in basal conditions at thermoneutrality, as this ratio was close to theoretical 3 NEFA and 1 glycerol per 1 TAG hydrolyzed. After cold exposure, this ratio decreased to 2, meaning that in average 1 FA from 1 TAG molecule was re-esterified back to newly-formed TAG. These results suggest, that the rate of TAG/FA cycling is higher in A/J mice (Fig. 5-5-2 A). In isoproterenol stimulated state, differences between strains were not detected, probably due to such a strong stimulation of lipolysis that subtle physiological differences in the function of involved enzymes were not detectable.

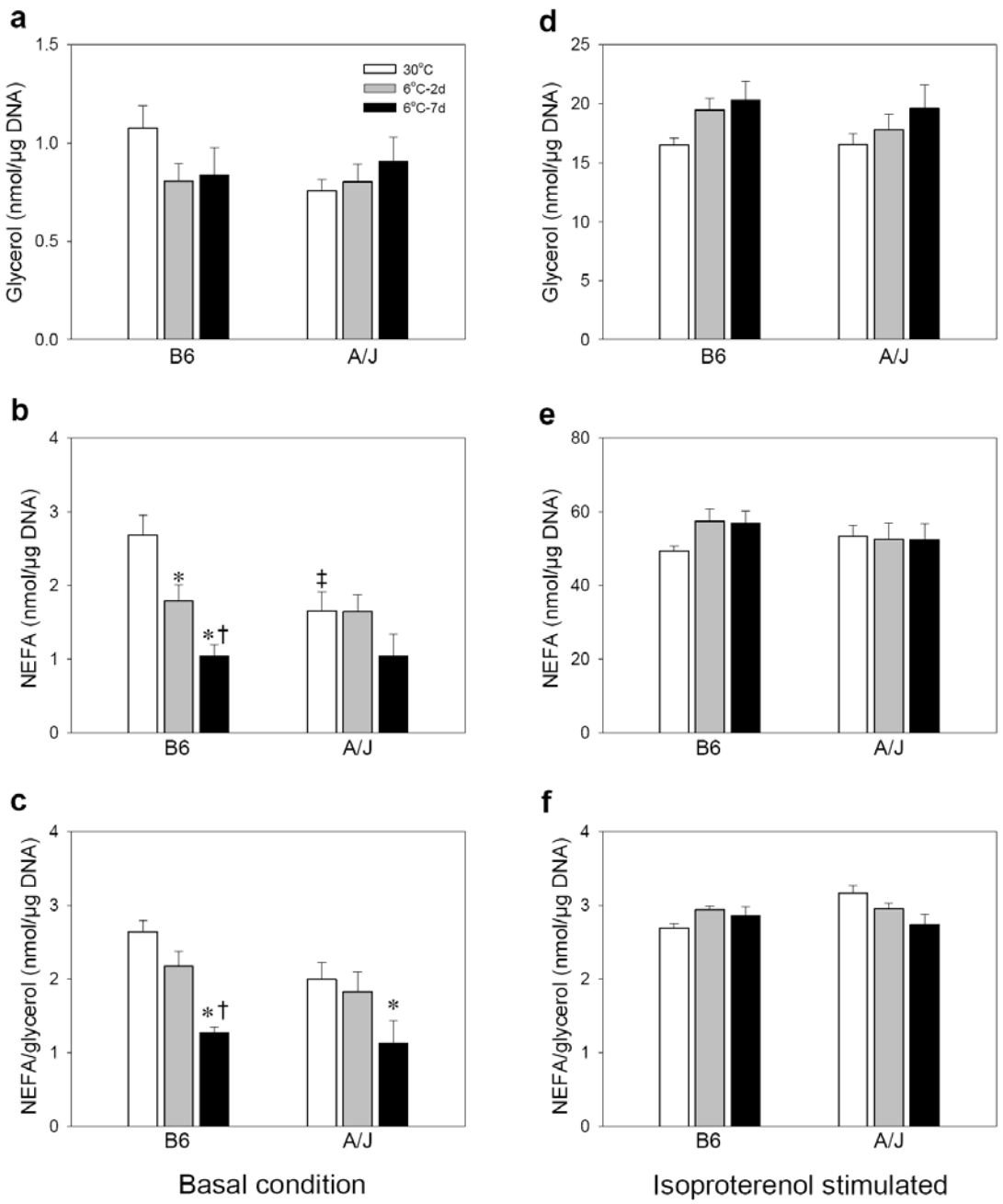

Fig. 5-5-2: *Ex vivo biochemical analysis of eWAT. (**A**), basal glycerol release from collagenase-diberated adipocytes from eWAT (n=8-10); (**B**), basal NEFA release from collagenase-diberated adipocytes from eWAT (n=8-10); (**C**), relative basal NEFA/glycerol ratio; (**D**), isoproterenol induced release of glycerol from collagenase-diberated adipocytes from eWAT (n=8-10); (**E**), isoproterenol induced NEFA release from collagenase-diberated adipocytes from eWAT (n=8-10); (**F**), relative isoproterenol induced NEFA/glycerol ratio. Data are mean ± SEM. *, different from 30°C within the strain; †, different from 6°C – 2d within the strain;‡, different between strains within the treatment.*

Morphology of Epididymal White Adipose Tissue

Lipolysis in adipose tissue is accompanied by morphologically visible changes in adipocyte appearance, as was previously reported (Giordano, Frontini et al. 2005). We found that after stimulation of lipolysis by cold exposure, only a subpopulation of adipocytes underwent shrinking process, and was surrounded by a morphologically unchanged unilocular adipocytes. We observed that after cold-stimulus-caused lipolysis morphologically unchanged unilocular adipocytes in eWAT decrease their size, and that adipocyte size was significantly higher in eWAT from A/J as compared to B6 mice, irrespective of ambient temperature. Mean adipocyte size was 1854±98 μm^2 in A/J 30^{o}C, 1314±70 μm^2 in A/J 6^o-7d, 1407±99 μm^2 in B6 30^{o}C, and 1126±64 μm^2 in B6 6^o-7d; with significant differences between A/J 30^{o}C and all other groups (one-way ANOVA). However, a subpopulation of morphologically paucilocular adipocytes emerged in cold-exposed animals (Fig. 5-5-3 A) and emergence of these probably lipolytically stimulated cells tended to be higher in A/J than B6 mice.

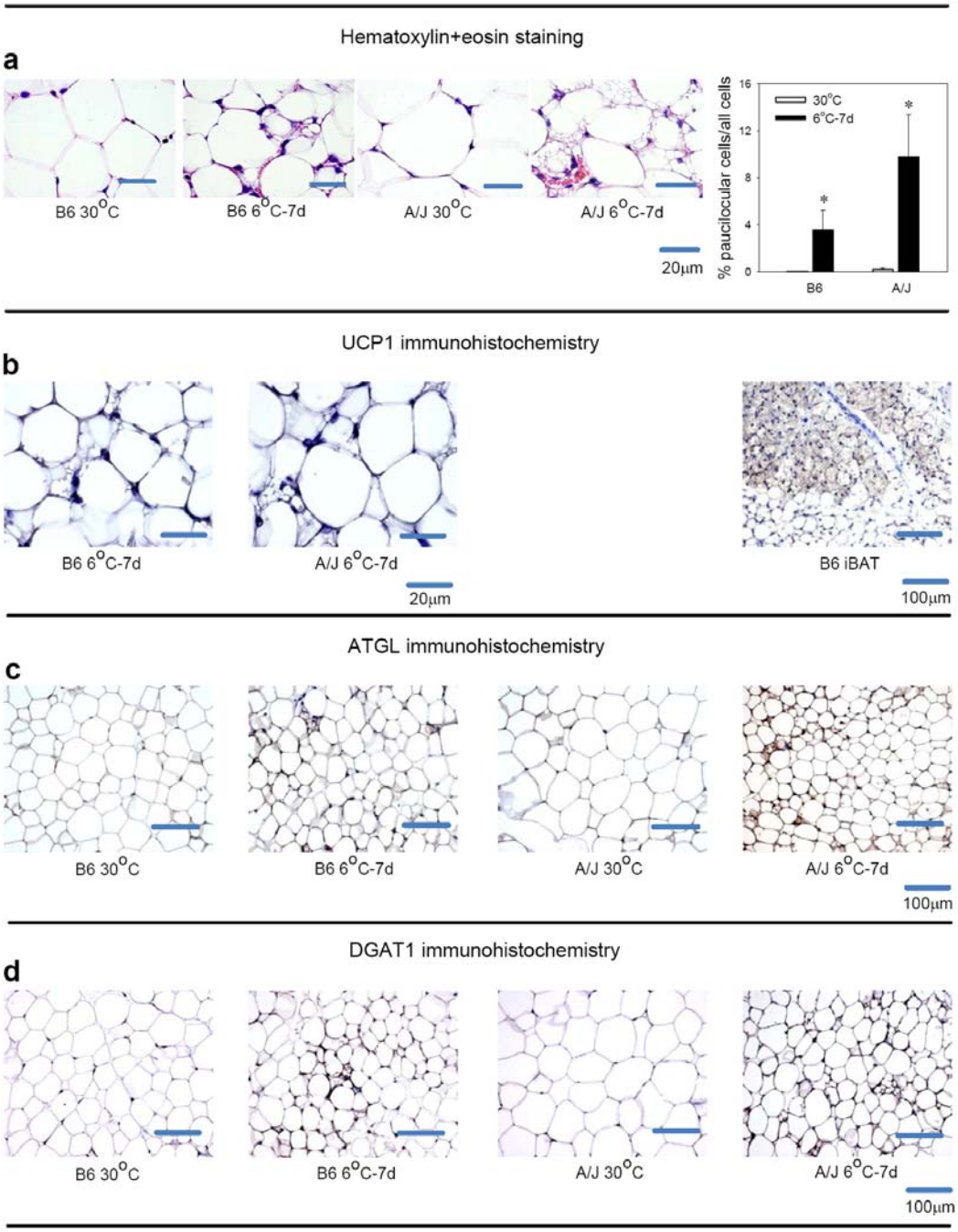

Fig. 5-5-3: *Histological characterisation of eWAT from mice exposed to thermoneutrality or to 6°C for 2 days. (**A**), representative images (hematoxylin and eosin staining) and quantification of paucilocular cells; (**B**),UCP1 immunohistochemistry; (**C**), ATGL immunohistochemistry; (**D**), DGAT1 immunohistochemistry; *, different from 30°C within the strain.*

In cold-exposed animals, increase of lipolysis and re-esterification was further revealed by immunohistochemistry for ATGL (Fig. 5-5-3 C) and DGAT1 (Fig. 5-5-3 D). A/J mice exhibited increased ATGL and DGAT1 immunostaining after cold exposure, as compared to B6, and this staining was mainly localized to smaller or paucilocular adipocytes.

Brite multilocular adipocytes, emerging within white adipose depots after various stimuli (Vitali, Murano et al. 2012, Frontini, Vitali et al. 2013), are defined by the presence of UCP1 protein. Therefore, we performed immunohistochemistry for UCP1 to test the possibility of brite-cell-emergence within eWAT. None of the paucilocular adipocytes detected was UCP1 positive, excluding the possibility of brite-cell induction in intraabdominal adipose depot (Fig. 5-5-3 B).

Gene Expression Analysis in Epididymal White Adipose Tissue

DGAT1 and 2 are essential for TAG synthesis in adipocytes (Harris, Haas et al. 2011). In hepatocytes, DGAT2 is essential for *de novo* synthesis of TAG, while DGAT1 functions primarily to re-esterify DAG and MAG formed after lipase-mediated hydrolysis of TAG (Zammit 2013). DGAT1 and 2 also differ in their K_m values for fatty acyl-CoA, with DGAT2 more active at lower and DGAT 1 more active at higher substrate concentrations. Moreover, DGAT1 possesses MGAT activity. This ability may be important in tissues with high re-esterification rate (Yen, 2008 #6664). Whereas *Dgat2* mRNA levels increased only after 7 days in cold in A/J mice and were induced after 2 days in cold in B6 mice, *Dgat1* mRNA levels were induced 2-fold in B6, and 3-fold in A/J mice even after 2 days in cold (Fig. 5-5-4 A). *Dgat2* mRNA expression in this study corresponds to mRNA expression of *Fasn* (Fig. 5-5-4 A) and *de-novo* FA-synthesis (Fig. 5-5-1 B), corresponding to a reported function of DGAT2 in TAG synthesis from *de-novo* synthetized FA. On the other hand, functional assessment of TAG synthesis may be overestimated by incorporation of labelled ^2H_2O into elongated FA, but equal mRNA expression of *Elovl5* in animals exposed to cold for 7 days (Fig. 5-5-4 A) suggests that this mechanism may not be involved in this case.

Re-esterification cycle requires supply of glycerol-3-phosphate. In white adipocytes, PEPC-K is a marker of this metabolic pathway, while glycerol-kinase doesn´t have such a high

activity in this tissue and is more connected to brown or brite adipocytes (2.1.1 Adipose Tissue Metabolism). *Pck1* expression was higher in A/J mice irrespective of external temperature and tended to increase in response to 4°C for 48h in A/J (Fig. 5-5-4 A). On the other hand, *Gk* expression did not differ between strains (Fig. 5-5-4 A).

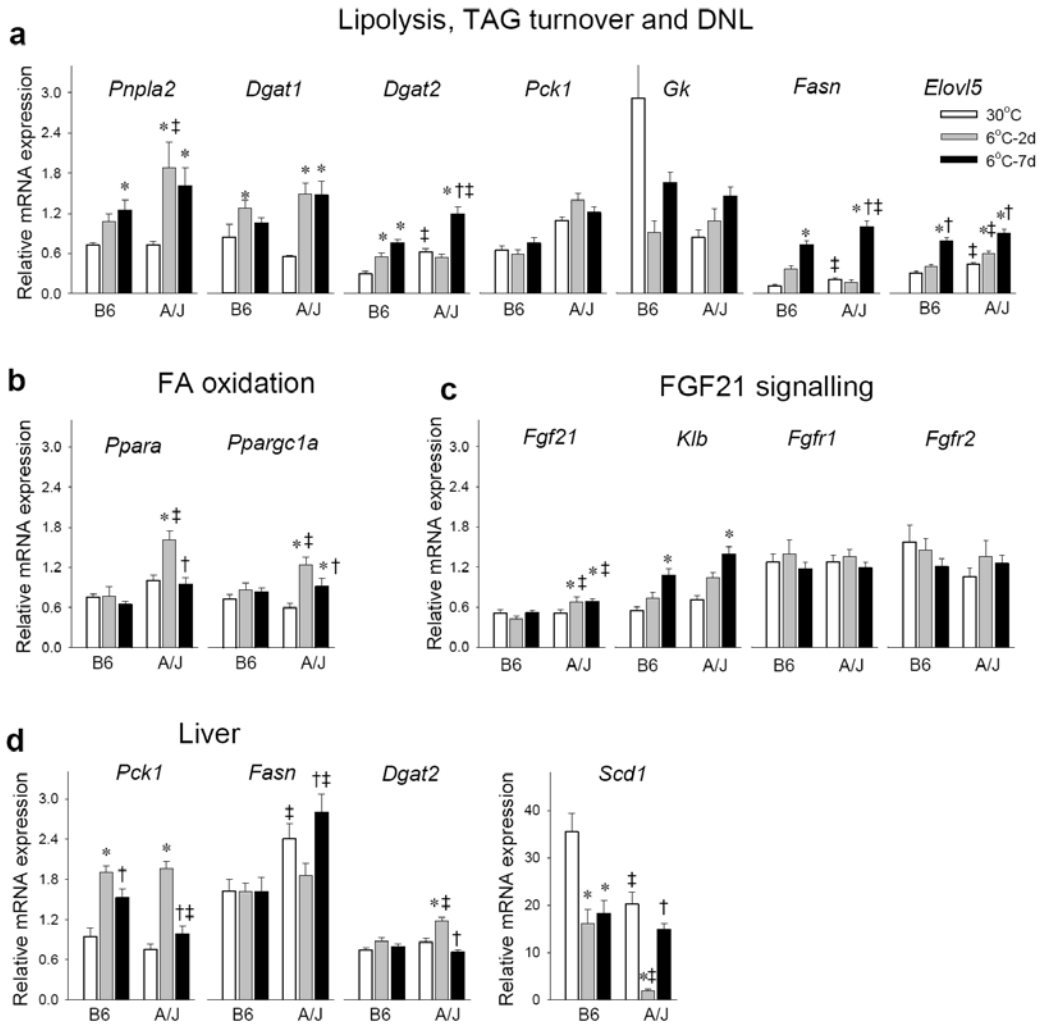

Fig. 5-5-4: *Gene expression analyses in eWAT (**A-C**) and liver (**D**). mRNA levels of Pnpla2, Dgat1, Dgat2, Pck1, Gk, Fasn, Elovl5, Ppara, Ppargc1a, Fgf21, Klb, Fgfr1, and Fgfr2 were analyzed in epididymal WAT and Pck1, Fasn and Scd1 were analyzed in liver. Data are mean ± SEM. a, different from 30°C within the strain; b, different from 6°C – 2d within the strain; c, different between strains within the treatment. *, different from 30°C within the strain; †, different from 6°C – 2d within the strain;‡, different between strains within the treatment.*

To conclude, re-esterification of FA released by excessive TAG lipolysis was confirmed functionally, histologically and on a level of mRNA expression of genes important in FA and TAG metabolism. A/J as compared to C57BL/6J mice exhibit higher flexibility to stress caused by cold exposure.

6 Discussion

6.1 Publication A

Specific goal 1: to evaluate influence of n-3 long chain fatty acids (n-3 LC-PUFA) and rosiglitazone, a drug from thiazolidinedione group, and their combination on metabolic flexibility in dietary obese mice, both at a whole-body and cellular level.

The principle finding of this study is that combined action of *n-3* LC-PUFA and rosiglitazone on dietary obese mice preserves metabolic flexibility. This improvement of whole-body metabolic flexibility may be accounted to improvement of muscle insulin sensitivity by a combined treatment as was shown by Kuda et al. (Kuda, Jelenik et al. 2009). Metabolic flexibility was expressed either as a ΔRQ between fasting and STD re-fed values or as a relative difference between PRCF curves from these two states. While ΔRQ is a relatively insensitive approach for metabolic flexibility assessment, comparison of PRCF curves from pooled RQ data enables to observe subtle changes in metabolic flexibility in fasting and re-fed state and to compare those two conditions.

The improvement of metabolic flexibility in cHF+F+ROSI group may be connected to lower final body weight of mice in this group or to direct effects on muscle metabolism. The difference between lean and obese humans with respect to metabolic flexibility is known for many years (Kelley, Goodpaster et al. 1999); however, relatively small differences in final body weights of experimental animals would not probably improve metabolic flexibility and muscle metabolism to such an extent as was observed in this study. The observed differences in skeletal muscle metabolism induced by interventions were more intervention- than weight-dependent.

The connection of metabolic flexibility to mitochondrial muscle metabolism was described both at the level of mitochondrial enzyme activities (Kelley, He et al. 2002), (Kelley, Goodpaster et al. 1999), (van de Weijer, Sparks et al. 2013) and mitochondrial content assessed by electron microscopy (Kelley, Goodpaster et al. 1999), (Chomentowski, Coen et al. 2011).

There is a possibility to indirectly estimate mitochondrial function from plasma acylcarnitine levels. As was reported, acylcarnitines in plasma reflect mitochondrial β-oxidation (Ramos-Roman, Sweetman et al. 2012); however, this connection does not directly reflect acylcarnitines levels in discrete tissues (Schooneman, Achterkamp et al. 2014), and as such, acylcarnitines in plasma cannot be considered as markers of skeletal muscle mitochondrial function. To avoid confounding effect of a variety of tissues contributing to plasma acylcarnitine pool, we focused on acylcarnitine analysis from skeletal muscle extracts. We observed on skeletal muscle metabolomics analysis from STD re-fed mice that *n-3* LC PUFA facilitates mitochondrial β-oxidation of fatty acids assessed as acylcarnitine levels, as tight correlations between discrete acylcarnitine species were observed. On the other hand, combined intervention probably enhanced insulin sensitivity through another mechanism, by modulation of metabolism of branched-chain fatty acids (BCAA). BCAA and related metabolites are strongly associated with insulin resistance (Newgard 2012). TZDs were shown to increase insulin sensitivity through BCAA metabolism in WAT, with the impact on BCAA metabolism in WAT and the impact on BCAA levels and insulin sensitivity in the muscle (Newgard 2012).

To conclude, the combined use of *n-3* LC-PUFA and rosiglitazone preserves metabolic flexibility with an additive effect as compared to single interventions. This statement is supported by INCA measurement and targeted metabolomics from skeletal muscle extracts.

6.2 Publication B

Specific goal 2: to evaluate metabolic flexibility in both genders of C57BL/6N mice challenged by high-fat diet.

We focused in this study on a model of high-fat diet induced obesity with respect to gender differences and metabolic flexibility. As was described in section 4.2, female mice of C57BL/6N strain increased their body weight more than male mice during the time-course of experiment, e.g. 35 weeks after weaning. At this time-point mice reached rather advanced age of 10 months. With the phenotype of increased body weight gain were associated other metabolic parameters, such as increased weight of adipose depots (eWAT and scWAT) and increased mean size of adipocytes at week 35. On the other hand, up till week 15, male gained more weight, so our model of investigating two time-points, in which male and female mice differed in their body weight gains, was prospective in the expected differences between metabolic parameters in genders.

Moreover, male and female mice differed in their metabolic flexibility. They not only differed in response to fasting/re-feeding protocol, but also in their response to glucose load during IPGTT. Fasting/re-feeding protocol reveals differences in natural setting where both source of dietary intervention and circadian rhythm of feeding and rest are respected. IPGTT, on the other hand, allows for precise control of experimental conditions and outcomes. Male mice displayed lower metabolic flexibility to fasting/re-feeding protocol with respect to glucose plasma levels; and higher plasma glucose levels and strikingly higher plasma insulin levels during IPGTT. This corresponds to previously published data of Hevener et al. (Hevener, Reichart et al. 2002), who found that female mice are protected from lipid-induced reductions in insulin action. Macotela et al. (Macotela, Boucher et al. 2009) reported that there are differences in insulin sensitivity in adipose tissue, regulated by physiological levels of sex steroids. The increased sensitivity to insulin in female mice, also observed in this article, may account for their lower insulin resistance.

Female mice consistently showed much higher levels of adiponectin in plasma as compared to males, including the biologically active HMW form (Waki, Yamauchi et al. 2003). Higher adiponectin levels were not dependent on a dietary intervention or duration of HF feeding. These data correspond to data in publication D, where higher adiponectin levels in C57BL/6J female mice persisted both in fasted and refed state, even at a time of weaning. Kim et al. (Kim, van de et al. 2007) suggested that adiponectin is a peripheral signal promoting storage of TAG in adipose tissue. The consequently reduced levels of TAG in liver and muscle enhance insulin sensitivity. This system may be valid not only for genetically manipulated mice, but also for different physiological situations, such as gender differences. Higher adiponectin levels may be connected also to inflammation of adipose tissue, because Ohashi et al. (Ohashi, Parker et al. 2010) reported that adiponectin functions as a regulator of macrophage polarization and may protect organism by favoring anti-inflammatory phenotype in macrophages.

The important result of this experiment is the connection of metabolically healthy female phenotype with less inflamed white adipose tissue. High-fat feeding causes increased inflammation, as was observed in many studies. Striessel et al. (Strissel, Stancheva et al. 2007) followed mice during development of obesity and found that adipose tissue inflammation progressively increases during time-course of high-fat feeding, and after a period of 20 weeks, a complete reconstruction of highly inflamed tissue by a population of smaller adipocytes succeeds. We also observed progressive increase of inflammation of both WAT depots between week 15 and 35, nevertheless we were unable to confirm published dependence of inflammation on increasing adipocyte size, because male and female mice showed a reverse relationship between those two variables.

In female mice, the capacity for enlargement is increased and it probably reflects the higher insulin sensitivity of female adipocytes. This fact may correspond to study of Khan et al. (Khan, Muise et al. 2009), where weakened extracellular scaffold due to KO of collagen VI enabled expansion of adipocytes without adverse metabolic effects. There remains an unanswered question of different mechanical properties of adipose tissue between male and female mice.

Gender dependent differences in inflammation of adipose tissue have been published. Grove et al. (Grove, Fried et al. 2010) found using both microarray approach and immunohistochemical assessment of CLS that high-fat diet increased inflammatory response in males as compared with females. This effect is probably sex-hormones-dependent, because ovariectomized mice adipose tissue gene expression resemble more male one according to inflammatory genes abundance. However, in this study a shorter exposition to high-fat diet was used (12 weeks after weaning) and female mice displayed lower fat mass; the size of adipocytes tended to be smaller in eWAT and was significantly smaller in scWAT.

To conclude, metabolic flexibility to carbohydrates exhibited in female C57BL/6N mice fed cHF diet using two independent tests is connected to higher leptin and adiponectin levels and bigger adipocyte size together with lower insulin resistance and inflammation of eWAT and scWAT.

6.3 Publication C

Specific goal 3: to evaluate whole body energy homeostasis challenged by chenodeoxycholic acid, with respect to BAT and WAT metabolism.

In this publication we tried to explore the possible effect of CDCA on adipose tissue and whole-body energy homeostasis. Bile acids, including CDCA, are known general metabolic integrators. Watanabe et al. (Watanabe, Houten et al. 2006) in their article referred about effects of cholic acid on reversal of dietary obesity. They accounted this phenomenon to increased energy expenditure of cholic acid-treated mice.

In 8-week reversion experiment, we confirmed weight-reducing effects of another bile acid, CDCA. CDCA displayed dose-dependent effects on body weight in used concentration of 1% and 0.5%, as compared to previously mentioned work, where they used 0.5% cholic acid. Nevertheless, we were not able to fully confirm declared similarity in food intake between dietary groups. This fact can be accounted to different formulation of food intake data – whereas we presented food intake data per mouse, Watanabe et al. used normalization to body weight, therefore, effects that influenced both body weight and food intake might be masked by this approach.

In 3-week reversion experiment we further addressed a question of impact of lowered caloric intake. The included PF group confirmed the suspected food-intake-caused body weight reduction, as most of the effects on body weight, weights of WAT depots and other connected metabolic parameters were similar between 1% CDCA and PF group. Nevertheless, in the case of food-intake independent decrease of adiposity was revealed, it could be accounted to induction of UCP1 dependent thermogenesis. We confirmed increase of both UCP1 mRNA and UCP1 protein content in BAT, as only the information at mRNA level is not sufficient for evaluation of BAT thermogenic function (Nedergaard and Cannon 2013). Moreover, we were able to detect induction of brite cells in scWAT present mainly in CDCA group. These facts

together confirmed some, but not considerable, effects of CDCA on brown cell abundance and function.

Any important effect on either UCP1-dependent or independent thermogenesis would have been mirrored in whole-body energy homeostasis. We tried to confirm previously published increase of EE caused by treatment by bile acids (Watanabe, Houten et al. 2006). We evaluated energy homeostasis in the third week of 3-week reversion experiment. During this time, mice were stabilized in their body weights and their food intake almost returned to values observed in cHF group. At this time point, the possible effects of body weight loss and food intake reduction should had been minimized and the discreet effect of CDCA should be retrieved. We were able to confirm decrease of RQ values, reported by Watanabe et al. (Watanabe, Houten et al. 2006), indicating increased dependence on lipid oxidation caused by bile acids. This decrease was more pronounced during night-phase of the 24h measurement, in agreement with previously mentioned article. Pattern of RQ values, as described in chapter 5.3, was highly dependent on dietary delivery; however, data evaluated as mean RQ revealed that there was not a significant difference. In an attempt to search for a more sensitive approach for RQ evaluation, we employed PRCF curves of pooled RQ values (see also chapter 2.2.2). This approach is much more sensitive in revealing subtle differences in distribution of measured values and also gives information on metabolic flexibility, as the shallower is the PRCF curve, the bigger is metabolic flexibility. In this experiment, we were not able to confirm differences in metabolic flexibility from PRCF curves, but, on the other hand, PRCF curve informed us about higher reliance on carbohydrate or lipid oxidation in the case of cHF and 1%CDCA group, respectively.

When comparing EE, we explored two possible adjustments of energy expenditure, first adjustment per mice and then adjustment per body weight. In both cases, the important information was whether 1% CDCA and PF group with similar body weights would display any differences in EE that could be attributed to CDCA effect. Even though the relations of CDCA and PF to cHF group EE were inverse in those two possible evaluations, there was no effect on EE that could be accounted to CDCA.

To sum up, our data were not able to confirm previously reported effects of bile acids on energy homeostasis and the detected differences in induction of brown adipocyte´s abundance and function probably do not have major impact on whole-body metabolism.

6.4 Publication D

Specific goal 4: to evaluate several aspects of metabolic flexibility by using intraperitoneal and oral glucose tolerance tests, INCA tests using glucose bolus and fasted-re-feeding setup.

The aim of this study was to compare glucose tolerance tests as a measure of metabolic flexibility to carbohydrates with tests using indirect calorimetry protocols. As a model, we used metabolically healthy mice at the time of weaning. As a second aim of this study, we were searching for a predicting factor(s) that differs between mouse strains and could predict their future differences in susceptibility to obesity.

We defined metabolic flexibility to carbohydrates either as the ability to withdraw glucose from blood during glucose tolerance tests (the ability of cells to react to insulin by increasing their glucose uptake or decreasing gluconeogenesis) or as an ability to oxidize carbohydrates visualized by indirect calorimetry measurement.

Metabolic flexibility to glucose is in laboratory practice often assessed as answer to glucose load either in the form of intraperitoneal or oral glucose tolerance test (IPGTT and OGTT). The ability to switch from lipid oxidation during fasting to glucose oxidation after glucose load is analyzed from glucose concentrations before and several time-points after a glucose application.

Assessment of metabolic flexibility by indirect calorimetry measurement is widely used in human studies. Measurements obtained during euglycemic-hyperinsulinemic clamps or meal tests indicate changes of whole body substrate oxidation between fasted and insulin-stimulated or refed state. In contrary, in animal studies, assessment of metabolic flexibility by indirect calorimetry is rare. Equivalents of human meal tests combined with indirect calorimetry measurements are nevertheless occasionally used (Kus, Prazak et al. 2008). Introduction of more sensitive approaches for metabolic flexibility assessment would possibly increase our knowledge of metabolic flexibility of mice models of obesity.

In our study we aimed to define several possible variants of indirect calorimetry tests. Whereas glucose tolerance tests reveal information on glucose concentration in plasma, indirect calorimetry is able to directly measure the substrate switching ability of the mouse model. When we compared different indirect calorimetry protocols, the best choice was a test where the maximal concentration of glucose (7.5 mg of glucose per gram of body weight) was used under thermoneutral conditions and, as a consequence, the maximal response of metabolism was observed. In this setup, the rate of metabolic switch between lipids and carbohydrates was statistically different between mice strains used. Measurements in room temperature together with lower glucose dose used (2 mg of glucose per gram of body weight) are probably the reasons, why Duivenvoorde et al (Duivenvoorde, van Schothorst et al. 2015) were not able to detect any differences in RQ increase between adult and aged mice using a similar protocol.

To validate artificial tests using glucose loads, we compared those tests with indirect calorimetry measurement during more physiological fasted/refed transition. Similar to the changes in substrate switching during previously mentioned INCA measurements, different ability to increase RQ during dark phase of the measurement was observed. Both types of tests reveal information on metabolic flexibility; nevertheless, the fasting-refed transition may be confounded by possible different caloric intake under physiological non-restricted conditions.

When comparing both genders of the two mice strains used, A/J mice resistant to diet-induced obesity and C57BL/6J mice prone to diet-induced obesity, we observed distinct differences in their metabolic flexibility. A/J mice exhibited lower plasma glucose levels acquired during intraperitoneal and oral glucose tolerance tests, mainly in the tests with lower glucose dose used (1 mg of glucose per g of body weight). Even more importantly, they exhibited higher metabolic flexibility in indirect calorimetry test performed under thermoneutral conditions (at a dose of 7.5 mg of glucose per g of body weight). Therefore, A/J mice are probably more efficient in glucose uptake and oxidation than C57BL/6J mice. A/J mice also manifested faster increase of RQ after food delivery and higher RQ in the refed state. Nevertheless, the rate of RQ increase after food delivery may be biased by different feeding patterns of both mice strains. To avoid this effect, we adjusted RQ values to different caloric

intake; and RQ values in A/J mice remained higher even after this correlation. In comparison with A/J mice, C57BL/6J mice show higher glucose plasma levels during glucose tolerance tests and lower metabolic flexibility together with slow increase of RQ after food delivery. Our results are in good agreement with Haramizu et al, who reported that A/J in comparison with C57BL/6J mice exhibited higher RQ during running exercise, lower running endurance capacity and lower fatty acid oxidation in muscle (Haramizu, Nagasawa et al. 2009). Different substrate preference between strains may be explained on a cell level by higher reported Pdk4 mRNA in C57BL/6J as compared to A/J mice (Kondo, Minegishi et al. 2006). Pdk4 inhibits pyruvate dehydrogenase complex by phosphorylation, reducing the conversion of pyruvate, which is produced from the oxidation of glucose and amino acids, to acetyl-CoA and contributing to the regulation of glucose metabolism. Phenotype differences between strains may possibly underlie different susceptibility to obesity in both mice strains with metabolically less flexible C57BL/6J mice being more susceptible to later diet-induced obesity.

Our findings concerning different metabolic flexibility extend those of Hall et al. (Hall, Poussin et al. 2010) and Poussin et al. (Poussin, Ibberson et al. 2011), who detected differences between A/J and C57BL/6J mice at the level of fatty acid oxidation in liver. On a high-fat diet, A/J mice increase preferentially peroxisomal beta-oxidation, and C57BL/6J mice increase preferentially mitochondrial beta-oxidation (Hall, Poussin et al. 2010). When further evaluating data from the same experiment, Poussin et al. used time dependent gene set enrichment analysis that revealed upregulation of 13 oxidative phosphorylation genes after initiation of high-fat feeding in the A/J, but not in the C57BL/6, mice livers (Poussin, Ibberson et al. 2011). Biochemical analysis using liver mitochondria from both strains of mice confirmed a rapid increase in the respiration rate by high-fat diet feeding in A/J but not C57BL/6 mice (Poussin, Ibberson et al. 2011). ATP production was the same in both types of mitochondria, indicating increased uncoupling of the A/J mitochondria (Poussin, Ibberson et al. 2011). Thus, our finding that A/J mice when compared to C57BL/6J mice exhibit higher metabolic flexibility measured by glucose tolerance tests and indirect calorimetry protocols, is in good agreement with differences in metabolic flexibility assessed by expression of several metabolically important genes in liver in the study of Poussin et al. (Poussin, Ibberson et al. 2011).

Both mice strains also differed in plasma levels of important metabolites and adipokines. Concerning leptin, as we and Surwitt et al. (Surwit, Edwards et al. 2000) observed, leptin levels shortly after weaning are higher in A/J as compared with C57BL/6J mice, even though data published by Watson et al. (Watson, Commins et al. 2000) indicated no difference between A/J and C57BL/6J mice shortly after weaning. The reason for the differences in leptin plasma levels may be attributed to the different age of the mice. Until weaning, mice have higher fat intake both from their breeding diet and mother's milk, and because we have measured mice 1 day after weaning, their metabolism was probably still set to a higher level of fat intake. When we take into account only mice on a high-fat diet during adulthood, A/J mice displayed higher leptin levels than C57BL/6J mice in study of Watson et al. (Watson, Commins et al. 2000) and in a study of Hall et al. (Hall, Poussin et al. 2010). Watson et al. (Watson, Commins et al. 2000) proposed that a disproportionately higher leptin expression in A/J compared with C57BL/6J mice may lessen their energetic efficiency by increasing non-shivering thermogenesis. Also in a study of Kaiyala et al. (Kaiyala and Schwartz 2011) leptin levels were connected with energy expenditure. Kaiyala et al. observed unexpectedly large effect of FM as a determinant of murine EE, with the influence of each gram of FM equaling cca 50% of the per-gram influence of LBM (Kaiyala and Schwartz 2011). FM may influence EE at least in part via changes of circulating leptin levels, as was exemplified by treatment of ob/ob mice with leptin and EE evaluation in this state. Nevertheless, in our study, higher leptin levels in A/J mice were not connected with higher energy expenditure in these animals. Higher leptin levels in A/J mice may be explained by reported higher fat mass in adult A/J as compared with C57BL/6J mice (significant only in males, (Gallou-Kabani, Vige et al. 2007)), but there is a lack of information on body composition of mice pups at the time of weaning. The difference in leptin plasma levels may be also explained by reported adipocyte hypertrophy in A/J mice in response to high-fat diet feeding, while C57BL/6J mice respond with adipocyte hyperplasia. This hyperplasia is most apparent in mesenteric adipose tissue, although it occurs to a lesser extent in gonadal tissue as well (Surwit, Feinglos et al. 1995).

As for adiponectin, its plasma levels are reported to be lower in A/J mice (as seen also in (Bullen, Bluher et al. 2007)). Lower adiponectin levels in A/J mice in our study could be

explained by higher energy intake in these mice during re-feeding, as it was reported that energy intake, but not dietary fat, plays an important role in maintaining blood adiponectin levels in mice (Qiao, Lee et al. 2011). Also, adiponectin is assumed to increase fatty acid oxidation in liver and skeletal muscle and through AMPK axis it may increase energy expenditure (Yamauchi, Kamon et al. 2002), but although C57BL/6J mice exhibited higher adiponectin plasma level, their energy expenditure did not differ from A/J mice. On the other hand, increased fatty acid oxidation caused by higher adiponectin levels in blood would be represented by lower RQ values, as was observed in our experiments in the case of C57BL/6J mice. This observation supports supposed effect of adiponectin on fatty acid oxidation increase.

To conclude, different glucose tolerance and indirect calorimetry tests were validated on A/J and C57BL/6J mice pups. The tests differ in their ability to detect metabolic flexibility differences. The most informative tests were oral and intraperitoneal glucose tolerance tests at a dose of 1 mg of glucose per gram of body weight and analogous INCA measurement using orally administered dose of 7.5 mg of glucose per gram of body weight performed at thermoneutrality, and fasted/refed measurement at thermoneutrality. When comparing both genders of the two mice strains, we propose that C57BL6/J mice, prone to high-fat-diet induced obesity, have a lower ability to switch between metabolic substrates and are not able to fully utilize glucose from blood, whereas A/J mice, resistant to high-fat-induced obesity, have a higher ability to switch to carbohydrate utilization and have lower glucose levels.

6.5 Publication E

Specific goal 5: to evaluate metabolic flexibility as a reaction metabolism to short-term cold exposure.

After cold exposure, thermogenic capacity of BAT non-shivering thermogenesis is insufficient to maintain body core temperature, thus heat must be generated by other sources, mainly by shivering. Thermogenic capacity of BAT gradually increases and after approximately 1 month of cold exposure it reaches its maximum. We employed a model of short-term cold exposure of 2 and 7 days, when metabolism starts to cope with cold-induced stress and pronounced alterations of BAT and WAT metabolism are suspected.

The principal finding of this study is induction of FA and TAG synthesis during cold-induced lipolysis in eWAT in obesity-resistant A/J mice. The results indicate a high rate of futile TAG/FA cycling in this intraabdominal depot under cold-stress conditions. Futile cycle is composed of two opposite metabolic pathways running simultaneously, which dissipate of energy in the form of heat. Futile cycle is sensitive to small changes in the activity of appropriate enzymes and allows for fine and fast tuning of FA release into circulation as well as for buffering of intracellular FA levels. Under stimulation of lipolysis, FA are detoxified by re-esterification into micro lipid droplets (Hashimoto, Segawa et al. 2012). We observed high stimulation of lipolysis mainly in A/J mice in the form of higher decrease in eWAT weight, increase of *Atgl* mRNA and ATGL immunostaining, as well as in the form of histologically determined adipocytes containing many lipid droplets. The process of re-esterification after cold stimulus confirmed by two independent methods is accompanied by increased *Dgat1* mRNA and DGAT1 immunostaining.

Resistance to obesity in A/J mice is accompanied only by higher re-esterification levels. Moreover, A/J mice responded to cold exposure by a decrease in leptin levels, with leptin being crucial for both UCP1-dependent (Commins, Watson et al. 1999) and –independent thermogenesis (Ukropec, Anunciado et al. 2006) in adipose tissue and skeletal muscle. Leptin

influences PEPC-K and through this pathway decreases glyceroneogenesis and FA re-esterification. Thus, leptin may be important metabolic signal to influence WAT metabolism.

To sum up, TAG/FA re-esterification represents important metabolic cycle, which may influence flexibility of FA supply under severe metabolic stress. This cycle is more pronounced in A/J as compared to B6 mice, in accordance with phenotype of resistance to high-fat induced phenotype.

7 Conclusions

Following conclusions could be made, corresponding to the specific aims of the thesis:

1. Whole-body metabolic flexibility assessment of *n-3* LC-PUFA and/or rosiglitazone treated mice revealed highest metabolic flexibility in a combination group. The method of evaluation – comparison of RQ from fasted and standard-diet-refed mice – is highly sensitive in revealing subtle differences in metabolic regulations.

2. Whole-body metabolic flexibility assessment of male and female C57BL/6N mice revealed that male mice challenged by high-fat diet display not only decreased metabolic flexibility with respect to glucose levels between fasted and re-fed state, but also highest metabolic disturbances in the form of high TAG levels in liver and inflammation in adipose tissue depots. The method of evaluation – comparison of physiologically relevant fasted and re-fed plasma metabolites – is superior to metabolic flexibility assessment by glucose tolerance tests.

3. Whole body energy homeostasis in mice challenged by chenodeoxycholic acid was revealed by evaluation of energy expenditure under ad-libitum or pair-fed conditions. Chenodeoxycholic acid treatment did not reveal any significant effect on energy homeostasis as compared to pair-fed group. The method of assessment – INCA measurement under ad-libitum or pair-fed conditions - is sensitive enough to reveal differences in energy expenditure; nevertheless, a negative result was obtained.

4. Whole body energy homeostasis was evaluated by several possible ways on pups of A/J and C57BL/6J mice at a time of weaning. Both glucose tolerance tests and INCA measurements under different conditions indicated higher metabolic flexibility of obesity-resistant A/J mice. The most beneficial assessments are oral glucose tolerance test using 1 mg glucose/g BW and INCA using glucose bolus 7.5 mg/g BW at thermoneutrality.

5. Whole body energy metabolism was influenced by cold exposure of A/J and C57BL/6J mice for 2 or 7 days. The reaction of WAT to severe metabolic stress indicated higher flexibility of WAT depots from A/J mice including higher re-esterification.

8 List of all publications

8.1 Publication A

Horakova O, Medrikova D, van Schothorst EM, Bunschoten A, Flachs P, Kus V, Kuda O, **Bardova K**, Janovska P, Hensler M, Rossmeisl M, Wang-Sattler R, Prehn C, Adamski J, Illig T, Keijer J, Kopecky J. *Preservation of metabolic flexibility in skeletal muscle by a combined use of n-3 PUFA and rosiglitazone in dietary obese mice.*

PLoS One, 2012, Vol. 7,8 :e43764, IF = 3.73

My personal contribution to this work includes participation on the accomplishment of experiments, and participation on metabolic flexibility and INCA analyses.

8.2 Publication B

Medrikova D, Jilkova ZM, **Bardova K**, Janovska P, Rossmeisl M, Kopecky J. *Sex differences during the course of diet-induced obesity in mice: adipose tissue expandability and glycemic control.*

International Journal of Obesity, 2012, Vol. 36, 2, p. 262-72. IF = 5.386

My personal contribution to this work includes participation on the accomplishment of experiments, and participation on metabolic flexibility and histological and immunohistochemical analyses.

8.3 Publication C

Teodoro JS*, Zouhar P*, Flachs P, **Bardova K**, Janovska P, Gomes AP, Duarte FV, Varela AT, Rolo AP, Palmeira CM, Kopecký J. *Enhancement of brown fat thermogenesis using chenodeoxycholic acid in mice.*

International Journal of Obesity, 2012, Vol. 38, 2, p. 216-223. IF = 5.386

* These authors contributed equally to this work.

My personal contribution to this publication includes participation on the accomplishment of experiments, accomplishment of INCA and histological and immunohistochemical analyses including statistical analysis.

8.4 Publication D

Bardova K, Horakova O, Janovska P, Hansikova J, Kus V, van Schothorst EM, Hoevenaars F, Uil M, Hensler M, Keijer J, Kopecky J. *Early differences in metabolic flexibility between obesity-resistant and obesity-prone mice.*
Biochimie, 2016, (Epub ahead of print), doi: 10.1016. IF = 2.963

My personal contribution to this publication includes planning all of the experiments, performing them, analyzing the data including statistical analyses, and writing the manuscript.

8.5 Publication E

Flachs P, Jones JG, Zouhar P, Adamcova K, Svobodova M, **Bardova K**, Janovska P, Hansikova J, Liisberg U, Keenan A, Madsen L, Kristiansen K and Kopecky J, *Induction of triacylglycerol/fatty acid futile cycling in white adipose tissue during cold exposure is linked to obesity-resistance in mice*

International Journal of Obesity, IF = 5.386, publication under preparation

My personal contribution to this publication includes participation in planning of the experiments, performing them and histological and immunohistochemical analyses.

9 Reference list

Abreu-Vieira, G., C. E. Hagberg, K. L. Spalding, B. Cannon and J. Nedergaard (2015). "Adrenergically stimulated blood flow in brown adipose tissue is not dependent on thermogenesis." Am J Physiol Endocrinol Metab **308**(9): E822-829.

Alberts, P., B. G. Johansson and R. A. McArthur (2005). Measurement and characterization of energy expenditure as a tool in the development of drugs for metabolic diseases, such as obesity and diabetes Current protocols in pharmacology. S. J. Enna, M. Williams, J. W. Ferkany et al., John Wiley and Sons, Inc.**:** 1-15.

Amano, S. U., J. L. Cohen, P. Vangala, M. Tencerova, S. M. Nicoloro, J. C. Yawe, Y. Shen, M. P. Czech and M. Aouadi (2014). "Local proliferation of macrophages contributes to obesity-associated adipose tissue inflammation." Cell Metab **19**(1): 162-171.

Andrikopoulos, S., A. R. Blair, N. Deluca, B. C. Fam and J. Proietto (2008). "Evaluating the glucose tolerance test in mice." Am J Physiol Endocrinol Metab **295**(6): E1323-1332.

Arch, J. R. S., D. Hislop, S. J. Y. Wang and J. R. Speakman (2006). "Some mathematical and technical issues in the measurement and interpretation of open-circuit indirect calorimetry in small animals." International Journal of Obesity **30**(9): 1322-1331.

Baggio, L. L. and D. J. Drucker (2007). "Biology of incretins: GLP-1 and GIP." Gastroenterology **132**(6): 2131-2157.

Barbatelli, G., I. Murano, L. Madsen, Q. Hao, M. Jimenez, K. Kristiansen, J. P. Giacobino, R. De Matteis and S. Cinti (2010). "The emergence of cold-induced brown adipocytes in mouse white fat depots is determined predominantly by white to brown adipocyte transdifferentiation." Am J Physiol Endocrinol Metab **298**(6): E1244-1253.

Bartness, T. J., Y. B. Shrestha, C. H. Vaughan, G. J. Schwartz and C. K. Song (2010). "Sensory and sympathetic nervous system control of white adipose tissue lipolysis." Mol Cell Endocrinol **318**(1-2): 34-43.

Bruss, M. D., C. F. Khambatta, M. A. Ruby, I. Aggarwal and M. K. Hellerstein (2010). "Calorie restriction increases fatty acid synthesis and whole body fat oxidation rates." Am.J.Physiol Endocrinol.Metab **298**(1): E108-E116.

Bullen, J. W., Jr., S. Bluher, T. Kelesidis and C. S. Mantzoros (2007). "Regulation of adiponectin and its receptors in response to development of diet-induced obesity in mice." Am J Physiol Endocrinol Metab **292**(4): E1079-1086.

Burnett, C. M. and J. L. Grobe (2014). "Dietary effects on resting metabolic rate in C57BL/6 mice are differentially detected by indirect (O2/CO2 respirometry) and direct calorimetry." Mol Metab **3**(4): 460-464.

Butler, A. A. and L. P. Kozak (2010). "A recurring problem with the analysis of energy expenditure in genetic models expressing lean and obese phenotypes." Diabetes **59**(2): 323-329.

Cannon, B. and J. Nedergaard (2004). "Brown adipose tissue: function and physiological significance." Physiol Rev. **84**(1): 277-359.

Cannon, B. and J. Nedergaard (2011). "Nonshivering thermogenesis and its adequate measurement in metabolic studies." J Exp Biol **214**(Pt 2): 242-253.

Carriere, A., Y. Jeanson, S. Berger-Muller, M. Andre, V. Chenouard, E. Arnaud, C. Barreau, R. Walther, A. Galinier, B. Wdziekonski, P. Villageois, K. Louche, P. Collas, C. Moro, C. Dani, F. Villarroya and L. Casteilla (2014). "Browning of white adipose cells by intermediate metabolites: an adaptive mechanism to alleviate redox pressure." Diabetes **63**(10): 3253-3265.

Celi, F. S. (2009). "Brown adipose tissue--when it pays to be inefficient." N Engl J Med **360**(15): 1553-1556.

Chomentowski, P., P. M. Coen, Z. Radikova, B. H. Goodpaster and F. G. Toledo (2011). "Skeletal muscle mitochondria in insulin resistance: differences in intermyofibrillar versus subsarcolemmal subpopulations and relationship to metabolic flexibility." J Clin Endocrinol Metab **96**(2): 494-503.

Cinti, S. (2006). "Morphology of the inflammatory state of the adipose organ in obese mice and human." Obesity and Metabolism **2** (2): 95-103.

Cinti, S. (2009). "Transdifferentiation properties of adipocytes in the adipose organ." Am J Physiol Endocrinol Metab **297**(5): E977-986.

Cinti, S., G. Mitchell, G. Barbatelli, I. Murano, E. Ceresi, E. Faloia, S. Wang, M. Fortier, A. S. Greenberg and M. S. Obin (2005). "Adipocyte death defines macrophage localization and function in adipose tissue of obese mice and humans." J Lipid Res. **46**(11): 2347-2355.

Collins, S., E. Yehuda-Shnaidman and H. Wang (2010). "Positive and negative control of Ucp1 gene transcription and the role of beta-adrenergic signaling networks." Int J Obes (Lond) **34 Suppl 1**: S28-33.

Commins, S. P., P. M. Watson, M. A. Padgett, A. udley, G. gyropulos and T. W. ttys (1999). "Induction of uncoupling protein expression in brown and white adipose tissue by leptin." Endocrinology **140**(1): 292-300.

Corvera, S. and O. Gealekman (2014). "Adipose tissue angiogenesis: impact on obesity and type-2 diabetes." Biochim Biophys Acta **1842**(3): 463-472.

Cypess, A. M., S. Lehman, G. Williams, I. Tal, D. Rodman, A. B. Goldfine, F. C. Kuo, E. L. Palmer, Y. Tseng, A. Doria, G. M. Kolodny and C. R. Kahn (2009). "Identification and Importance of Brown Adipose Tissue in Adult Humans." New England Journal of Medicine **360**(15): 1509-1517.

Duivenvoorde, L. P., E. M. van Schothorst, H. J. Swarts and J. Keijer (2015). "Assessment of metabolic flexibility of old and adult mice using three noninvasive, indirect calorimetry-based treatments." J Gerontol A Biol Sci Med Sci **70**(3): 282-293.

Elia, M. and G. Livesey (1988). "Theory and validity of indirect calorimetry during net lipid synthesis." Am J Clin Nutr **47**(4): 591-607.

Enerback, S., A. Jacobsson, E. M. Simpson, C. Guerra, H. Yamashita, M. E. Harper and L. P. Kozak (1997). "Mice lacking mitochondrial uncoupling protein are cold-sensitive but not obese." Nature **387**: 90-94.

Even, P. C., A. Mokhtarian and A. Pele (1994). "Practical aspects of indirect calorimetry in laboratory animals." Neurosci Biobehav Rev **18**(3): 435-447.

Even, P. C. and N. A. Nadkarni (2012). "Indirect calorimetry in laboratory mice and rats: principles, practical considerations, interpretation and perspectives." Am J Physiol Regul.Integr.Comp Physiol **303**(5): R459-R476.

Ferrannini, E. (1988). "The theoretical bases of indirect calorimetry: a review." Metabolism **37**(3): 287-301.

Fromme, T. and M. Klingenspor (2011). "Uncoupling protein 1 expression and high-fat diets." Am J Physiol Regul Integr Comp Physiol **300**(1): R1-8.

Frontini, A., A. Giordano and S. Cinti (2012). "Endothelial cells of adipose tissues: a niche of adipogenesis." Cell Cycle **11**(15): 2765-2766.

Frontini, A., A. Vitali, J. Perugini, I. Murano, C. Romiti, D. Ricquier, M. Guerrieri and S. Cinti (2013). "White-to-brown transdifferentiation of omental adipocytes in patients affected by pheochromocytoma." Biochim Biophys Acta **1831**(5): 950-959.

Fujisaka, S., I. Usui, A. Bukhari, M. Ikutani, T. Oya, Y. Kanatani, K. Tsuneyama, Y. Nagai, K. Takatsu, M. Urakaze, M. Kobayashi and K. Tobe (2009). "Regulatory mechanisms for adipose tissue M1 and M2 macrophages in diet-induced obese mice." Diabetes **58**(11): 2574-2582.

Galgani, J. E., C. Moro and E. Ravussin (2008). "Metabolic flexibility and insulin resistance." Am J Physiol Endocrinol Metab **295**(5): E1009-1017.

Gallou-Kabani, C., A. Vige, M. S. Gross, J. P. Rabes, C. Boileau, C. Larue-Achagiotis, D. Tome, J. P. Jais and C. Junien (2007). "C57BL/6J and A/J mice fed a high-fat diet delineate components of metabolic syndrome." Obesity (Silver.Spring) **15**(8): 1996-2005.

Giordano, A., A. Frontini, I. Murano, C. Tonello, M. A. Marino, M. O. Carruba, E. Nisoli and S. Cinti (2005). "Regional-dependent increase of sympathetic innervation in rat white adipose tissue during prolonged fasting." J Histochem Cytochem **53**(6): 679-687.

Giordano, A., I. Murano, E. Mondini, J. Perugini, A. Smorlesi, I. Severi, R. Barazzoni, P. E. Scherer and S. Cinti (2013). "Obese adipocytes show ultrastructural features of stressed cells and die of pyroptosis." J Lipid Res **54**(9): 2423-2436.

Giordano, A., A. Smorlesi, A. Frontini, G. Barbatelli and S. Cinti (2014). "White, brown and pink adipocytes: the extraordinary plasticity of the adipose organ." Eur J Endocrinol **170**(5): R159-171.

Golozoubova, V., B. Cannon and J. Nedergaard (2006). "UCP1 is essential for adaptive adrenergic nonshivering thermogenesis." Am J Physiol Endocrinol Metab **291**(2): E350-357.

Grove, K. L., S. K. Fried, A. S. Greenberg, X. Q. Xiao and D. J. Clegg (2010). "A microarray analysis of sexual dimorphism of adipose tissues in high-fat-diet-induced obese mice." Int.J.Obes.(Lond) **34**(6): 989-1000.

Haase, J., U. Weyer, K. Immig, N. Kloting, M. Bluher, J. Eilers, I. Bechmann and M. Gericke (2014). "Local proliferation of macrophages in adipose tissue during obesity-induced inflammation." Diabetologia **57**(3): 562-571.

Hall, D., C. Poussin, V. R. Velagapudi, C. Empsen, M. Joffraud, J. S. Beckmann, A. E. Geerts, Y. Ravussin, M. Ibberson, M. Oresic and B. Thorens (2010). "Peroxisomal and microsomal lipid pathways associated with resistance to hepatic steatosis and reduced pro-inflammatory state." J Biol Chem **285**(40): 31011-31023.

Haramizu, S., A. Nagasawa, N. Ota, T. Hase, I. Tokimitsu and T. Murase (2009). "Different contribution of muscle and liver lipid metabolism to endurance capacity and obesity susceptibility of mice." J. Appl. Physiol. **106**(3): 871-879.

Harris, C. A., J. T. Haas, R. S. Streeper, S. J. Stone, M. Kumari, K. Yang, X. Han, N. Brownell, R. W. Gross, R. Zechner and R. V. Farese, Jr. (2011). "DGAT enzymes are required for triacylglycerol synthesis and lipid droplets in adipocytes." J Lipid Res **52**(4): 657-667.

Hashimoto, T., H. Segawa, M. Okuno, H. Kano, H. O. Hamaguchi, T. Haraguchi, Y. Hiraoka, S. Hasui, T. Yamaguchi, F. Hirose and T. Osumi (2012). "Active involvement of micro-lipid droplets and lipid-droplet-associated proteins in hormone-stimulated lipolysis in adipocytes." J Cell Sci **125**(Pt 24): 6127-6136.

Heldmaier, G. (1975). "The effect of short daily cold exposures on development of brown adipose tissue in mice." J.Comp.Physiol. 98: 161-168.

Hevener, A., D. Reichart, A. Janez and J. Olefsky (2002). "Female rats do not exhibit free fatty acid-induced insulin resistance." Diabetes **51**(6): 1907-1912.

Himms-Hagen, J., A. Melnyk, M. C. Zingaretti, E. Ceresi, G. Barbatelli and S. Cinti (2000). "Multilocular fat cells in WAT of CL-316243-treated rats derive directly from white adipocytes." Am.J.Physiol Cell Physiol **279**(3): C670-C681.

Hue, L. and H. Taegtmeyer (2009). "The Randle cycle revisited: a new head for an old hat." Am.J.Physiol Endocrinol.Metab **297**(3): E578-E591.

Jo, J., O. Gavrilova, S. Pack, W. Jou, S. Mullen, A. E. Sumner, S. W. Cushman and V. Periwal (2009). "Hypertrophy and/or Hyperplasia: Dynamics of Adipose Tissue Growth." PLoS Comput Biol **5**(3): e1000324.

Joe, A. W., L. Yi, Y. Even, A. W. Vogl and F. M. Rossi (2009). "Depot-specific differences in adipogenic progenitor abundance and proliferative response to high-fat diet." Stem Cells **27**(10): 2563-2570.

Kaiyala, K. J., G. J. Morton, B. G. Leroux, K. Ogimoto, B. Wisse and M. W. Schwartz (2010). "Identification of body fat mass as a major determinant of metabolic rate in mice." Diabetes **59**(7): 1657-1666.

Kaiyala, K. J. and D. S. Ramsay (2011). "Direct animal calorimetry, the underused gold standard for quantifying the fire of life." Comp Biochem Physiol A Mol Integr Physiol **158**(3): 252-264.

Kaiyala, K. J. and M. W. Schwartz (2011). "Toward a more complete (and less controversial) understanding of energy expenditure and its role in obesity pathogenesis." Diabetes **60**(1): 17-23.

Kajimura, S., P. Seale, K. Kubota, E. Lunsford, J. V. Frangioni, S. P. Gygi and B. M. Spiegelman (2009). "Initiation of myoblast to brown fat switch by a PRDM16-C/EBP-beta transcriptional complex." Nature **460**(7259): 1154-1158.

Karpe, F., J. R. Dickmann and K. N. Frayn (2011). "Fatty acids, obesity, and insulin resistance: time for a reevaluation." Diabetes **60**(10): 2441-2449.

Kelley, D. E., B. Goodpaster, R. R. Wing and J. A. Simoneau (1999). "Skeletal muscle fatty acid metabolism in association with insulin resistance, obesity, and weight loss." American Journal of Physiology-Endocrinology and Metabolism **277**(6): E1130-E1141.

Kelley, D. E., J. He, E. V. Menshikova and V. B. Ritov (2002). "Dysfunction of mitochondria in human skeletal muscle in type 2 diabetes." Diabetes **51**(10): 2944-2950.

Kelley, D. E. and L. J. Mandarino (2000). "Fuel selection in human skeletal muscle in insulin resistance: a reexamination." Diabetes **49**(5): 677-683.

Khan, T., E. S. Muise, P. Iyengar, Z. V. Wang, M. Chandalia, N. Abate, B. B. Zhang, P. Bonaldo, S. Chua and P. E. Scherer (2009). "Metabolic dysregulation and adipose tissue fibrosis: role of collagen VI." Mol.Cell Biol. **29**(6): 1575-1591.

Kim, J. Y., W. E. van de, M. Laplante, A. Azzara, M. E. Trujillo, S. M. Hofmann, T. Schraw, J. L. Durand, H. Li, G. Li, L. A. Jelicks, M. F. Mehler, D. Y. Hui, Y. Deshaies, G. I. Shulman, G. J. Schwartz and P. E. Scherer (2007). "Obesity-associated improvements in metabolic profile through expansion of adipose tissue." J Clin.Invest **117**(9): 2621-2637.

Kondo, H., Y. Minegishi, Y. Komine, T. Mori, I. Matsumoto, K. Abe, I. Tokimitsu, T. Hase and T. Murase (2006). "Differential regulation of intestinal lipid metabolism-related genes in obesity-resistant A/J vs. obesity-prone C57BL/6J mice." Am J Physiol Endocrinol.Metab **291**(5): E1092-E1099.

Kozak, L. P., R. A. Koza, R. Anunciado-Koza, T. Mendoza and S. Newman (2012). "Inherent plasticity of brown adipogenesis in white fat of mice allows for recovery from effects of post-natal malnutrition." Plos One **7**(2): e30392.

Kuda, O., T. Jelenik, Z. Jilkova, P. Flachs, M. Rossmeisl, M. Hensler, L. Kazdova, N. Ogston, M. Baranowski, J. Gorski, P. Janovska, V. Kus, J. Polak, V. Mohamed-Ali, R. Burcelin, S. Cinti, M. Bryhn and J. Kopecky (2009). "n-3 Fatty acids and rosiglitazone improve insulin sensitivity through additive stimulatory effects on muscle glycogen synthesis in mice fed a high-fat diet." Diabetologia **52**(5): 941-951.

Kus, V., T. Prazak, P. Brauner, M. Hensler, O. Kuda, P. Flachs, P. Janovska, D. Medrikova, M. Rossmeisl, Z. Jilkova, B. Stefl, E. Pastalkova, Z. Drahota, J. Houstek and J. Kopecky (2008). "Induction of muscle thermogenesis by high-fat diet in mice: association with obesity-resistance." Am J Physiol Endocrinol Metab **295**(2): E356-367.

Lasar, D., A. Julius, T. Fromme and M. Klingenspor (2013). "Browning attenuates murine white adipose tissue expansion during postnatal development." Biochim.Biophys.Acta **1831**(5): 960-968.

Lee, M. J., Y. Wu and S. K. Fried (2012). "Adipose tissue heterogeneity: Implication of depot differences in adipose tissue for obesity complications." Mol.Aspects Med.

Lee, Y. H., A. P. Petkova, A. A. Konkar and J. G. Granneman (2015). "Cellular origins of cold-induced brown adipocytes in adult mice." FASEB J **29**(1): 286-299.

Li, P., Z. Zhu, Y. Lu and J. G. Granneman (2005). "Metabolic and cellular plasticity in white adipose tissue II: role of peroxisome proliferator-activated receptor-alpha." Am J Physiol Endocrinol Metab **289**(4): E617-E626.

Livesey, G. and M. Elia (1988). "Estimation of energy expenditure, net carbohydrate utilization, and net fat oxidation and synthesis by indirect calorimetry: evaluation of errors with special reference to the detailed composition of fuels." Am J Clin Nutr **47**(4): 608-628.

Longo, K. A., S. Charoenthongtrakul, D. J. Giuliana, E. K. Govek, T. McDonagh, P. S. Distefano and B. J. Geddes (2010). "The 24-hour respiratory quotient predicts energy intake and changes in body mass." Am J Physiol Regul Integr Comp Physiol **298**(3): R747-754.

Ma, X., P. Lee, D. J. Chisholm and D. E. James (2015). "Control of adipocyte differentiation in different fat depots; implications for pathophysiology or therapy." Front Endocrinol (Lausanne) **6**: 1.

Macotela, Y., J. Boucher, T. T. Tran and C. R. Kahn (2009). "Sex and depot differences in adipocyte insulin sensitivity and glucose metabolism." Diabetes **58**(4): 803-812.

McLaughlin, T., A. Deng, G. Yee, C. Lamendola, G. Reaven, P. S. Tsao, S. W. Cushman and A. Sherman (2010). "Inflammation in subcutaneous adipose tissue: relationship to adipose cell size." Diabetologia **53**(2): 369-377.

Morris, D. L., K. W. Cho, J. L. Delproposto, K. E. Oatmen, L. M. Geletka, G. Martinez-Santibanez, K. Singer and C. N. Lumeng (2013). "Adipose tissue macrophages function as antigen-presenting cells and regulate adipose tissue CD4+ T cells in mice." Diabetes **62**(8): 2762-2772.

Mottillo, E. P., P. Balasubramanian, Y. H. Lee, C. Weng, E. E. Kershaw and J. G. Granneman (2014). "Coupling of lipolysis and de novo lipogenesis in brown, beige, and white adipose tissues during chronic beta3-adrenergic receptor activation." J Lipid Res **55**(11): 2276-2286.

Murano, I., G. Barbatelli, A. Giordano and S. Cinti (2009). "Noradrenergic parenchymal nerve fiber branching after cold acclimatisation correlates with brown adipocyte density in mouse adipose organ." J Anat **214**(1): 171-178.

Murano, I., J. M. Rutkowski, Q. A. Wang, Y. R. Cho, P. E. Scherer and S. Cinti (2013). "Time course of histomorphological changes in adipose tissue upon acute lipoatrophy." Nutr Metab Cardiovasc Dis **23**(8): 723-731.

Naukkarinen, J., S. Heinonen, A. Hakkarainen, J. Lundbom, K. Vuolteenaho, L. Saarinen, S. Hautaniemi, A. Rodriguez, G. Fruhbeck, P. Pajunen, T. Hyotylainen, M. Oresic, E. Moilanen, A. Suomalainen, N. Lundbom, J. Kaprio, A. Rissanen and K. H. Pietilainen (2014). "Characterising metabolically healthy obesity in weight-discordant monozygotic twins." Diabetologia **57**(1): 167-176.

Nedergaard, J. and B. Cannon (2013). "UCP1 mRNA does not produce heat." Biochimica et Biophysica Acta.

Newgard, C. B. (2012). "Interplay between Lipids and Branched-Chain Amino Acids in Development of Insulin Resistance." Cell Metab **15**(5): 606-614.

Nishimura, S., I. Manabe, M. Nagasaki, Y. Hosoya, H. Yamashita, H. Fujita, M. Ohsugi, K. Tobe, T. Kadowaki, R. Nagai and S. Sugiura (2007). "Adipogenesis in obesity requires close interplay between differentiating adipocytes, stromal cells, and blood vessels." Diabetes **56**(6): 1517-1526.

Ohashi, K., J. L. Parker, N. Ouchi, A. Higuchi, J. A. Vita, N. Gokce, A. A. Pedersen, C. Kalthoff, S. Tullin, A. Sams, R. Summer and K. Walsh (2010). "Adiponectin promotes macrophage polarization toward an anti-inflammatory phenotype." Journal of Biological Chemistry **285**(9): 6153-6160.

Poussin, C., M. Ibberson, D. Hall, J. Ding, J. Soto, E. D. Abel and B. Thorens (2011). "Oxidative phosphorylation flexibility in the liver of mice resistant to high-fat diet-induced hepatic steatosis." Diabetes **60**(9): 2216-2224.

Qiao, L., B. Lee, B. Kinney, H. S. Yoo and J. Shao (2011). "Energy Intake and Adiponectin Gene Expression." Am.J.Physiol Endocrinol.Metab **300**(5): E809-816.

Ramos-Roman, M. A., L. Sweetman, M. J. Valdez and E. J. Parks (2012). "Postprandial changes in plasma acylcarnitine concentrations as markers of fatty acid flux in overweight and obesity." Metabolism **61**(2): 202-212.

Reshef, L., Y. Olswang, H. Cassuto, B. Blum, C. M. Croniger, S. C. Kalhan, S. M. Tilghman and R. W. Hanson (2003). "Glyceroneogenesis and the triglyceride/fatty acid cycle." Journal of Biological Chemistry **278**(33): 30413-30416.

Riachi, M., J. Himms-Hagen and M. E. Harper (2004). "Percent relative cumulative frequency analysis in indirect calorimetry: application to studies of transgenic mice." Can.J Physiol Pharmacol. **82**(12): 1075-1083.

Rosenwald, M., A. Perdikari, T. Rulicke and C. Wolfrum (2013). "Bi-directional interconversion of brite and white adipocytes." Nat Cell Biol **15**(6): 659-667.

Sanchez-Gurmaches, J. and D. A. Guertin (2014). "Adipocyte lineages: tracing back the origins of fat." Biochim Biophys Acta **1842**(3): 340-351.

Schooneman, M. G., N. Achterkamp, C. A. Argmann, M. R. Soeters and S. M. Houten (2014). "Plasma acylcarnitines inadequately reflect tissue acylcarnitine metabolism." Biochim Biophys Acta.

Shaham, O., R. Wei, T. J. Wang, C. Ricciardi, G. D. Lewis, R. S. Vasan, S. A. Carr, R. Thadhani, R. E. Gerszten and V. K. Mootha (2008). "Metabolic profiling of the human response to a glucose challenge reveals distinct axes of insulin sensitivity." Mol Syst Biol **4**: 214.

Shi, Y. and D. Cheng (2009). "Beyond triglyceride synthesis: the dynamic functional roles of MGAT and DGAT enzymes in energy metabolism." Am J Physiol Endocrinol Metab **297**(1): E10-18.

Simonson, D. C. and R. A. DeFronzo (1990). "Indirect calorimetry: methodological and interpretative problems." Am J Physiol **258**(3 Pt 1): E399-412.

Smorlesi, A., A. Frontini, A. Giordano and S. Cinti (2012). "The adipose organ: white-brown adipocyte plasticity and metabolic inflammation." Obes.Rev. **13 Suppl 2**: 83-96.

Spalding, K. L., E. Arner, P. O. Westermark, S. Bernard, B. A. Buchholz, O. Bergmann, L. Blomqvist, J. Hoffstedt, E. Naslund, T. Britton, H. Concha, M. Hassan, M. Ryden, J. Frisen and P. Arner (2008). "Dynamics of fat cell turnover in humans." Nature **453**(7196): 783-787.

Sparks, L. M., M. Pasarica, O. Sereda, L. deJonge, S. Thomas, H. Loggins, H. Xie, J. M. Miles and S. R. Smith (2009). "Effect of adipose tissue on the sexual dimorphism in metabolic flexibility." Metabolism **58**(11): 1564-1571.

Storlien, L., N. D. Oakes and D. E. Kelley (2004). "Metabolic flexibility." Proc.Nutr.Soc. **63**(2): 363-368.

Strissel, K. J., Z. Stancheva, H. Miyoshi, J. W. Perfield, J. DeFuria, Z. Jick, A. S. Greenberg and M. S. Obin (2007). "Adipocyte death, adipose tissue remodeling, and obesity complications." Diabetes **56**(12): 2910-2918.

Surwit, R. S., C. L. Edwards, S. Murthy and A. E. Petro (2000). "Transient effects of long-term leptin supplementation in the prevention of diet-induced obesity in mice." Diabetes **49**(7): 1203-1208.

Surwit, R. S., M. N. Feinglos, J. Rodin, A. Sutherland, A. E. Petro, E. C. Opara, C. M. Kuhn and M. Rebuffe-Scrive (1995). "Differential effects of fat and sucrose on the development of obesity and diabetes in C57BL/6J and A/J mice." Metabolism **44**(5): 645-651.

Tang, W., D. Zeve, J. M. Suh, D. Bosnakovski, M. Kyba, R. E. Hammer, M. D. Tallquist and J. M. Graff (2008). "White fat progenitor cells reside in the adipose vasculature." Science **322**(5901): 583-586.

Tran, K. V., O. Gealekman, A. Frontini, M. C. Zingaretti, M. Morroni, A. Giordano, A. Smorlesi, J. Perugini, R. De Matteis, A. Sbarbati, S. Corvera and S. Cinti (2012). "The vascular endothelium of the adipose tissue gives rise to both white and brown fat cells." Cell Metab **15**(2): 222-229.

Turner, P. V., E. Vaughn, J. Sunohara-Neilson, J. Ovari and F. Leri (2012). "Oral gavage in rats: animal welfare evaluation." J Am Assoc Lab Anim Sci **51**(1): 25-30.

Ukropcova, B., O. Sereda, L. de Jonge, I. Bogacka, T. Nguyen, H. Xie, G. A. Bray and S. R. Smith (2007). "Family history of diabetes links impaired substrate switching and reduced mitochondrial content in skeletal muscle." Diabetes **56**(3): 720-727.

Ukropec, J., R. P. Anunciado, Y. Ravussin, M. W. Hulver and L. P. Kozak (2006). "UCP1-independent thermogenesis in white adipose tissue of cold-acclimated Ucp1-/- mice." J Biol.Chem. **281**(42): 31894-31908.

van de Weijer, T., L. M. Sparks, E. Phielix, R. C. Meex, N. A. van Herpen, M. K. Hesselink, P. Schrauwen and V. B. Schrauwen-Hinderling (2013). "Relationships between mitochondrial function and metabolic flexibility in type 2 diabetes mellitus." PLoS One **8**(2): e51648.

van Herpen, N. A., V. B. Schrauwen-Hinderling, G. Schaart, R. P. Mensink and P. Schrauwen (2011). "Three weeks on a high-fat diet increases intrahepatic lipid accumulation and decreases metabolic flexibility in healthy overweight men." J Clin Endocrinol Metab **96**(4): E691-695.

Van Klinken, J. B., S. A. van den Berg, L. M. Havekes and K. Willems Van Dijk (2012). "Estimation of activity related energy expenditure and resting metabolic rate in freely moving mice from indirect calorimetry data." PLoS One **7**(5): e36162.

Virtanen, K. A., M. E. Lidell, J. Orava, M. Heglind, R. Westergren, T. Niemi, M. Taittonen, J. Laine, N. J. Savisto, S. Enerback and P. Nuutila (2009). "Functional brown adipose tissue in healthy adults." New England Journal of Medicine **360**(15): 1518-1525.

Virtue, S., P. Even and A. Vidal-Puig (2012). "Below thermoneutrality, changes in activity do not drive changes in total daily energy expenditure between groups of mice." Cell Metab **16**(5): 665-671.

Virtue, S. and A. Vidal-Puig (2013). "Assessment of brown adipose tissue function." Front Physiol **4**: 128.

Viscarra, J. A. and R. M. Ortiz (2013). "Cellular mechanisms regulating fuel metabolism in mammals: role of adipose tissue and lipids during prolonged food deprivation." Metabolism **62**(7): 889-897.

Vitali, A., I. Murano, M. C. Zingaretti, A. Frontini, D. Ricquier and S. Cinti (2012). "The adipose organ of obesity-prone C57BL/6J mice is composed of mixed white and brown adipocytes." J Lipid Res **53**(4): 619-629.

Voet, D. and J. G. Voetov (1994). Biochemie2. Praha, Victoria Publishing.

Vosselman, M. J., A. A. van der Lans, B. Brans, R. Wierts, M. A. van Baak, P. Schrauwen and W. D. van Marken Lichtenbelt (2012). "Systemic beta-Adrenergic Stimulation of Thermogenesis Is Not Accompanied by Brown Adipose Tissue Activity in Humans." Diabetes **61**(12): 3106-3113.

Waki, H., T. Yamauchi, J. Kamon, Y. Ito, S. Uchida, S. Kita, K. Hara, Y. Hada, F. Vasseur, P. Froguel, S. Kimura, R. Nagai and T. Kadowaki (2003). "Impaired multimerization of human adiponectin mutants associated with diabetes - Molecular structure and multimer formation of adiponectin." Journal of Biological Chemistry **278**(41): 40352-40363.

Wang, Q. A., C. Tao, R. K. Gupta and P. E. Scherer (2013). "Tracking adipogenesis during white adipose tissue development, expansion and regeneration." Nat Med **19**(10): 1338-1344.

Wang, T., Y. Zang, W. Ling, B. E. Corkey and W. Guo (2003). "Metabolic partitioning of endogenous fatty acid in adipocytes." Obes.Res. **11**(7): 880-887.

Wasser, S. K., S. L. Monfort, J. Southers and D. E. Wildt (1994). "Excretion rates and metabolites of oestradiol and progesterone in baboon (Papio cynocephalus cynocephalus) faeces." J Reprod Fertil **101**(1): 213-220.

Watanabe, M., S. M. Houten, C. Mataki, M. A. Christoffolete, B. W. Kim, H. Sato, N. Messaddeq, J. W. Harney, O. Ezaki, T. Kodama, K. Schoonjans, A. C. Bianco and J. Auwerx (2006). "Bile acids induce energy expenditure by promoting intracellular thyroid hormone activation." Nature **439**(7075): 484-489.

Watson, P. M., S. P. Commins, R. J. Beiler, H. C. Hatcher and T. W. Gettys (2000). "Differential regulation of leptin expression and function in A/J vs. C57BL/6J mice during diet-induced obesity." Am.J.Physiol Endocrinol.Metab. **279**(2): E356-E365.

Weir, J. B. (1949). "New methods for calculating metabolic rate with special reference to protein metabolism." J Physiol **109**(1-2): 1-9.

Wurie, H. R., L. Buckett and V. A. Zammit (2012). "Diacylglycerol acyltransferase 2 acts upstream of diacylglycerol acyltransferase 1 and utilizes nascent diglycerides and de novo synthesized fatty acids in HepG2 cells." FEBS J **279**(17): 3033-3047.

Xue, Y., N. Petrovic, R. Cao, O. Larsson, S. Lim, S. Chen, H. M. Feldmann, Z. Liang, Z. Zhu, J. Nedergaard, B. Cannon and Y. Cao (2009). "Hypoxia-independent angiogenesis in adipose tissues during cold acclimation." Cell Metab **9**(1): 99-109.

Yamauchi, T., J. Kamon, Y. Minokoshi, Y. Ito, H. Waki, S. Uchida, S. Yamashita, M. Noda, S. Kita, K. Ueki, K. Eto, Y. Akanuma, P. Froguel, F. Foufelle, P. Ferre, D. Carling, S. Kimura, R. Nagai, B. B. Kahn and T. Kadowaki (2002). "Adiponectin stimulates glucose utilization and fatty-acid oxidation by activating AMP-activated protein kinase1." Nat.Med. **8**(11): 1288-1295.

Ye, L., J. Wu, P. Cohen, L. Kazak, M. J. Khandekar, M. P. Jedrychowski, X. Zeng, S. P. Gygi and B. M. Spiegelman (2013). "Fat cells directly sense temperature to activate thermogenesis." Proc Natl Acad Sci U S A **110**(30): 12480-12485.

Zammit, V. A. (2013). "Hepatic triacylglycerol synthesis and secretion: DGAT2 as the link between glycaemia and triglyceridaemia." Biochem J **451**(1): 1-12.

Zhao, X., A. Peter, J. Fritsche, M. Elcnerova, A. Fritsche, H. U. Haring, E. D. Schleicher, G. Xu and R. Lehmann (2009). "Changes of the plasma metabolome during an oral glucose tolerance test: is there more than glucose to look at?" Am.J.Physiol Endocrinol.Metab **296**(2): E384-E393.

OPEN ACCESS Freely available online

PLOS ONE

Preservation of Metabolic Flexibility in Skeletal Muscle by a Combined Use of *n*-3 PUFA and Rosiglitazone in Dietary Obese Mice

Olga Horakova[1☯], Dasa Medrikova[1☯], Evert M. van Schothorst[2], Annelies Bunschoten[2], Pavel Flachs[1], Vladimir Kus[1], Ondrej Kuda[1], Kristina Bardova[1], Petra Janovska[1], Michal Hensler[1], Martin Rossmeisl[1], Rui Wang-Sattler[3], Cornelia Prehn[4], Jerzy Adamski[4], Thomas Illig[3¤], Jaap Keijer[2], Jan Kopecky[1]*

1 Department of Adipose Tissue Biology, Institute of Physiology Academy of Sciences of the Czech Republic v.v.i., Prague, Czech Republic, **2** Department of Human and Animal Physiology, Wageningen University, Wageningen, The Netherlands, **3** Research Unit of Molecular Epidemiology, Helmholtz Zentrum München, Neuherberg, Germany, **4** Institute of Experimental Genetics, Genome Analysis Center, Helmholtz Zentrum München, Neuherberg, Germany

Abstract

Insulin resistance, the key defect in type 2 diabetes (T2D), is associated with a low capacity to adapt fuel oxidation to fuel availability, i.e., metabolic inflexibility. This, in turn, contributes to a further damage of insulin signaling. Effectiveness of T2D treatment depends in large part on the improvement of insulin sensitivity and metabolic adaptability of the muscle, the main site of whole-body glucose utilization. We have shown previously in mice fed an obesogenic high-fat diet that a combined use of *n*-3 long-chain polyunsaturated fatty acids (*n*-3 LC-PUFA) and thiazolidinediones (TZDs), anti-diabetic drugs, preserved metabolic health and synergistically improved muscle insulin sensitivity. We investigated here whether *n*-3 LC-PUFA could elicit additive beneficial effects on metabolic flexibility when combined with a TZD drug rosiglitazone. Adult male C57BL/6N mice were fed an obesogenic corn oil–based high-fat diet (cHF) for 8 weeks, or randomly assigned to various interventions: cHF with *n*-3 LC-PUFA concentrate replacing 15% of dietary lipids (cHF+F), cHF with 10 mg rosiglitazone/kg diet (cHF+ROSI), cHF+F+ROSI, or chow-fed. Indirect calorimetry demonstrated superior preservation of metabolic flexibility to carbohydrates in response to the combined intervention. Metabolomic and gene expression analyses in the muscle suggested distinct and complementary effects of the interventions, with *n*-3 LC-PUFA supporting complete oxidation of fatty acids in mitochondria and the combination with *n*-3 LC-PUFA and rosiglitazone augmenting insulin sensitivity by the modulation of branched-chain amino acid metabolism. These beneficial metabolic effects were associated with the activation of the switch between glycolytic and oxidative muscle fibers, especially in the cHF+F+ROSI mice. Our results further support the idea that the combined use of *n*-3 LC-PUFA and TZDs could improve the efficacy of the therapy of obese and diabetic patients.

Citation: Horakova O, Medrikova D, van Schothorst EM, Bunschoten A, Flachs P, et al. (2012) Preservation of Metabolic Flexibility in Skeletal Muscle by a Combined Use of *n*-3 PUFA and Rosiglitazone in Dietary Obese Mice. PLoS ONE 7(8): e43764. doi:10.1371/journal.pone.0043764

Editor: Stephane Blanc, Institut Pluridisciplinaire Hubert Curien, France

Received March 29, 2012; **Accepted** July 25, 2012; **Published** August 31, 2012

Funding: The research leading to these results has received funding from the Czech Science Foundation (303/08/0664), RVO: 67985823, EPAX AS (Norway), the European Union's Seventh Framework Programme FP7 2007–2013 under grant agreement n° 244995 (BIOCLAIMS), and the EFSD New Horizons research grant. This project has been also in part supported by a Grant from the German Federal Ministry of Education and Research (BMBF) to the German Center Diabetes Research (DZD). The funders had no role in study design, data collection and analysis, decision to publish, or preparation of the manuscript.

Competing Interests: The authors have read the journal's policy and have the following conflict: The research leading to these results has been funded in part by EPAX AS (Norway). There are no patents, products in development, or marketed products to declare. This does not alter the authors' adherence to all the PLoS ONE policies on sharing data and materials.

* E-mail: kopecky@biomed.cas.cz

☯ These authors contributed equally to this work.

¤ Current address: Hannover Unified Biobank, Hannover Medical School, Hannover, Germany

Introduction

Combined treatments with multiple mechanisms of action are required for a better handling of metabolic diseases associated with obesity [1–4]. Thus, dietary, lifestyle, and pharmacological interventions should all be considered in the therapy of patients with type 2 diabetes (**T2D**), the major metabolic disease triggered by obesity [5].

Naturally occurring *n*-3 long-chain polyunsaturated fatty acids (***n*-3 LC-PUFA**), namely eicosapentaenoic acid (**EPA**; 20:5n-3) and docosahexaenoic acid (**DHA**; 22:6n-3) are now regarded as healthy constituents of diets for diabetic patients [6–8]. These lipids, which are abundant in sea fish, act as hypolipidemics and augment the efficacy of the lipid-lowering drugs [4], and reduce cardiac events and decrease progression of atherosclerosis (reviewed in ref. [7,9,10]). Numerous animal studies demonstrated reduced accumulation of body fat in response to dietary *n*-3 LC-PUFA supplementation [11–18], especially when combined with calorie restriction [19], reflecting possibly reduced proliferation of fat cells [12,20], and/or metabolic changes in the liver [15,21], adipose tissue [13,19], and intestine [22]. In contrast, only few randomized clinical trials demonstrated a reduction of adiposity after *n*-3 LC-PUFA supplementation [23–26], while other studies in humans

could not reveal any anti-obesity effect of *n*-3 LC-PUFA [27,28]. Moreover, in rodents, *n*-3 LC-PUFA prevented [14,21,29–31] and even reversed [14,32] insulin resistance induced by high-fat feeding, while *n*-3 LC-PUFA had little effect on glycemic control and insulin sensitivity in diabetic patients [23,33,34].

Impairment of insulin sensitivity represents the key defect in T2D. It is associated with a low capacity to adapt fuel oxidation to fuel availability, i.e., metabolic inflexibility [35,36]. This results in lower glucose oxidation during insulin-stimulated conditions and in relatively low activation of lipid catabolism when lipids represent the main metabolic fuel, which further support accumulation of ectopic fat and lipotoxicity with a deleterious effect on insulin signaling [35]. Recent studies based on metabolomics suggest that both incomplete mitochondrial fatty acid oxidation and abnormal metabolism of branched-chain amino acids (**BCAA**) [37,38] could contribute to insulin resistance, especially in the context of high fat-feeding in rodents and/or obesity (reviewed in [39]). In turn, this novel mechanistic insight may help to develop causal and more effective treatment strategies for T2D patients.

In our previous studies, we sought to learn whether *n*-3 LC-PUFA could augment the effects of anti-diabetic drugs, namely thiazolidinediones (**TZDs**). Thus, using a model of dietary obese mice and euglycemic-hyperinsulinemic clamps to measure insulin sensitivity, we have demonstrated that the combined use of *n*-3 LC-PUFA and TZD rosiglitazone, both administered at a relatively low dose (a 'combined intervention'), exerted synergistic effects in prevention as well as reversal of insulin resistance [14]. These effects reflected a synergistic improvement in muscle insulin sensitivity [14], depending possibly in part on the induction of adiponectin [14,32]. The combined intervention also exerted additivity in the counteraction of both dyslipidemia [14,32] and low-grade inflammation of adipose tissue [14]. Also pioglitazone, a TZD used currently in treatment of diabetic patients [40], prevented both dyslipidemia and impairment of glucose homeostasis more efficiently in the combination with *n*-3 LC-PUFA as compared with the single intervention [32]. In addition, rosiglitazone, at the low dose used [14,32], but not pioglitazone [32], augmented the anti-obesity effect of *n*-3 LC-PUFA. Changes in plasma metabolome suggested that the anti-obesity effect of the combined intervention reflected induction of fatty acid β-oxidation [32].

Motivated by our findings revealing synergistic effect of the combined use of *n*-3 LC-PUFA and rosiglitazone on muscle insulin sensitivity in dietary obese mice (refs. [14,32]; see also above), and by the fact that skeletal muscle is the main site of glucose uptake [35], we aimed to verify a hypothesis that improvement of metabolic flexibility is an important part of the beneficial effects of the combined intervention. We also sought to learn what are the mechanisms underlying the improvement of muscle insulin sensitivity in response to the combined intervention. To examine this, we applied our established treatment protocol to high-fat diet-fed mice [14,32]. Indirect calorimetry results indicated superior preservation of metabolic flexibility to carbohydrates in response to the combined intervention. Moreover, metabolomic analysis as well as evaluation of gene expression in skeletal muscle revealed (i) partially distinct mechanisms of action of *n*-3 LC-PUFA and rosiglitazone, and (ii) additive activation of the switch between glycolytic and oxidative muscle fibers in response to the combined intervention.

Results

Assessment of Intervention

In agreement with our previous experiments [14,32], when adult mice (see Fig. 1A) were randomly assigned to an obesogenic high-fat diet (**cHF**) or to the following cHF-based diets supplemented with (i) *n*-3 LC-PUFA (**cHF+F**); (ii) a low dose of rosiglitazone (**cHF+ROSI**); and (iii) both *n*-3 LC-PUFA concentrate and rosiglitazone (**cHF+F+ROSI**), only the combined intervention prevented development of obesity during 8 weeks of the high-fat feeding experiment (Table 1). As observed before [14,32], food consumption was not significantly affected by any of the interventions (data not shown).

To evaluate plasma parameters at the end of the experiment at week 8, a 'diet-switch protocol' was applied (see Fig 1 and Methods), similarly as in the case of indirect calorimetry, which was performed during week 6 (see below). Thus, mice, which were fed during the whole experiment various cHF-based diets, were fasted during the light phase of the day and re-fed standard low-fat (**Chow**) diet during the night. Plasma was collected and glycemia was measured in (i) mice with *ad libitum* access to various cHF-based diets, before fasting, and (ii) mice re-fed Chow overnight. In the mice before fasting, the combined intervention strongly reduced plasma levels of triglycerides, even when compared with the mice fed Chow diet. Moreover, both *n*-3 LC-PUFA containing diets (cHF+F and cHF+F+ROSI) decreased NEFA levels in plasma (Table 1). Glycemia was not affected by any of the interventions (Table 1), in spite of the synergistic improvement of muscle insulin sensitivity in response to the combined intervention observed already before [14,32]. Feeding cHF diet increased plasma insulin levels as compared with the Chow mice, while the combined intervention counteracted this effect (see also refs [14,32]).

In the animals fasted during the day and re-fed Chow overnight, the hypolipidemic effects of *n*-3 LC-PUFA containing diets disappeared, and insulin levels in all the groups were similar to the Chow-fed control mice. Glycemia was similar in all the animals maintained on various cHF-based diets during the experiment, while insulin levels tended to be lower in the cHF+F+ROSI as compared with the cHF mice (Table 1). In addition, the combination intervention prevented cHF-induced elevation of β-hydroxybutyrate levels in plasma, while the single interventions had no effect (Table 1).

Assessment of Metabolic Flexibility

During week 6 of the experiment, indirect calorimetry was performed, using the diet-switch protocol mentioned above, i.e., during the course of the subsequent periods of (i) feeding various cHF-based diets, (ii) fasting, and (iii) re-feeding Chow diet (i.e., low-fat diet with a carbohydrate/fat ratio of 16.3, wt/wt, as compared with the corresponding ratio of 1.0 in the case of the cHF-based diets; see Methods and ref. [14]). Neither oxygen consumption ($\boldsymbol{\dot{V}O_2}$), nor respiratory exchange ratio (**RER;** calculated as carbon dioxide production, $\boldsymbol{\dot{V}CO_2}$, divided by $\dot{V}O_2$), the marker of fuel partitioning, were affected by any of the interventions, except for (i) a slight depression of $\dot{V}O_2$ in the cHF+F+ROSI mice during fasting (Table 2), and (ii) an increase in RER during re-feeding Chow diet in response to all the interventions. This increase was similar in the cHF and cHF+ROSI mice (Fig. 2B, Table 2), while the cHF+F mice exhibited a transiently higher induction during the second half of the dark phase of the day (Fig. 2B). Mice subjected to the combined intervention displayed the highest induction, which prevailed even during the light phase of the day (Fig. 2B). Percent relative cumulative frequency (**PRCF**) curves were constructed, based on RER values pooled from all animals within a given dietary group. This was done for the fasting and Chow periods (Fig. 2C). The values of log EC_{50} of PRCF (50^{th} percentile value) correspond to median RER values [41]. This robust approach confirmed the RER data, indicating a shift from lipid to

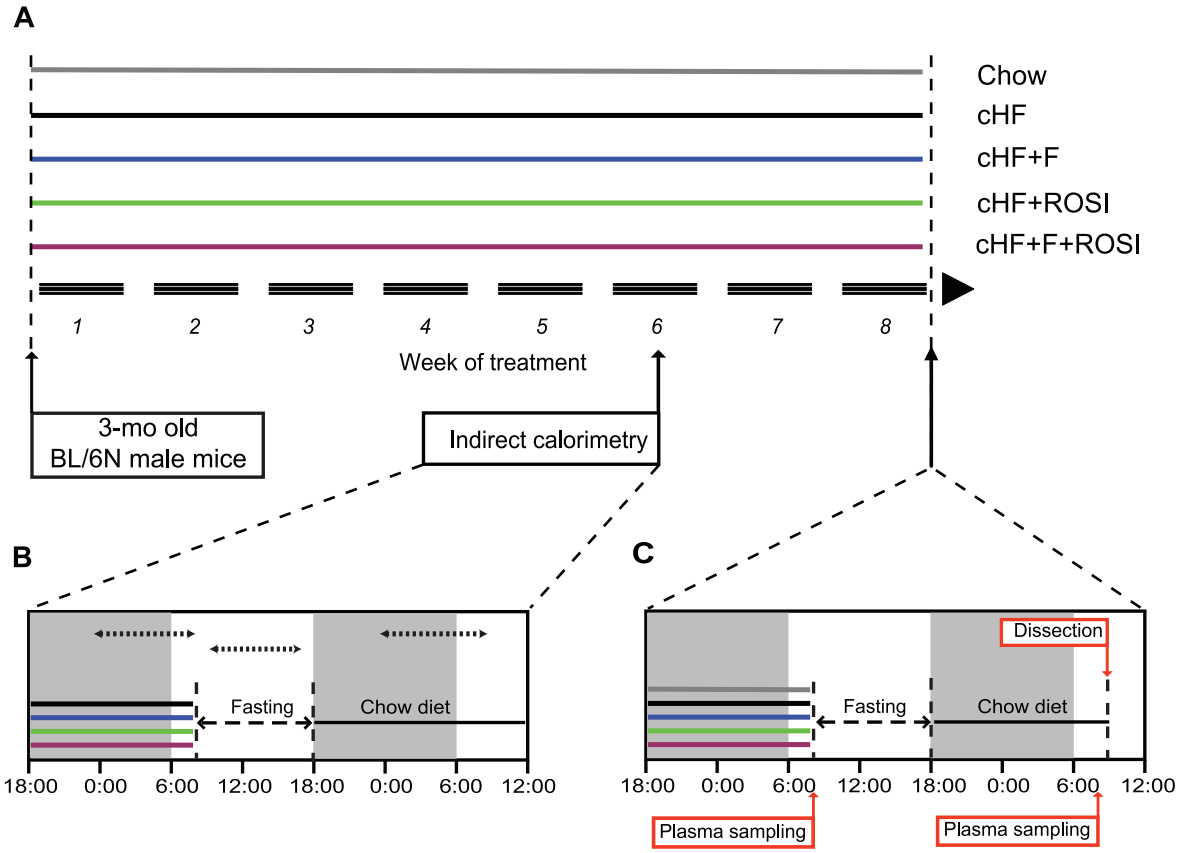

Figure 1. Overview of experimental setup. Starting at 3 months of age, subgroups of mice were fed either Chow or cHF diets, or subjected to various interventions (cHF+F, cHF+ROSI, and cHF+F+ROSI diets), which lasted for 8 weeks (**A**). During week 6 of the experiment, indirect calorimetry was performed using the 'diet-switch protocol' (**B**). At the end of the experiment, animals were killed either following the diet-switch protocol when re-fed Chow diet (**C**), or without any additional manipulations, while offered various cHF-based diets (not shown). White and grey background (**B, C**), light and dark phase of the day, respectively. Dotted arrow lines (**B**), periods of data collection for calculation of the mean values of $V0_2$, RER, and PRCF (see Table 1 and Fig. 2).
doi:10.1371/journal.pone.0043764.g001

carbohydrate oxidation in response to re-feeding mice Chow diet, with the highest flexibility in the mice subjected to the combined intervention (Fig. 2C and Table 2).

Targeted Metabolomic Analysis in Skeletal Muscle

To characterize the role of muscle, the major organ of energy utilization, in the differential modulation of metabolic flexibility by the treatments, targeted metabolomics analysis in the muscle was performed in mice re-fed Chow diet (see also Fig. 1). Concentrations of 163 metabolites (Table S1) providing sets of hexoses, amino acids, sugars, acylcarnitines and phospholipids were measured using flow injection analysis/thermospray mass spectrometry (**FIA-MS**) with Biocrates Absolute*IDQ*™ targeted metabolomics technology.

Partial least squares-discriminant analysis (**PLS-DA**) of the data separated mice into three distinct groups, namely the cHF mice, the cHF+ROSI mice, and the group of mice fed the diets containing *n*-3 LC-PUFA (both cHF+F and the cHF+F+ROSI mice; Fig. 3A). The first PLS-DA component (X-axis) showed a strong separation between the mice fed diets containing or not *n-3* LC PUFA, while the second PLS-DA component (Y-axis) showed a separation between the cHF mice and the cHF+ROSI mice. A loading scatter plot was constructed to determine the variables (metabolites) discriminating between the groups (Fig. 3B). Concerning the PLS-DA component 1, the most influential metabolites were glycerophospholipids, reflecting a difference in fatty acid composition of the diets. Most of sphingolipids were associated with the cHF+F and cHF+F+ROSI mice (Fig. 3B and Fig. S1). The metabolites having the greatest influence on the separation of the cHF mice were acylcarnitines and amino acids (Fig. 3B and Fig. S1).

We generated heat maps of the correlation matrices of all pairwise correlations of muscle acylcarnitines (Fig. 4). These metabolites are formed in mitochondria, equilibrate with their cognate acyl CoAs and provide a detailed signature of mitochondrial fatty acid metabolism. Obesity accelerates fatty acid metabolism with possible accumulation of incomplete oxidation products, which may exacerbate insulin resistance [37,38,42]. Strong associations between all 14 acylcarnitines reflect complete β-oxidation of fatty acids, while reciprocal association between short-chain and long-chain acylcarnitines reflect a metabolic block, when fatty acids are metabolised only partially [37,42]. Furthermore, acetylcarnitine (**C2**) can be used as a marker of acetyl-CoA levels, whereas odd-chain acylcarnitines, namely propionyl-L-carnitine (**C3**) and isovalerlycarnitine (**C5**), are primarily derived from catabolism of BCAA [37–39]. Our analysis revealed several hotspots and patterns, which discriminated between the interventions. The interpretations given above indicate that *n*-3 LC PUFA improved efficiency of β-oxidation (Fig. 4A vs Fig. 4B), while rosiglitazone alone had only a negligible

Table 1. Growth characteristics and plasma parameters.

	Chow	cHF	cHF+F	cHF+ROSI	cHF+F+ROSI
Body weight (g)					
Initial	24.7±0.8	25.9±0.5	26.2±0.5	25.1±0.3	25.5±0.4
Final	31.4±1.0	37.6±1.1[f]	34.8±1.1	37.4±1.2[f]	32.3±0.8[a,c]
Body weight gain	5.7±0.5	11.7±1.3[f]	8.6±1.0	12.2±1.1[f]	6.8±0.9[a,c]
Plasma parameters					
cHF-based diets					
Triglycerides (mmol/l)	0.70±0.05	0.90±0.11	0.55±0.06	0.55±0.04[f]	0.46±0.03[a,f]
NEFA (mmol/l)	0.56±0.06	0.48±0.08	0.30±0.03[f]	0.44±0.05	0.33±0.05[f]
Glucose (mmol/l)	15.1±0.6	14.6±0.4	14.1±0.3	14.6±0.6	14.1±0.4
Insulin (nmol/l)	0.13±0.01	0.38±0.07[f]	0.24±0.03	0.30±0.03	0.19±0.05[a]
Re-fed Chow					
Triglycerides (mmol/l)	0.69±0.13	0.84±0.17	0.63±0.06	0.47±0.06	0.56±0.10
NEFA (mmol/l)	0.39±0.11	0.33±0.03	0.46±0.06	0.35±0.04	0.27±0.07
Glucose (mmol/l)	18.3±1.11	15.5±1.1	13.4±0.8[f]	16.2±0.7	15.2±0.5[f]
Insulin (nmol/l)	0.11±0.02	0.15±0.02	0.12±0.03	0.16±0.03	0.09±0.01
β-HB (μmol/l)	46.0±7.5	95.4±18.1[f]	68.1±6.9[f]	94.3±11.1[f]	35.2±6.4[a,c]
n	6	8–10	8–10	8–10	8–10

Three-month-old mice were placed on various diets and killed 8 weeks thereafter. Plasma parameters were followed as described in Methods, either in mice with free access to various cHF-based diets, or when mice were re-fed Chow (using the diet-switch protocol; see also Fig. 1C). BHB, β-hydroxybutyrate in the animals re-fed Chow.
[a]Significantly different from cHF;
[b]significantly different from cHF+F;
[c]significantly different from cHF+ROSI;
[d]significantly different from cHF+F+ROSI (ANOVA).
[f]Significantly different from Chow (*t*-test).
doi:10.1371/journal.pone.0043764.t001

effect (Fig. 4A vs Fig. 4C). The combined intervention resulted in a strong regulation of the metabolism of BCAA (C3 and C5 hotspots) and specifically unmasked the involvement of the hydroxylated C4 metabolite (**C4-OH**; Fig. 4D), i.e., either hydroxybutyrylcarnitine or malonylcarnitine (Table S1). This was supported by analysis at the level of individual metabolites, which revealed that even side-chain (C>10) acylcarnitines, arising from incomplete mitochondrial β-oxidation [37,42], were significantly reduced in response to the *n*-3 LC-PUFA, while they were not affected by rosiglitazone. Levels of shorter side-chain (C<10) acylcarnitines did not change, while levels of odd-chain acylcarnitines (C3+C5) tended to be decreased by all the interventions. Together with the heatmap analysis, these results suggest different mechanisms engaged in the beneficial effects of the single interventions on insulin sensitivity. Thus, *n*-3 LC-PUFA ameliorate lipid-induced mitochondrial stress [37,42], while the combination with *n*-3 LC-PUFA and rosiglitazone probably augments insulin sensitivity by the modulation of branched-chain amino acid metabolism [37,38]. Furthermore, C4-OH levels were decreased by all the interventions (Table S1 and Fig. 5A) and *n*-3 LC-PUFA, especially in combination with rosiglitazone, exerted a suppressive effect on the concentration of free amino acids in the muscle (Table S1 and Fig. 5B). Glucogenic amino acids, namely glycine and serine, were more affected than amino acids that are both glucogenic and ketogenic, like tyrosine (Fig. 5B). These results are in favour of the synergistic improvement of muscle insulin sensitivity by the combined intervention (see Discussion).

In accordance with the changes in their plasma levels and amelioration of obesity-associated low-grade inflammation [32], the content of most of lysophosphatidylcholines (**lysoPCs**) were reduced in response to *n*-3 LC-PUFA also in the muscle, specifically lysoPCs with polyunsaturated fatty acids C18:2-, C20:3-, and C20:4- side chains (Table S1 and Fig. 5C). The combined intervention tended to exert the most pronounced effects. Levels of sphingolipids (**SM**) were hardly regulated, except for hydroxysphingomyeline C24:1 [**SM(OH) C24:1**], which was strongly induced by *n*-3 LC-PUFA, especially in the combined intervention, while rosiglitazone alone had the opposite effect (Table S1 and Fig. 4D).

Gene Expression in Skeletal Muscle

To investigate the effects of the interventions on gene expression in the skeletal muscle, whole genome microarray analysis was performed in mice re-fed Chow diet. As the initial step, three groups were compared, being the cHF+F and cHF+ROSI versus the control cHF mice. Non-stringent analysis of the results suggested that both single interventions regulated genes engaged in various biological processes, with only a partial overlap, and with a stronger effect of *n*-3 LC PUFA (Table 3). The stronger effect of *n*-3 LC PUFA agrees with the stronger effects observed for metabolomic data as analyzed by PLS-DA (Fig. 3A).

To examine the most prominent changes, genes with a significant regulation with an absolute fold change (**FC**) ≥1.5 were selected (Table S3). In total, 18 and 12 well annotated genes were detected when the effects of *n*-3 LC PUFA (Table S2; 12 genes down-regulated, 6 genes up-regulated in the cHF+F mice), and rosiglitazone (Table S3; 5 genes down-regulated, 7 genes up-regulated in the cHF+ROSI mice), respectively, were compared. All detected genes were unique, and mostly specific for the different interventions, while their number was very small compared to the number of genes detectable using the Agilent oligonucleotide arrays (see Methods).

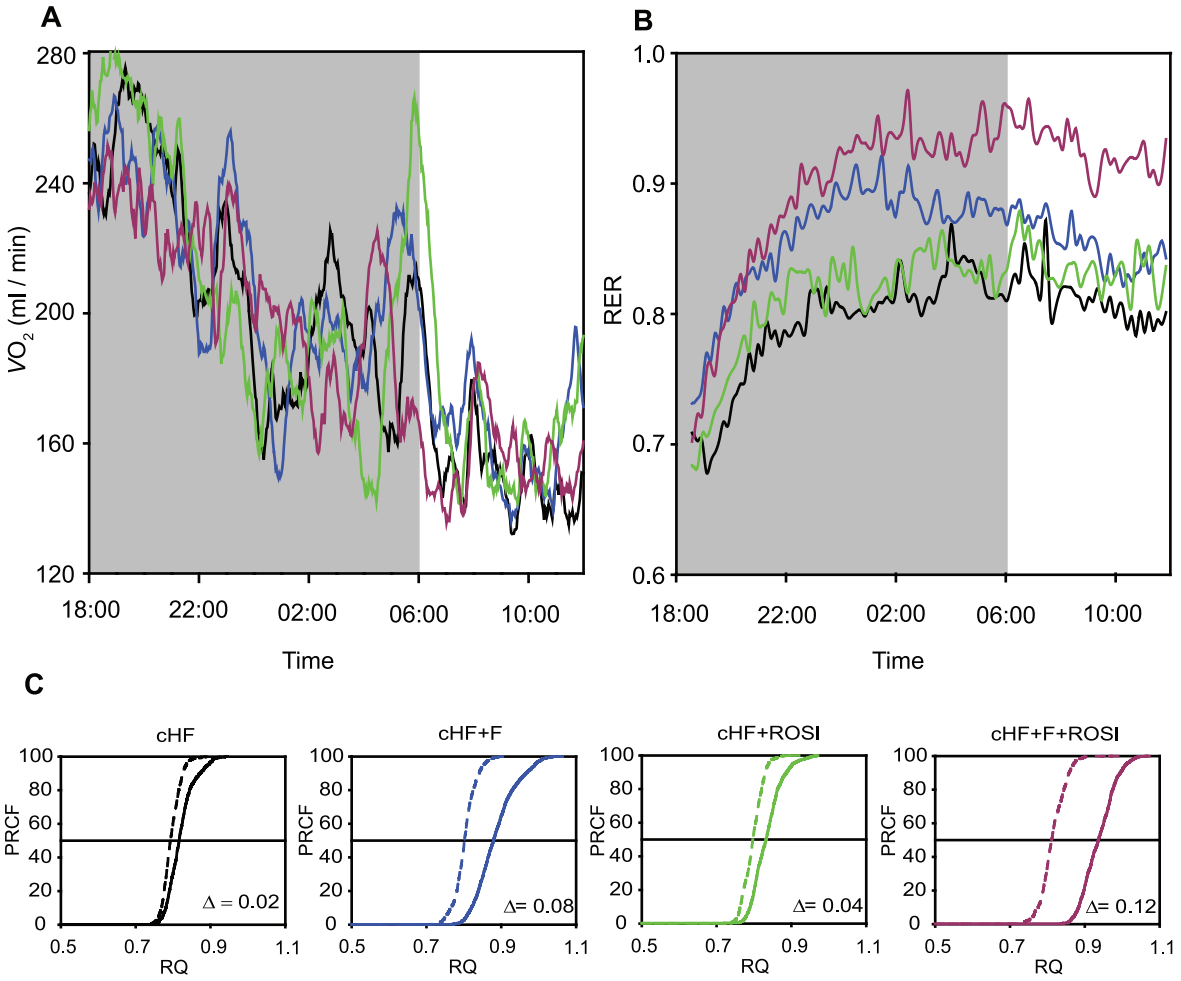

Figure 2. Indirect calorimetry. During week 6 of the experiment, in mice fed cHF diet, or mice subjected to various interventions (cHF+F, cHF+ROSI, and cHF+F+ROSI diets; *n*+5; mice randomly chosen from each subgroup, see Table 1), indirect calorimetry was performed using the diet-switch protocol (Fig. 1B). Thus, during the first part of the measurements (between 6.00 p.m. and 8.00 a.m.), animals had *ad libitum* access to water and various cHF-based diets. After that period, the diets were removed and the animals fasted for 10 hours (between 8.00 a.m. and 6.00 p.m.). At the beginning of the dark phase of the day cycle (at 6.00 p.m.), all the subgroups were offered Chow diet and the measurements continued for 20 more hours. **A** and **B**. Oxygen consumption (**A**) and RER values (**B**) during re-feeding Chow diet (mean values). **C**. Plots of PRCF of RER values during the periods of fasting (broken lines; data collected between 9.00 a.m. and 5.00 p.m.) and re-feeding Chow (solid lines; data collected between 0.00 p.m. and 8.00 a.m.). Each curve represents the data pooled from all mice within a given group ($n = 5$; see above; ~1,200 RER measurements per curve). For the means over different periods of the measurements and for the statistical analysis of these data, see Table 2.
doi:10.1371/journal.pone.0043764.g002

As the second step, we sought to find the genes, which could be additively/synergistically affected by the combined intervention by direct comparison of the cHF+F+ROSI versus cHF+ROSI mice. A higher number of genes was regulated as compared with the sum of genes regulated by single interventions (Table 3). Focusing on the most regulated genes using FC ≥1.5 as a threshold again, in total 39 well-annotated genes were identified to be differentially expressed, with most of these showing a lower expression in the cHF+F+ROSI mice (Table S4). The total number of differentially expressed genes, as well as the extent of their regulation was still relatively small (4 genes detected with FC ≥2.0; Table S4).

Detailed inspection of the expression data (Tables S2, S3, and S4) uncovered 10 genes, which were highly relevant with respect to a functional interpretation. Therefore, expression of these genes was verified using real-time quantitative RT-PCR (**qRT-PCR**) analysis across all the dietary groups. In addition, 5 genes, which were not identified using the microarrays, but could help the functional interpretation, were also included (for the complete list of genes, see Tables S5). Since the main focus of the analyses was on the characterisation of the muscle involvement in the differential effects of the interventions on metabolic flexibility, gene expression was evaluated not only in the animals re-fed Chow diet (see above), but also in mice from a separate experiment, which were killed when fed the cHF-based diets (see Methods and Fig. 1).

Several genes involved in carbohydrate metabolism showed significant changes in expression (Fig. 6A): (i) pyruvate dehydrogenase kinase 4 (***Pdk4***), a regulatory enzyme limiting oxidation of glucose by inhibiting the pyruvate dehydrogenase complex [43], (ii) fructose-1,6-bisphophatase 2 (***Fbp2***), a key enzyme of gluconeogenesis catalyzing the hydrolysis of fructose 1,6-bisphosphate to fructose 6-phosphate and inorganic phosphate [44], and (iii) glucose transporter 4 (***Glut4***), which is essential for the insulin-stimulated glucose uptake in muscle cells [45]. Changes in *Pdk4* expression suggested improved metabolic flexibility in response to all the interventions, as demonstrated by the down-regulation of

Table 2. Indirect calorimetry.

	cHF	cHF+F	cHF+ROSI	cHF+F+ROSI
VO_2 (ml/min)				
Original diets	2.00±0.04	1.99±0.09	1.97±0.04	1.97±0.06
Fasting	1.83±0.06	1.83±0.03	1.94±0.08	1.69±0.04[b]
Re-feeding Chow	1.85±0.06	1.90±0.06	1.86±0.06	1.81±0.04
RER				
Original diets	0.84±0.01	0.84±0.01	0.83±0.01	0.87±0.01
Fasting	0.80±0.01	0.80±0.01	0.80±0.01	0.81±0.01
Re-feeding Chow	0.85±0.03	0.89±0.02	0.84±0.02	0.94±0.02[ab]
ΔRER	0.05±0.02	0.08±0.01	0.04±0.01	0.12±0.01[ab]

At 6 weeks after the initiation of the experiment, oxygen consumption (VO_2) and carbon dioxide production were recorded every 2 min using indirect calorimetry. The measurements were performed following the diet-switch protocol in individual mice (Fig. 1B). During the first part of the measurements (between 6.00 p.m. and 8.00 a.m.), animals had *ad libitum* access to water and various cHF-based diets. After that period, the animals were fasted for 10 hours. At the beginning of the dark cycle at 6.00 p.m., all subgroups were switched to Chow diet, and the measurements continued for 20 more hours ('Re-feeding Chow '). The measurements were performed under the 12-hour light-dark cycle (lights on from 6:00 a.m.) at ambient temperature of 22°C. Data are means±SE ($n = 5$; mice randomly chosen from each subgroup, see Table 1) expressed for the following three time-periods (i) from 0.00 p.m. to 8.00 a.m., feeding various cHF-based diets; (ii) from 9.00 a.m. to 5 p.m., fasting; and (iii) from 0.00 p.m. to 8.00 a.m., re-feeding Chow. ΔRER, the difference in RER between mice re-fed Chow diet and fasted mice.

[a]Significantly different from cHF diet;

[b]significantly different from cHF+ROSI diet (ANOVA).

doi:10.1371/journal.pone.0043764.t002

this gene in mice re-fed Chow diet (Fig. 6A), and they were verified using Western blot analysis (Fig. 7). In the case of *Fbp2*, only the rosiglitazone-based interventions could improved the flexibility, as revealed by the pronounced down-regulation of this gene in the mice re-fed Chow diet (Fig. 6A). Only in the case of *Glut4*, the combined intervention tended to increase the expression, independent on the actual feeding status (Fig. 6A).

Lipid metabolism was clearly regulated as well; genes encoding (i) acyl-CoA thioesterase 1 (***Acot1***), a mitochondrial enzyme hydrolyzing medium- and long-chain acyl-CoAs to the free fatty acid and CoASH [46], (ii) carnitine palmitoyltransferase 1b (muscle form; ***Cpt1b***), the rate-limiting transporter of activated fatty acids for mitochondrial β-oxidation in the muscle [47], and (iii) CD36 protein (***Cd36***), acting as a plasma membrane, TZD-inducible fatty acid transporter [48], were all regulated by the interventions (Fig. 6B). Both *Acot1* and *Cpt1b* showed a relatively strong response, while especially changes in *Cpt1b* expression suggested additive improvement of metabolic flexibility in response to the combined intervention. In contrast to the strong regulation of *Cpt1b* (Fig. 6B), expression of the liver isoform of the enzyme (***Cpt1a***) was not affected (Tables S5).

Furthermore, important changes were found in the expression of genes marking slow (oxidative) muscle fibres [49,50], especially (i) myosin heavy polypeptides, ***Myh6*** and ***Myh7***, and (ii) troponin C 1 (***Tnnc1***; Fig. 6C). In the mice killed when fed the cHF-based diets, increased expression was observed for all these genes, suggesting additive/synergistic induction of the oxidative fibers, while in the mice re-fed Chow diet, expression of these genes was mostly down-regulated (*Myh6* and *Myh7*), with *Tnnc1* showing the strongest response to the combined intervention (Fig. 6C). The gene encoding peroxisome proliferator-activated receptor γ coactivator 1α, (***Pgc1α***), which stimulates the conversion of muscle fiber type towards oxidative type [51,52], was regulated by rosiglitazone but not by *n*-3 LC PUFA (Fig. 6D).

Finally, among other genes showing a strong regulation, genes encoding enzymes involved in the production of lipid mediators from various PUFA [53], including a member of the cytochrome P450 family genes (***Cyp1a1***; Fig. 6E), were identified. In both cases, combined intervention resulted in the strongest induction, independent of the actual feeding status.

Discussion

Indirect calorimetry performed in this study proved an additive improvement in metabolic flexibility in response to the combined use of *n*-3 LC-PUFA and rosiglitazone in mice fed an obesogenic high-fat diet. These results are in agreement with the changes of plasma metabolite levels during the fasted to re-fed transition, as well as with the synergistic improvement of muscle insulin sensitivity by the combined intervention in these animals [14,32]. The beneficial effect on metabolic flexibility was observed during a switch from lipid to carbohydrate fuel. As reported recently by the group of Blaak, "the ability to switch from fat oxidation to carbohydrate oxidation after a meal is already impaired in the prediabetic state, suggesting this may be an early factor in the development toward type 2 diabetes" [54]. Interestingly, in our animals with *ad libitum* access to high-fat diet, no differences between the treatments in fuel partitioning were found, also in accordance with the lack of correlation between fasting RER and insulin sensitivity in some human studies (reviewed in [36]).

It is not known whether the effect of the combined intervention on metabolic flexibility merely reflects the reduced accumulation of body fat, when rosiglitazone is administered at a relatively low dose in the combination with *n*-3 LC-PUFA (see also [14,32]), or whether it depends on direct effects on muscle metabolism. However, several pieces of evidence are in favor of the latter possibility. Thus, (i) in agreement with a previous study in rats [55], cHF+F diet, but not cHF+ROSI diet, increased RER values in mice re-fed Chow, in spite of the absence of an effect on body weight by neither of the single intervention; (ii) both metabolomic and gene expression analyses in the muscle documented several body weight-independent changes induced by the interventions (see below); and (iii) dietary supplementation with *n*-3 LC-PUFA, either in combination with rosiglitazone [14,32] or pioglitazone [32] resulted in a synergistic induction of adiponectin, while elevated adiponectin levels were found to be associated with enhanced metabolic flexibility [56].

Metabolic Profiling in the Muscle

Targeted metabolomic analysis in the muscle revealed relatively subtle differences between the interventions. This could be explained by the fact that the set of the measured metabolites lacked specific markers of carbohydrate metabolism, the process affected the most during the fasted to re-fed transition. Nevertheless, the levels of glucogenic amino acids were regulated as expected, with the strongest response induced by the combined intervention. Changes in the regulation and levels of acylcarnitines suggested distinct and complementary effects of *n*-3 LC-PUFA and rosiglitazone, with *n*-3 LC PUFA supporting mitochondrial β-oxidation (see [37,38,42]), and the combined intervention augmenting insulin sensitivity by the modulation of BCAA metabolism (see [37,38]). In fact, in a previous study [57], the insulin-senzitizing potency of TZDs was shown to correlate with modulation of BCAA metabolism in WAT, with the impact on BCAA levels and insulin sensitivity in the muscle (see [39]). All the

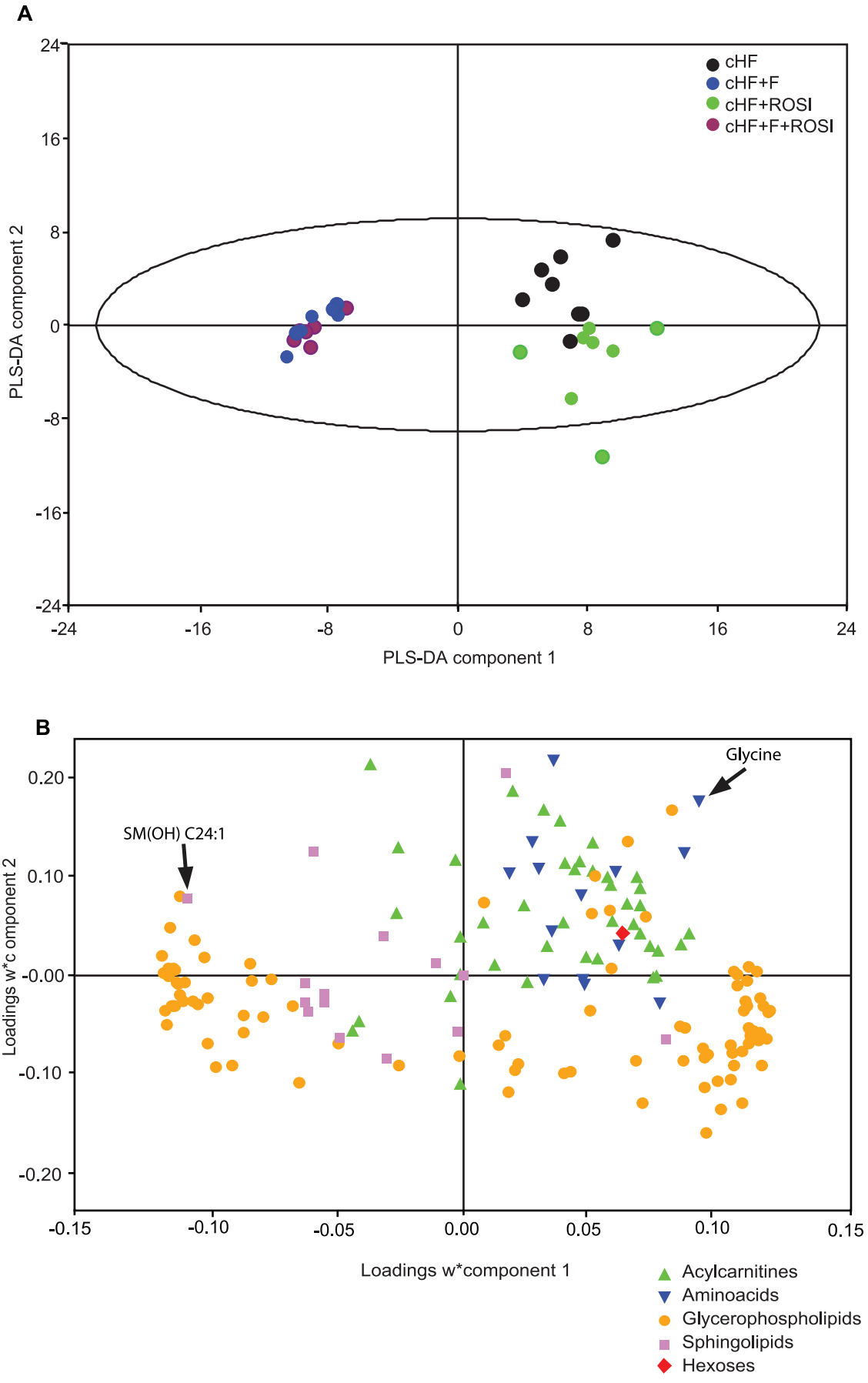
A
cHF
cHF+F
cHF+ROSI
cHF+F+ROSI
PLS-DA component 2
PLS-DA component 1
24
16
8
0
-8
-16
-24
B
Glycine
SM(OH) C24:1
Loadings w*c omponent 2
Loadings w*component 1
0.20
0.10
-0.00
-0.10
-0.20
-0.15
-0.10
-0.05
0.00
0.05
0.10
0.15
Acylcarnitines
Aminoacids
Glycerophospholipids
Sphingolipids
Hexoses

Figure 3. The effects of various interventions on gastrocnemius muscle metabolome. At 3 month of age, subgroups of mice were fed cHF diet, or subjected to various interventions using cHF-based diets (cHF+F, cHF+ROSI, and cHF+F+ROSI). Animals were killed while re-fed Chow diet (see the diet-switch protocol and Fig. 1). Targeted metabolomics analysis was performed in gastrocnemius muscle extracts. In total, concentrations of 163 metabolites were determined using FIA-MS with the Biocrates AbsoluteIDQ™ technology (see Table S1) and PLS-DA was performed. **A**. 2D-score scatter plot of the first (X-axis) and the second (Y-axis) PLS-DA component are shown for selected groups of mice ($n = 7–8$; mice randomly chosen from each subgroup, see Table 1). Mice were fed cHF (black circles), cHF+ROSI (green circles), cHF+F (blue circles), or cHF+F+ROSI (violet circles) diets. **B**. Corresponding loading scatter plot. Acylcarnitines (green triangle), amino acids (inverted blue triangle), glycerophospholipids (yellow circles), sphingolipids (violet circles) and sum of hexoses (red diamante) are shown. The score (**A**) and loading (**B**) plots complement each other. The position of objects (muscle sample) in a given direction in the score plot is determined by variables (metabolites) lying in same direction in the loading plot. For identification of the individual metabolites shown in **B**, see Fig. S1.
doi:10.1371/journal.pone.0043764.g003

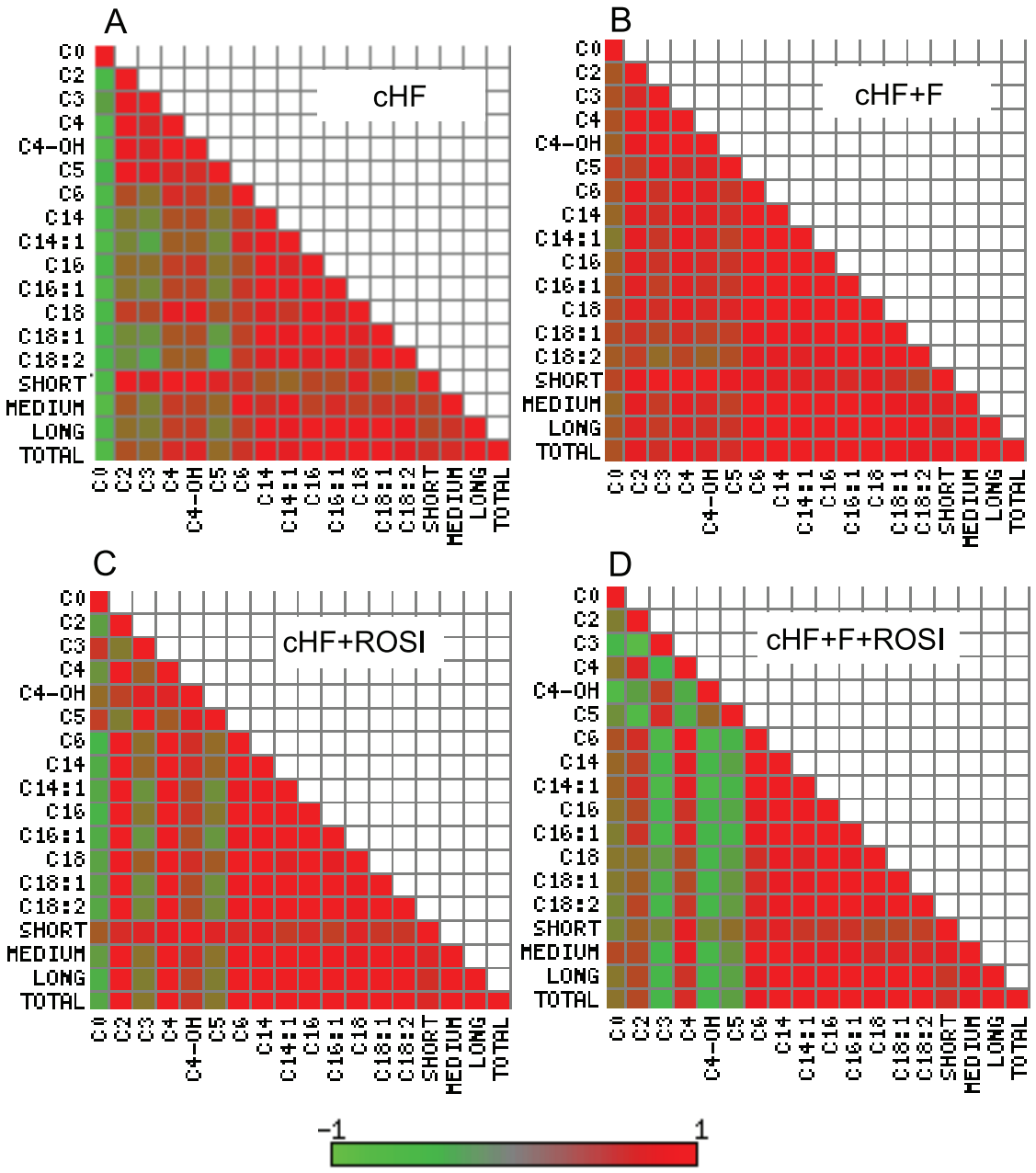

Figure 4. Heatmap analysis of the effects of various interventions on selected analytes in the muscle. Analysis was performed in mice re-fed Chow diet (see Fig. 1 and Fig. 3). Heatmap representations of the pairwise correlation matrix were generated using selected muscle metabolites in mice fed cHF (**A**), cHF+F (**B**), cHF+ROSI (**C**), and cHF+F+ROSI (**D**) diets. Each square represents Pearson correlation coefficient between the metabolite in the row with that in the column. The strength of correlation (red, positive; green, negative) is expressed as a color intensity, see the color scale bar. CX, acylcarnitine with the chain of X carbons; SHORT, sum of acylcarnitines C3-C7; MEDIUM, sum of carnitines C8-C13; LONG, sum of acylcarnitines C14–18; TOTAL, sum of all acylcarnitines.
doi:10.1371/journal.pone.0043764.g004

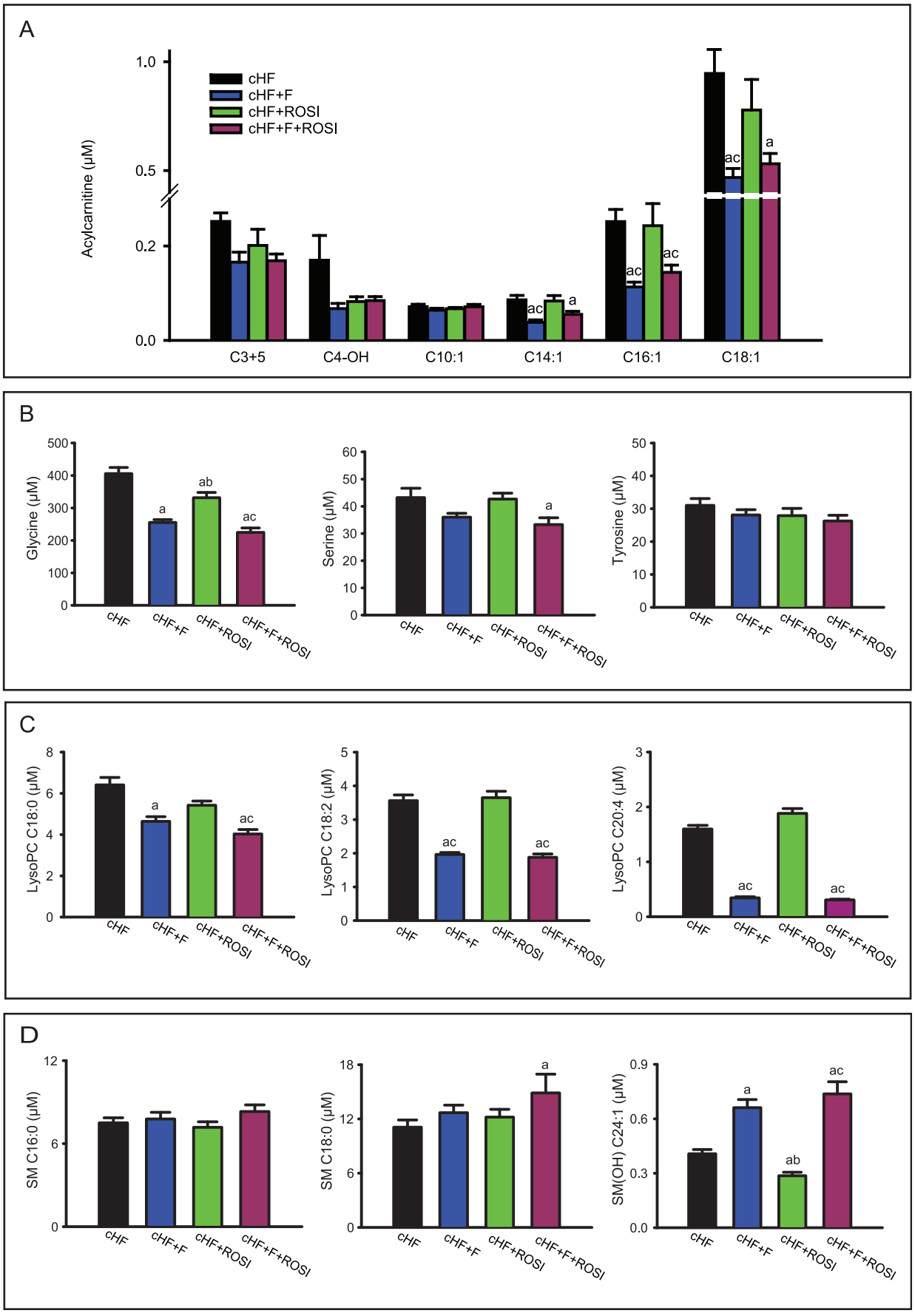
A
Acylcarnitine (µM)
1.0
0.5
0.2
0.0
cHF
cHF+F
cHF+ROSI
cHF+F+ROSI
C3+5
C4-OH
C10:1
C14:1
C16:1
C18:1
ac
a
B
Glycine (µM)
Serine (µM)
Tyrosine (µM)
C
LysoPC C18:0 (µM)
LysoPC C18:2 (µM)
LysoPC C20:4 (µM)
D
SM C16:0 (µM)
SM C18:0 (µM)
SM(OH) C24:1 (µM)
ab

Figure 5. Concentrations of selected metabolites in gastrocnemius muscle extracts. Analysis was performed in mice re-fed Chow diet (see Fig. 3 and Table 1). **A.** Carnitines: propionyl-L-carnitine and isovalerlycarnitine (C3+C5); malonyl-L-carnitine (C4-OH); and various even-chain monounsaturated acylcarnitines (C10:1, C14:1, C16:1, and C18:1; individual acylcarnitines are denoted by their side chain; see Table S1). **B**. Amino acids. **C.** Lysophosphatidylcholines: stearoyl lysophasphatidylcholine (lysoPC C18:0); linoleoyl lysophosphatidylcholine (lysoPC C18:2); and arachidonoyl lysophasphatidylcholine (lysoPC C20:4). **D.** Sphingolipids: palmitoyl sphingomyeline (SM C16:0); stearoyl sphingomyeline (SM C18:0); and hydroxysphingomyeline [SM(OH) C24:1]. **D.** Data are means±SE ($n = 7–8$). Dietary groups are: cHF (black bars), cHF+F (blue bars); cHF+ROSI (green bars) and cHF+F+ROSI (violet bars). [a]Significantly different from cHF; [b]significantly different from cHF+F; [c]significantly different from cHF+ROSI (ANOVA).
doi:10.1371/journal.pone.0043764.g005

treatments decreased C4-OH, while its regulation with respect to the levels of other metabolites emerged as a unique marker of the effect of the combined intervention on muscle metabolome. This analyte could be either hydroxybutyrylcarnitine or malonylcarnitine, reflecting either the muscle levels of β-hydroxybutyrate and β-hydroxybutyryl-CoA [58], or α-hydroxybutyrate and α-hydroxybutyryl-CoA [59], or malonyl-CoA. All these metabolites could support muscle insulin sensitivity [14,32] since (i) muscle β-hydroxybutyrate represents a strong marker and a possible causal factor for insulin resistance, which correlates with plasma NEFA levels [59]; (ii) α-hydroxybutyrate, a marker of mitochondrial redox status, is linked to the regulation of BCAA [59] and it was recently identified as an early biomarker of insulin resistance [60]; and (iii) malonyl-CoA is the key lipogenic intermediate controlling mitochondrial activity of β-oxidation by inhibiting CPT-1 (ref. [47]; see below).

Importantly, only the combined intervention could suppress plasma levels of β-hydroxybutyrate in mice re-fed Chow diet. In contrast, in the animals with *ad libitum* access to the cHF-based diets, or in fasted mice, no difference in the levels of β-hydroxybutyrate between was observed the interventions [32]. Formation of β-hydroxybutyrate occurs in the liver, as a by-product of β-oxidation when carbohydrates are scarce. Therefore, the marked suppression of the plasma β-hydroxybutyrate levels by the combined intervention suggests that, in addition to the beneficial muscle metabolic flexibility, also the adaptability of hepatic metabolism is synergistically improved. That this effect only occurred in the animals that switched to carbohydrate fuels supported the improvement in hepatic insulin sensitivity.

Chronic inflammation in obesity triggers insulin resistance [61], depending also on macrophage accumulation in the muscle and inflammatory state of muscle cells [62]. Therefore, we sought to detect changes in muscle metabolome, which could document anti-inflammatory effects of the treatments. Indeed, levels of several lysoPCs were decreased by the interventions, and the combined intervention tended to exert the strongest effect, in accordance with the notion that lysoPCs are associated with obesity-induced low-grade systemic inflammation (reviewed in [32]), and that phospholipase A2-derived lysoPC exert adverse effects on insulin responsiveness of myocytes [63].

Table 3. Differentially expressed, unique genes classified in biological processes.

	Upregulated		Downregulated		Total	
Single interventions	**cHF+F**	**cHF+ROSI**	**cHF+F**	**cHF+ROSI**	**cHF+F**	**cHF+ROSI**
Immune response	17	1	24	4	41	5
Development	15	5	12	2	27	7
G-protein signaling	9	0	13	0	22	0
Angiogenesis	11	4	10	8	21	12
Cell cycle	3	3	15	7	18	10
Transport	4	0	4	0	8	0
Total:	27	7	42	15	69	22
Combined intervention	**Upregulated**	**Downregulated**	**Total**			
Development	29	21	50			
Muscle contraction	8	18	26			
Apoptosis and survival	10	7	17			
Cell adhesion	2	12	14			
Angiogenesis	5	9	14			
Immune response	4	10	14			
Transcription	6	7	13			
G protein signaling	5	7	12			
Regulation of lipid metabolism	3	7	10			
Trafficking	5	1	6			
Total:	77	99	176			

Single interventions, unique genes with absolute FC ≥1.2 significantly different from cHF; combined intervention, unique genes with absolute FC ≥1.2 significantly different from cHF+F (*t*-test). Genes were manually classified in biological processes using scientific literature and bioinformatical resources, following initial MetaCore pathway analysis.
doi:10.1371/journal.pone.0043764.t003

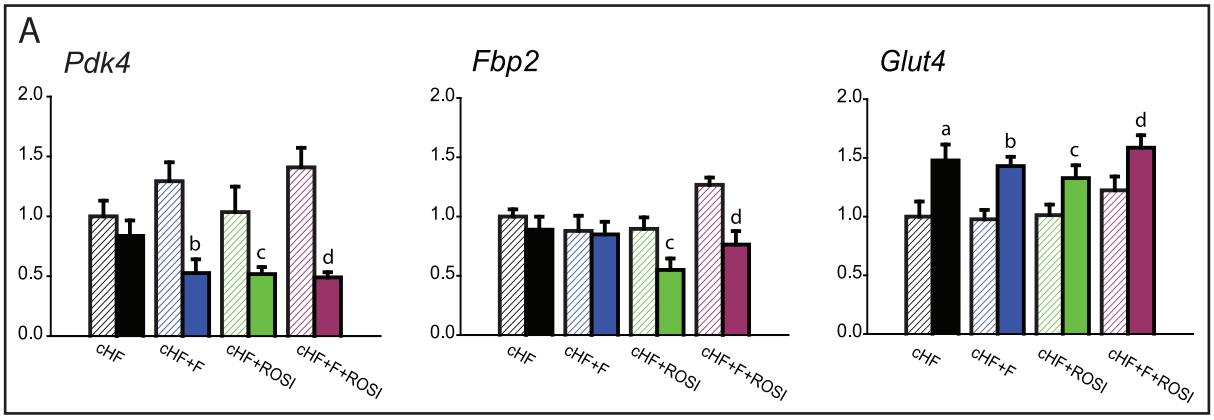

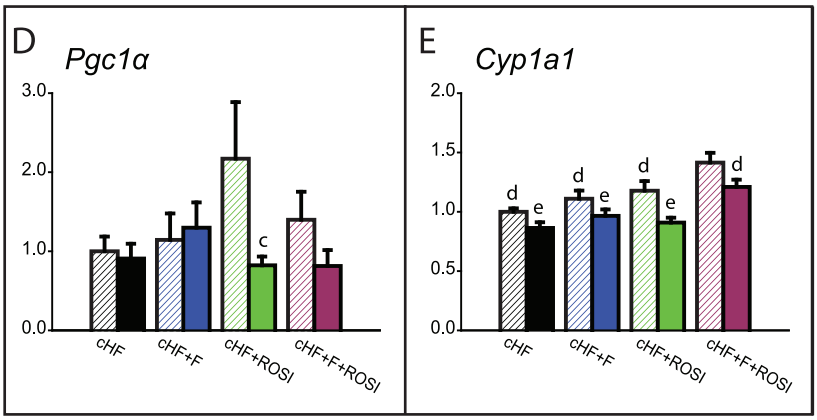

Figure 6. Expression of selected genes in gastrocnemius muscle. Mice were killed either without any additional manipulations, that is, while offered various 'original' cHF-based diets (OrD; crossed bars), or following the diet-switch protocol when re-fed Chow diet (full bars); see Fig. 1. **A**.Genes involved in carbohydrate metabolism: pyruvate dehydrogenase kinase isozyme 4 (*Pdk4*); fructose-1,6-bisphosphatase isoenzyme 2 (*Fbp2*); and glucose transporter type 4 (*Glut4*). **B**. Genes involved in lipid metabolism: acyl-CoA thioesterase 1 (*Acot1*); carnitine palmitoyltransferase 1b

(*Cpt1b*); and CD36 antigen (*Cd36*). **C**. Slow muscle (oxidative) fiber genes: myosin, heavy polypeptide 6 (*Myh6*); myosin, heavy polypeptide 7 (*Myh7*); and troponin C type 1 (*Tnnc1*). **D.** *Pgc1α*. **E.** Cytochrome P450, family 1, subfamily a, polypeptide 1 (*Cyp1a1*). Data are means±SE ($n = 7$–8). See also Table S6. [a]Significantly different from cHF, OrD; [b]significantly different from cHF+F, OrD; [c]significantly different from cHF+ROSI, OrD; [d]significantly different from cHF+F+ROSI, OrD; [e]significantly different from cHF+F+ROSI, re-fed Chow (ANOVA).
doi:10.1371/journal.pone.0043764.g006

Interestingly, we have found here a specific pattern of regulation of SM(OH) C24:1 levels in the muscle, with the opposite effects by the single interventions, while combined intervention strongly increased the levels of this metabolite. As we have found before, SM(OH) C24:1 represents the most strongly associated single metabolite with a genetic variant of serine-palmitoyltransferase [64], the rate-limiting enzyme in the synthesis of ceramides and sphingomyelins. Activity of this enzyme is increased in response to the treatments, which enhances insulin sensitivity, like aerobic training [65] or pioglitazone [66]. Moreover, the involvement of ceramide-derived sphingosines in the activation of AMP-activated protein kinase by adiponectin, downstream from the adiponectin receptors, was recently suggested [67]. This mechanism, which should operate in the muscle, suggests a new role for the sphingolipid metabolism [66] with respect to its long-disputed role in affecting muscle insulin sensitivity [65,66,68–70]. Our results further support the importance of SM(OH) C24:1 as a marker of the muscle sphingosines metabolism.

Gene Expression in the Muscle

Expression profiling in the muscle indicated a higher number of genes regulated in response to the combined intervention as compared with any of the single interventions, suggesting multiple mechanisms of action. Identification of the key metabolic genes was enabled by the quantitative comparison of the expression under the different metabolic states, i.e. in the animals relying mostly on either carbohydrate (mice re-fed Chow) or lipid fuels (mice with *ad libitum* access to the cHF-based diets). This approach revealed the involvement of both glycolysis and fatty acid oxidation in the preservation of the adaptability of muscle metabolism (see also ref. [71]); and moreover, it identified several candidates, namely *Pdk4*, *Fbp2* and *Cpt1b*, which could be involved in the additive effects of the combined intervention. That *Cpt1b* but not *Cpt1a* was regulated substantiates the view that *Cpt1b* was important for the modulation of fuel partitioning and β-oxidation by all the interventions, since it is primarily *Cpt1b* which is more sensitive to the inhibition by malonyl-CoA [47]. Previous studies suggested that oxidative (slow) muscle fibers could be important for metabolic flexibility [36,49]. As compared with the glycolytic fibers, the oxidative fibers contain more mitochondria [72] and they are more insulin sensitive and more abundant in the muscle of insulin-sensitive than insulin-resistant human subjects [68]. Indeed, our unbiased analysis uncovered that several oxidative fibers genes, namely *Myh6*, *Myh7*, and *Tnnc1* were regulated in

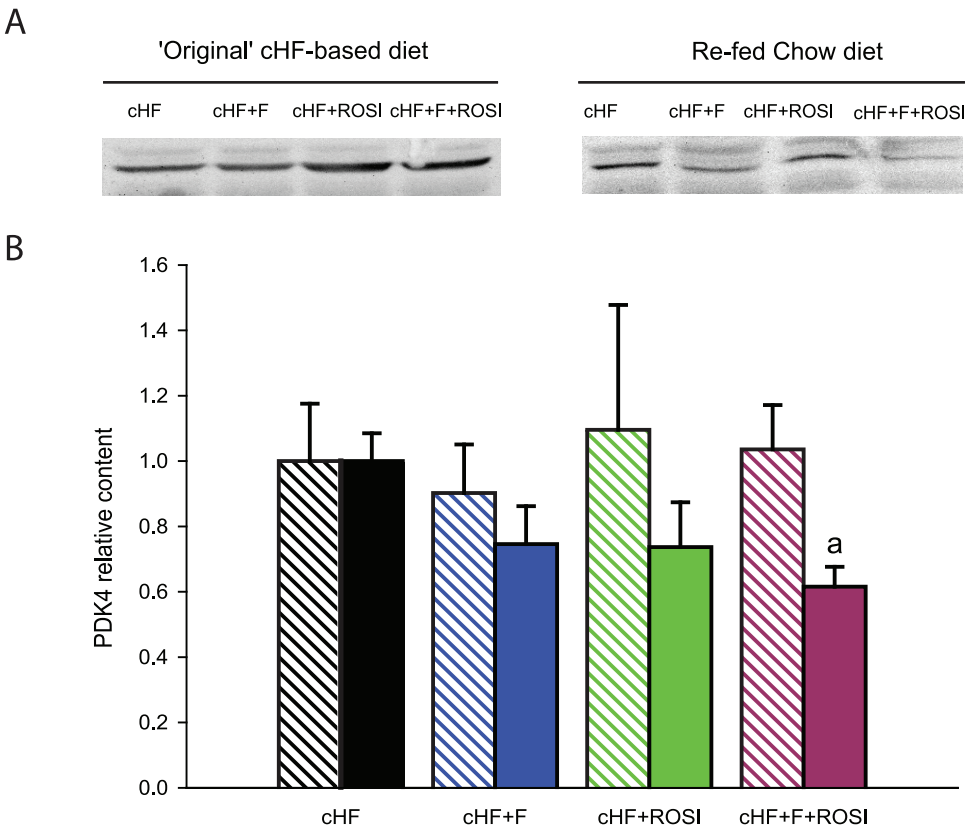

Figure 7. Content of PDK4 protein in gastrocnemius muscle. Mice were killed either without any additional manipulations, that is, while offered the 'original' cHF-based diet in fed state (crossed bars), or following the diet-switch protocol when re-fed Chow diet (full bars). **A**. Representative Western blot analysis. **B**. Quantification of PDK4 protein in skeletal muscle. Values are means±S.E. ($n = 5$–8). [a]Significantly different from mice offered the cHF+F+ROSI diet (ANOVA).
doi:10.1371/journal.pone.0043764.g007

accordance with their involvement in metabolic flexibility. Our results suggest that the combined intervention potentiated the switch between the oxidative and glycolytic fibres, which is activated in response to the change of metabolic fuels. Thus, the combined intervention exhibited the most pronounced regulation of the oxidative fibres genes, while inducing their highest expression when the animals had *ad libitum* access to the cHF-based diets, and the lowest expression in the animals re-fed Chow. Interestingly, expression of *Pgc1α*, the master regulator of mitochondrial biogenesis and the marker of the slow muscle fibers [51,52], matched the changes in the expression of the oxidative fibres genes only to a limited extent.

With respects to the anti-inflammatory effects of the interventions, meaningful changes in the expression of *Cyp1a1* were found, showing additive induction by the combination treatment. This gene is inducible by both TZDs [73], and PUFA [74], acts both as epoxygenase and hydroxylase, while producing PUFA-derived lipid mediators, with EPA-derived lipid mediators exerting presumably anti-inflammatory effects [53].

Conclusions

Our results indicate that the combined use *n*-3 LC-PUFA and rosiglitazone preserve metabolic flexibility of mice fed an obesogenic high-fat diet, with a stronger, additive, effect as compared with any of the interventions applied individually (Fig. 8). Indirect calorimetry demonstrated that especially metabolic flexibility to carbohydrates was preserved in response to the combined intervention, also in agreement with the previously observed synergistic improvement of muscle insulin sensitivity under these conditions. Metabolomic and gene expression analyses suggested that both carbohydrate and lipid metabolism contribute to a better adaptability to fluctuating metabolic fuels and they highlighted the importance of mitochondrial fatty acid oxidation in the adaptability of muscle metabolism, while modulation of BCAA metabolism may be essential for the beneficial effect of the combined intervention on muscle insulin sensitivity. Our results further support the idea that dietary supplementation using *n*-3 LC-PUFA could improve the efficacy of TZDs, as well as other insulin-sensitizing and hypolipidemic pharmaceuticals used for the treatment of obese and type 2 diabetic patients.

Methods

Animals and Treatments

Male C57BL/6N mice (Charles River Laboratories, Sulzfeld, Germany) were maintained at 22°C on 12-h light-dark cycle (light from 6.00 a.m.) with free access to water and Chow diet (extruded Ssniff R/M-H diet; Ssniff Spezialdieten GmbH, Soest, Germany; with lipid, carbohydrate, and protein content ~3.4, 55.3, and 19.3% wt/wt, respectively; energy density, 16.3 kJ/g). As described before [14,32], three-month-old mice (Fig. 1) were randomly assigned (2 animals per cage) to cHF diet (lipid content ~35% wt/wt, mainly corn oil; and carbohydrate, and protein content ~35.4, and 20.5% wt/wt, respectively) or to the following 'interventions' using isocaloric cHF-based diets (energy density, 22.8 kJ/g), namely (i) cHF+F, cHF diet supplemented with *n*-3 LC-PUFA concentrate (46% DHA, 14% EPA, wt/wt, as triglycerides; product EPAX 1050 TG; EPAX a.s., Aalesund, Norway), which replaced 15% wt/wt of dietary lipids; (ii) cHF+ROSI, cHF diet supplemented with 10 mg rosiglitazone/kg diet (Avandia; GlaxoSmithKline, USA); and (iii) cHF+F+ROSI, cHF diet supplemented with both *n*-3 LC-PUFA concentrate and rosiglitazone. Chow diet-fed control mice were also included in the study. During the experiment lasting for 8 weeks (week 1– week 8), fresh ration of food was distributed daily and food consumption and body weights were recorded once a week. For the detailed fatty acid composition of lipids of all the diets, see [14].

Animals were killed by cervical dislocation under pentobarbital anesthesia (between 9.00 a.m. and 11.00 a.m.), (i) either when allowed free access to different cHF-based diets ($n = 8$), or (ii) using a 'diet-switch protocol' (Fig. 1) when the animals were first fasted for 10 hours during the light phase of the day (between 8.00 a.m. and 6.00 p.m.), than re-fed Chow (starting at 6.00 p.m.), and killed the following day ($n = 10$). In the second case, glycemia was evaluated and EDTA-plasma for measurement of various metabolites (see below) was collected in fed state, at 7.00 a.m., either before the initiation of the fasting period (when fed various cHF-based diets), or before the killing (when re-fed Chow; Fig. 1). In both cases, gastrocnemius muscle was dissected for RNA analysis (see below).

The animal experiments were specifically approved by the Animal Care and Use Committee of the Institute of Physiology Academy of Sciences of the Czech Republic v.v.i. (Approval Number: 172/2009) and conducted under the guidelines.

Indirect Calorimetry

To evaluate energy expenditure, as well as metabolic flexibility to the high-carbohydrate meal, indirect calorimetry was performed using system INCA (Somedic, Horby, Sweden) [19,41] during week 6 of the experiment (Fig. 1) in singly caged mice (Eurostandard type II mouse plastic cages, ~ 6,000 ml; Techniplast, Milan, Italy), which were placed in sealed measuring chambers equipped with thermostatically controlled heat exchangers at 22°C. VO_2 and VCO_2 were recorded every 2 min under a constant airflow rate (1000 ml/min). The diet-switch protocol (see above and Fig. 1) was used, allowing for the evaluation of metabolic flexibility, which was assessed as the induction in RER in response to the re-feeding Chow diet, following the period of fasting. Alternatively, to assess the change in fuel partitioning more accurately, PRCF curves were constructed based on RER values pooled from all animals within a given dietary group during the specific period of the measurement. Provided that PRCF curves represent the normally distributed data, the values of log EC_{50} of PRCF (50^{th} percentile value) correspond to RER values [41].

Metabolite Quantification

NEFA, triglycerides, and β-hydroxybutyrate in EDTA-plasma and glycemia were assessed as before [32]. In addition, targeted metabolomics analysis was performed using extracts [75] from skeletal muscle (100 mg aliquots; samples collected in our previous study [32]) to determine concentrations of 163 metabolites using a targeted metabolomics kit (AbsoluteIDQTM kit p150, Biocrates Life Sciences AG, Innsbruck, Austria) based on FIA-MS as before [32,64]. Concentrations of all analyzed metabolites are reported in μM. For the general information on biological roles of the metabolites, see [64]. In short, 14 amino acids, sum of hexoses, free carnitine, 26 acylcarnitines, 14 hydroxy- and dicarboxy-acylcarnitines, 10 sphingomyelins, 5 hydroxysphingomyelins, 38 diacyl-phosphatidylcholines, 39 acyl-alkyl-phospatidylcholines, and 15 lysophosphatidylcholines were quantified. For the full list of the measured metabolites and the abbreviations to denote them, see Table S1.

Gene Expression in Skeletal Muscle

Total RNA was isolated from gastrocnemius muscle samples stored in RNA*later* (Ambion, Austin, TX, USA) at −20°C using TRI Reagent (Sigma-Aldrich, St. Louis, MO, USA) according to the manufacturer's instruction. After extraction, RNA was purified

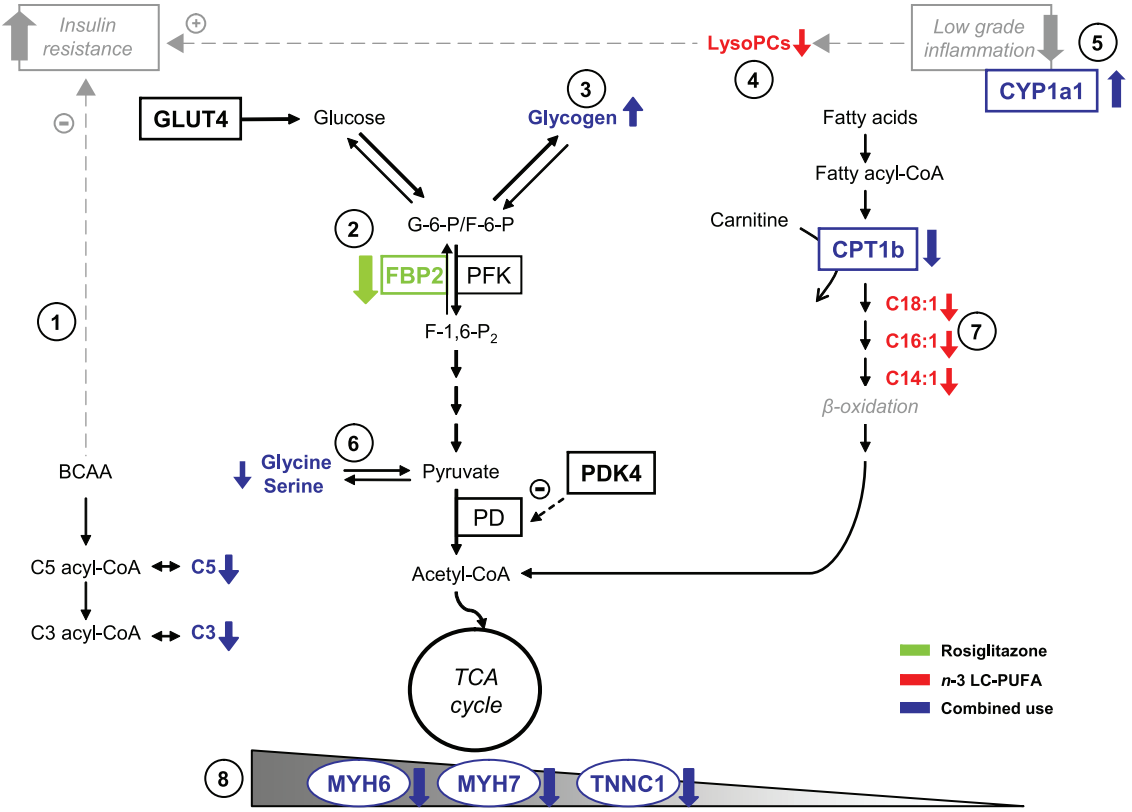

Figure 8. Synopsis of the results of metabolomic and gene expression analyses in the muscle. Metabolomic and gene expression analyses suggested complementary effects of the single interventions, with rosiglitazone augmenting insulin sensitivity by the modulation of branched-chain amino acid metabolism, especially when combined with *n*-3 LC-PUFA (1), and *n*-3 LC-PUFA supporting specifically complete oxidation of fatty acids in mitochondria (7). These beneficial metabolic effects were associated with inhibition of low grade tissue inflammation (5) and the activation of the switch between glycolytic and oxidative muscle fibers (8), especially in the combined intervention. Moreover, rosiglitazone inhibited gene expression of fructose-1,6-bisphosphatase 2 - a key enzyme of gluconeogenesis (2), while the concentrations of most of lysophosphatidylcholines were reduced in response to *n*-3 LC-PUFA (4). Glucogenic amino acids, namely glycine and serine, were affected by the combined intervention (6). As we published previously [14], the combined intervention also exerted synergistic stimulatory effect on muscle glycogen synthesis (3). Altered metabolites (bold font) and altered transcripts (bold font, rectangle) are marked. BCAA, branched-chain amino acids; C, acylcarnitine; CPT1b, carnitine palmitoyltransferase 1b; CYP1a1, member of the cytochrome P450 family genes; FBP2, fructose-1,6-bisphosphatase 2; GLUT4, glucose transporter 4; lysoPCs, lysophosphatidylcholines; PD, pyruvate dehydrogenase; PDK4 pyruvate dehydrogenase kinase 4; PFK, phosphofructokinase; MYH6 and MYH7, myosin heavy polypeptide; TCA cycle, tricarboxylic acid cycle; TNNC1, troponin C1.
doi:10.1371/journal.pone.0043764.g008

by using RNeasy columns (Qiagen, Venlo, The Netherlands). RNA concentration and purity were measured using the NanoDrop spectrophotometer (IsoGen Life Science, Maarsen, The Netherlands). The integrity of RNA was checked with Experion automated electrophoresis system (BioRad, Veenendaal, The Netherlands). Levels of selected gene transcripts in total muscle RNA from individual mice were evaluated using real-time qRT-PCR [13] and appropriate primers (see Table S5).

Muscle total RNA isolated from individual mice was also analyzed using Agilent whole genome 44K mouse gene expression arrays (Agilent Technologies, Inc., Santa Clara, CA, USA), similarly as described before (ref. [76]; see Supporting Information S1). The arrays contain 43,379 probes (excluding controls). Differential gene expression was assessed in two subsequent microarray analyses using a reference pool design. In the first analysis mice ($n = 7$–8) of the cHF, cHF+F, and cHF+ROSI treatment groups were assessed and in the second analysis, the cHF+ROSI and cHF+F+ROSI were assessed. In total, after removing probes that were below two times the background, 20,721 probes remained in the first study and 25,922 probes in the second study. Quality control and data handling was done as described [76]. More detailed information, including data analysis, is provided in Supporting Information S1. The gene expression studies are deposited in Gene Expression Omnibus of NCBI with GEO accession number GSE36718.

Western Blot Analysis of Protein Levels of PDK4

Frozen muscles (50 mg) were homogenized in 0.3 ml of ice-cold lysis buffer (20 mmol/l Tris, pH 7.4; 1 mmol/l EDTA; 1% deoxycholate; 1% Triton X-100; 1 mmol/l phenylmethylsulfonyl fluoride; 10 µg/ml aprotinin; 10 µg/ml leupeptin and Phosphatase-Inhibitor-Mix I [Serva, Heidelberg, Germany]). Tissue lysates were centrifuged at 15,000 g for 10 minutes at 4°C. Protein concentration in supernatant was determined by bicinchoninic acid assay. 50 µg protein was separated by 10% sodium dodecylsulphate-polyacrylamide gel electrophoresis and transferred to Immobilon-FL membranes (Millipore, Billerica, MA, USA). The membranes were then probed with rabbit antibodies against PDK4 (1:200; Abgent, San Diego, CA, USA). Secondary antibody conjugated to IRDye 800CW (Li-COR, Lincoln, NE, USA) was used for detection. Membranes were scanned using an Odyssey IR scanner (LI-COR). The results were quantified using AIDA image analysis software (Raytest, Straubenhardt, Germany).

Statistical Analysis

Growth characteristics, plasma parameters, indirect calorimetry data, and metabolite concentration profile data were analyzed using ANOVA and paired *t*-test as before [19,32]. All values are presented as means±SE. Comparisons were judged to be significant at $p \leq 0.05$. Correlation matrices were computed using MS Excel. Gene array data was processed with MetaCore Pathway analysis software (GeneGo, Carlsbad, CA, USA). PLS-DA was performed using Umetrics SIMCA-P+12 statistical software (Umetrics AB, Umea, Sweden) as before [32]. When the PLS-DA score plot showed significantly separated groups, a loading scatter plot was constructed to determine the variables influencing their separation.

Supporting Information

Figure S1 The effects of various interventions on gastrocnemius muscle metabolome - detailed loading scatter plot. Identification of the metabolites shown in the simplified loading scatter plot (Fig. 3B). Acylcarnitines (green triangle), aminoacids (inverted blue triangle), lysophosphatidylcholines (yellow circles), diacyl phosphatidylcholines (orange circles), acyl-alkyl phosphatidylcholines (red circles), sphingolipids (violet circles) and sum of hexoses (dark green diamante) are shown. Individual metabolites are indicated by unique numbers (see Table S1 for the name of each metabolite).
(EPS)

Table S1 List of all 163 metabolites measured in skeletal muscle extracts - targeted metabolomics analysis. In short, 14 amino acids, sum of hexoses (H1), free carnitine (C0), 26 acylcarnitines (C2, C3,…C18:2), 14 hydroxy- and dicarboxy-acylcarnitines (C-3OH, C4-OH, C5-DC,…C18:1-OH), 10 sphingomyelins (SM C16:0, SM C16:1,… SM C26:1), 5 hydroxysphingomyelins [SM(OH)C14:1… SM(OH)C24:1], 38 diacyl-phosphatidylcholines (PC aa C24:0 …PC aa C42:6), 39 acyl-alkyl-phospatidylcholines (PC ae C30:0… PC ae C44:6), and 15 lyso-phosphatidylcholines (lysoPC a C6:0….lysoPC a C28:1) were identified in extracts of skeletal muscle from animals subjected to various interventions and killed when re-fed Chow (see Methods and Fig. 1). Concentrations of all analysed metabolites are reported in μM. All metabolites above were determined using flow injection analysis/thermospray mass spectrometry (**FIA-MS**) with Biocrates Absolute*IDQ*^{TM} targeted metabolomics technology. Data are means±SE ($n = 7$–8).
(XLS)

Table S2 Differentially regulated probesets expressed in cHF+F versus control cHF dietary groups. The data provided represents only the statistical significant differentially expressed probesets of the microarrays (cHF: $n = 8$, cHF+F: $n = 8$) which showed a mean absolute fold change ≥1.5 (cHF+F/cHF).
(DOC)

Table S3 Differentially regulated probesets expressed in cHF+ROSI versus cHF dietary groups. The data provided represents only the statistical significant differentially expressed probesets of the microarrays (cHF+ROSI: $n = 8$, cHF: $n = 8$) which showed a mean absolute fold change ≥1.5 (cHF+ROSI/cHF).
(DOC)

Table S4 Differentially regulated probesets expressed in cHF+F+ROSI versus cHF+ROSI dietary groups. The data provided represents only the statistical significant differentially expressed probesets of the microarrays (cHF+F+ROSI: $n = 8$, cHF+ROSI: $n = 8$) which showed a mean absolute fold change ≥1.5 (cHF+F+ROSI/cHF+ROSI).
(DOC)

Table S5 Real-time quantitative RT-PCR analysis: genes and primers.
(DOC)

Table S6 Real-time quantitative RT-PCR analysis in skeletal muscle. At the end of the experiment, mice were killed either without any additional manipulations, that is, while offered the 'original' cHF-based diets (OrD), or following the 'diet-switch protocol' when re-fed Chow diet; see Fig. 1. Control mice maintained on Chow diet throughout the intervention and killed in *ad libitum* fed state were also analyzed. Data are means±SE ($n = 7$–8). For gene symbols, see Table S5. [a] Significantly different from cHF, OrD. [b] significantly different from cHF+F, OrD. [c] significantly different from cHF+ROSI, OrD. [d] significantly different from cHF+F+ROSI, OrD. [e] Significantly different from cHF, Re-fed Chow. [f] significantly different from cHF+F, Re-fed Chow. [g] significantly different from cHF+ROSI, Re-fed Chow. [h] significantly different from cHF+F+ROSI, Re-fed Chow (Two-way ANOVA). [i] significantly different from Chow (t-test).
(DOC)

Supporting Information S1
(DOC)

Acknowledgments

We thank Dr. Werner Römisch-Margl, Julia Scarpa, Katharina Sckell and Arsin Sabunchi for the metabolomics measurements performed at the Helmholtz Centrum München, Genome Analysis Center, Neuherberg, Germany.

Author Contributions

Conceived and designed the experiments: J. Kopecky. Performed the experiments: OH DM EMS AB OK VK KB PJ MH CP JA. Analyzed the data: OK DM EMS PF J. Kopecky J. Keijer CP JA MR RW-S TI. Wrote the paper: OH DM PF OK MR EMS J. Keijer J. Kopecky.

References

1. Bays HE, Maki KC, McKenney J, Snipes R, Meadowcroft A, et al. (2010) Long-term up to 24-month efficacy and safety of concomitant prescription omega-3-acid ethyl esters and simvastatin in hypertriglyceridemic patients. Curr Med Res Opin 26: 907–915.
2. Reyes-Soffer G, Rondon-Clavo C, Ginsberg HN (2011) Combination therapy with statin and fibrate in patients with dyslipidemia associated with insulin resistance, metabolic syndrome and type 2 diabetes mellitus. Expert Opin Pharmacother 12: 1429–1438.
3. Nathan DM, Buse JB, Davidson MB, Ferrannini E, Holman RR, et al. (2008) Management of hyperglycaemia in type 2 diabetes mellitus: a consensus algorithm for the initiation and adjustment of therapy. Update regarding the thiazolidinediones. Diabetologia 51: 8–11.
4. Yokoyama M, Origasa H, Matsuzaki M, Matsuzawa Y, Saito Y, et al. (2007) Effects of eicosapentaenoic acid on major coronary events in hypercholesterolaemic patients (JELIS): a randomised open-label, blinded endpoint analysis. Lancet 369: 1090–1098.
5. Edelstein SL, Knowler WC, Bain RP, Andres R, Barrett-Connor EL, et al. (1997) Predictors of progression from impaired glucose tolerance to NIDDM: an analysis of six prospective studies. Diabetes 46: 701–710.
6. MacLean CH, Mojica WA, Morton SC, Pencharz J, Hasenfeld Garland R, et al. (2004) Effects of omega-3 fatty acids on lipids and glycemic control in type II diabetes and the metabolic syndrome and on inflammatory bowel disease, rheumatoid arthritis, renal disease, systemic lupus erythrematosus, and osteoporosis. Summary, Evidence Report. AHRQ Publication No.04-E012–1.
7. Nettleton JA, Katz R (2005) n-3 long-chain polyunsaturated fatty acids in type 2 diabetes: a review. J Am Diet Assoc 105: 428–440.
8. Kromhout D, Geleijnse JM, de Goede J, Oude Griep LM, Mulder BJ, et al. (2011) n-3 fatty acids, ventricular arrhythmia-related events, and fatal

myocardial infarction in postmyocardial infarction patients with diabetes. Diabetes Care 34: 2515–2520.
9. Ruxton CH, Reed SC, Simpson MJ, Millington KJ (2007) The health benefits of omega-3 polyunsaturated fatty acids: a review of the evidence. J Hum Nutr Diet 17: 449–459.
10. Flachs P, Rossmeisl M, Bryhn M, Kopecky J (2009) Cellular and molecular effects of *n*-3 polyunsaturated fatty acids on adipose tissue biology and metabolism. Clinical Sciences 116: 1–16.
11. Ikemoto S, Takahashi M, Tsunoda N, Maruyama K, Itakura H, et al. (1996) High-fat diet-induced hyperglycemia and obesity in mice: Differential effects of dietary oils. Metabolism 45: 1539–1546.
12. Ruzickova J, Rossmeisl M, Prazak T, Flachs P, Sponarova J, et al. (2004) Omega-3 PUFA of marine origin limit diet-induced obesity in mice by reducing cellularity of adipose tissue. Lipids 39: 1177–1185.
13. Flachs P, Horakova O, Brauner P, Rossmeisl M, Pecina P, et al. (2005) Polyunsaturated fatty acids of marine origin upregulate mitochondrial biogenesis and induce beta-oxidation in white fat. Diabetologia 48: 2365–2375.
14. Kuda O, Jelenik T, Jilkova Z, Flachs P, Rossmeisl M, et al. (2009) n-3 Fatty acids and rosiglitazone improve insulin sensitivity through additive stimulatory effects on muscle glycogen synthesis in mice fed a high-fat diet. Diabetologia 52: 941–951.
15. Sato A, Kawano H, Notsu T, Ohta M, Nakakuki M, et al. (2010) Antiobesity effect of eicosapentaenoic acid in high-fat/high-sucrose diet-induced obesity: importance of hepatic lipogenesis. Diabetes 59: 2495–2504.
16. Hill JO, Peters JC, Lin D, Yakubu F, Greene H, et al. (1993) Lipid accumulation and body fat distribution is influenced by type of dietary fat fed to rats. Int J Obes Relat Metab Disord 17: 223–236.
17. Belzung F, Raclot T, Groscolas R (1993) Fish oil n-3 fatty acids selectively limit the hypertrophy of abdominal fat depots in growing rats fed high-fat diets. Am J Physiol 264: R1111–R1118.
18. Raclot T, Groscolas R, Langin D, Ferre P (1997) Site-specific regulation of gene expression by n-3 polyunsaturated fatty acids in rat white adipose tissues. J Lipid Res 38: 1963–1972.
19. Flachs P, Ruhl R, Hensler M, Janovska P, Zouhar P, et al. (2011) Synergistic induction of lipid catabolism and anti-inflammatory lipids in white fat of dietary obese mice in response to calorie restriction and n-3 fatty acids. Diabetologia 54: 2626–2638.
20. Hensler M, Bardova K, Jilkova ZM, Wahli W, Meztger D, et al. (2011) The inhibition of fat cell proliferation by n-3 fatty acids in dietary obese mice. Lipids Health Dis 10: 128.
21. Jelenik T, Rossmeisl M, Kuda O, Jilkova ZM, Medrikova D, et al. (2010) AMP-activated protein kinase {alpha}2 subunit is required for the preservation of hepatic insulin sensitivity by *n*-3 polyunsaturated fatty acids. Diabetes 59: 2737–2746.
22. van Schothorst EM, Flachs P, Franssen-van Hal NL, Kuda O, Bunschoten A, et al. (2009) Induction of lipid oxidation by polyunsaturated fatty acids of marine origin in small intestine of mice fed a high-fat diet. BMC Genomics 10: 110.
23. Mori TA, Bao DQ, Burke V, Puddey IB, Watts GF, et al. (1999) Dietary fish as a major component of a weight-loss diet: effect on serum lipids, glucose, and insulin metabolism in overweight hypertensive subjects. Am J Clin Nutr 70: 817–825.
24. Couet C, Delarue J, Ritz P, Antoine JM, Lamisse F (1997) Effect of dietary fish oil on body fat mass and basal fat oxidation in healthy adults. Int J Obes 21: 637–643.
25. Kunesova M, Braunerova R, Hlavaty P, Tvrzicka E, Stankova B, et al. (2006) The influence of n-3 polyunsaturated fatty acids and very low calorie diet during a short-term weight reducing regimen on weight loss and serum fatty acid composition in severely obese women. Physiol Res 55: 63–72.
26. Thorsdottir I, Tomasson H, Gunnarsdottir I, Gisladottir E, Kiely M, et al. (2007) Randomized trial of weight-loss-diets for young adults varying in fish and fish oil content. Int J Obes (Lond) 31: 1560–1566.
27. Krebs JD, Browning LM, McLean NK, Rothwell JL, Mishra GD, et al. (2006) Additive benefits of long-chain n-3 polyunsaturated fatty acids and weight-loss in the management of cardiovascular disease risk in overweight hyperinsulinaemic women. Int J Obes (Lond) 30: 1535–1544.
28. Munro IA, Garg ML (2012) Dietary supplementation with n-3 PUFA does not promote weight loss when combined with a very-low-energy diet. Br J Nutr 1–9.
29. Storlien LH, Kraegen EW, Chisholm DJ, Ford GL, Bruce DG, et al. (1987) Fish oil prevents insulin resistance induced by high-fat feeding in rats. Science 237: 885–888.
30. Neschen S, Morino K, Dong J, Wang-Fischer Y, Cline GW, et al. (2007) *n*-3 fatty acids preserve insulin sensitivity in vivo in a PPAR{alpha}-dependent manner. Diabetes 56: 1034–1041.
31. Jucker BM, Cline GW, Barucci N, Shulman GI (1999) Differential effects of safflower oil versus fish oil feeding on insulin-stimulated glycogen synthesis, glycolysis, and pyruvate dehydrogenase flux in skeletal muscle: a 13C nuclear magnetic resonance study. Diabetes 48: 134–140.
32. Kus V, Flachs P, Kuda O, Bardova K, Janovska P, et al. (2011) Unmasking differential effects of rosiglitazone and pioglitazone in the combination treatment with *n*-3 fatty acids in mice fed a high-fat diet. Plos One 6: e27126.
33. Fasching P, Ratheiser K, Waldhausl W, Rohac M, Osterrode W, et al. (1991) Metabolic effects of fish-oil supplementation in patients with impaired glucose tolerance. Diabetes 40: 583–589.
34. Pelikanova T, Kohout M, Valek J, Kazdova L, Base J (1993) Metabolic effects of omega-3 fatty acids in type 2 (non-insulin-dependent) diabetic patients. Ann N Y Acad Sci 683: 272–278.
35. Kelley DE, Mandarino LJ (2000) Fuel selection in human skeletal muscle in insulin resistance: a reexamination. Diabetes 49: 677–683.
36. Galgani JE, Moro C, Ravussin E (2008) Metabolic flexibility and insulin resistance. Am J Physiol Endocrinol Metab 295: E1009–E1017.
37. Koves TR, Ussher JR, Noland RC, Slentz D, Mosedale M, et al. (2008) Mitochondrial overload and incomplete fatty acid oxidation contribute to skeletal muscle insulin resistance. Cell Metab 7: 45–56.
38. Newgard CB, An J, Bain JR, Muehlbauer MJ, Stevens RD, et al. (2009) A branched-chain amino acid-related metabolic signature that differentiates obese and lean humans and contributes to insulin resistance. Cell Metab 9: 311–326.
39. Newgard CB (2012) Interplay between Lipids and Branched-Chain Amino Acids in Development of Insulin Resistance. Cell Metab 15: 606–614.
40. Punthakee Z, Bosch J, Dagenais G, Diaz R, Holman R, et al. (2012) Design, history and results of the Thiazolidinedione Intervention with vitamin D Evaluation (TIDE) randomised controlled trial. Diabetologia 55: 36–45.
41. Kus V, Prazak T, Brauner P, Hensler M, Kuda O, et al. (2008) Induction of muscle thermogenesis by high-fat diet in mice: association with obesity-resistance. Am J Physiol Endocrinol Metab 295: E356–E367.
42. Mihalik SJ, Goodpaster BH, Kelley DE, Chace DH, Vockley J, et al. (2010) Increased levels of plasma acylcarnitines in obesity and type 2 diabetes and identification of a marker of glucolipotoxicity. Obesity (Silver Spring) 18: 1695–1700.
43. Kwon HS, Harris RA (2004) Mechanisms responsible for regulation of pyruvate dehydrogenase kinase 4 gene expression. Adv Enzyme Regul 44: 109–121.
44. Tillmann H, Stein S, Liehr T, Eschrich K (2000) Structure and chromosomal localization of the human and mouse muscle fructose-1,6-bisphosphatase genes. Gene 247: 241–253.
45. James DE, Brown R, Navarro J, Pilch PF (1988) Insulin-regulatable tissues express a unique insulin-sensitive glucose transport protein. Nature 333: 183–185.
46. Hunt MC, Rautanen A, Westin MA, Svensson LT, Alexson SE (2006) Analysis of the mouse and human acyl-CoA thioesterase (ACOT) gene clusters shows that convergent, functional evolution results in a reduced number of human peroxisomal ACOTs. FASEB J 20: 1855–1864.
47. McGarry JD, Mills SE, Long CS, Foster DW (1983) Observations on the affinity for carnitine, and malonyl-CoA sensitivity, of carnitine palmitoyltransferase I in animal and human tissues. Demonstration of the presence of malonyl-CoA in non-hepatic tissues of the rat. Biochem J 214: 21–28.
48. Todd MK, Watt MJ, Le J, Hevener AL, Turcotte LP (2007) Thiazolidinediones enhance skeletal muscle triacylglycerol synthesis while protecting against fatty acid-induced inflammation and insulin resistance. Am J Physiol Endocrinol Metab 292: E485–E493.
49. Schiaffino S (2010) Fibre types in skeletal muscle: a personal account. Acta Physiol (Oxf) 199: 451–463.
50. Kischel P, Bastide B, Stevens L, Mounier Y (2001) Expression and functional behavior of troponin C in soleus muscle fibers of rat after hindlimb unloading. J Appl Physiol 90: 1095–1101.
51. Lin J, Wu H, Tarr PT, Zhang CY, Wu Z, et al. (2002) Transcriptional co-activator PGC-1 alpha drives the formation of slow-twitch muscle fibres. Nature 418: 797–801.
52. Russell AP, Feilchenfeldt J, Schreiber S, Praz M, Crettenand A, et al. (2003) Endurance training in humans leads to fiber type-specific increases in levels of peroxisome proliferator-activated receptor-gamma coactivator-1 and peroxisome proliferator-activated receptor-alpha in skeletal muscle. Diabetes 52: 2874–2881.
53. Arnold C, Konkel A, Fischer R, Schunck W-H (2010) Cytochrome P-450-dependent metabolism of omega 6 and omega-3 long-chain polyunsaturated fatty acids. Pharmacological Reports 62: 536–547.
54. Corpeleijn E, Mensink M, Kooi ME, Roekaerts PM, Saris WH, et al. (2008) Impaired skeletal muscle substrate oxidation in glucose-intolerant men improves after weight loss. Obesity (Silver Spring) 16: 1025–1032.
55. Rustan AC, Hustvedt BE, Drevon CA (1993) Dietary supplementation of very long-chain n-3 fatty acids decreases whole body lipid utilization in the rat. J Lipid Res 34: 1299–1309.
56. Asterholm IW, Scherer PE (2010) Enhanced metabolic flexibility associated with elevated adiponectin levels. Am J Pathol 176: 1364–1376.
57. Hsiao G, Chapman J, Ofrecio JM, Wilkes J, Resnik JL, et al. (2011) Multi-tissue, selective PPARgamma modulation of insulin sensitivity and metabolic pathways in obese rats. Am J Physiol Endocrinol Metab 300: E164–E174.
58. An J, Muoio DM, Shiota M, Fujimoto Y, Cline GW, et al. (2004) Hepatic expression of malonyl-CoA decarboxylase reverses muscle, liver and whole-animal insulin resistance. Nat Med 10: 268–274.
59. Adams SH (2011) Emerging perspectives on essential amino acid metabolism in obesity and the insulin-resistant state. Advances in Nutrition 2: 445–456.
60. Gall WE, Beebe K, Lawton KA, Adam KP, Mitchell MW, et al. (2010) alpha-hydroxybutyrate is an early biomarker of insulin resistance and glucose intolerance in a nondiabetic population. PLoS ONE 5: e10883.
61. Lee YS, Li P, Huh JY, Hwang IJ, Lu M, et al. (2011) Inflammation is necessary for long-term but not short-term high-fat diet-induced insulin resistance. Diabetes 60: 2474–2483.

62. Varma V, Yao-Borengasser A, Rasouli N, Nolen GT, Phanavanh B, et al. (2009) Muscle inflammatory response and insulin resistance: synergistic interaction between macrophages and fatty acids leads to impaired insulin action. Am J Physiol Endocrinol Metab 296: E1300–E1310.
63. Han MS, Lim YM, Quan W, Kim JR, Chung KW, et al. (2011) Lysophosphatidylcholine as an effector of fatty acid-induced insulin resistance. J Lipid Res 52: 1234–1246.
64. Illig T, Gieger C, Zhai G, Romisch-Margl W, Wang-Sattler R, et al. (2010) A genome-wide perspective of genetic variation in human metabolism. Nat Genet 42: 137–141.
65. Blachnio-Zabielska A, Zabielski P, Baranowski M, Gorski J (2011) Aerobic training in rats increases skeletal muscle sphingomyelinase and serine palmitoyltransferase activity, while decreasing ceramidase activity. Lipids 46: 229–238.
66. Baranowski M, Blachnio A, Zabielski P, Gorski J (2007) Pioglitazone induces de novo ceramide synthesis in the rat heart. Prostaglandins Other Lipid Mediat 83: 99–111.
67. Holland WL, Miller RA, Wang ZV, Sun K, Barth BM, et al. (2011) Receptor-mediated activation of ceramidase activity initiates the pleiotropic actions of adiponectin. Nat Med 17: 55–63.
68. Coen PM, Dube JJ, Amati F, Stefanovic-Racic M, Ferrell RE, et al. (2010) Insulin resistance is associated with higher intramyocellular triglycerides in type I but not type II myocytes concomitant with higher ceramide content. Diabetes 59: 80–88.
69. Schmitz-Peiffer C, Biden TJ (2008) Protein kinase C function in muscle, liver, and beta-cells and its therapeutic implications for type 2 diabetes. Diabetes 57: 1774–1783.
70. Samuel VT, Shulman GI (2012) Mechanisms for insulin resistance: common threads and missing links. Cell 148: 852–871.
71. Szendroedi J, Roden M (2008) Mitochondrial fitness and insulin sensitivity in humans. Diabetologia 51: 2155–2167.
72. Essen B, Jansson E, Henriksson J, Taylor AW, Saltin B (1975) Metabolic characteristics of fibre types in human skeletal muscle. Acta Physiol Scand 95: 153–165.
73. Kim HG, Han EH, Jeong HG (2008) Effect of troglitazone on CYP1A1 induction. Toxicology 246: 166–171.
74. Zhou GD, Zhu H, Phillips TD, Wang J, Wang SZ, et al. (2011) Effects of Dietary Fish Oil on the Depletion of Carcinogenic PAH-DNA Adduct Levels in the Liver of B6C3F1 Mouse. Plos One 6: e26589.
75. Romisch-Margl W, Prehn C, Bogumil R, Rohring C, Suhre K, et al. (2012) Procedure for tissue sample preparation and metabolite extraction for high-troughput targeted metabolomics. Metabolomics 8: 133–142.
76. van Helden YG, Godschalk RW, Heil SG, Bunschoten A, Hessel S, et al. (2010) Downregulation of Fzd6 and Cthrc1 and upregulation of olfactory receptors and protocadherins by dietary beta-carotene in lungs of Bcmo1−/− mice. Carcinogenesis 31: 1329–1337.

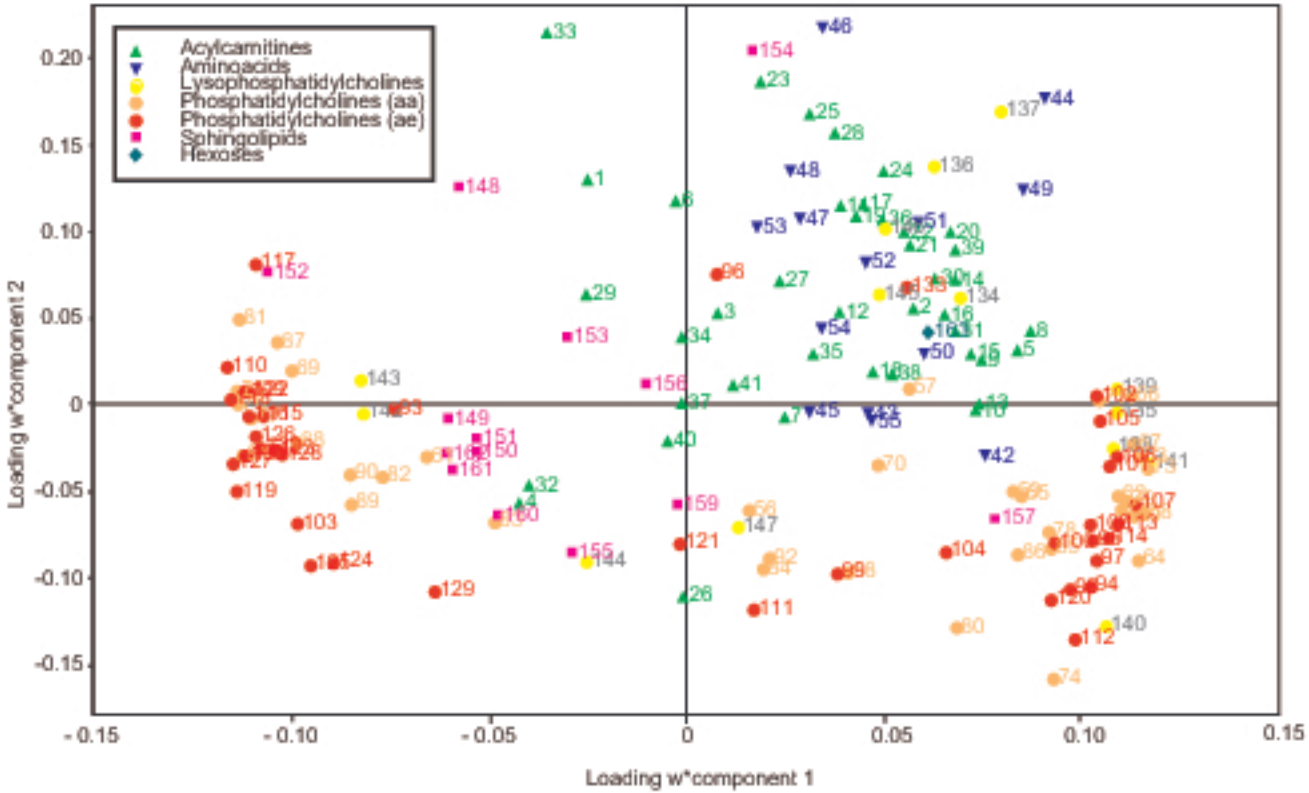
Acylcarnitines
Aminoacids
Lysophosphatidylcholines
Phosphatidylcholines (aa)
Phosphatidylcholines (ae)
Sphingolipids
Hexoses
Loading w*component 2
Loading w*component 1
0.20
0.15
0.10
0.05
0
-0.05
-0.10
-0.15
-0.15
-0.10
-0.05
0
0.05
0.10
0.15

Supporting Information

Expression profiling using microarrays

The Two-color whole mouse genome (4 x 44 k) Agilent oligo microarray kits (G4122F, Agilent Technologies, Inc. Santa Clara, CA) were used to analyse gene expression in individual mice. Preparation of samples and the microarray hybridization were performed according to the manufacturer's protocol with a few modifications as described previously [1] and with arrays rotating at 10 rpm. Briefly, cDNA was synthesized for each animal using 1 μg of gastrocnemius muscle total RNA using the Agilent Low-RNA Input Fluorescent Linear Amplification kit without addition of spikes. In the first study, individual samples from the cHF, cHF+F, and cHF+ROSI groups were used; in the latter case, we also included samples from another group of mice, subjected to an intervention using a higher dose of rosiglitazone admixed to the cHF diet (i.e., 100 mg rosiglitazone/kg diet) for the reference pool, but these samples were excluded for data analysis in this study. In the second study, only cHF+ROSI and cHF+F+ROSI were analyzed. In both studies, samples were split in two equal amounts, to synthesize cyanine 3-cytidine triphosphate (Cy3) and cyanine 5-cytidine triphosphate (Cy5) labeled cRNA using half the amounts per dye as indicated by the manufacturer. Labeled cRNA was purified using RNeasy columns (Qiagen, Venlo, The Netherlands). Cy3 and Cy5 concentration, A_{260}/A_{280} ratio and cRNA concentration were determined using the NanoDrop spectrophotometer (IsoGen Life Science, Maarsen, The Netherlands) and yield and specific activity of each reaction were calculated according to the manufacturer's protocol. Overall, thirty-nine of the forty samples met the criteria of cRNA yield higher than 825 ng and the specific activity higher than 8 pmol Cy3 or Cy5 per μg cRNA (the sample that did not met the criteria was excluded from further analysis). Then, all Cy3-labeled cRNA samples were pooled on an equimolar basis and subsequently used as a common reference pool. Individual 825 ng Cy5-labeled cRNA and 825 ng pooled Cy3-labeled cRNA were fragmented in 1x fragmentation and 1x blocking agent at 60°C for 30 min, afterward mixed with GEx Hybridization Buffer HI-RPM and hybridized in the Agilent Microarray Hybridization Chamber rotating at 10 rpm at 65°C for 17 hours. After hybridization, slides were washed according to the wash protocol. Arrays were scanned with an Agilent scanner with 10% and 100% laser-power intensities. All used chemicals and instruments were by Agilent Technologies, unless otherwise stated.

Microarray data analysis

Per study, signal intensities for each spot were quantified using Feature Extraction software version 10.5.1.1 (Agilent Technologies, Inc. Santa Clara, CA). Quality control of each microarray was performed visually using quality control graphs from Feature Extraction and M-A plots and boxplots using limmaGUI in R (Bioconductor, Seattle, WA, USA). After quality control, data from all arrays were imported into GeneMaths XT 2.12 (Applied Maths, Sint-Martens-Latem, Belgium). Median spot values with a mean Cy-5 and Cy-3 signal/background ratio over all arrays lower than two were excluded; remaining data were log-transformed. The log-transformed Cy5 signal was normalized against Cy3 intensities as described before [2]. Since cHF+ROSI was used for both microarray studies, we analysed coherence between the hybridisation studies. This indicated that data are very reproducible (data not shown), as reported previously [3]. Pathway analysis was performed using MetaCore (GeneGo, Carlsbad, CA, USA), GO overrepresentation analysis, and mining of scientific literature.

References

1. van Helden YG, Godschalk RW, Heil SG, Bunschoten A, Hessel S, Amengual J, Bonet ML, von LJ, van Schooten FJ, Keijer J (2010) Downregulation of Fzd6 and Cthrc1 and upregulation of olfactory receptors and protocadherins by dietary beta-carotene in lungs of Bcmo1-/- mice. Carcinogenesis 31: 1329-1337.

2. Pellis L, Franssen-van Hal NL, Burema J, Keijer J (2003) The intraclass correlation coefficient applied for evaluation of data correction, labeling methods, and rectal biopsy sampling in DNA microarray experiments. Physiol Genomics 16: 99-106.

3. van Schothorst EM, Pagmantidis V, de Boer VC, Hesketh J, Keijer J (2007) Assessment of reducing RNA input for Agilent oligo microarrays. Anal Biochem 363: 315-317.

Table S1

List of all 163 metabolites measured in skeletal muscle extracts - targeted metabolomics analysis.

Carnitines (Acylcarnitines)						
			cHF	**cHF+F**	**cHF+ROSI**	**cHF+F+ROSI**
Abbreviation	*Order*	*Full biochemical name*	*means ± SE*	*means ± SE*	*means ± SE*	*means ± SE*
C0	1	Carnitine	57.76 ± 5.151	60.60 ± 2.002	49.76 ± 2.971	53.27 ± 2.081
C10	2	Decanoylcarnitine	0.100 ± 0.007	0.070 ± 0.005	0.094 ± 0.008	0.082 ± 0.006
C10:1	3	Decenoylcarnitine	0.071 ± 0.005	0.064 ± 0.004	0.067 ± 0.003	0.071 ± 0.005
C10:2	4	Decadienylcarnitine	0.017 ± 0.001	0.020 ± 0.002	0.018 ± 0.002	0.021 ± 0.001
C12	5	Dodecanoylcarnitine	0.137 ± 0.011	0.074 ± 0.008	0.134 ± 0.011	0.092 ± 0.008
C12-DC	6	Dodecenoylcarnitine	0.080 ± 0.001	0.078 ± 0.001	0.077 ± 0.002	0.077 ± 0.002
C12:1	7	Dodecanedioylcarnitine	0.078 ± 0.005	0.071 ± 0.005	0.079 ± 0.004	0.077 ± 0.004
C14	8	Tetradecanoylcarnitine	0.412 ± 0.041	0.170 ± 0.0024	0.390 ± 0.043	0.220 ± 0.028
C14:1	9	Tetradecenoylcarnitine	0.086 ± 0.009	0.038 ± 0.01	0.083 ± 0.011	0.055 ± 0.006
C14:1-OH	10	Hydroxytetradecenoylcarnitine	0.031 ± 0.003	0.018 ± 0.002	0.032 ± 0.004	0.020 ± 0.002
C14:2	11	Tetradecadienylcarnitine	0.030 ± 0.004	0.016 ± 0.002	0.022 ± 0.004	0.022 ± 0.002
C14:2-OH	12	Hydroxytetradecadienylcarnitine	0.011 ± 0.001	0.008 ± 0.001	0.010 ± 0.001	0.010 ± 0.000
C16	13	Hexadecanoylcarnitine	1.821 ± 0.247	0.873 ± 0.091	1.904 ± 0.318	1.018 ± 0.109
C16-OH	14	Hydroxyhexadecanoylcarnitine	0.064 ± 0.012	0.027 ± 0.005	0.055 ± 0.007	0.037 ± 0.003
C16:1	15	Hexadecenoylcarnitine	0.252 ± 0.026	0.113 ± 0.010	0.243 ± 0.047	0.144 ± 0.015
C16:1-OH	16	Hydroxyhexadecenoylcarnitine	0.042 ± 0.005	0.022 ± 0.003	0.039 ± 0.006	0.029 ± 0.003
C16:2	17	Hexadecadienylcarnitine	0.076 ± 0.009	0.037 ± 0.007	0.057 ± 0.013	0.052 ± 0.007
C16:2-OH	18	Hydroxyhexadecadienylcarnitine	0.018 ± 0.002	0.012 ± 0.001	0.017 ± 0.002	0.016 ± 0.001
C18	19	Octadecanoylcarnitine	0.294 ± 0.047	0.187 ± 0.030	0.233 ± 0.034	0.195 ± 0.021
C18:1	20	Octadecenoylcarnitine	0.946 ± 0.104	0.468 ± 0.041	0.778 ± 0.140	0.532 ± 0.047
C18:1-OH	21	Hydroxyoctadecenoylcarnitine	0.053 ± 0.009	0.027 ± 0.003	0.044 ± 0.006	0.035 ± 0.003
C18:2	22	Octadecadienylcarnitine	0.631 ± 0.065	0.328 ± 0.043	0.510 ± 0.104	0.404 ± 0.036
C2	23	Acetylcarnitine	16.36 ± 1.545	13.10 ± 1.072	12.49 ± 1.159	12.74 ± 0.535
C3	24	Propionylcarnitine	0.159 ± 0.012	0.105 ± 0.017	0.125 ± 0.019	0.105 ± 0.010
C4-OH (C3-DC)	25	Hydroxybutyrylcarnitine (Malonylcarnitine)	0.170 ± 0.052	0.067 ± 0.011	0.082 ± 0.009	0.084 ± 0.008
C3-OH	26	Hydroxypropionylcarnitine	0.065 ± 0.003	0.069 ± 0.003	0.071 ± 0.004	0.067 ± 0.002
C3:1	27	Propenoylcarnitine	0.016 ± 0.002	0.015 ± 0.001	0.015 ± 0.001	0.013 ± 0.001
C4	28	Butyrylcarnitine	0.340 ± 0.072	0.177 ± 0.028	0.219 ± 0.021	0.199 ± 0.023
C4:1	29	Butenylcarnitine	0.011 ± 0.002	0.011 ± 0.001	0.010 ± 0.000	0.012 ± 0.001
C5	30	Valerylcarnitine	0.093 ± 0.007	0.061 ± 0.004	0.084 ± 0.012	0.064 ± 0.005
C5-DC (C6-OH)	31	Glutarylcarnitine (Hydroxyhexanoylcarnitine)	0.026 ± 0.003	0.017 ± 0.001	0.025 ± 0.002	0.018 ± 0.001
C5-M-DC	32	Methylglutarylcarnitine	0.016 ± 0.001	0.018 ± 0.001	0.017 ± 0.001	0.018 ± 0.002
C5-OH (C3-DC-M)	33	Hydroxyvalerylcarnitine (Methylmalonylcarnitine)	0.191 ± 0.009	0.190 ± 0.009	0.157 ± 0.007	0.185 ± 0.004
C5:1	34	Tiglylcarnitine	0.024 ± 0.002	0.024 ± 0.002	0.023 ± 0.001	0.022 ± 0.001
C5:1-DC	35	Glutaconylcarnitine	0.009 ± 0.001	0.008 ± 0.001	0.009 ± 0.000	0.008 ± 0.001
C6 (C4:1-DC)	36	Hexanoylcarnitine (Fumarylcarnitine)	0.122 ± 0.011	0.076 ± 0.011	0.103 ± 0.007	0.095 ± 0.010
C6:1	37	Hexenoylcarnitine	0.012 ± 0.001	0.012 ± 0.001	0.012 ± 0.001	0.012 ± 0.001
C7-DC	38	Pimelylcarnitine	0.024 ± 0.002	0.019 ± 0.001	0.023 ± 0.001	0.021 ± 0.001
C8	39	Octanoylcarnitine	0.122 ± 0.008	0.090 ± 0.005	0.113 ± 0.005	0.099 ± 0.005
C8:1	40	Octenoylcarnitine	0.012 ± 0.001	0.011 ± 0.001	0.012 ± 0.001	0.014 ± 0.001
C9	41	Nonaylcarnitine	0.014 ± 0.001	0.014 ± 0.001	0.014 ± 0.001	0.013 ± 0.001
Amino Acids						

			cHF	cHF+F	cHF+ROSI	cHF+F+ROSI
Abbreviation		*Full biochemical name*	*means ± SE*	*means ± SE*	*means ± SE*	*means ± SE*
Arg	42	Arginine	20.79 ± 1.11	15.40 ± 0.54	21.94 ± 1.86	15.93 ± 1.28
Gln	43	Glutamine	373.6 ± 17.24	310.6 ± 11.55	375.13 ± 21.24	347.86 ± 20.55
Gly	44	Glycine	405.9 ± 18.81	255.5 ± 8.63	331.5 ± 16.34	226.29 ± 14.21
His	45	Histidine	31.95 ± 2.07	27.83 ± 1.14	32.04 ± 1.79	29.94 ± 2.01
Met	46	Methionine	22.98 ± 0.96	19.57 ± 0.88	19.05 ± 1.23	17.69 ± 0.78
Orn	47	Ornithine	6.37 ± 0.72	4.77 ± 0.34	5.42 ± 0.45	5.27 ± 0.41
Phe	48	Phenylalanine	15.76 ± 0.75	14.01 ± 0.43	14.29 ± 0.76	13.77 ± 0.68
Pro	49	Proline	53.51 ± 2.00	39.64 ± 1.25	48.41 ± 2.88	37.49 ± 1.17
Ser	50	Serine	43.23 ± 3.42	36.03 ± 1.42	42.69 ± 2.16	33.29 ± 2.51
Thr	51	Threonine	39.14 ± 3.39	30.51 ± 1.50	35.01 ± 2.10	26.69 ± 2.32
Trp	52	Tryptophan	8.242 ± 0.25	7.191 ± 0.15	7.851 ± 0.39	7.56 ± 0.18
Tyr	53	Tyrosine	31.03 ± 2.06	28.10 ± 1.62	27.89 ± 2.20	26.27 ± 1.74
Val	54	Valine	50.25 ± 1.77	42.96 ± 2.02	48.31 ± 2.99	45.67 ± 3.83
xLeu	55	Leucine / Isoleucine	63.74± 3.10	54.86 ± 3.60	65.13 ± 5.44	55.20 ± 2.85
Glycerophospholipids						
			cHF	**cHF+F**	**cHF+ROSI**	**cHF+F+ROSI**
Abbreviation		*Full biochemical name*	*means ± SE*	*means ± SE*	*means ± SE*	*means ± SE*
PC aa C24:0	56	Phosphatidylcholine diacyl C24:0	0.055 ± 0.002	0.055 ± 0.006	0.058 ± 0.002	0.055 ± 0.003
PC aa C26:0	57	Phosphatidylcholine diacyl C26:0	0.515 ± 0.004	0.495 ± 0.012	0.516 ± 0.07	0.492 ± 0.008
PC aa C28:1	58	Phosphatidylcholine diacyl C28:1	0.118 ± 0.003	0.111 ± 0.007	0.128 ± 0.006	0.44 ± 0.008
PC aa C30:0	59	Phosphatidylcholine diacyl C30:0	7.445 ± 0.507	5.619 ± 0.388	8.150 ± 0.500	6.209 ± 0.684
PC aa C30:2	60	Phosphatidylcholine diacyl C30:2	0.235 ± 0.007	0.106 ± 0.008	0.283 ± 0.014	0.112 ± 0.011
PC aa C32:0	61	Phosphatidylcholine diacyl C32:0	10.22 ± 1.117	13.44 ± 0.947	10.42 ± 0.814	16.84 ± 2.658
PC aa C32:1	62	Phosphatidylcholine diacyl C32:1	19.04 ± 1.100	7.907 ± 0.560	22.52 ± 1.599	9.044 ± 0.938
PC aa C32:2	63	Phosphatidylcholine diacyl C32:2	7.013 ± 0.381	2.293 ± 0.124	8.011 ± 0.429	2.466 ± 0.232
PC aa C32:3	64	Phosphatidylcholine diacyl C32:3	0.941 ± 0.036	0.325 ± 0.015	1.236 ± 0.056	0.368± 0.023
PC aa C34:1	65	Phosphatidylcholine diacyl C34:1	34.64 ± 2.882	22.23 ± 1.958	39.26 ± 3.795	28.10 ± 4.859
PC aa C34:2	66	Phosphatidylcholine diacyl C34:2	105.0 ± 7.411	30.72 ± 2.98	110.6 ± 7.117	33.62 ± 4.147
PC aa C34:3	67	Phosphatidylcholine diacyl C34:3	10.203 ± 0.686	2.883 ± 0.161	11.50 ± 0.718	3.261 ± 0.293
PC aa C34:4	68	Phosphatidylcholine diacyl C34:4	3.668 ± 0.179	0.726 ± 0.040	4.704 ± 0.230	0.754 ± 0.058
PC aa C36:0	69	Phosphatidylcholine diacyl C36:0	4.283 ± 0.232	7.220 ± 0.650	3.780 ± 0.306	8.023 ± 0.058
PC aa C36:1	70	Phosphatidylcholine diacyl C36:1	2.678 ± 0.315	2.014 ± 0.290	2.920 ± 0.388	2.839 ± 0.647
PC aa C36:2	71	Phosphatidylcholine diacyl C36:2	23.375 ± 2.090	7.480 ± 0.803	24.70 ± 2.530	8.747 ± 1.423
PC aa C36:3	72	Phosphatidylcholine diacyl C36:3	26.738 ± 2.185	6.139 ± 0.481	34.04 ± 2.90	7.046 ± 0.885
PC aa C36:4	73	Phosphatidylcholine diacyl C36:4	106.325 ± 5.355	18.157 ± 1.483	127.4 ± 6.471	17.93 ± 1.840
PC aa C36:5	74	Phosphatidylcholine diacyl C36:5	6.936 ± 0.382	5.036 ± 0.372	9.200 ± 0.529	5.729 ± 0.588
PC aa C36:6	75	Phosphatidylcholine diacyl C36:6	6.090 ± 0.369	16.33 ± 1.187	4.790 ± 0.206	17.94 ± 1.624
PC aa C38:0	76	Phosphatidylcholine diacyl C38:0	1.017 ± 0.062	2.769 ± 0.206	0.848 ± 0.067	3.197 ± 0.439
PC aa C38:1	77	Phosphatidylcholine diacyl C38:1	0.469 ± 0.036	1.247 ± 0.115	0.418 ± 0.036	1.454 ± 0.220
PC aa C38:3	78	Phosphatidylcholine diacyl C38:3	1.784 ± 0.156	0.905 ± 0.113	2.216 ± 0.266	1.135 ± 0.214
PC aa C38:4	79	Phosphatidylcholine diacyl C38:4	16.700 ± 1.076	1.226 ± 0.084	21.79 ± 2.305	1.095 ± 0.128
PC aa C38:5	80	Phosphatidylcholine diacyl C38:5	43.18 ± 3.104	36.12 ± 4.288	54.18 ± 4.171	42.49 ± 7.620
PC aa C38:6	81	Phosphatidylcholine diacyl C38:6	140.6 ± 4.367	206.9 ± 4.913	120.3 ± 5.716	231.7 ± 4.999
PC aa C40:1	82	Phosphatidylcholine diacyl C40:1	0.196 ± 0.015	0.266 ± 0.025	0.202 ± 0.015	0.343 ± 0.055
PC aa C40:2	83	Phosphatidylcholine diacyl C40:2	0.057 ± 0.006	0.069 ± 0.008	0.062 ± 0.007	0.101 ± 0.019

PC aa C40:3	84	Phosphatidylcholine diacyl C40:3	0.062 ± 0.004	0.060 ± 0.007	0.071 ± 0.006	0.079 ± 0.014
PC aa C40:4	85	Phosphatidylcholine diacyl C40:4	0.732 ± 0.059	0.345 ± 0.025	0.945 ± 0.127	0.397 ± 0.039
PC aa C40:5	86	Phosphatidylcholine diacyl C40:5	3.221 ± 0.276	1.927 ± 0.256	4.034 ± 0.485	2.554 ± 0.574
PC aa C40:6	87	Phosphatidylcholine diacyl C40:6	19.24 ± 1.414	38.00 ± 4.054	14.44 ± 1.313	46.54 ± 8.737
PC aa C42:0	88	Phosphatidylcholine diacyl C42:0	0.020 ± 0.001	0.036 ± 0.004	0.019 ± 0.001	0.043 ± 0.006
PC aa C42:1	89	Phosphatidylcholine diacyl C42:1	0.062 ± 0.013	0.146 ± 0.022	0.075 ± 0.012	0.220 ± 0.064
PC aa C42:2	90	Phosphatidylcholine diacyl C42:2	0.048 ± 0.008	0.095 ± 0.015	0.051 ± 0.006	0.140 ± 0.027
PC aa C42:4	91	Phosphatidylcholine diacyl C42:4	0.046 ± 0.004	0.169 ± 0.015	0.046 ± 0.005	0.224 ± 0.039
PC aa C42:5	92	Phosphatidylcholine diacyl C42:5	0.078 ± 0.02	0.075 ± 0.006	0.090 ± 0.012	0.090 ± 0.012
PC aa C42:6	93	Phosphatidylcholine diacyl C42:6	0.413 ± 0.017	0.497 ± 0.030	0.405 ± 0.020	0.592 ± 0.096
PC ae C30:0	94	Phosphatidylcholine acyl-alkyl C30:0	0.297 ± 0.017	0.198 ± 0.012	0.355 ± 0.014	0.227 ± 0.016
PC ae C30:1	95	Phosphatidylcholine acyl-alkyl C30:1	0.107 ± 0.009	0.051 ± 0.002	0.132 ± 0.010	0.060 ± 0.008
PC ae C30:2	96	Phosphatidylcholine acyl-alkyl C30:2	0.091 ± 0.003	0.089 ± 0.003	0.088 ± 0.002	0.087 ± 0.003
PC ae C32:1	97	Phosphatidylcholine acyl-alkyl C32:1	0.911 ± 0.068	0.453 ± 0.032	1.153 ± 0.082	0.531 ± 0.068
PC ae C32:2	98	Phosphatidylcholine acyl-alkyl C32:2	0.226 ± 0.010	0.152 ± 0.011	0.275 ± 0.018	0.168 ± 0.014
PC ae C34:0	99	Phosphatidylcholine acyl-alkyl C34:0	0.369 ± 0.039	0.331 ± 0.031	0.431 ± 0.036	0.426 ± 0.074
PC ae C34:1	100	Phosphatidylcholine acyl-alkyl C34:1	2.351 ± 0.178	1.447 ± 0.128	2.830 ± 0.241	1.733 ± 0.277
PC ae C34:2	101	Phosphatidylcholine acyl-alkyl C34:2	1.886 ± 0.133	0.855 ± 0.069	2.140 ± 0.149	0.935 ± 0.110
PC ae C34:3	102	Phosphatidylcholine acyl-alkyl C34:3	0.853 ± 0.060	0.418 ± 0.036	0.890 ± 0.071	0.417 ± 0.047
PC ae C36:0	103	Phosphatidylcholine acyl-alkyl C36:0	0.175 ± 0.009	0.282 ± 0.022	0.191 ± 0.008	0.316 ± 0.029
PC ae C36:1	104	Phosphatidylcholine acyl-alkyl C36:1	0.670 ± 0.055	0.522 ± 0.056	0.782 ± 0.070	0.669 ± 0.126
PC ae C36:2	105	Phosphatidylcholine acyl-alkyl C36:2	1.509 ± 0.121	0.611 ± 0.053	1.629 ± 0.143	0.720 ± 0.119
PC ae C36:3	106	Phosphatidylcholine acyl-alkyl C36:3	0.701 ± 0.049	0.275 ± 0.024	0.793 ± 0.057	0.324 ± 0.046
PC ae C36:4	107	Phosphatidylcholine acyl-alkyl C36:4	1.355 ± 0.072	0.369 ± 0.030	1.688 ± 0.106	0.374 ± 0.039
PC ae C36:5	108	Phosphatidylcholine acyl-alkyl C36:5	1.198 ± 0.082	0.628 ± 0.051	1.451 ± 0.120	0.660 ± 0.070
PC ae C38:0	109	Phosphatidylcholine acyl-alkyl C38:0	8.810± 0.269	15.89 ± 0.871	7.735 ± 0.437	18.529 ± 1.435
PC ae C38:1	110	Phosphatidylcholine acyl-alkyl C38:1	0.624 ± 0.019	1.356 ± 0.057	0.480 ± 0.028	1.544 ± 0.099
PC ae C38:2	111	Phosphatidylcholine acyl-alkyl C38:2	0.305 ± 0.019	0.299 ± 0.026	0.358 ± 0.038	0.398 ± 0.067
PC ae C38:3	112	Phosphatidylcholine acyl-alkyl C38:3	0.261 ± 0.012	1.157 ± 0.014	0.344 ± 0.024	0.200 ± 0.022
PC ae C38:4	113	Phosphatidylcholine acyl-alkyl C38:4	1.416 ± 0.095	0.377 ± 0.033	1.836 ± 0.168	0.407 ± 0.054
PC ae C38:5	114	Phosphatidylcholine acyl-alkyl C38:5	1.298 ± 0.082	0.578 ± 0.050	1.629 ± 0.126	0.634 ± 0.082
PC ae C38:6	115	Phosphatidylcholine acyl-alkyl C38:6	3.735 ± 0.199	7.273 ± 0.556	3.514 ± 0.271	7.854 ± 0.888
PC ae C40:0	116	Phosphatidylcholine acyl-alkyl C40:0	14.60 ± 0.722	31.07 ± 2.285	13.20 ± 0.863	39.39 ± 6.448
PC ae C40:1	117	Phosphatidylcholine acyl-alkyl C40:1	20.25 ± 0.911	33.64 ± 2.16	14.03 ± 0.774	37.49 ± 4.038
PC ae C40:2	118	Phosphatidylcholine acyl-alkyl C40:2	0.683 ± 0.026	1.560 ± 0.072	0.569 ± 0.029	1.873 ± 0.171
PC ae C40:3	119	Phosphatidylcholine acyl-alkyl C40:3	0.055 ± 0.003	0.191 ± 0.013	0.064 ± 0.004	0.245 ± 0.025
PC ae C40:4	120	Phosphatidylcholine acyl-alkyl C40:4	0.234 ± 0.018	0.133 ± 0.010	0.309 ± 0.031	0.162 ± 0.019
PC ae C40:5	121	Phosphatidylcholine acyl-alkyl C40:5	0.608 ± 0.043	0.624 ± 0.044	0.668 ± 0.060	0.735 ± 0.074
PC ae C40:6	122	Phosphatidylcholine acyl-alkyl C40:6	2.218 ± 0.143	6.117 ± 0.594	1.743 ± 0.156	7.326 ± 1.305
PC ae C42:0	123	Phosphatidylcholine acyl-alkyl C42:0	0.402 ± 0.013	0.622 ± 0.037	0.400 ± 0.018	0.794 ± 0.142
PC ae C42:1	124	Phosphatidylcholine acyl-alkyl C42:1	0.289 ± 0.017	0.521 ± 0.049	0.348 ± 0.032	0.683 ± 0.143
PC ae C42:2	125	Phosphatidylcholine acyl-alkyl C42:2	0.406 ± 0.028	0.793 ± 0.066	0.504 ± 0.042	1.100 ± 0.176
PC ae C42:3	126	Phosphatidylcholine acyl-alkyl C42:3	0.992 ± 0.052	2.903 ± 0.289	0.909 ± 0.048	3.673 ± 0.511
PC ae C42:4	127	Phosphatidylcholine acyl-alkyl C42:4	0.026 ± 0.005	1.730 ± 0.144	0.024 ± 0.003	2.583 ± 0.332
PC ae C42:5	128	Phosphatidylcholine acyl-alkyl C42:5	0.390 ± 0.007	0.484 ± 0.020	0.390 ± 0.010	0.544 ± 0.042
PC ae C44:3	129	Phosphatidylcholine acyl-alkyl C44:3	0.170 ± 0.012	0.247 ± 0.028	0.206 ± 0.018	0.351 ± 0.074
PC ae C44:4	130	Phosphatidylcholine acyl-alkyl C44:4	0.151 ± 0.010	1.965 ± 0.227	0.135 ± 0.006	2.989 ± 0.640
PC ae C44:5	131	Phosphatidylcholine acyl-alkyl C44:5	0.147 ± 0.013	10.32 ± 1.381	0.088 ± 0.005	14.739 ± 2.714
PC ae C44:6	132	Phosphatidylcholine acyl-alkyl C44:6	0.020 ± 0.002	0.053 ± 0.006	0.019 ± 0.001	0.073 ± 0.011
lysoPC a C14:0	133	Lysophosphatidylcholine acyl C14:0	1.009 ± 0.020	0.940 ± 0.015	0.989 ± 0.022	0.941 ± 0.022

lysoPC a C16:0	134	Lysophosphatidylcholine acyl C16:0	10.17 ± 0.545	8.479 ± 0.209	9.810 ± 0.387	8.296 ± 0.358
lysoPC a C16:1	135	Lysophosphatidylcholine acyl C16:1	0.294 ± 0.018	0.122 ± 0.007	0.313 ± 0.024	0.125 ± 0.003
lysoPC a C17:0	136	Lysophosphatidylcholine acyl C17:0	0.208 ± 0.012	0.172 ± 0.009	0.186 ± 0.009	0.150 ± 0.005
lysoPC a C18:0	137	Lysophosphatidylcholine acyl C18:0	6.411 ± 0.363	4.644 ± 0.228	5.424 ± 0.204	4.031 ± 0.214
lysoPC a C18:1	138	Lysophosphatidylcholine acyl C18:1	1.449 ± 0.065	0.860 ± 0.023	1.550 ± 0.072	0.910 ± 0.048
lysoPC a C18:2	139	Lysophosphatidylcholine acyl C18:2	3.561 ± 0.172	1.964 ± 0.058	3.650 ± 0.192	1.937 ± 0.115
lysoPC a C20:3	140	Lysophosphatidylcholine acyl C20:3	0.280 ± 0.014	0.144 ± 0.013	0.372 ± 0.016	0.166 ± 0.011
lysoPC a C20:4	141	Lysophosphatidylcholine acyl C20:4	1.598 ± 0.067	0.343 ± 0.020	1.883 ± 0.088	0.307 ± 0.014
lysoPC a C24:0	142	Lysophosphatidylcholine acyl C24:0	0.356 ± 0.007	0.394 ± 0.016	0.349 ± 0.009	0.445 ± 0.014
lysoPC a C26:0	143	Lysophosphatidylcholine acyl C26:0	0.221 ± 0.009	0.260 ± 0.015	0.209 ± 0.011	0.296 ± 0.011
lysoPC a C26:1	144	Lysophosphatidylcholine acyl C26:1	2.081 ± 0.027	2.121 ± 0.022	2.114 ± 0.020	2.134 ± 0.021
lysoPC a C28:0	145	Lysophosphatidylcholine acyl C28:0	0.205 ± 0.007	0.177 ± 0.009	0.197 ± 0.012	0.186 ± 0.007
lysoPC a C28:1	146	Lysophosphatidylcholine acyl C28:1	0.139 ± 0.008	0.121 ± 0.003	0.131 ± 0.003	0.129 ± 0.007
lysoPC a C6:0	147	Lysophosphatidylcholine acyl C6:0	0.006 ± 0.001	0.005 ± 0.001	0.007 ± 0.002	0.007 ± 0.001
Sphingolipids						
			cHF	**cHF+F**	**cHF+ROSI**	**cHF+F+ROSI**
Abbreviation		*Full biochemical name*	*means ± SE*	*means ± SE*	*means ± SE*	*means ± SE*
SM (OH) C14:1	148	Hydroxysphingomyeline C14:1	0.225 ± 0.008	0.243 ± 0.017	0.190 ± 0.012	0.254 ± 0.016
SM (OH) C16:1	149	Hydroxysphingomyeline C16:1	0.391 ± 0.020	0.466 ± 0.030	0.387 ± 0.031	0.545 ± 0.069
SM (OH) C22:1	150	Hydroxysphingomyeline C22:1	0.229 ± 0.024	0.280 ± 0.025	0.234 ± 0.024	0.363 ± 0.061
SM (OH) C22:2	151	Hydroxysphingomyeline C22:2	0.099 ± 0.11	0.131 ± 0.015	0.100 ± 0.015	0.170 ± 0.035
SM (OH) C24:1	152	Hydroxysphingomyeline C24:1	0.408 ± 0.024	0.661 ± 0.045	0.287 ± 0.019	0.737 ± 0.067
SM C16:0	153	Sphingomyeline C16:0	7.508 ± 0.024	7.784 ± 0.481	7.185 ± 0.401	8.323 ± 0.480
SM C16:1	154	Sphingomyeline C16:1	0.674 ± 0.034	0.618 ± 0.031	0.572 ± 0.026	0.570 ± 0.015
SM C18:0	155	Sphingomyeline C18:0	11.08 ± 0.801	12.68 ± 0.839	12.20 ± 0.867	14.90 ± 2.079
SM C18:1	156	Sphingomyeline C18:1	1.219 ± 0.18	1.260 ± 0.089	1.207 ± 0.063	1.324 ± 0.118
SM.C20:2	157	Sphingomyeline C20:2	0.070 ± 0.016	0.026 ± 0.006	0.094 ± 0.016	0.022 ± 0.005
SM C22:3	158	Sphingomyeline C22:3	0.000 ± 0.000	0.000 ± 0.000	0.000 ± 0.000	0.000 ± 0.000
SM C24:0	159	Sphingomyeline C24:0	0.750 ± 0.084	0.761 ± 0.095	0.824 ± 0.094	1.037 ± 0.196
SM C24:1	160	Sphingomyeline C24:1	1.394 ± 0.164	1.937 ± 0.295	1.593 ± 0.238	2.747 ± 0.680
SM C26:0	161	Sphingomyeline C26:0	0.007 ± 0.002	0.014 ± 0.002	0.008 ± 0.002	0.016 ± 0.004
SM C26:1	162	Sphingomyeline C26:1	0.009 ± 0.002	0.019 ± 0.004	0.009 ± 0.003	0.020 ± 0.004
Sugars						
			cHF	**cHF+F**	**cHF+ROSI**	**cHF+F+ROSI**
Abbreviation		*Full biochemical name*	*means ± SE*	*means ± SE*	*means ± SE*	*means ± SE*
H1	163	Sum of Hexose	201.00 ± 17.86	129.66 ± 16.64	190.38 ± 21.40	153.57 ± 15.99

In short, 14 amino acids, sum of hexoses (H1), free carnitine (C0), 26 acylcarnitines (C2, C3,...C18:2), 14 hydroxy- and dicarboxy-acylcarnitines (C-3OH, C4-OH, C5-DC,...C18:1-OH), 10 sphingomyelins (SM C16:0, SM C16:1,… SM C26:1), 5 hydroxysphingomyelins [SM(OH)C14:1… SM(OH)C24:1], 38 diacyl-phosphatidylcholines (PC aa C24:0 …PC aa C42:6), 39 acyl-alkyl-phospatidylcholines (PC ae C30:0… PC ae C44:6), and 15 lyso-phosphatidylcholines (lysoPC a C6:0….lysoPC a C28:1) were identified in extracts of skeletal muscle from animals subjected to various interventions and killed when re-fed Chow (see Methods and Fig. 1). Concentrations of all analysed metabolites are reported in μM. All metabolites above were determined using flow injection analysis/thermospray mass spectrometry (**FIA-MS**) with Biocrates Absolute*IDQ*^{TM} targeted metabolomics technology. Data are means±SE (n=7–8).

Table S2 Differentially regulated probesets expressed in cHF+F versus control cHF dietary groups

Probe name	Gene symbol	Description	Fold change
Down-regulated			
A_52_P682382	*Scd1*	stearoyl-Coenzyme A desaturase 1	-2.04
A_52_P262219	*Fos*	FBJ osteosarcoma oncogene	-2.03
A_52_P657360	*Tnni1*	troponin I, skeletal, slow 1	-1.79
A_51_P143162	*Myh7*	myosin, heavy polypeptide 7, cardiac muscle, beta	-1.77
A_51_P512210	*Myh6*	myosin, heavy polypeptide 6, cardiac muscle, alpha	-1.70
A_51_P461894	*Tnnc1*	troponin C, cardiac/slow skeletal	-1.65
A_52_P362772	*AK048349*	16 days embryo head cDNA, RIKEN full-length enriched library, clone:C130051M16 product:SNF1-like kinase, full insert sequence	-1.62
A_51_P189814	*Cldn5*	claudin 5	-1.61
A_51_P293069	*9630055N22Rik*	RIKEN cDNA 9630055N22 gene	-1.56
A_51_P451574	*Acot1*	acyl-CoA thioesterase 1	-1.56
A_52_P763309	*AK033367*	16 days embryo lung cDNA, RIKEN full-length enriched library, clone:8430406N14 product:unclassifiable, full insert sequence	-1.54
A_51_P462153	*Tpm3*	tropomyosin 3, gamma	-1.51
Up-regulated			
A_52_P651784	*LOC672434*	PREDICTED: similar to S-adenosylmethionine decarboxylase 1	1.55
A_52_P1115511	*6030422H21Rik*	13 days embryo male testis cDNA, RIKEN full-length enriched library, clone:6030422H21 product:unclassifiable, full insert sequence	1.59
A_51_P331570	*Trib3*	tribbles homolog 3	1.62
A_52_P184149	*Mthfd2*	methylenetetrahydrofolate dehydrogenase (NAD+ dependent), methenyltetrahydrofolate cyclohydrolase	1.64
A_52_P645855	*D5Ertd593e*	DNA segment, Chr 5, ERATO Doi 593, expressed	1.65
A_51_P369762	*Itgb1bp3*	integrin beta 1 binding protein 3	1.86

The data provided represents only the statistical significant differentially expressed probesets of the microarrays (cHF: n=8, cHF+F: n=8) which showed a mean absolute fold change ≥ 1.5 (cHF+F/cHF).

Table S3 Differentially regulated probesets expressed in cHF+ROSI versus cHF dietary groups

Probe name	Gene symbol	Description	Fold change
Down-regulated			
A_51_P235945	*Hp*	haptoglobin	-1.96
A_51_P350453	*Pdk4*	pyruvate dehydrogenase kinase, isoenzyme 4	-1.88
A_51_P109369	*Fbxo32*	F-box protein 32	-1.55
A_52_P380379	*Ucp3*	uncoupling protein 3 (mitochondrial, proton carrier)	-1.52
A_51_P415395	*3300001A09Rik*	RIKEN cDNA 3300001A09 gene	-1.51
Up-regulated			
A_51_P389479	*1190003J15Rik*	18-day embryo whole body cDNA, RIKEN full-length enriched library, clone:1190003J15 product:hypothetical Transthyretin/Transthyretin-related containing protein, full insert sequence	1.51
A_52_P1179878	*AK036012*	16 days neonate cerebellum cDNA, RIKEN full-length enriched library, clone:9630027C04 product:unclassifiable, full insert sequence	1.51
A_52_P1115511	*6030422H21Rik*	13 days embryo male testis cDNA, RIKEN full-length enriched library, clone:6030422H21 product:unclassifiable, full insert sequence	1.55
A_51_P230269	*H2-Q10*	histocompatibility 2, Q region locus 10	1.60
A_51_P283456	*Cyp2e1*	cytochrome P450, family 2, subfamily e, polypeptide 1	1.63
A_51_P238576	*Cyp4a14*	cytochrome P450, family 4, subfamily a, polypeptide 14	1.90
A_52_P348256	*Mup1*	major urinary protein 1	1.93

The data provided represents only the statistical significant differentially expressed probesets of the microarrays (cHF+ROSI: n=8, cHF: n=8) which showed a mean absolute fold change ≥ 1.5 (cHF+ROSI/cHF).

Table S4 Differentially regulated probesets expressed in cHF+F+ROSI versus cHF+ROSI dietary groups

Probe name	Gene symbol	Description	Fold change
Down-regulated			
A_51_P501844	*Cyp26b1*	cytochrome P450, family 26, subfamily b, polypeptide 1	-2.15
A_51_P369426	*Zmynd17*	0 day neonate head cDNA, RIKEN full-length enriched library, clone:4833444M15	-2.12
A_51_P133684	*Csrp3*	cysteine and glycine-rich protein 3	-1.86
A_52_P381484	*Spon2*	spondin 2, extracellular matrix protein	-1.81
A_52_P576720	*Calm4*	calmodulin 4	-1.80
A_51_P324814	*Krt18*	keratin 18	-1.79
A_52_P556140	*Vapb*	vesicle-associated membrane protein, associated protein B and C	-1.78
A_52_P408826	*9530083O12Rik*	adult male urinary bladder cDNA, RIKEN full-length enriched library, clone:9530083O12 product:unclassifiable, full insert sequence.	-1.78
A_52_P682382	*Scd1*	stearoyl-Coenzyme A desaturase 1	-1.78
A_51_P194230	*Zic1*	zinc finger protein of the cerebellum 1	-1.74
A_52_P622680	*Chmp4b*	chromatin modifying protein 4B	-1.72
A_52_P677718	*Tatdn2*	TatD DNase domain containing 2	-1.66
A_51_P104418	*Dusp10*	dual specificity phosphatase 10	-1.65
A_51_P111462	*Arl15*	ADP-ribosylation factor-like 15	-1.65
A_52_P591431	*Tra2a*	transformer 2 alpha homolog (Drosophila)	-1.61
A_51_P235977	*4933401F05Rik*	adult male testis cDNA, RIKEN full-length enriched library, clone:4933401F05 product:hypothetical Serine proteases, trypsin family containing protein, full insert sequence	-1.60
A_52_P659312	*Spsb4*	splA/ryanodine receptor domain and SOCS box containing 4	-1.59
A_51_P294535	*Unc5b*	unc-5 homolog B (C. elegans)	-1.58
A_51_P324450	*Pbp2*	phosphatidylethanolamine binding protein 2	-1.58
A_52_P486964	*NAP051367-1*	Unknown	-1.56
A_51_P200529	*Mpst*	mercaptopyruvate sulfurtransferase	-1.55

A_51_P100505	*AK054424*	2 days pregnant adult female ovary cDNA, RIKEN full-length enriched library, clone:E330024G11 product:unclassifiable, full insert sequence.	-1.55
A_51_P346445	*Hspb7*	heat shock protein family, member 7 (cardiovascular)	-1.54
A_51_P335000	*Fhl1*	four and a half LIM domains 1	-1.51
A_51_P260265	*Hoxd4*	homeo box D4	-1.51
A_51_P316243	*C330024D12Rik*	ES cells cDNA, RIKEN full-length enriched library, clone:C330024D12 product:hypothetical Pyrrolidone carboxyl peptidase (pyroglutamate aminopeptidase) structure containing protein, full insert sequence.	-1.50
Up-regulated			
A_51_P458130	*Tph1*	tryptophan hydroxylase 1	1.51
A_52_P430194	*Smox*	0 day neonate eyeball cDNA, RIKEN full-length enriched library, clone:E130115D16 product:POLYAMINE OXIDASE ISOFORM-3 homolog [Homo sapiens], full insert sequence.	1.51
A_51_P112734	*Slc7a8*	solute carrier family 7 (cationic amino acid transporter, y+ system), member 8	1.52
A_52_P1179878	*AK036012*	16 days neonate cerebellum cDNA, RIKEN full-length enriched library, clone:9630027C04 product:unclassifiable, full insert sequence.	1.52
A_51_P279693	*Cyp1a1*	cytochrome P450, family 1, subfamily a, polypeptide 1	1.55
A_51_P499020	*Fbp2*	fructose bisphosphatase 2	1.56
A_52_P706912	*AK035307*	adult male urinary bladder cDNA, RIKEN full-length enriched library, clone:9530013H21 product:unclassifiable, full insert sequence.	1.57
A_52_P175376	*Tcfcp2l1*	transcription factor CP2-like 1	1.57
A_52_P355480	*TC1677116*	Q4QRG7_BRARE (Q4QRG7) Zgc:113884, partial (10%)	1.58
A_52_P453884	*Foxo1*	forkhead box O1	1.65
A_52_P835711	*AK043497*	10 days neonate cortex cDNA, RIKEN full-length enriched library, clone:A830001K22 product:unclassifiable, full insert sequence.	1.73
A_51_P331570	*Trib3*	tribbles homolog 3 (Drosophila)	1.93
A_51_P369762	*Itgb1bp3*	integrin beta 1 binding protein 3	2.11
A_52_P184149	*Mthfd2*	methylenetetrahydrofolate dehydrogenase (NAD+ dependent), methenyltetrahydrofolate cyclohydrolase	2.16

The data provided represents only the statistical significant differentially expressed probesets of the microarrays (cHF+F+ROSI: *n*=8, cHF+ROSI: *n*=8) which showed a mean absolute fold change ≥ 1.5 (cHF+F+ROSI/cHF+ROSI).

Table S5 Real-time quantitative RT-PCR analysis: genes and primers

Gene symbol	Gene name	Accession number (RefSeq)	Forward primer (5' – 3')	Reverse primer (5' – 3')
Acot1	acyl-CoA thioesterase 1	NM_012006.2	AGCGCTGGCATGCACCTCCTG	TTCCCCAACCTCCAAACCATCATA
CD36	CD36 antigen	NM_001159558.1	TCCTTGGCATGGTAGAGAT	ACCAAAGATGTAGCCAGTGTA
Cpt1a	carnitine palmitoyltransferase 1a, liver	NM_013495.2	GCAGCTCGCACATTACAAGGACAT	ACTATGTGTCCTGTGGCGGGGGCT
Cpt1b	carnitine palmitoyltransferase 1b, muscle	NM_009948.2	GGATGATGGCTACGGGGTCTCTTA	AGGGCAGCTGGGGTATCTCTTTTC
Cyp1a1	cytochrome P450, family 1, subfamily a	NM_009992.4	TCCCCCACAGCACCACAAGAGATA	AGAGTGCCGCTGGGGGTGAGAAA
eEf2	eukaryotic translation elongation factor 2	NM_007907.2	GAAACGCGCAGATGTCCAAAAGTC	GCCGGGCTGCAAGTCTAAGG
Fbp2	fructose bisphosphatase 2	NM_007994.3	CCATGAGCCCGCTTCCCTTTGT	GGCGCTGTTCTGACCGTGACCT
Glut4	solute carrier family 2 (facilitated glucose transporter), member 4	NM_009204.2	ACCGGCTGGGCTGATGTGTCT	GCCGACTCGAAGATGCTGGTTGAATAG
Gpd1	glycerol-3-phosphate dehydrogenase 1 (soluble)	NM_005276.2	GCAGACACCCAACTTTCGCATCA	CCGCCGCCTTGGTGTTGTCA
Myh6	myosin, heavy polypeptide 6, cardiac muscle, alpha	NM_010856.4	TCCGTGCAGATAGAGATGAATAAG	CCCGCTGGAGGTTGTCG
Myh7	myosin, heavy polypeptide 7, cardiac muscle, beta	NM_080728.2	GGCTAACCTGGAGAAGATGTGC	CCCGCTGGCTGGTGAGG
Myl2	myosin, light polypeptide 2, regulatory, cardiac, slow	NM_010861.3	CCGAGGGCAAAGGGTCACTG	GGGGAAAGGCTGCGAACATCT
Pdk4	pyruvate dehydrogenase kinase, isoenzyme 4	NM_013743.2	GGCTTGCCAATTTCTCGTCTCTA	TTCGCCAGGTTCTTCGGTTCC
Pgc1a	peroxisome proliferative activated receptor, gamma, coactivator 1	NM_008904.2	CCCAAAGGATGCGCTCTCGTT	TGCGGTGTCTGTAGTGGCTTGATT
Scd1	stearoyl-Coenzyme A desaturase 1	NM_009127.4	ACTGGGGCTGCTAATCTCTGGGTGTA	GGCTTTATCTCTGGGGTGGGTTTGTTA
Srebp1	sterol regulatory element binding transcription factor 1	NM_011480.3	GCTTCCGGCCTGCTATGA	CAGGGCCTCGGTGTGCTC
Tnnc1	troponin C, cardiac/slow skeletal	NM_009393.2	CGATGGCCGAATTGACTATGACGA	TGGGTGGAGGGGGAGAACAGG
Trib3	tribbles homolog 3	NM_175093.2	TTCCTACCGGGGCTGTCTTCTCTG	AGCCCGGCCTGATTTGTGGTC
Ucp3	uncoupling protein 3 (mitochondrial, proton carrier)	NM_009464.3	AGAACCATCGCCAGGGAGGAAGGA	CACCGGGGAGGCCACCACTGT

Table S6 Real-time quantitative RT-PCR analysis in skeletal muscle

Gene symbol	Chow	cHF		cHF+F		cHF+ROSI		cHF+F+ROSI	
		OrD	Re-fed Chow	OrD	Re-fed Chow	OrD	Re-fed Chow	OrD	Re-fed Chow
Acot1	0.54 ± 0.06	1.00 ± 0.15^{i}	1.00 ± 0.09^{i}	1.28 ± 0.14^{i}	0.66 ± 0.05^{b}	1.12 ± 0.10^{i}	0.73 ± 0.05^{ci}	1.34 ± 0.11^{i}	0.66 ± 0.08^{d}
CD36	0.97 ± 0.08	1.00 ± 0.11^{d}	1.19 ± 0.07	1.30 ± 0.10^{i}	1.07 ± 0.06	1.19 ± 0.16	1.12 ± 0.07	1.51 ± 0.08^{i}	1.17 ± 0.10^{d}
Cpt1a	1.49 ± 0.31	1.00 ± 0.19	1.72 ± 0.37^{a}	1.36 ± 0.22	1.37 ± 0.19	1.15 ± 0.28	1.15 ± 0.12	1.61 ± 0.15	1.86 ± 0.30
Cpt1b	0.69 ± 0.35	1.00 ± 0.13	2.18 ± 0.53^{a}	0.69 ± 0.14	1.93 ± 0.30^{bi}	1.05 ± 0.17	1.65 ± 0.29	1.30 ± 0.18	1.48 ± 0.41
Cyp1a1	0.92 ± 0.08	1.00 ± 0.03^{d}	0.86 ± 0.05^{h}	1.10 ± 0.07^{d}	0.97 ± 0.05^{h}	1.18 ± 0.08^{d}	0.91 ± 0.041^{h}	1.41 ± 0.08^{i}	1.21 ± 0.06^{di}
Fbp2	0.52 ± 0.11	1.00 ± 0.06^{i}	0.89 ± 0.11	0.88 ± 0.13	0.85 ± 0.11	0.90 ± 0.10^{i}	0.55 ± 0.10^{c}	1.27 ± 0.06^{i}	0.76 ± 0.11^{d}
Glut4	1.68 ± 0.18	1.00 ± 0.13^{i}	1.48 ± 0.14^{a}	0.98 ± 0.08^{i}	1.43 ± 0.08^{b}	1.01 ± 0.09^{i}	1.33 ± 0.11^{c}	1.22 ± 0.12^{i}	1.59 ± 0.11^{d}
Gpd1	1.05 ± 0.09	1.00 ± 0.07	0.85 ± 0.06	0.84 ± 0.06^{d}	0.97 ± 0.07	0.86 ± 0.10	0.90 ± 0.05	1.11 ± 0.05^{b}	1.05 ± 0.07
Myh6	0.33 ± 0.09	1.00 ± 0.26	2.09 ± 0.33^{i}	1.21 ± 0.54	1.48 ± 0.47^{i}	1.25 ± 0.59	1.74 ± 0.55^{i}	2.19 ± 0.46^{i}	0.93 ± 0.31
Myh7	0.68 ± 0.11	1.00 ± 0.42	2.23 ± 0.26^{ai}	1.05 ± 0.31	1.65 ± 0.36^{i}	1.45 ± 0.60	1.47 ± 0.29^{i}	1.81 ± 0.47^{i}	1.30 ± 0.31
Myl2	1.17 ± 0.28	1.00 ± 0.23	1.93 ± 0.17^{ai}	1.01 ± 0.19	2.44 ± 0.22^{bi}	1.42 ± 0.31	2.46 ± 0.31^{ci}	1.23 ± 0.20	1.43 ± 0.34^{dfg}
Pdk4	0.41 ± 0.05	1.00 ± 0.13^{i}	0.84 ± 0.13	1.29 ± 0.16^{i}	0.53 ± 0.12^{b}	1.03 ± 0.21	0.52 ± 0.06^{c}	1.41 ± 0.16^{i}	0.49 ± 0.04^{d}
Pgc1a	0.81 ± 0.33	1.00 ± 0.19	0.91 ± 0.19	1.14 ± 0.33	1.30 ± 0.32	2.17 ± 0.72	0.82 ± 0.11^{c}	1.40 ± 0.35	0.81 ± 0.20
Scd1	1.55 ± 0.30	1.00 ± 0.09	1.15 ± 0.14	0.59 ± 0.08^{ci}	0.64 ± 0.08^{i}	1.52 ± 0.32^{d}	1.02 ± 0.07^{c}	0.75 ± 0.11^{i}	0.73 ± 0.15^{i}
Srebp1	2.79 ± 0.43	1.00 ± 0.12^{i}	1.70 ± 0.35^{ai}	0.85 ± 0.11^{i}	1.35 ± 0.21^{i}	1.10 ± 0.16	2.09 ± 0.29^{c}	1.24 ± 0.18	1.38 ± 0.18^{i}
Tnnc1	0.23 ± 0.07	1.00 ± 0.28	1.15 ± 0.16^{i}	1.12 ± 0.33	0.97 ± 0.19^{i}	1.27 ± 0.32	1.42 ± 0.42	1.73 ± 0.34^{i}	0.74 ± 0.15^{d}
Trib3	1.51 ± 0.14	1.00 ± 0.08^{i}	1.06 ± 0.11^{i}	1.09 ± 0.07^{i}	1.81 ± 0.24^{be}	0.98 ± 0.05^{i}	1.41 ± 0.06^{c}	1.56 ± 0.09^{ac}	2.09 ± 0.15^{degi}
Ucp3	0.88 ± 0.23	1.00 ± 0.12	1.21 ± 0.31	1.02 ± 0.10	1.00 ± 0.17	0.98 ± 0.21	0.81 ± 0.12	1.14 ± 0.10	1.45 ± 0.17

At the end of the experiment, mice were killed either without any additional manipulations, that is, while offered the 'original' cHF-based diets (OrD), or following the 'diet-switch protocol' when re-fed Chow diet; see Fig. 1. Control mice maintained on Chow diet throughout the intervention and killed in ad libitum fed state were also analyzed. Data are means±SE (n=7–8). For gene symbols, see Table S5.

[a] Significantly different from cHF, OrD.

[b] significantly different from cHF+F, OrD.

[c] significantly different from cHF+ROSI, OrD.

[d] significantly different from cHF+F+ROSI, OrD.

[e] Significantly different from cHF, Re-fed Chow.
[f] significantly different from cHF+F, Re-fed Chow.
[g] significantly different from cHF+ROSI, Re-fed Chow.
[h] significantly different from cHF+F+ROSI, Re-fed Chow (Two-way ANOVA).
[i] significantly different from Chow (t-test).

International Journal of Obesity (2012) 36, 262–272
 0307-0565/12
www.nature.com/ijo

ORIGINAL ARTICLE

Sex differences during the course of diet-induced obesity in mice: adipose tissue expandability and glycemic control

D Medrikova, ZM Jilkova, K Bardova, P Janovska, M Rossmeisl and J Kopecky

Department of Adipose Tissue Biology, Institute of Physiology Academy of Sciences of the Czech Republic v.v.i., Prague, Czech Republic

Objective: Adverse effects of obesity on glucose homeostasis are linked to low-grade adipose tissue inflammation and accumulation of lipids in non-adipose tissues. The goal of this study was to evaluate the role of adipose tissue plasticity in a less severe deterioration of glucose homeostasis in females compared with males during the course of high-fat (HF) feeding in mice.
Design: Mice of the C57BL/6N strain were fed either a chow or obesogenic HF diet for up to 35 weeks after weaning. Metabolic markers and hormones in plasma, glucose homeostasis, adipocyte size and inflammatory status of gonadal (gWAT) and subcutaneous (scWAT) adipose depots and liver steatosis were evaluated at 15 and 35 weeks of HF feeding.
Results: HF-fed males were heavier than females until week ~20, after which the body weights stabilized at a similar level (55–58 g) in both sexes. Greater weight gain and fat accumulation in females were associated with larger adipocytes in gWAT and scWAT at week 35. Although adipose tissue macrophage infiltration was in general less frequent in scWAT, it was reduced in both fat depots of female as compared with male mice; however, the expression of inflammatory markers in gWAT was similar in both sexes at week 35. In females, later onset of the impairment of glucose homeostasis and better insulin sensitivity were associated with higher plasma levels of adiponectin (weeks 0, 15 and 35) and reduced hepatosteatosis (weeks 15 and 35).
Conclusions: Compared with males, female mice demonstrate increased capacity for adipocyte enlargement in response to a long-term HF feeding, which is associated with reduced adipose tissue macrophage infiltration and lower fat deposition in the liver, and with better insulin sensitivity. Our data suggest that adipose tissue expandability linked to adiponectin secretion might have a role in the sex differences observed in obesity-associated metabolic disorders.
International Journal of Obesity (2012) **36,** 262–272; doi:10.1038/ijo.2011.87; published online 3 May 2011

Keywords: sex differences; inflammation; adipose tissue expandability; insulin sensitivity; mice

Introduction

Human[1,2] as well as animal studies[3–7] demonstrate less severe obesity-related metabolic disorders including peripheral tissue insulin resistance and dyslipidemia (i.e., the components of metabolic syndrome), and/or later onset of these adverse phenotypes in female than in male subjects. However, mechanisms underlying a relatively low susceptibility of females to metabolic syndrome remain largely unknown.

Correspondence: Dr J Kopecky, Department of Adipose Tissue Biology, Institute of Physiology Academy of Sciences of the Czech Republic v.v.i.,Videnska 1083, 142 20 Prague, Czech Republic.
E-mail: kopecky@biomed.cas.cz
Received 22 July 2010; revised 23 February 2011; accepted 13 March 2011; published online 3 May 2011

Adverse effects of obesity depend largely on (1) the anatomical site of excessive fat accumulation,[8,9] which differ between the sexes,[1,10,11] and (2) on whether the growth of adipose tissue is reached by hyperplasia or hypertrophy of adipocytes. Hyperplasia, rather than hypertrophy, represents a less harmful phenotype associated with a faster turnover of fat cells.[12] Larger adipocytes are less insulin-sensitive than smaller ones,[7,13,14] and small adipocytes can store more extra fat, while limiting the ectopic accumulation of lipids in non-adipose tissues and lipotoxicity.[15] It was suggested that adipose tissue expandability is a more important determinant of obesity-associated metabolic disorders than the absolute amount of adipose tissue an individual possesses.[16] Moreover, larger fat cells are associated with a low-grade adipose tissue inflammation, another key factor linking obesity with insulin resistance.[13,14,17–19] Enhanced secretion of chemoattractants in obese state, like monocyte

chemoattractant protein-1 (MCP-1), is believed to promote migration of macrophages[20,21] as well as other immune cells[22] into the tissue accompanied by the phenotypic switch of macrophages to proinflammatory state.[23,24] Higher release of proinflammatory cytokines, like tumor necrosis factor α (TNFα) and interleukin 6, into circulation may disrupt insulin signaling in other tissues.[25–27] Recent studies in mice[19,28] showed that high-fat (HF) diet-induced obesity is associated with increased macrophage infiltration and inflammation in gonadal fat (gWAT) and to a lower extent also in subcutaneous fat (scWAT). Inflammatory state in gWAT is correlated with systemic insulin resistance[28] and with hepatic triglyceride (TAG) content in rodents.[20,21] It is believed that increased macrophage infiltration of adipose tissue in obesity is triggered by dead adipocytes,[29] and that adipocyte size is an important determinant in cell death.[30] At the same time, clearance of dead adipocytes by surrounding macrophages is required for remodeling of adipose tissue.[28] Thus, fat cell size and macrophage infiltration represent interdependent variables affecting adipose tissue expandability.

In contrast to proinflammatory cytokines, the major adipokines released from adipocytes, namely leptin and adiponectin, protect insulin signaling from lipotoxic damage via increasing activity of AMP-activated protein kinase (AMPK; see Yamauchi *et al.*[31]), reflecting the key role of AMPK in the control of lipid metabolism, as well as by other mechanisms.[32] Although secretion of leptin and leptinemia correlate with adiposity, adiponectin is downregulated in obese and diabetic subjects.[33] This may have a major impact on health because of the anti-diabetic, anti-inflammatory and anti-atherogenic effects of adiponectin.[34–37]

Most of the above studies were performed on male subjects. However, studies in humans[38–40] as well as in mice[19] suggest that lower adipose tissue macrophage infiltration[19] and/or smaller fat cell size[19,40] in female subjects could contribute to the sex differences in propensity to the disorders of the metabolic syndrome. In this study performed in mice, we tested a hypothesis that because of a higher stimulation of lipogenesis and a stronger antilipolytic effect of insulin in female adipocytes, especially those in gWAT,[4,7] (1) prolonged HF feeding may eventually result in larger fat cells in female than in male animals, and that (2) glycemic control may be less affected by excessive adiposity in female than in male mice, even in the presence of larger adipocytes in the females. During the course of a long-term (35 weeks) HF feeding, body weights of male and female mice reached their maxima at a similar level. Adipocytes in both gWAT and scWAT became eventually larger in female than in male mice, whereas the density of macrophages in adipose tissue remained lower in females. Our results suggest that adiponectin, rather than adipose tissue-derived proinflammatory cytokines, is associated with the differential effects of extreme dietary obesity on insulin sensitivity and hepatic steatosis in female and male mice. It is plausible that adipose tissue in female subjects is genetically programmed to store more lipids than in males, thus constituting an important mechanism of harmless lipid storage.

Materials and methods

Animals and treatments

All experiments were performed using the F1 generation of male and female C57BL/6N mice imported from Charles River Laboratories (Sulzfeld, Germany; 20 mice of each sex) maintained (3–4 mice of the same sex per cage) at 22 °C on a 12-h light–dark cycle (light switched on from 0600 h), and allowed free access to food and water. Four weeks after birth (week 0), mice were randomly assigned either to (1) chow (ST; lipid content ~3.4% wt/wt; extruded Ssniff R/M-H diet, SSNIFF Spezialdieten GmbH, Soest, Germany) with protein, fat and carbohydrate forming 33, 9 and 58 energy percent or to (2) HF diet (lipid content ~35% wt/wt, mainly corn oil) with protein, fat and carbohydrate forming 15, 59 and 26 energy percent, respectively (see Kuda *et al.*[41] for further details regarding the HF diet composition, including fatty acid composition of dietary lipids). During the treatments, fresh rations were distributed three times a week. Body weight of each mouse was monitored weekly, food intake per cage was monitored weekly between weeks 4 and 14 after weaning, and every second week between weeks 17 and 30 after weaning, except for the week right after the glucose tolerance tests (see below and Figure 1). At week 15 or at week 35 after weaning, 10 mice of each sex were

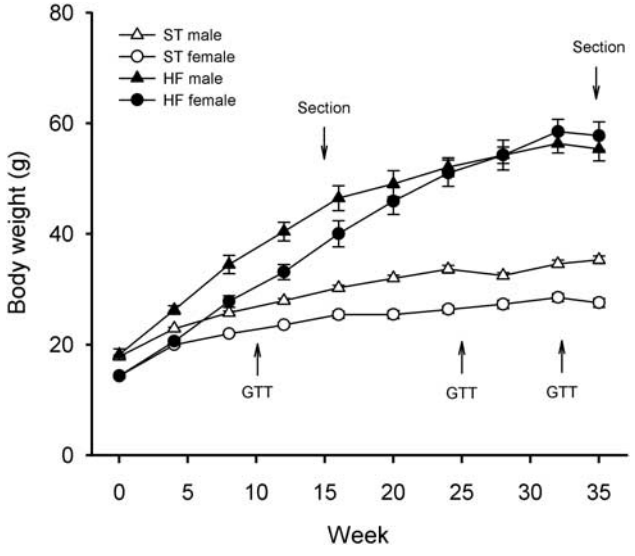

Figure 1 Growth curves. Mice of both sexes were weaned to either ST or HF diet at 4 weeks of age (week 0). Some mice ($n=10$ from each sex) were killed at week 15, whereas the remaining mice were killed at week 35. Data are shown as means ± s.e. ($n=20$ between weeks 0 and 15; and $n=10$ between weeks 16 and 35). Intraperitoneal glucose tolerance test (GTT) was performed at weeks 10, 25 and 33.

killed under the influence of diethyl ether anesthesia, by cervical dislocation, in a random-fed state. Truncal plasma was collected and stored at −80 °C. Liver, gWAT and dorsolumbar scWAT (i.e., fat depot forming a continuum with the inguinal fat[42]) were rapidly dissected. Liver samples were snap-frozen in liquid nitrogen and stored at −80 °C for further histological analysis. Samples of gWAT for mRNA analysis were stored at −80 °C in RNA Later (Ambion, Austin, TX, USA). Corresponding contralateral adipose tissue depots were used for light microscopy and immunohistochemical analysis (see below).

All experiments were performed in accordance with the directive of the European Communities Council (68/609/EEC), and the *Principles of Laboratory Animal Care* (NIH publication no. 85-23, revised 1985).

Plasma metabolites, hormones and enzymes

Non-esterified fatty acids and TAG were determined in EDTA–plasma using respective enzymatic photometric tests: NEFA-C (Wako Chemicals, Neuss, Germany) and Triacylglycerols Liquid (Pliva-Lachema Diagnostika, Brno, Czech Republic). Blood glucose was measured using calibrated glucometers OneTouch Ultra (Life Scan, Milpitas, CA, USA). Multimeric forms of adiponectin were determined similarly as before,[43] using western blotting and primary rabbit anti-mouse polyclonal antibodies (BioVendor, Brno, Czech Republic), followed by secondary donkey anti-rabbit IgG infrared dye conjugated antibodies (IR Dye 800; Rockland, Gilbertsville, PA, USA). Membranes were scanned using Odyssey IR imager (Li-Cor Biosciences, Lincoln, NE, USA). Plasma insulin levels were determined by the Sensitive Rat Insulin RIA Kit, and leptin content was assessed using a Mouse Leptin RIA Kit (both kits from LINCO Research, St Charles, MO, USA).

Tissue TAG content

Tissue fragments were digested in 0.15 ml of 3 M alcoholic KOH (70 °C, 2 h) and glycerol in the solubilisate was assessed by Triacylglycerols Liquid (Pliva-Lachema Diagnostika) as before.[44] TAG content was calculated relative to a Lyonorm Calibrator (Pliva-Lachema Diagnostika).

Adipose tissue DNA content

The DNA content was measured fluorometrically after overnight digestion of the tissue using proteinase K as before.[45] Calf-thymus DNA (Sigma-Aldrich, Prague, Czech Republic) was used as a standard.

Light microscopy and immunohistochemical analysis

Adipose tissue samples were fixed in 10% neutral buffered formalin (Sigma-Aldrich) and embedded in paraffin. Sections (5 μm) were stained with hematoxylin–eosin stain for morphometry, or processed to detect MAC-2/galectin positive macrophages aggregated in crown-like structures (CLS) surrounding dead adipocytes, using antibodies by Cedarlane Laboratories (Burlington, NC, USA) as described before.[29] Liver lipids were detected in cryosections (8 μm) of the tissue, fixed in 10% neutral-buffered formalin and stained with a saturated solution of Oil red O (Sigma-Aldrich) in 70% ethanol; sections were counterstained with hematoxylin. Digital images were captured by Olympus AX70 light microscope and a DP 70 camera (Olympus, Tokyo, Japan). Morphometric analysis was performed using Imaging Software NIS-Elements AR 3.0 (Laboratory Imaging, Prague, Czech Republic). The morphometry data are based on measurements of ∼500 cells taken randomly from 3 to 6 different sections per animal.

Glucose homeostasis

An intraperitoneal glucose tolerance test was performed after overnight fasting (15–16 h), at weeks 10, 25 and 33 (Figure 1). Blood glucose was assessed by tail bleeds at the baseline (fasting blood glucose; just before the glucose injection) and at 15, 30, 60, 120 and 180 min after the injection of D-glucose (1 g kg^{-1} body weight). Results were expressed as area under the curve for glucose.[44] Blood samples collected at the baseline were also used to measure insulinemia. In addition, to assess changes of glycemia in response to fasted-to-fed transition, mice scheduled for killing at week 35 were subjected to tail bleeding at week 15. Before the bleeding, one half of the mice within each experimental group was either (1) fasted for 14 h (food was absent in the cage between 0800 and 2200 h; i.e., fasted state), or (2) fasted for 10 h (between 0800 and 1800 h and allowed free access to food for the following 3 h; i.e., re-fed state). In each mouse, blood glucose was assessed in both fasted and re-fed state, while altering the above protocols during two subsequent days (adapted procedure, following Viollet *et al.*[46]).

Gene expression analysis

Total RNA was isolated from gWAT using TRIzol Reagent (Invitrogen, Carlsbad, CA, USA). Total RNA (1 μg) was reverse transcribed to cDNA and gene expression was evaluated by quantitative real-time PCR, using the LightCycler Instrument 480 (Roche Diagnostics, Mannheim, Germany) and qPCR kit LightCycler 480 SYBR Green I Master (Roche Diagnostics). Oligonucleotide primers were designed using Lasergene software (DNAStar, Madison, WI, USA). The following primer pairs were used: MCP-1 (forward, 5′-GTTAACGCCCCACTCAC-3′, reverse, 5′-GGTTCCGATCCAGGTTT-3′); tumor necrosis factor α (TNFα; forward, 5′-GAAGTTCCCAAATGGCCTCCCTCTC-3′, reverse, 5′-GCCACTCCAGCTGCTCCTCCACTTG-3′); macrosialin (CD68; forward, 5′-CACTTCGGGCCATGTTTCTCTTG-3′, reverse, 5′-AGGGGCTGGTAGGTTGATTGTCGT-3′). Levels of transcripts were standardized using the gene encoding eukaryotic translation elongation

factor 2 (eEF2; forward, 5′-GAAACGCGCAGATGTCCAAAA GTC-3′, reverse, 5′-GCCGGGCTGCAAGTCTAAGG-3′).

Statistics

All values are presented as means ± s.e. Data were analyzed by two-way analysis of variance using SigmaStat (SSI, San Jose, CA, USA) statistical software. The Holm–Sidak test for multiple comparisons was used. Changes in glycemia (Figure 3a) and in plasma insulin levels (Figure 3d) in individual mice were analyzed using repeated measures analysis of variance. Threshold of significance was defined at $P \leqslant 0.05$.

Results

Growth characteristics

At the time of weaning, body weight of male mice was significantly higher than that of females, and males remained heavier during the whole 35-week-period of ST feeding (Figure 1 and Table 1). Within a couple of weeks after weaning, mice of both sexes fed HF diet became significantly heavier than their respective ST-fed controls. During ~20 initial weeks, HF-fed male mice showed higher body weight than females, whereas females gained weight faster than males, and from week 20 onward, females showed equal body weight as males, and even tended to be heavier than males eventually (Figure 1). Thus, females gained more weight during the 35-week feeding period compared with males (Table 1). Food consumption remained stable with age in both sexes and dietary groups. HF-fed males showed the same caloric intake as ST-fed males, whereas caloric intake was higher in HF-fed than ST-fed females. Inter-sex differences in caloric intake were not observed, except for ST-fed female mice, during weeks 4–14, showing lower food intake than ST-fed males (Table 1).

In ST-fed mice, at both weeks 15 and 35, no significant differences in weight of either gWAT or scWAT were observed between the sexes, but male mice tended to accumulate more fat. The opposite situation was observed in HF-fed mice, in which females displayed the tendency for a greater accumulation of fat in both depots at week 15. The difference was even more pronounced at week 35, with males showing smaller fat depots, especially in the case of gWAT (~3.8-fold difference) as compared with corresponding female mice (Table 1). Similar trends were observed after normalization of depot weights to total body weight (Table 1).

HF feeding increased the weight of the liver. However, at both week 15 and 35 (as well as in ST-fed mice at week 35), the liver was smaller in female than in male mice (Table 1). Female mice were less prone to HF diet-induced liver steatosis, as revealed by the biochemical analysis of the tissue (Table 1) and by its histological staining for lipids (Figure 2). However, no differences were detected between the sexes with respect to lipid accumulation in skeletal muscle (not shown).

Table 1 Growth characteristics, adiposity, and liver weight and TAG content

	ST		*HF*	
	Male	*Female*	*Male*	*Female*
BW (g)				
Week 0	17.8 ± 0.2	14.3 ± 0.3[a]	18.2 ± 1.0	14.3 ± 0.3[a]
Week 15	28.5 ± 0.4	24.1 ± 0.4[a]	43.6 ± 1.9[b]	36.4 ± 1.7[a,b]
Week 35	35.3 ± 0.7	27.6 ± 0.8[a]	55.4 ± 2.2[b]	57.7 ± 2.6[b]
BWG (g)				
Week 15	11.6 ± 0.6	10.6 ± 0.5	27.2 ± 1.4[b]	23.1 ± 2.3[a,b]
Week 35	17.5 ± 0.6	13.2 ± 0.6	37.2 ± 1.8[b]	43.4 ± 2.4[b]
FC (kJ per day)				
Week 4–14	66.3 ± 0.7	56.2 ± 1.4[a]	69.5 ± 2.4	68.5 ± 3.6[b]
Week 17–30	64.8 ± 1.1	61.1 ± 2.3	66.7 ± 4.1	70.6 ± 2.0[b]
gWAT (mg)				
Week 15	484 ± 31	364 ± 26	1881 ± 158[b]	2147 ± 301[b]
Week 35	1032 ± 107	711 ± 97	1565 ± 95	5989 ± 470[a,b]
gWAT (% of BW)				
Week 15	1.8 ± 0.1	1.62 ± 0.1	4.8 ± 0.4[b]	5.87 ± 0.5[a,b]
Week 35	2.9 ± 0.3	2.5 ± 0.3	2.8 ± 02	10.2 ± 0.5[a,b]
scWAT (mg)				
Week 15	217 ± 14	195 ± 11	797 ± 95[b]	873 ± 117[b]
Week 35	312 ± 35	271 ± 24	1297 ± 113[b]	1590 ± 133[a,b]
scWAT (% of BW)				
Week 15	0.8 ± 0.0	0.8 ± 0.1	2.0 ± 0.2[b]	2.4 ± 0.2[b]
Week 35	0.9 ± 01	1.0 ± 0.1	2.3 ± 0.2[b]	2.7 ± 0.2[a,b]
Liver (mg)				
Week 15	1247 ± 55	1144 ± 29	1606 ± 130[b]	1236 ± 56[a]
Week 35	1544 ± 51	1160 ± 56[a]	2541 ± 231[b]	1806 ± 111[a,b]
Liver (% of BW)				
Week 15	4.6 ± 0.2	4.9 ± 0.1	4.0 ± 0.1[b]	3.6 ± 0.1[a,b]
Week 35	4.4 ± 0.1	4.2 ± 0.1	4.5 ± 0.3	3.1 ± 0.1[a,b]
Liver TAG (mg/g of tissue)				
Week 15	28 ± 1	32 ± 3	109 ± 20[b]	72 ± 6[a,b]
Week 35	34 ± 3	38 ± 3	197 ± 27[b]	121 ± 8[a,b]

Abbreviations: BW, body weight; BWG, body weight gain since week 0; FC, mean food consumption; gWAT, gonadal white adipose tissue; HF, high fat; scWAT, subcutaneous white adipose tissue; ST, standard; TAG, triglycerides. [a]Significant differences between sexes within diet. [b]Significant differences between diets within sex (ANOVA). Male and female mice, weaned at 4 weeks of age (week 0), on ST or HF diet were analyzed after 15 or 35 weeks ($n = 10$) of feeding their respective diets. Data are shown as means ± s.e.

Plasma markers

Levels of lipids and several hormones were measured in plasma of mice killed in *ad libitum*-fed state at weeks 15 and 35 (Table 2). In ST-fed mice, levels of TAG decreased with age, and especially at week 35, female had lower TAG levels than male mice, whereas no age- or sex-specific differences in

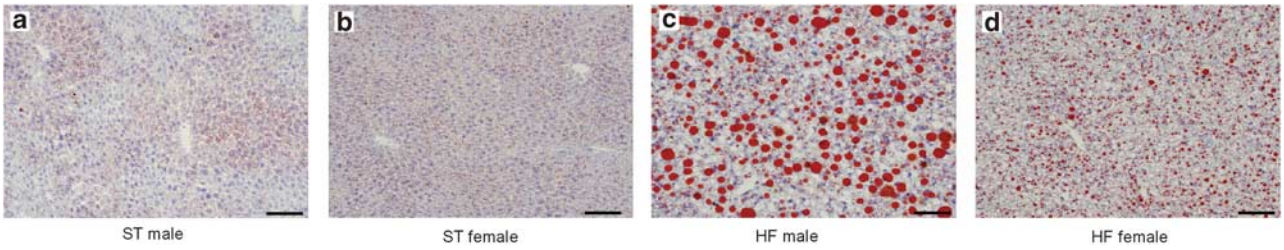

Figure 2 Liver histology. Oil-red O staining showing triglyceride accumulation (red color) in the liver (sections counterstained with hematoxylin) of male and female mice at 35 weeks after weaning to either ST or HF diet. Scale bar, 0.1 mm.

Table 2 Plasma lipids and hormones

	ST		*HF*	
	Male	*Female*	*Male*	*Female*
TAG (mmol l^{-1})				
Week 15	1.20 ± 0.12	1.01 ± 0.05	1.66 ± 0.21[a]	1.21 ± 0.14[b]
Week 35	0.97 ± 0.11	0.61 ± 0.04[b]	0.96 ± 0.03	0.92 ± 0.06[a]
NEFA (mmol l^{-1})				
Week 15	0.51 ± 0.04	0.48 ± 0.03	0.59 ± 0.06	0.62 ± 0.06
Week 35	0.40 ± 0.05	0.39 ± 0.03	0.41 ± 0.06	0.46 ± 0.03
Cholesterol (mmol l^{-1})				
Week 15	1.77 ± 0.11	1.54 ± 0.10	4.08 ± 0.30[a]	3.55 ± 0.20[a]
Week 35	1.96 ± 0.10	1.47 ± 0.06	4.78 ± 0.38[a]	4.08 ± 0.25[a,b]
Insulin (ng ml^{-1})				
Week 15	0.88 ± 0.21	0.38 ± 0.04[b]	2.71 ± 0.54[a]	1.15 ± 0.23[a,b]
Week 35	0.97 ± 0.16	0.21 ± 0.03[b]	4.68 ± 0.45[a]	2.30 ± 0.46[a,b]
Leptin (ng ml^{-1})				
Week 15	6.2 ± 0.7	8.8 ± 0.8	45.5 ± 7.6[a]	41.7 ± 8.0[a]
Week 35	17.7 ± 2.0	9.1 ± 1.7[b]	71.9 ± 4.7[a]	89.6 ± 2.8[a,b]
Adiponectin (AU)				
Week 15				
HMW	0.45 ± 0.03	0.62 ± 0.05[b]	0.33 ± 0.02[a]	0.63 ± 0.03[b]
MMW	0.46 ± 0.02	0.65 ± 0.04[b]	0.44 ± 0.02	0.60 ± 0.03[b]
LMW	0.02 ± 0.00	0.02 ± 0.00	0.01 ± 0.00	0.02 ± 0.00[b]
Total	0.94 ± 0.05	1.29 ± 0.08[b]	0.78 ± 0.03[a]	1.25 ± 0.05[b]
Week 35				
HMW	0.46 ± 0.04	0.86 ± 0.10[b]	0.40 ± 0.06	0.63 ± 0.07[a,b]
MMW	0.55 ± 0.03	0.80 ± 0.06[b]	0.50 ± 0.02	0.78 ± 0.07[b]
LMW	0.04 ± 0.01	0.03 ± 0.00	0.02 ± 0.00[a]	0.03 ± 0.00
Total	1.06 ± 0.06	1.69 ± 0.15[b]	0.92 ± 0.07	1.44 ± 0.13[b]

Abbreviations: AU, arbitrary units; HF, high fat; HMW, high-molecular-weight adiponectin; LMW, low-molecular-weight adiponectin; MMW, medium-molecular-weight adiponectin; NEFA, non-esterified fatty acids; ST, standard; TAG, triglycerides. [a]Significant differences between diets within the sexes (ANOVA). [b]Significant differences between sexes within diet. Male and female mice, weaned at 4 weeks of age, on ST or HF diet were analyzed after 15 or 35 weeks ($n=10$) of feeding their respective diets. Data are shown as means ± s.e.

non-esterified fatty acids or cholesterol levels were observed. Except for non-esterified fatty acids, plasma lipid levels were increased in response to HF feeding; TAG levels were lower in the older mice, and they were also lower in female than in male mice at week 15. No other age- or sex-dependent differences were observed in plasma lipid levels in HF-fed mice, excepting of cholesterol that was lower in female mice at week 35 (Table 2).

Plasma insulin levels in random-fed state in ST-fed mice were lower in female than in male mice, with the lowest levels observed in females at week 35. Insulin levels increased with HF feeding and with its duration, suggesting induction of insulin resistance; however, female mice were partially protected, as observed at both week 15 (~2.4-fold difference in plasma insulin) and week 35 (~2.0-fold difference in plasma insulin) (Table 2).

Plasma leptin levels in ST-fed mice increased with age, and at week 35, the levels were lower in female than in male mice. Leptin levels increased with HF feeding and with its duration, with female mice at week 35 showing higher levels than the corresponding male mice (Table 2).

Levels of total adiponectin (for a representative western blot, see Supplementary Figure 1), especially of its biologically active high-molecular-weight (HMW) form, which is implicated in enhancement of insulin sensitivity,[47] tended to be decreased by HF feeding, and HMW adiponectin levels were significantly depressed by HF diet at week 15 in male mice and at week 35 in females. Nevertheless, the levels of both total as well as HMW adiponectin were always higher in female than in male mice, with the HMW adiponectin in HF-fed mice showing a bigger difference between the sexes at week 15 than at week 35 (~1.9-fold vs ~1.6-fold difference, respectively; Table 2). Moreover, in a separate experiment, we have observed higher plasma total adiponectin in female mice already at the time of weaning at 4 weeks of age (0.68 ± 0.04 vs 1.03 ± 0.06 AU in males and females, respectively; $n=9$, $P\leqslant0.01$), with even doubled levels of HMW form (0.24 ± 0.1 vs 0.49 ± 0.3 AU in males and females, respectively; $P\leqslant0.01$).

Glucose homeostasis

When evaluated at week 15, mice of both genders fed ST diet, as well as female mice fed HF diet, were able to decrease substantially glycemia during fasting, but HF-fed male mice were not able to do so, indicating metabolic inflexibility to glucose in these mice (Figure 3a).

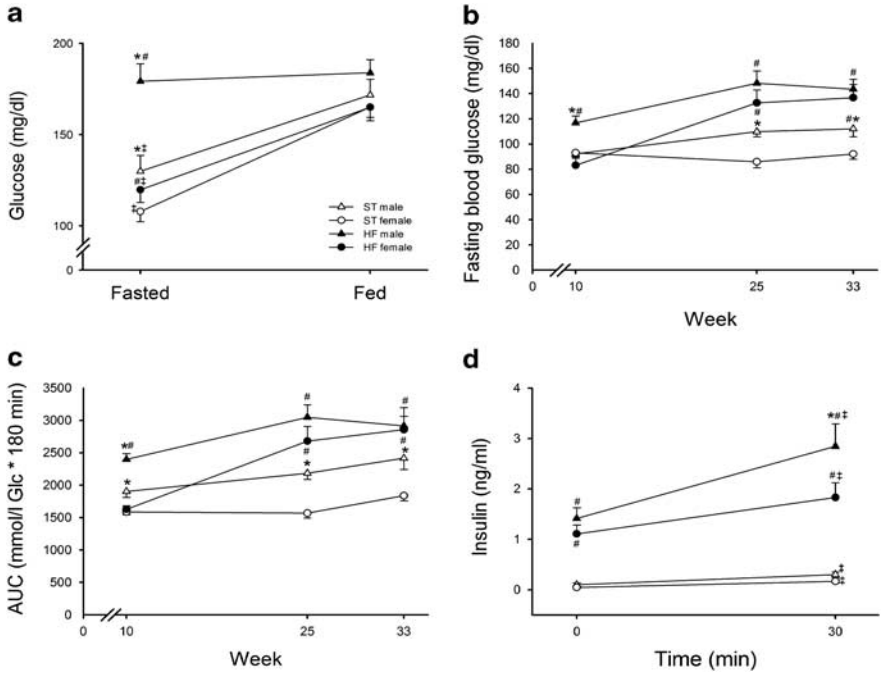

Figure 3 Glucose homeostasis. (**a**) Plasma glucose levels in fasted and fed mice at week 15 (see text for details). (**b–d**) Intraperitoneal glucose tolerance test was performed at weeks 10, 25 and 33, after weaning to either ST or HF diet (see also Supplementary Figure 1). (**b**) Fasting blood glucose at time 0 of the glucose tolerance tests performed at weeks 10, 25 and 33. (**c**) Area under the glycemic curve (AUC) of the tests performed at weeks 10, 25 and 33. (**d**) Plasma insulin levels at time 0 and 30 min of the test performed at week 33. Data are shown as means ± s.e. ($n = 10$; at week 10, one half of the mice was randomly selected for the testing). *Significant difference between the sexes within the same diet, #significant difference between the diets within the same sex (ANOVA); ‡significant difference before and after the respective treatment (RM ANOVA).

To assess the sex differences in the development of HF diet-induced insulin resistance, intraperitoneal glucose tolerance test was performed at weeks 10, 25 and 33 (Figures 3b, c and Supplementary Figure 2). Fasting blood glucose levels at the baseline (Figure 3b), as well as area under the curve derived from glycemic curves (Figure 3c), suggested better glucose tolerance in female than in male mice fed ST diet at all three time points analyzed (except for glycemia at week 10), with a mild deterioration of glucose homeostasis with aging. HF feeding aggravated glucose intolerance in both male and female mice. However, in contrast to male mice, which became strongly affected already at week 10, deterioration of glucose tolerance in response to HF feeding in female mice required longer period to develop, with a significant effect observed at week 25, and even more pronounced effect at week 33, when mice of both sexes showed identical values of both fasting blood glucose and area under the curve for glycemia during the test.

To further characterize glucose homeostasis at week 33, plasma insulin levels were also determined at the baseline and at 30 min after the glucose injection (Figure 3d), that is, at the time of presumed highest insulin response (when plasma glucose levels reach the peak values; see Supplementary Figure 1). In ST-fed mice, insulin levels at the baseline and at 30 min after the glucose injection were similar in both sexes (Figure 3d). In the HF-fed mice, already the baseline insulin levels were higher than in the ST-fed mice and the levels increased further in response to glucose reaching significantly higher levels in male than in female mice (Figure 3d).

Adipose tissue morphology and inflammation

Further analysis was performed to characterize the possible links between sex-dependent effects of HF feeding on glucose homeostasis, and changes in adipose tissue morphology and inflammation. Histological analysis combined with morphometry revealed that in ST-fed mice, mean area of adipocytes was larger in gWAT as compared with scWAT. However, the mean size of adipocytes was comparable between the sexes and it did not differ between weeks 15 and 35 (Figures 4e, i, g and k). In both sexes and in both fat depots, HF feeding significantly increased the adipocyte size at week 15 as well as at week 35. As observed before,[28] mean adipocyte size in gWAT (Figures 4e and i), but not in scWAT (Figures 4g and k), decreased with age. The shift in the mean size of adipocyte in gWAT with the duration of HF feeding reflected relatively high preponderance of small adipocytes at week 35 (Supplementary Figure 3). In contrast to gWAT, no major difference in the adipocyte size distribution between weeks 15 and 35 was observed in scWAT (Supplementary Figure 4). At week 15, mean size of adipocytes in both gWAT and scWAT of

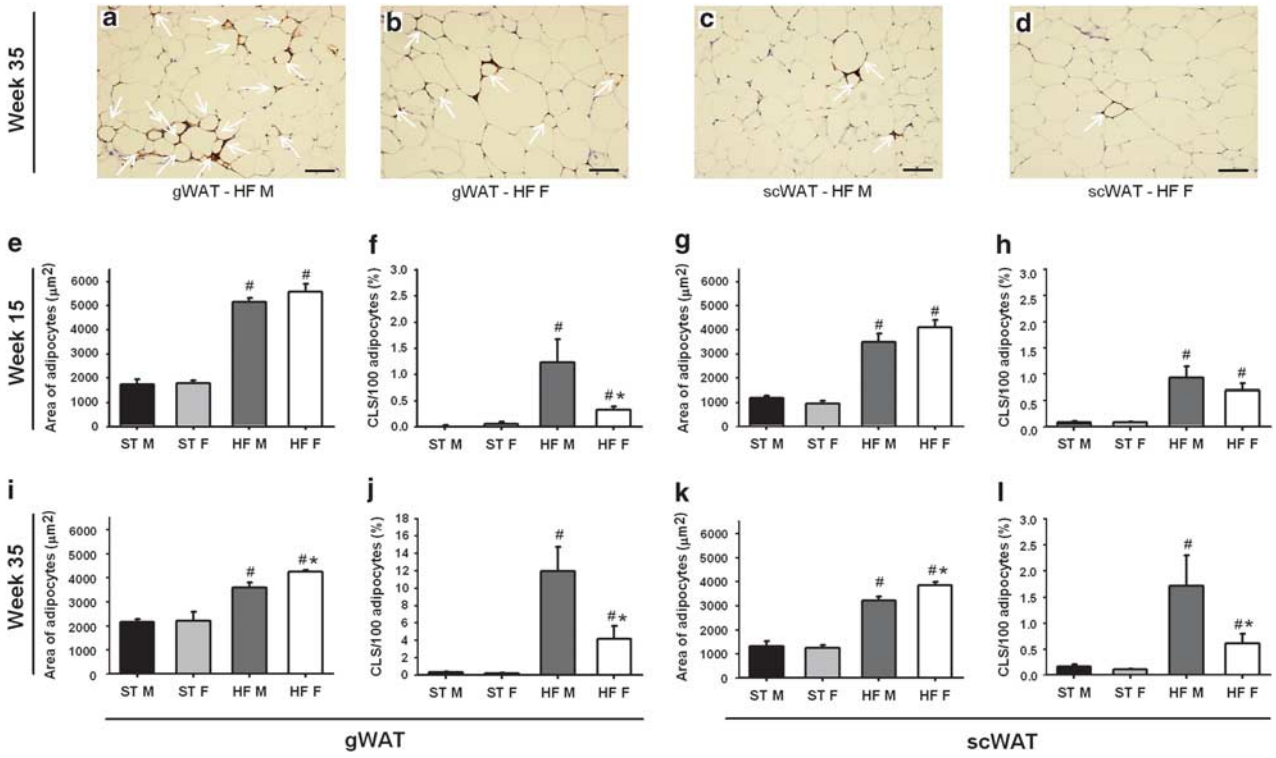

Figure 4 Adipose tissue histology—morphometry of adipocytes and macrophage infiltration. (**a–d**) Immunodetection of MAC-2-positive macrophages aggregated in crown-like structures (CLS; brownish color indicated by arrows) in gWAT and scWAT of male (M) and female (F) mice at 35 weeks after weaning to either ST or HF diet. Sections were counterstained with hematoxylin–eosin stain. Scale bar, 0.1 mm. At week 15 (**e–h**) and week 35 (**i–l**), size of adipocytes was evaluated by morphometric analysis in hematoxylin–eosin stained sections of gWAT (**e** and **i**) and scWAT (**g** and **k**) in both sexes. Frequency of CLS in gWAT (**f** and **j**) and scWAT (**h** and **l**) in both sexes. Data are shown as means ± s.e. ($n = 8$; within each group, mouse with the lowest and with the highest body weight, respectively, were not analyzed). *Significant difference between the sexes within the same diet; #significant difference between the diets within the same sex (ANOVA).

HF-fed female mice tended to be larger than in male mice fed the same diet (Figures 4e and g) and at week 35, the mean size of adipocytes in both fat depots was significantly larger in female compared with male mice (Figures 4i and k).

HF diet-induced hypertrophy of adipose tissue was associated with increased content of macrophages, immunodetected as CLS aggregates surrounding individual adipocytes (Figures 4a–d), and indicating induction of low-grade adipose tissue inflammation.[29] Thus, whereas CLS could be hardly detected in any sample of adipose tissue of ST-fed mice (Figures 4f, j, h and l), the CLS density was significantly higher in fat depots of HF-fed mice (Figure 4f, j, h and l), and it increased further several fold in gWAT, with a small increase in scWAT, between weeks 15 and 35 (Figures 4f, j, h and l). Although the degree of adipose tissue macrophage infiltration is usually correlated with size of adipocytes (see Introduction), adipose tissue of female mice contained much less CLS than their male counterparts. This was most apparent in both fat depots at week 35 (Figures 4j and l), as well as in gWAT at week 15 (Figure 4f).

In addition to the histological analysis, cellularity of gWAT was characterized using estimation of tissue DNA. At week 15, lower DNA concentration was found in HF-fed than in ST-fed mice, regardless of the sex (Figure 5a). At week 35, a different picture was observed. There was no difference between the ST-fed male and female mice; however, HF feeding increased the DNA concentration only in male mice (Figure 5b).

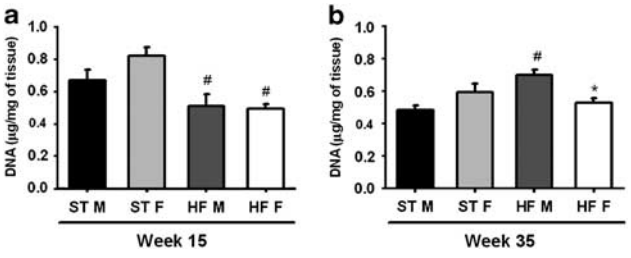

Figure 5 DNA quantification in gWAT of male (M) and female (F) mice fed ST or HF diet at week 15 (**a**) and week 35 (**b**). Data are means ± s.e. ($n = 7$–10). *significant difference between the sexes within the same diet; #significant difference between the diets within the same sex (ANOVA).

Gene expression

To further characterize the inflammatory status of adipose tissue in HF-fed mice, expression of several proinflammatory

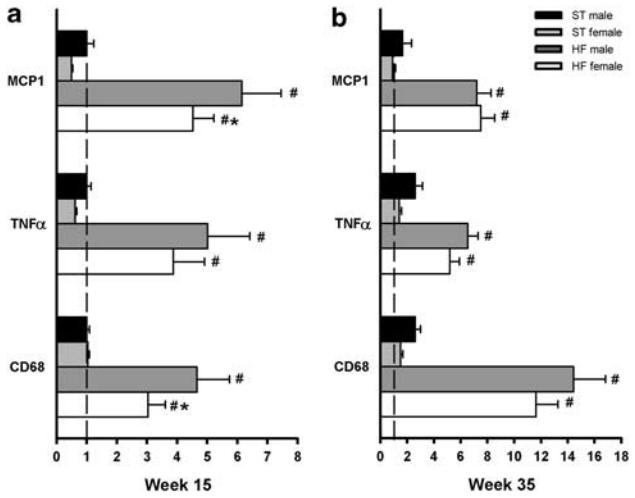

Figure 6 Quantification of gene expression in gWAT of male and female mice fed ST or HF diet at (**a**) week 15 and (**b**) week 35. Expression of selected genes was evaluated using qRT-PCR and standardized relative to ST diet-fed male mice at week 15. Data are shown as means ± s.e. ($n = 7$–10). *significant difference between the sexes within the same diet; #significant difference between the diets within the same sex (ANOVA).

markers was assessed in gWAT, which showed higher induction of macrophage infiltration in response to HF diet than scWAT (see above). In both sexes, HF feeding markedly increased expression of genes for MCP-1, TNFα and CD68, with a stronger induction in mice fed HF diet for the longer time (Figure 6). At week 15, all these genes showed lower expression in female than in male mice (although the difference in TNFα did not reach statistical significance; Figure 6a). At week 35, only a trend for lower expression in female mice was observed with TNFα and CD68 (Figure 6b).

Discussion

In this study, using a murine model of HF diet-induced morbid obesity, we showed that the weight gain, mass of both scWAT and gWAT fat depots, and mean size of adipocytes in these fat depots were all significantly increased in female compared with male mice in response to HF diet administered from weaning for a period of 35 weeks, that is, HF feeding of a very long duration until 10 months of age. At this time point, the body weight was stabilized and reached a similar level in both sexes. Although the total content of body lipids was not assessed at the end of HF feeding, it was also likely increased in females, as supported by their increased plasma leptin levels. Until week 15, males gained more weight and their body mass was higher than in females until week 20. In mice fed a low-fat ST diet, males were heavier, tended to accumulate more fat than females, whereas no effect on adipocyte size was found during the study. We verified the hypothesis (see Introduction) that the capacity for enlargement is increased in adipocytes of female compared with male mice in response to a long-term HF feeding, possibly reflecting the higher insulin sensitivity of the female adipocytes. In contrast to similar studies performed previously,[6,7,19] the sex-dependent metabolic phenotypes observed in this mouse model of dietary obesity could not be attributed to a lower body weight gain, adiposity and/or smaller fat cells in females. Most of the results were confirmed by an independent experiment on a separate cohort of animals (not shown).

Study of Grove *et al.*,[19] published recently in this journal, showed less inflamed gWAT in female than in male C57BL/6 mice fed HF diet for 12 weeks after weaning, with female mice having lower fat mass. Moreover, in female mice, the size of adipocytes tended to be smaller in gWAT, whereas it was significantly smaller in scWAT.[19] In our experiments, adipose tissue inflammation was assessed, as the density of CLS was also much lower in gWAT of female compared with male mice at week 15, that is, the time point when no significant differences in the size of adipocytes were observed between the sexes. However, in contrast to the study by Grove *et al.*,[19] we have prolonged the HF feeding until the week 35, when adipocytes within each fat depot were larger in female compared with male mice. Also at this time point, we observed sex-dependent differences in the CLS accumulation in gWAT and scWAT with females having much lower macrophage accumulation in both fat depots. These results are supported by the data on DNA concentration in gWAT, namely at week 35. At this time, HF-fed mice showed equal (female mice) or higher (male mice) tissue DNA concentration as compared with the ST-fed mice, in spite of larger adipocytes in the HF-fed animals, in agreement with an increased infiltration of adipose tissue with immune cells in response to HF feeding[22] and with the prominent inflammatory changes occurring in the male mice.

That female mice had lower inflammatory response was a surprising observation, as it is generally believed that macrophage infiltration and inflammation of adipose tissue in obesity is correlated with adipocyte hypertrophy.[13,14,19,29,30,36] Moreover, in agreement with the published data on extensive remodeling of gWAT in male mice during the course of HF diet-induced obesity,[28] our data document smaller adipocytes and lower mass of gWAT depot in males at week 35 than at week 15. In contrast, the mass of gWAT in HF-fed female mice was ~2.8-fold bigger at week 35 than at week 15, indicating very different patterns of gWAT remodeling in the two sexes. Our data also confirmed fat depot-specific differences[19,28] in the induction of adipose tissue macrophage infiltration by HF diet, with a relatively small infiltration in scWAT at either week 15 or 35, compared with a much stronger infiltration in gWAT, which increased ~10-fold between weeks 15 and 35.

Our observation that hypertrophy of adipocytes can be dissociated from adipose tissue inflammation is not without precedent. Thus, the genetic disruption of MCP-1 receptor gene,[48] transport protein lipocalin-2,[49] or disruption of the gene for a component of extracellular matrix, namely

collagen VI,[17] resulted in larger adipocytes, lower adipose tissue inflammation and attenuated insulin resistance in male mice fed the HF diet. These data suggest a role for extracellular matrix in the mechanisms underlying adipocyte death, due to restriction of adipocytes' enlargement and shear stress.[17] However, we could not find any differences between the sexes regarding the gene expression of the components of extracellular matrix, including collagen VI and lumican (not shown). This suggests that other mechanism(s) than the extracellular matrix-dependent shear stress contributed to reduced inflammation in females' adipose tissue.

Our data confirm the previously observed (see Introduction) sex differences at the level of glycemic control, documenting an earlier onset of glucose intolerance in male as compared with female mice challenged with HF diet. Although blood glucose clearance during the glucose tolerance test was similar in mice of both sexes at the end of the long-term HF feeding, lower levels of plasma insulin were required in females to maintain the same glucose tolerance as males. We have also examined whether the differences in glycemic control reflected sex-dependent changes in the expression of proinflammatory markers in adipose tissue. Consistent with the previous findings,[20,26,50,51] we observed profound increases in the expression of proinflammatory markers such as MCP-1, TNFα and macrophage marker CD68 in adipose tissue of mice of both sexes during the course of HF diet-induced obesity. In agreement with the sex-dependent differences in macrophage infiltration of gWAT, the expression of MCP-1, TNFα and CD68 was lower in gWAT of females at week 15, however, unexpectedly, no significant differences in the expression of selected genes (MCP-1, TNFα and CD68) were observed between the sexes at week 35. The lack of correlation between macrophage infiltration and expression of the inflammatory cytokines in gWAT at week 35 remains to be explained. However, it is compatible with other results showing that the absence of MCP-1 does not limit the recruitment of macrophages to gWAT,[52] and the lack of a correlation between macrophage content in gWAT and the levels of proinflammatory cytokines in plasma in mice fed HF diet.[19,28] In fact, the previous study[19] in mice fed HF diet for 12 weeks after weaning showed similar plasma levels of TNFα, interleukin-6, interleukin-1β, MCP-1 and granulocyte-macrophage colony-stimulating factor in male and female mice, in spite of a robust sexual dimorphism in macrophage infiltration and in the expression of genes for inflammatory markers in gWAT. Therefore, the above results suggest that macrophage-released proinflammatory cytokines may not have a major role in the differential induction of systemic insulin resistance by HF diet in male and female mice. On the other hand, macrophages in adipose tissue could contribute to sex-dependent tissue remodeling during the course of HF feeding.[28] This would be in agreement with the concept (see above) that increased expandability of adipose tissue, reflected by a higher capacity for adipocyte enlargement and lower macrophage infiltration, could counteract ectopic fat deposition and lipotoxicity in females.

Adiponectin or estrogens should be considered among the factors contributing to the sex-dependent differences in insulin sensitivity, as both hormones possess anti-inflammatory properties and protect from insulin resistance.[34,53,54] In fact, female mice consistently showed much higher levels of adiponectin in plasma compared with males, including the biologically active HMW form,[47] and this feature was independent of the type of diet, expression of inflammatory markers in adipose tissue and duration of HF feeding. These results are in accordance with other animal[36,55,56] as well as human[57,58] studies showing higher adiponectin levels in females and suggesting involvement of adipose tissue expandability in the beneficial metabolic effects of adiponectin.[36]. Adiponectin may preserve insulin sensitivity in females by various mechanisms, including the activation of AMPK,[31] as well as by promoting the switch between proinflammatory (M1) and anti-inflammatory (M2) macrophages in adipose tissue.[59] Thus, relatively low levels of hepatic steatosis in female mice exposed to HF diet could be explained, at least in part, by the AMPK-mediated effect of adiponectin. Indeed, higher phosphorylation of hepatic AMPK was observed in adult female as compared with male mice fed HF diet, suggesting a higher AMPK activity in the females (Jelenik *et al.*, unpublished results). However, the involvement of possible sexual dimorphism in macrophage polarization in response to adiponectin and HF diet remains an open question (see Supplementary Tables 2 and 4).[19]

An important question remains to be answered, whether the increased capacity for adipocyte enlargement in female as compared with male mice is also relevant to human obesity. A carefully conducted study in human subjects has not shown any significant differences between the sexes regarding the curvilinear relationship between body fat mass and fat cell volume in subcutaneous fat, whereas only a trend for adipocytes in women to grow bigger could be observed (see Figures 1a and b of Spalding *et al.*[60]). In this respect, further studies should focus on human subjects with morbid obesity.

In conclusion, in a model of morbid obesity induced in C57BL/6N mice by a long-term (35 weeks) HF feeding, females eventually accumulated more fat and showed larger adipocytes compared with males. In spite of larger adipocytes in gWAT as well as in scWAT, the frequency of dead adipocytes, marked by macrophage infiltration of adipose tissue, was reduced in female compared with male mice. Lower plasma levels of insulin together with a markedly increased adiponectin and less pronounced hepatosteatosis imply better insulin sensitivity in female mice during the course of HF feeding, independent of the expression of proinflammatory cytokines in adipose tissue. Our results suggest an increased intrinsic capacity for adipocyte enlargement in females in the face of a relatively mild tissue remodeling and macrophage infiltration. Thus, adipose tissue expandability linked to secretion of adiponectin can substantially contribute to a greater resistance of female mice to deterioration of glycemic control during the development of dietary obesity.

Conflict of interest

The authors declare no conflict of interest.

Acknowledgements

The research has received funding from the European Union's Seventh Framework Program FP7 2007-2013 under grant agreement no. 244995 (BIOCLAIMS Project), the Czech Science Foundation (303/08/0664), COST Action Mitofood (FA0602), the MSMT of the Czech Republic (OC08008), and EPAX a.s. (Aalesund, Norway). We thank Pavel Flachs for the critical reading of the manuscript.

References

1 Krotkiewski M, Bjorntorp P, Sjostrom L, Smith U. Impact of obesity on metabolism in men and women. Importance of regional adipose tissue distribution. *J Clin Invest* 1983; **72**: 1150–1162.
2 Frias JP, Macaraeg GB, Ofrecio J, Yu JG, Olefsky JM, Kruszynska YT. Decreased susceptibility to fatty acid-induced peripheral tissue insulin resistance in women. *Diabetes* 2001; **50**: 1344–1350.
3 Priego T, Sanchez J, Pico C, Palou A. Sex-differential expression of metabolism-related genes in response to a high-fat diet. *Obesity (Silver Spring)* 2008; **16**: 819–826.
4 Guerre-Millo M, Leturque A, Girard J, Lavau M. Increased insulin sensitivity and responsiveness of glucose metabolism in adipocytes from female versus male rats. *J Clin Invest* 1985; **76**: 109–116.
5 Hevener A, Reichart D, Janez A, Olefsky J. Female rats do not exhibit free fatty acid-induced insulin resistance. *Diabetes* 2002; **51**: 1907–1912.
6 Trevaskis JL, Meyer EA, Galgani JE, Butler AA. Counterintuitive effects of double-heterozygous null melanocortin-4 receptor and leptin genes on diet-induced obesity and insulin resistance in C57BL/6J mice. *Endocrinology* 2008; **149**: 174–184.
7 Macotela Y, Boucher J, Tran TT, Kahn CR. Sex and depot differences in adipocyte insulin sensitivity and glucose metabolism. *Diabetes* 2009; **58**: 803–812.
8 Wajchenberg BL. Subcutaneous and visceral adipose tissue: their relation to the metabolic syndrome. *Endocr Rev* 2000; **21**: 697–738.
9 Cnop M, Landchild MJ, Vidal J, Havel PJ, Knowles NG, Carr DR *et al*. The concurrent accumulation of intra-abdominal and subcutaneous fat explains the association between insulin resistance and plasma leptin concentrations: distinct metabolic effects of two fat compartments. *Diabetes* 2002; **51**: 1005–1015.
10 Enzi G, Gasparo M, Biondetti PR, Fiore D, Semisa M, Zurlo F. Subcutaneous and visceral fat distribution according to sex, age, and overweight, evaluated by computed tomography. *Am J Clin Nutr* 1986; **44**: 739–746.
11 Clegg DJ, Brown LM, Woods SC, Benoit SC. Gonadal hormones determine sensitivity to central leptin and insulin. *Diabetes* 2006; **55**: 978–987.
12 Arner E, Westermark PO, Spalding KL, Britton T, Ryden M, Frisen J *et al*. Adipocyte turnover: relevance to human adipose tissue morphology. *Diabetes* 2010; **59**: 105–109.
13 Okuno A, Tamemoto H, Tobe K, Ueki K, Mori Y, Iwamoto K *et al*. Troglitazone increases the number of small adipocytes without the change of white adipose tissue mass in obese zucker rats. *J Clin Invest* 1998; **101**: 1354–1361.
14 Kubota N, Terauchi Y, Miki H, Tamemoto H, Yamauchi T, Komeda K *et al*. PPAR gamma mediates high-fat diet-induced adipocyte hypertrophy and insulin resistance. *Mol Cell* 1999; **4**: 597–609.
15 Danforth Jr E. Failure of adipocyte differentiation causes type II diabetes mellitus? *Nat Genet* 2000; **26**: 13.
16 Virtue S, Vidal-Puig A. It's not how fat you are, it's what you do with it that counts. *PLoS Biol* 2008; **6**: e237.
17 Khan T, Muise ES, Iyengar P, Wang ZV, Chandalia M, Abate N *et al*. Metabolic dysregulation and adipose tissue fibrosis: role of collagen VI. *Mol Cell Biol* 2009; **29**: 1575–1591.
18 Halberg N, Khan T, Trujillo ME, Wernstedt-Asterholm I, Attie AD, Sherwani S *et al*. Hypoxia-inducible factor 1alpha induces fibrosis and insulin resistance in white adipose tissue. *Mol Cell Biol* 2009; **29**: 4467–4483.
19 Grove KL, Fried SK, Greenberg AS, Xiao XQ, Clegg DJ. A microarray analysis of sexual dimorphism of adipose tissues in high-fat-diet-induced obese mice. *Int J Obes (Lond)* 2010; **34**: 989–1000.
20 Kanda H, Tateya S, Tamori Y, Kotani K, Hiasa K, Kitazawa R *et al*. MCP-1 contributes to macrophage infiltration into adipose tissue, insulin resistance, and hepatic steatosis in obesity. *J Clin Invest* 2006; **116**: 1494–1505.
21 Kamei N, Tobe K, Suzuki R, Ohsugi M, Watanabe T, Kubota N *et al*. Overexpression of monocyte chemoattractant protein-1 in adipose tissues causes macrophage recruitment and insulin resistance. *J Biol Chem* 2006; **281**: 26602–26614.
22 Anderson EK, Gutierrez DA, Hasty AH. Adipose tissue recruitment of leukocytes. *Curr Opin Lipidol* 2010; **21**: 172–177.
23 Lumeng CN, Bodzin JL, Saltiel AR. Obesity induces a phenotypic switch in adipose tissue macrophage polarization. *J Clin Invest* 2007; **117**: 175–184.
24 Lumeng CN, Delproposto JB, Westcott DJ, Saltiel AR. Phenotypic switching of adipose tissue macrophages with obesity is generated by spatiotemporal differences in macrophage subtypes. *Diabetes* 2008; **57**: 3239–3246.
25 Hotamisligil GS, Murray DL, Choy LN, Spiegelman BM. Tumor necrosis factor alpha inhibits signaling from the insulin receptor. *Proc Natl Acad Sci USA* 1994; **91**: 4854–4858.
26 Xu H, Barnes GT, Yang Q, Tan G, Yang D, Chou CJ *et al*. Chronic inflammation in fat plays a crucial role in the development of obesity-related insulin resistance. *J Clin Invest* 2003; **112**: 1821–1830.
27 de Luca C, Olefsky JM. Inflammation and insulin resistance. *FEBS Lett* 2008; **582**: 97–105.
28 Strissel KJ, Stancheva Z, Miyoshi H, Perfield JW, DeFuria J, Jick Z *et al*. Adipocyte death, adipose tissue remodeling, and obesity complications. *Diabetes* 2007; **56**: 2910–2918.
29 Cinti S, Mitchell G, Barbatelli G, Murano I, Ceresi E, Faloia E *et al*. Adipocyte death defines macrophage localization and function in adipose tissue of obese mice and humans. *J Lipid Res* 2005; **46**: 2347–2355.
30 Monteiro R, de Castro PMST, Calhau C, Azevedo I. Adipocyte size and liability to cell death. *Obesity Surgery* 2006; **16**: 804–806.
31 Yamauchi T, Kamon J, Minokoshi Y, Ito Y, Waki H, Uchida S *et al*. Adiponectin stimulates glucose utilization and fatty-acid oxidation by activating AMP-activated protein kinase. *Nat Med* 2002; **8**: 1288–1295.
32 Carling D. The AMP-activated protein kinase cascade–a unifying system for energy control. *Trends Biochem Sci* 2004; **29**: 18–24.
33 Hotta K, Funahashi T, Arita Y, Takahashi M, Matsuda M, Okamoto Y *et al*. Plasma concentrations of a novel, adipose-specific protein, adiponectin, in type 2 diabetic patients. *Arterioscler Thromb Vasc Biol* 2000; **20**: 1595–1599.
34 Berg AH, Combs TP, Du X, Brownlee M, Scherer PE. The adipocyte-secreted protein Acrp30 enhances hepatic insulin action. *Nat Med* 2001; **7**: 947–953.
35 Yamauchi T, Kamon J, Waki H, Terauchi Y, Kubota N, Hara K *et al*. The fat-derived hormone adiponectin reverses insulin resistance associated with both lipoatrophy and obesity. *Nat Med* 2001; **7**: 941–946.

36 Kim JY, van de WE, Laplante M, Azzara A, Trujillo ME, Hofmann SM *et al*. Obesity-associated improvements in metabolic profile through expansion of adipose tissue. *J Clin Invest* 2007; **117**: 2621–2637.
37 Okamoto Y, Kihara S, Ouchi N, Nishida M, Arita Y, Kumada M *et al*. Adiponectin reduces atherosclerosis in apolipoprotein E-deficient mice. *Circulation* 2002; **106**: 2767–2770.
38 Cancello R, Tordjman J, Poitou C, Guilhem G, Bouillot JL, Hugol D *et al*. Increased infiltration of macrophages in omental adipose tissue is associated with marked hepatic lesions in morbid human obesity. *Diabetes* 2006; **55**: 1554–1561.
39 Tordjman J, Guerre-Millo M, Clement K. Adipose tissue inflammation and liver pathology in human obesity. *Diabetes Metab* 2008; **34**: 658–663.
40 Hou XG, Moser S, Sarr MG, Thompson GB, Que FG, Jensen MD. Visceral and subcutaneous adipose tissue diacylglycerol acyltransferase activity in humans. *Obesity (Silver Spring)* 2009; **17**: 1129–1134.
41 Kuda O, Jelenik T, Jilkova Z, Flachs P, Rossmeisl M, Hensler M *et al*. n-3 Fatty acids and rosiglitazone improve insulin sensitivity through additive stimulatory effects on muscle glycogen synthesis in mice fed a high-fat diet. *Diabetologia* 2009; **52**: 941–951.
42 Cinti S. *The Adipose Organ*. Editrice Kurtis: Milano, Italy, 1999.
43 Polak J, Kovacova Z, Jacek M, Klimcakova E, Kovacikova M, Vitkova M *et al*. An increase in plasma adiponectin multimeric complexes follows hypocaloric diet-induced weight loss in obese and overweight pre-menopausal women. *Clin Sci (Lond)* 2007; **112**: 557–565.
44 Rossmeisl M, Jelenik T, Jilkova Z, Slamova K, Kus V, Hensler M *et al*. Prevention and reversal of obesity and glucose intolerance in mice by DHA-derivatives. *Obesity (Silver Spring)* 2009; **17**: 1023–1031.
45 Ruzickova J, Rossmeisl M, Prazak T, Flachs P, Sponarova J, Vecka M *et al*. Omega-3 PUFA of marine origin limit diet-induced obesity in mice by reducing cellularity of adipose tissue. *Lipids* 2004; **39**: 1177–1185.
46 Viollet B, Andreelli F, Jorgensen SB, Perrin C, Geloen A, Flamez D *et al*. The AMP-activated protein kinase alpha2 catalytic subunit controls whole-body insulin sensitivity. *J Clin Invest* 2003; **111**: 91–98.
47 Waki H, Yamauchi T, Kamon J, Ito Y, Uchida S, Kita S *et al*. Impaired multimerization of human adiponectin mutants associated with diabetes - Molecular structure and multimer formation of adiponectin. *J Biol Chem* 2003; **278**: 40352–40363.
48 Weisberg SP, Hunter D, Huber R, Lemieux J, Slaymaker S, Vaddi K *et al*. CCR2 modulates inflammatory and metabolic effects of high-fat feeding. *J Clin Invest* 2006; **116**: 115–124.
49 Law IK, Xu A, Lam KS, Berger T, Mak TW, Vanhoutte PM *et al*. Lipocalin-2 deficiency attenuates insulin resistance associated with aging and obesity. *Diabetes* 2010; **59**: 872–882.
50 Hotamisligil GS, Shargill NS, Spiegelman BM. Adipose expression of tumor necrosis factor-alpha: direct role in obesity-linked insulin resistance. *Science* 1993; **259**: 87–91.
51 Takahashi K, Mizuarai S, Araki H, Mashiko S, Ishihara A, Kanatani A *et al*. Adiposity elevates plasma MCP-1 levels leading to the increased CD11b-positive monocytes in mice. *J Biol Chem* 2003; **278**: 46654–46660.
52 Inouye KE, Shi H, Howard JK, Daly CH, Lord GM, Rollins BJ *et al*. Absence of CC chemokine ligand 2 does not limit obesity-associated infiltration of macrophages into adipose tissue. *Diabetes* 2007; **56**: 2242–2250.
53 Ghisletti S, Meda C, Maggi A, Vegeto E. 17beta-estradiol inhibits inflammatory gene expression by controlling NF-kappaB intracellular localization. *Mol Cell Biol* 2005; **25**: 2957–2968.
54 Vegeto E, Belcredito S, Etteri S, Ghisletti S, Brusadelli A, Meda C *et al*. Estrogen receptor-alpha mediates the brain antiinflammatory activity of estradiol. *Proc Natl Acad Sci USA* 2003; **100**: 9614–9619.
55 Combs TP, Berg AH, Rajala MW, Klebanov S, Iyengar P, Jimenez-Chillaron JC *et al*. Sexual differentiation, pregnancy, calorie restriction, and aging affect the adipocyte-specific secretory protein adiponectin. *Diabetes* 2003; **52**: 268–276.
56 Combs TP, Pajvani UB, Berg AH, Lin Y, Jelicks LA, Laplante M *et al*. A transgenic mouse with a deletion in the collagenous domain of adiponectin displays elevated circulating adiponectin and improved insulin sensitivity. *Endocrinology* 2004; **145**: 367–383.
57 Spranger J, Kroke A, Mohlig M, Bergmann MM, Ristow M, Boeing H *et al*. Adiponectin and protection against type 2 diabetes mellitus. *Lancet* 2003; **361**: 226–228.
58 Snijder MB, Heine RJ, Seidell JC, Bouter LM, Stehouwer CD, Nijpels G *et al*. Associations of adiponectin levels with incident impaired glucose metabolism and type 2 diabetes in older men and women: the hoorn study. *Diabetes Care* 2006; **29**: 2498–2503.
59 Ohashi K, Parker JL, Ouchi N, Higuchi A, Vita JA, Gokce N *et al*. Adiponectin promotes macrophage polarization toward an anti-inflammatory phenotype. *J Biol Chem* 2010; **285**: 6153–6160.
60 Spalding KL, Arner E, Westermark PO, Bernard S, Buchholz BA, Bergmann O *et al*. Dynamics of fat cell turnover in humans. *Nature* 2008; **453**: 783–787.

Supplementary Information accompanies the paper on International Journal of Obesity website (http://www.nature.com/ijo)

Online-Supplement

Supplementary Figure 1 Representative Western blot with detection of multimeric forms of murine adiponectin in plasma at week 35. HMW, high molecular weight adiponectin; MMW, medium molecular weight adiponectin; LMW, low molecular weight adiponectin; ST, standard diet; HF, high-fat diet; F, female; M, male (see also Table 2 of the main text).

Supplementary Figure 2 Intraperitoneal glucose tolerance test. Plasma glucose levels following intraperitoneal glucose injection (time 0) to fasted mice at week 33 (see also Fig. 1 of the main text).

Supplementary Figure 3 Adipocyte diameter distribution in gWAT of mice of both sexes fed HF diet at 15 week and week 35. (**a**) male mice; (**b**), female mice (see also Fig. 4e,i of the main text).

Supplementary Figure 4 Adipocyte diameter distribution in scWAT of mice of both sexes fed HF at 15 week and week 35. (**a**) male mice; (**b**), female mice (see also Fig. 4g,k of the main text).

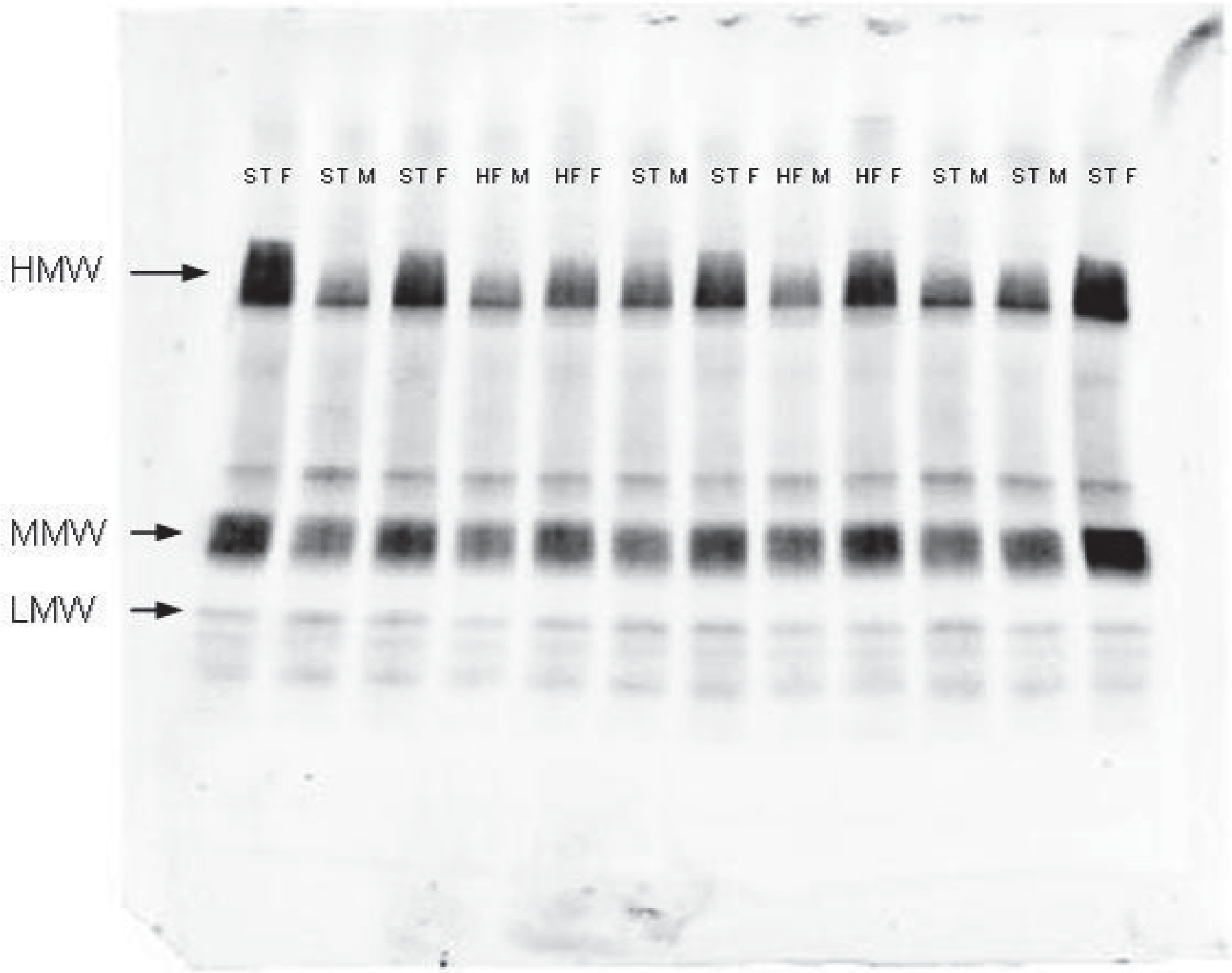
ST F
ST M
ST F
HF M
HF F
ST M
ST F
HF M
HF F
ST M
ST M
ST F
HMW
MMW
LMW

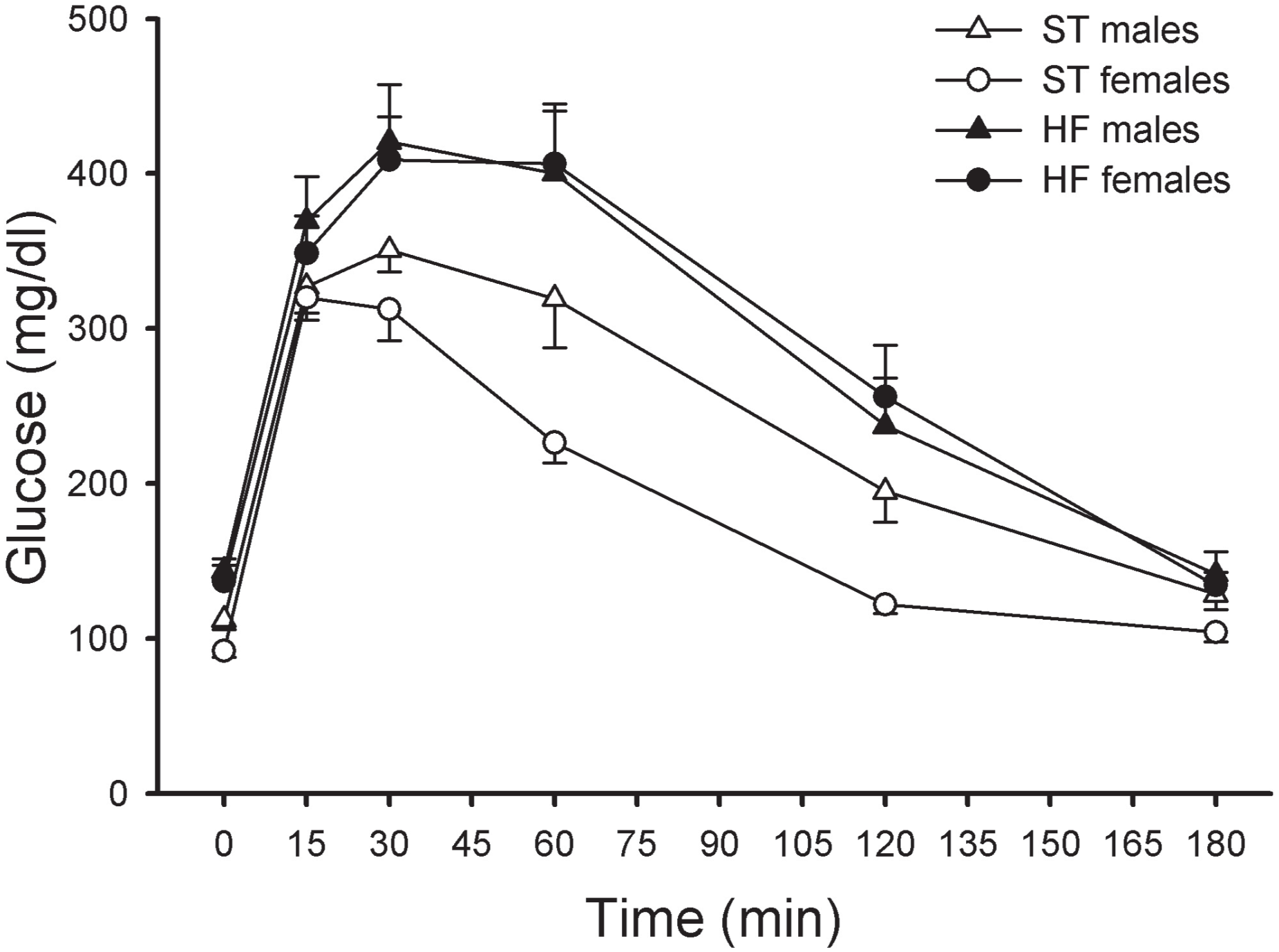
ST males
ST females
HF males
HF females
Glucose (mg/dl)
500
400
300
200
100
0
0
15
30
45
60
75
90
105
120
135
150
165
180
Time (min)

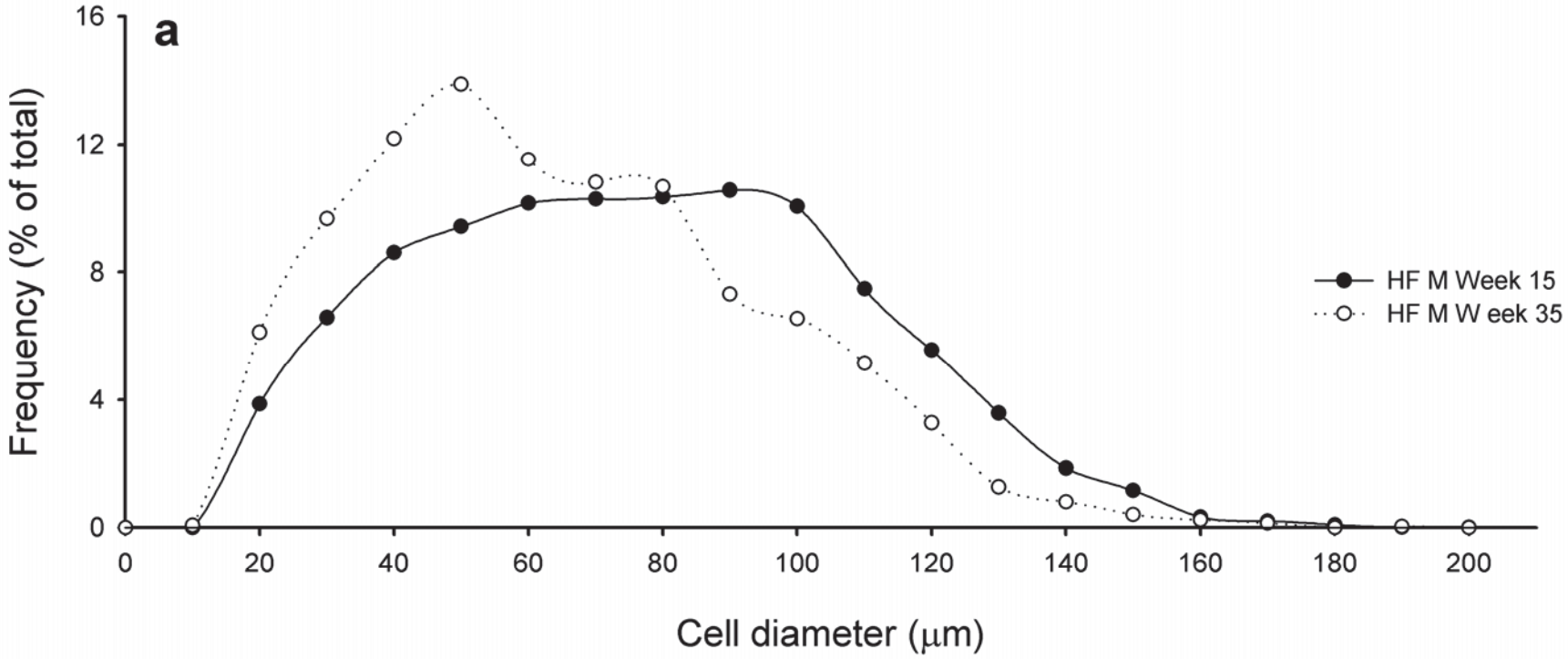
a
Frequency (% of total)
16
12
8
4
0
0
20
40
60
80
100
120
140
160
180
200
Cell diameter (μm)
HF M Week 15
HF M W eek 35

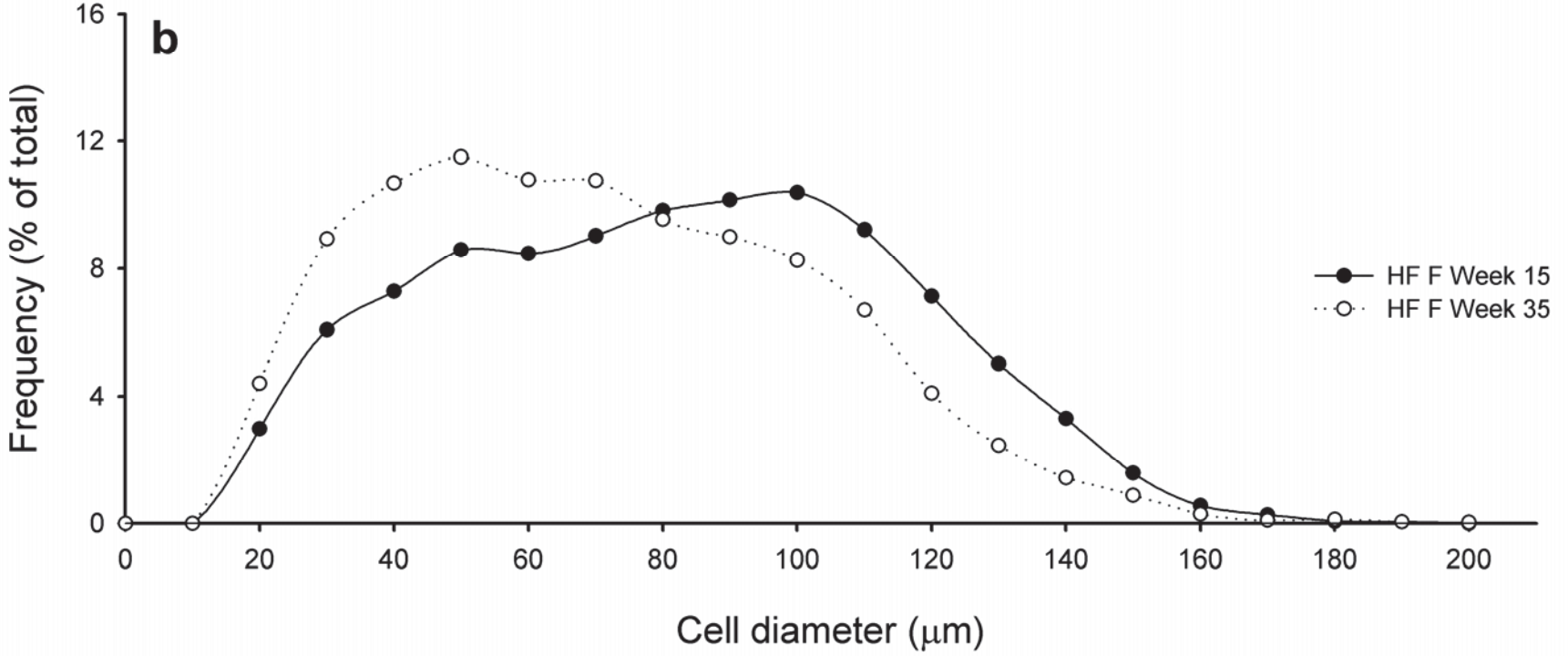
b
Frequency (% of total)
16
12
8
4
0
0
20
40
60
80
100
120
140
160
180
200
Cell diameter (μm)
HF F Week 15
HF F Week 35

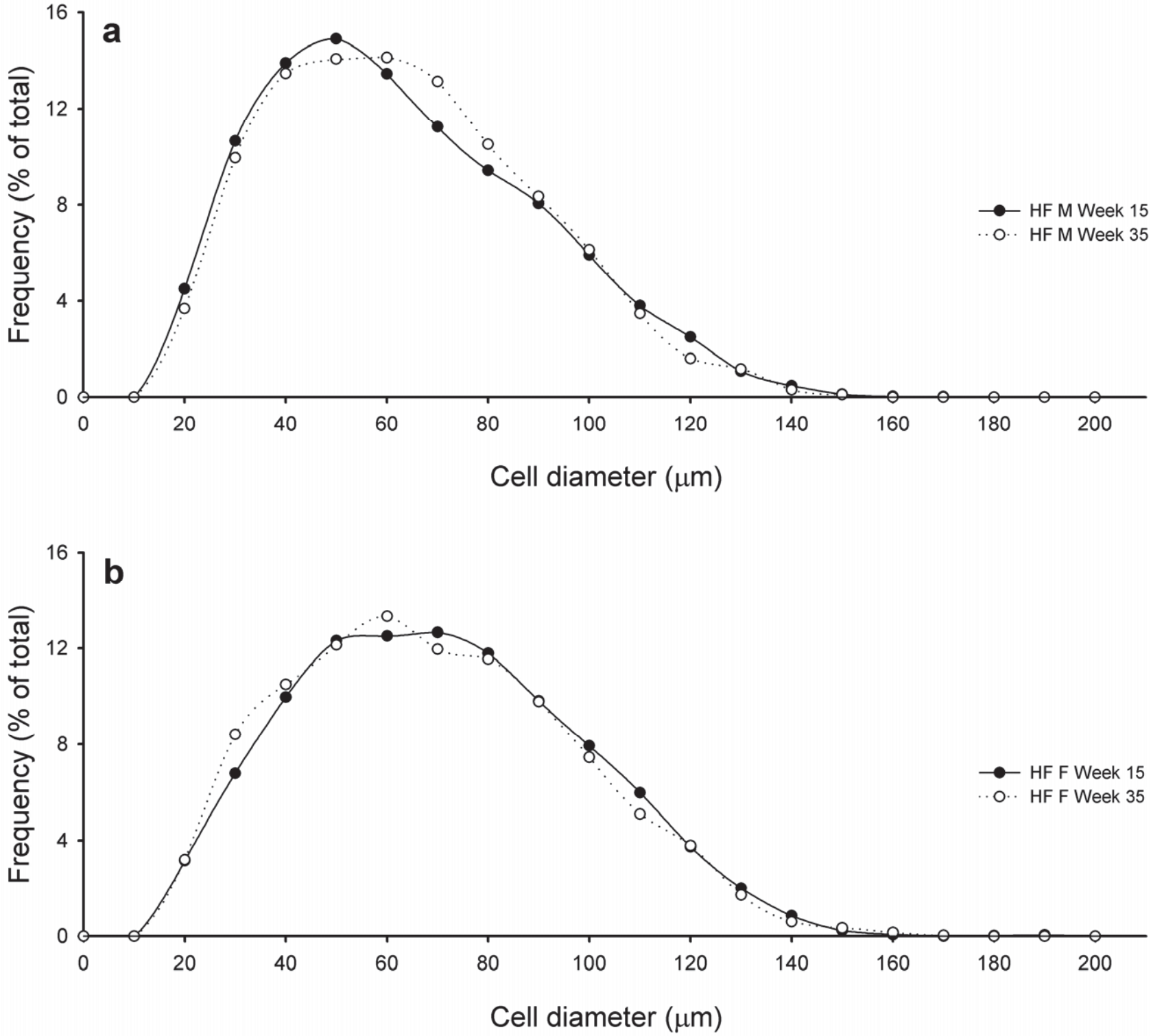
a
Frequency (% of total)
16
12
8
4
0
0
20
40
60
80
100
120
140
160
180
200
Cell diameter (μm)
HF M Week 15
HF M Week 35
b
Frequency (% of total)
16
12
8
4
0
0
20
40
60
80
100
120
140
160
180
200
Cell diameter (μm)
HF F Week 15
HF F Week 35

International Journal of Obesity (2014) **38,** 1027–1034

www.nature.com/ijo

ORIGINAL ARTICLE

Enhancement of brown fat thermogenesis using chenodeoxycholic acid in mice

JS Teodoro[1,2,5], P Zouhar[3,5], P Flachs[3], K Bardova[3], P Janovska[3], AP Gomes[1,2], FV Duarte[1,2], AT Varela[1,2], AP Rolo[1,4], CM Palmeira[1,2] and J Kopecký[3]

OBJECTIVE: Besides their role in lipid absorption, bile acids (BAs) can act as signalling molecules. Cholic acid was shown to counteract obesity and associated metabolic disorders in high-fat-diet (cHF)-fed mice while enhancing energy expenditure through induction of mitochondrial uncoupling protein 1 (UCP1) and activation of non-shivering thermogenesis in brown adipose tissue (BAT). In this study, the effects of another natural BA, chenodeoxycholic acid (CDCA), on dietary obesity, UCP1 in both interscapular BAT and in white adipose tissue (brite cells in WAT), were characterized in dietary-obese mice.

RESEARCH DESIGN: To induce obesity and associated metabolic disorders, male 2-month-old C57BL/6J mice were fed cHF (35% lipid wt wt^{-1}, mainly corn oil) for 4 months. Mice were then fed either (i) for 8 weeks with cHF or with cHF with two different doses (0.5%, 1%; wt wt^{-1}) of CDCA (8-week reversion); or (ii) for 3 weeks with cHF or with cHF with 1% CDCA, or pair-fed (PF) to match calorie intake of the CDCA mice fed *ad libitum*; mice on standard chow diet were also used (3-week reversion).

RESULTS: In the 8-week reversion, the CDCA intervention resulted in a dose-dependent reduction of obesity, dyslipidaemia and glucose intolerance, which could be largely explained by a transient decrease in food intake. The 3-week reversion revealed mild CDCA-dependent and food intake-independent induction of UCP1-mediated thermogenesis in interscapular BAT, negligible increase of UCP1 in subcutaneous WAT and a shift from carbohydrate to lipid oxidation.

CONCLUSIONS: CDCA could reverse obesity in cHF-fed mice, mainly in response to the reduction in food intake, an effect probably occuring but neglected in previous studies using cholic acid. Nevertheless, CDCA-dependent and food intake-independent induction of UCP1 in BAT (but not in WAT) could contribute to the reduction in adiposity and to the stabilization of the lean phenotype.

International Journal of Obesity (2014) **38,** 1027–1034; doi:10.1038/ijo.2013.230

Keywords: white adipose tissue; uncoupling protein 1; energy expenditure; bile acids

INTRODUCTION

Bile acids (BAs) are essential for lipid absorption in the intestine. More recently, it was discovered that BAs administration could improve several parameters of lipid metabolism.[1] Thus, BAs could beneficially influence the health status of both patients and experimental models (reviewed in Teodoro *et al.*[2]). This finding made BAs a promising new tool for the treatment of metabolic syndrome—that is, the cluster of diseases associated with obesity.

BAs could act as signalling molecules through activation of the farnesoid X receptor (FXR).[3] FXR activation influences glucose and lipid metabolism; namely, it decreases plasma triglyceride (TG) levels by inhibiting lipogenesis and by increasing TG clearance.[3,4] Accordingly, FXR-null mice are obese and hypertriglyceridaemic.[5] FXR is also important for prevention of insulin resistance[6] and hypoglycaemia during fasting,[7] production of hepatic glycogen[8] and differentiation of adipocytes.[9] Moreover, the positive metabolic effect of BAs on glucose control and weight reduction could be mediated by G protein-coupled receptor 5 (TGR5).[10] However, some BAs are not competent activators of TGR5. The most potent natural activator of FXR, chenodeoxycholic acid (CDCA), used as a drug for the treatment of gallstones,[11] has been reported to be both a potent and a not very effective activator of TGR5.[10,12–14] Therefore, the mechanism by which BAs accomplish their beneficial metabolic functions is not yet fully understood.

A new insight into the mechanism of action of BAs was provided by the finding of Watanabe *et al.*[15] that BAs, namely, cholic acid, promote non-shivering thermogenesis in the interscapular brown adipose tissue (BAT) in mice and in skeletal muscle in humans. In BAT, energy expenditure (EE) is mediated by mitochondrial uncoupling protein 1 (UCP1)[16], and induction of the UCP1-based thermogenesis has been proposed as a possible therapeutic strategy against obesity and diabetes.[17,18] The BAs' binding to TGR5 in BAT leads to elevation of cAMP level and consequent activation of thyroid hormone-converting enzyme type 2 iodothyronine deiodinase.[15] BAs therefore facilitate thyroid hormone stimulatory influence on BAT thermogenesis. In fact, treatment with cholic acid was able to reverse diet-induced weight gain.[15] Also, other studies confirmed the ability of BAs to stimulate UCP1-mediated non-shivering thermogenesis in BAT.[10,19,20]

The interest in UCP1-mediated thermogenesis was boosted recently by the discovery of functional BAT in adult humans,[21] as well as by the finding of *Ucp1*-expressing adipocytes,[22–24] which

[1]Center for Neuroscience and Cell Biology, Faculty of Science and Technology, University of Coimbra, Coimbra, Portugal; [2]Department of Life Sciences, Faculty of Science and Technology, University of Coimbra, Coimbra, Portugal; [3]Department of Adipose Tissue Biology, Institute of Physiology Academy of Sciences of the Czech Republic v.v.i., Prague, Czech Republic and [4]Department of Biology, University of Aveiro, Aveiro, Portugal. Correspondence: Dr J Kopecký, Department of Adipose Tissue Biology, Institute of Physiology Academy of Sciences of the Czech Republic v.v.i., Videnska 1083, Prague 14220, Czech Republic.
E-mail: kopecky@biomed.cas.cz
[5]These authors contributed equally to this work.
Received 7 August 2013; revised 11 November 2013; accepted 24 November 2013; accepted article preview online 6 December 2013; advance online publication, 14 January 2014

could be induced in several white adipose tissue (WAT) depots in mice in response to various stimuli and represent a potential target for induction of fat burning (these cells are annotated 'brite' adipocytes in this article, as in Petrovic *et al.*;[25] reviewed in Wu *et al.*[17]). However, whether the brite cells reflect transdifferentiation of white adipocytes[26] or the existence of distinct brown and brite cell lineages (reviewed in Wu *et al.*[17]) is a subject of debate. Similarly, the origin of Ucp1-expressing adipocytes in humans (reviewed in Jespersen *et al.*[27]) and, importantly, the magnitude of energy dissipation in brite cells with respect to that in classical BAT, as well as the contribution of energy dissipation occurring in brite cells to total energy balance (compare Wu *et al.*,[17] and Nedergaard and Cannon[28]), remain all controversial.

We focused here on whether CDCA (similarly to cholic acid; see above) could influence energy balance and reverse the dietary obesity. Our results demonstrated a strong anti-obesity effect of CDCA, which could be explained in large by a transient decrease in food intake. The results suggest that induction of UCP1-mediated thermogenesis in adipocytes in BAT rather than in brite cells could contribute to stabilization of the lean phenotype under these conditions.

MATERIALS AND METHODS

Animals care and diet

C57BL/6J mice were obtained from the Jackson Laboratory (Bar Harbor, ME, USA) and bred at the Institute of Physiology for several generations. Single-caged male mice were maintained at 20 °C on a 12:12-hr light–dark cycle.

Two different experiments were conducted. In the first experiment (8-week reversion), 2-month-old mice were subjected to the high-fat-diet feeding (cHF, lipid content ~35.2% wt wt^{-1}, mainly corn oil, energy density 22.8 kJ g^{-1}; this diet was proven to be obesogenic in C57BL/6J mice, and it contained 15%, 59% and 26% energy as protein, fat and carbohydrate, respectively)[29] for another 4 months to induce obesity and associated metabolic disorders. After that, the animals were randomly divided into three experimental groups ($n = 10$–12 per group) and fed for 8 weeks either the cHF diet, the cHF diet supplemented with 0.5% CDCA (wt wt^{-1}) or the cHF diet supplemented with 1% CDCA (wt wt^{-1}, 95% pure; Sigma-Aldrich, St Louis, MO, USA). All the diets were fed *ad libitum*. Body weight (BW) and food intake were measured every week. During week 6 of the intervention, some of the animals (five mice randomly selected in each group) were subjected to an oral glucose tolerance test (see below). At the end of week 8, all the mice were killed in the morning in fed state by means of cervical dislocation. Plasma was collected (see below), and following tissues were also dissected: liver, gastrocnemius muscle, interscapular BAT, epididymal WAT and subcutaneous WAT (scWAT) from the dorsolumbar region. Moreover, faeces were also collected for further analysis.

In the second experiment (3-week reversion), adult mice already fed the cHF diet for 4 months (see above) were randomly assigned to one of the following: 1) a cHF diet, 2) a cHF diet containing 1% CDCA or 3) a cHF diet with food intake limited to that of animals on 1% CDCA (pair-fed group (PF); $n = 8$ per group). Animals fed standard laboratory chow (STD diet, lipid content ~3.4% wt wt^{-1}, energy density 13.0 kJ g^{-1}; contained 33, 9 and 58% energy as protein, fat and carbohydrate, respectively; extruded Ssniff R/M-H diet, Ssniff Spezialdieten GmbH, Soest, Germany) since weaning at 4 weeks of age were also included in the experiment ($n = 7$). The experiment continued for next 3 weeks. BW and food intake were measured four times each week (see Figures 1c and d). Between day 15 and day 17, indirect calorimetry was performed. At the end of the experiment, mice were killed as described above.

All experiments were performed in accordance with the guidelines for the use and care of laboratory animals of the Institute of Physiology, the directive of the European Communities Council (2010/63/EU) and the Principles of Laboratory Animal Care (NIH publication no. 85–23, revised 1985).

Evaluation of plasma parameters, glucose homeostasis and TG content in tissues and faeces

Blood was collected and analysed as described previously;[30] glycaemia, plasma levels of non-esterified fatty acids, TG, cholesterol, insulin and multimeric forms of adiponectin were evaluated. The remaining plasma was frozen at −80 °C for measurement of the activity of liver enzymes, as previously described.[31] Oral glucose tolerance test was conducted as described in Medrikova *et al.*[30] TG content in tissues and faeces was assessed.[32]

Light microscopy and immunohistology analysis

Adipose tissue samples were fixed in 10% neutral buffered formalin (Sigma-Aldrich) and embedded in paraffin. Sections (5 μm) were stained with haematoxylin–eosin for morphometry, or processed to detect UCP1-positive cells, using a rabbit anti-hamster UCP1 antibody.[33] Sections were deparaffinized and rehydrated, and 10 mM sodium citrate (pH 6.0) was used for antigen retrieval. Immunohistological detection of UCP1 was performed as follows: a) incubation with 3% hydrogen peroxide in methanol at room temperature for 10 min; b) incubation with the diluted goat serum 1:50 at room temperature for 30 min; c) incubation with the primary antibody diluted 1:4000 at 4 °C overnight; d) incubation with the secondary antibody anti-rabbit IgG biotinylated (Vector laboratories, Burlingame, CA, USA) 1:200 at room temperature for 1 h; e) incubation with ABC (Vectastain ABC kit, Vector laboratories) at room temperature for 1 h; f) visualization using diaminobenzidine. For each treatment, a negative control without the primary antibody was used. BAT was used as a positive control for UCP1 immunoreactivity. Digital images were captured using an Olympus AX70 light microscope and a DP 70 camera (Olympus, Tokyo, Japan). Morphometric analysis was performed using Imaging Software NIS-Elements AR3.0 (Laboratory Imaging, Prague, Czech Republic). The morphometry data are based on measurements of ~800 cells taken randomly from two to three different sections per animal (see Medrikova *et al.*[30]).

RNA isolation and real-time PCR

Total RNA was isolated from flash-frozen tissue (kit from Qiagen GmbH, Hilden, Germany). RNA yields were quantified using a Nanodrop instrument (Thermo Scientific, Waltham, MA, USA). Complementary DNA was produced using 1 μg of RNA with a Bio-Rad iScript cDNA synthesis kit (Bio-Rad, Hercules, CA, USA). Gene expression was evaluated using real-time PCR, LightCycler (Roche Diagnostics, Mannheim, Germany) and MiniOpticon (Bio-Rad) equipments. Primers used and their sequences are described in Supplementary Table S1.

Quantification of UCP1 using Western blots

Tissue membranous fraction was prepared using 70 mg interscapular BAT or 100 mg scWAT samples, by homogenization in a buffer containing 250 mM sucrose, 50 mM Tris, 5 mM Na-EDTA, 174 μg ml^{-1} phenylmethanesulphonylfluoride, 1 μg ml^{-1} aprotinin, leupeptin and pepstatin, followed by centrifugation at 100 000 *g*, for 45 min, at 4 °C. Membranous sample aliquots (2–5 μg protein) were then analysed using western blots and 10% polyacrylamide gels.[33] Immunodetection of UCP1 was performed similarly to the detection of adiponectin multimeric forms in plasma,[30] except that anti-UCP1 antibody (1:500)[33] and a secondary infrared dye-conjugated antibody (1:5000) were used. Mitochondria isolated from interscapular BAT of adult C57BL/6J mice reared at 4 °C were used to quantify the relative UCP1 content in each sample (the detection limit for UCP1 was about 0.5 μg of BAT mitochondrial protein and relative UCP1 content in whole interscapular BAT was also calculated. Protein was measured using bicinchoninic acid.[34]

Indirect calorimetry

To evaluate EE and fuel partitioning, indirect calorimetry was performed using INCA system from Somedic (Horby, Sweden).[35,36] Briefly, the measurements were performed in individually caged mice (Eurostandard type II mouse plastic cages; ~6000 ml; Techniplast, Milan, Italy), with the cages placed in a sealed measuring chamber equipped with thermostatically controlled heat exchangers at 22 °C. Oxygen consumption (VO_2) and carbon dioxide production (VCO_2) were recorded every 2 min under a constant airflow rate (1000 ml min^{-1}) for 24 h, starting at 0800 hours. EE was calculated using the following equation: $EE\ (cal) = 3.9 \times VO_2\ (ml) + 1.1 \times VCO_2\ (ml)$.[37,38] The level of substrate partitioning was estimated by calculating respiratory quotient (RQ; that is, VCO_2/VO_2 ratio). To compare subtle differences between groups, the percent relative cumulative frequency (PRCF) curves were constructed on the basis of RQ values pooled from all the animals within a given dietary group ($n = 7$–8) during the whole measurement

period, as described before.[35] Provided that the PRCF curves represent the normally distributed data, the values of 50th percentile of PRCF (EC_{50}) based on each individual animal correspond to RQ values.

Statistical analysis

All values are reported as means ± s.e.m. Statistical significance was analysed as indicated by one-way ANOVA with a Holm–Sidac correction in SigmaPlot 10 software (Systat Software, Point Richmond, CA, USA). The PRCF curves were analysed using nonlinear regression using SigmaPlot. Differences in EE were evaluated by ANCOVA using NCSS software. Differences were considered significant when $P<0.05$.

RESULTS

Reversal of dietary obesity and associated disorders in response to CDCA

First, the effects of CDCA admixed to the cHF diet (0.5% and 1% CDCA) were examined in the 8-week reversion of dietary obesity. Immediately following the switch to the CDCA-containing diets, food intake rapidly decreased reflecting the dose of CDCA, and it returned to the level observed in the control cHF-fed mice within 2–3 weeks of the intervention (Figure 1a). This transient drop due to habituation of mice to the new diets was not accompanied by any changes in plasma levels of liver transaminases (Table 1), arguing against hepatotoxic effects of CDCA. The transient decrease in food intake coincided with a CDCA dose-dependent decrease in BW (Figure 1b), with a maximum reduction reached by the end of week 2 of the intervention. Surprisingly, in spite of the normalization of food intake in the CDCA-intervention groups following week 2, the depression of BW lasted stable till the end of the experiment at week 8 (Figure 1b).

At week 8, plasma lipid levels (namely, TG and cholesterol) were decreased by the CDCA interventions, with a dose-dependent effect on TG levels, and maximum effect on cholesterol levels observed already at the lower CDCA dose (Table 1). Dose-dependent lowering of glycaemia, insulinaemia and glucose intolerance (manifested by changes of area under curve in glucose tolerance test) in response to CDCA documented improvement of glucose homeostasis by the interventions, which was in accordance with the increase in the ratio of high molecular weight adiponectin/total adiponectin plasma levels (Table 1). Lipid (TG and cholesterol) content in faeces was slightly decreased by CDCA treatment, independently of the dose.

Changes in BW could be explained by the changes in adiposity, as documented by weights of both epididymal WAT and scWAT (Table 1). Furthermore, the CDCA intervention prevented ectopic TG accumulation in liver and muscle (Table 1). Thus, the 8-week reversion experiment revealed strong normalization of BW and obesity-associated phenotypes in response to the CDCA intervention. However, it remained to be established what was the contribution of the transient decrease in food intake to the lasting effects of the intervention.

Reduction of adiposity in response to CDCA in a pair-feeding experiment

To dissect the role of the transient decrease in food intake and the CDCA-induced metabolic effects in the anti-obesity effect of the drug, the 3-week reversion experiment was conducted (Figures 1c and d), in which PF animals were also included. The duration of intervention was shortened to 3 weeks, in order to focus on the period when the decline in food intake occurred (see above). The transient decrease in food intake in the CDCA mice, normalized within 3 weeks (Figure 1c), was associated with a drop in BW, almost to the level of mice fed the STD diet since weaning (Figure 1d). This drop could be explained by the decrease in food intake, as it was also observed in the PF mice (Figure 1d). The animals maintained the decreased BW even after reaching the normal food consumption (Figures 1c and d).

Adipose tissue in the 3-week reversion experiment

Dietary obesity was associated with a strong increase in adiposity, as indicated by the differences in weights of all fat depots analysed in the STD mice and the cHF mice (Table 2). Weights of epididymal WAT and scWAT depots, as well as interscapular BAT, were significantly decreased in the PF mice (Table 2).

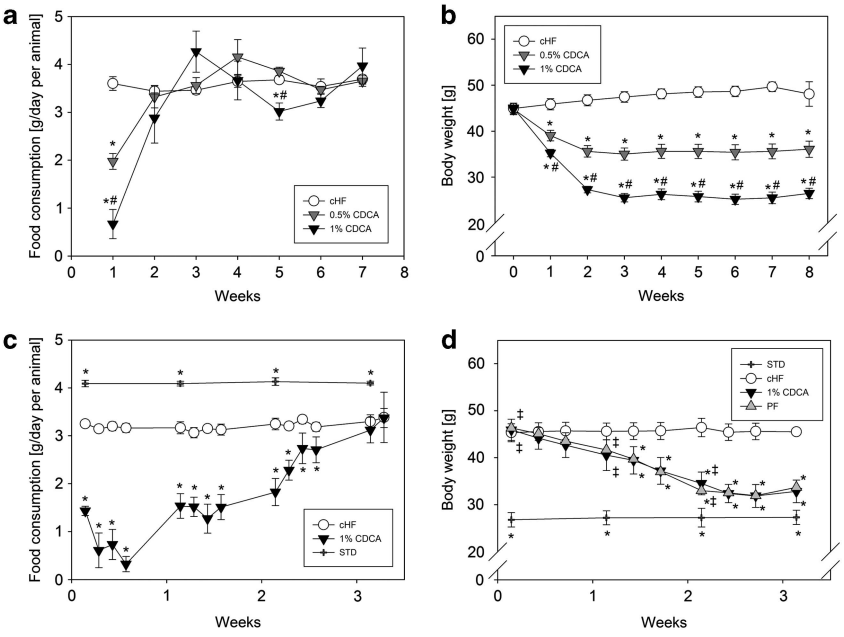

Figure 1. Growth curves and food intake. (**a**, **b**) Food intake (**a**) and growth curve (**b**) during the 8-week reversion experiment ($n=10$–12); (**c**, **d**) food intake (**c**) and growth curve (**d**) during the 3-week reversion experiment ($n=8$, except for STD, where $n=4$). Data are means ± s.e.m. *Significantly different in comparison to the cHF group; #significantly different in comparison to the 0.5% CDCA group (only in **a** and **b**); ‡significantly different in comparison to the STD group (only in **d**). cHF, high-fat diet; 0.5 and 1% CDCA, high-fat diet supplemented with 0.5% and 1% CDCA, respectively; PF, pair-fed group; STD, standard chow diet.

Table 1. Parameters measured in plasma, tissues and faeces at the end of the 8-week reversion experiment

	cHF	*0.5% CDCA*	*1% CDCA*
Plasma levels			
TG (mmol l^{-1})	1.56 ± 0.12	1.08 ± 0.12[a]	0.83 ± 0.10[a]
NEFA (mmol l^{-1})	0.86 ± 0.04	0.85 ± 0.04	0.65 ± 0.04[a,b]
Cholesterol (mmol l^{-1})	5.27 ± 0.26	3.15 ± 0.26[a]	2.70 ± 0.42[a]
Glucose (mg dl^{-1})	257 ± 10	191 ± 13[a]	143 ± 19[a]
Insulin (ng ml^{-1})	4.53 ± 0.43	0.71 ± 0.10[a]	0.19 ± 0.03[a]
Adiponectin HMW (AU)	0.43 ± 0.03	0.47 ± 0.04	0.62 ± 0.07[a]
Total (AU)	1.02 ± 0.06	0.98 ± 0.07	1.20 ± 0.10
HMW/totals	0.42 ± 0.02	0.48 ± 0.03	0.51 ± 0.03
Aspartate transaminase (uCAT l^{-1})	3.02 ± 0.32	3.01 ± 0.39	3.26 ± 0.30
Alanine transaminase (uCAT l^{-1})	1.12 ± 0.16	0.62 ± 0.03	0.88 ± 0.08
Oral glucose tolerance test			
Total AUC (mmol l^{-1} Glc 180 min)	3042 ± 189	2524 ± 158[a]	1654 ± 82[a,b]
Weight of tissues			
eWAT (mg)	2241 ± 105	1419 ± 147[a]	513 ± 66[a,b]
scWAT (mg)	1295 ± 60	612 ± 102[a]	191 ± 19[a,b]
Liver (mg)	2328 ± 132	1873 ± 95	2060 ± 204
Tissue TG content			
Liver TG (mg g^{-1} tissue)	377 ± 41	49 ± 6[a]	30 ± 1[a,b]
Muscle TG (mg g^{-1} tissue)	113 ± 11	50 ± 7[a]	35 ± 7[a]
Faeces lipid content			
TG (mg g^{-1})	62.8 ± 14	47.5 ± 4.7	49.2 ± 2.9
Cholesterol (mg g^{-1})	12.3 ± 0.8	10.4 ± 0.4[a]	10.5 ± 0.3[a]

Abbreviations: AUC, area under the curve; CDCA, chenodeoxycholic acid; cHF, high-fat diet; eWAT, epididymal WAT; HMW, high molecular weight; NEFA, non-esterified fatty acid; scWAT, subcutaneous WAT; TG, plasma triglyceride. Data are means ± s.e.m. ($n = 10$–12, except for oral glucose tolerance test, where $n = 5$; see Materials and Methods). [a]Significant differences in comparison to the cHF group. [b]Significant differences in comparison to the 0.5% CDCA group.

Table 2. Fat depots at the end of the 3-week reversion experiment

	STD	*cHF*	*1% CDCA*	*PF*
Weight of tissues				
eWAT (mg)	553 ± 94[a]	2490 ± 208	899 ± 147[a]	979 ± 154[a]
scWAT (mg)	183 ± 14[a]	1163 ± 168	417 ± 78[a]	498 ± 83[a]
Interscapular BAT (mg)	121 ± 19[a]	228 ± 20	92 ± 9[a]	125 ± 17[a]
Average adipocyte area				
scWAT (μm^2)	1040 ± 190[a]	3474 ± 240	1652 ± 193[a]	2191 ± 186[a,b]

Abbreviations: BAT, brown adipose tissue; CDCA, chenodeoxycholic acid; cHF, high-fat diet; eWAT, epididymal WAT; PF, pair-fed group; scWAT, subcutaneous WAT; STD, standard chow diet. Data are shown as means ± s.e.m. ($n = 8$, except for STD, where $n = 4$; see Materials and Methods). [a]Significant differences in comparison to the cHF group. [b]Significant differences in comparison to the STD group.

Morphometry of adipocytes in scWAT indicated that the differences in adiposity were reflected by the size of adipocytes (Table 2). A similar conclusion could be made by a simple inspection of histological sections from both interscapular BAT (Figure 2a) and scWAT (Figure 3a). Weights of all fat depots analysed, as well as the size of adipocytes in scWAT, tended to be smaller in the CDCA as compared with the PF mice, but the differences were not statistically significant (Table 2).

To learn whether the reduction in BW and adiposity in response to both PF and CDCA intervention could be explained by induction of UCP1-mediated thermogenesis, as previously observed in the case of cholic acid,[15] *Ucp1* gene transcript levels in the interscapular BAT were quantified. As compared with the cHF mice, *Ucp1* gene expression was highly induced in the CDCA mice (Figure 2b), which was also in accordance with the increased expression of the *Prdm16* gene (which is essential for *Ucp1* gene expression and for the activation of the UCP1-mediated thermogenesis[39]) as well as the induction of selected markers of mitochondrial biogenesis (such as *Ppargc1a*, *Slc25a4* and *Cox4i1*; Figure 2b). On the other hand, no induction of these genes could be observed in the PF mice (Figure 2b). Total thermogenic activity of interscapular BAT could be assessed by evaluation of UCP1 content per depot.[28] Therefore, UCP1 was quantified in the membranous fraction prepared from interscapular BAT using western blots (data not shown). Although total UCP1 content was similar in the STD, cHF and PF mice, it was significantly increased in response to the CDCA intervention, and it was ~1.5-fold higher in the CDCA as compared with the cHF mice (Figure 2c).

Also in scWAT of the CDCA and PF mice, *Ucp1* gene transcript was detected. No *Ucp1* gene transcript could be detected in the cHF mice, and the transcript levels were much higher in the CDCA as compared with the PF mice. However, even in the CDCA mice, *Ucp1* transcript levels in scWAT were at least three orders of magnitude lower as compared with those in interscapular BAT of these mice (compare *Y* axes in Figures 2b and 3b, where *Ucp1* transcript levels were estimated under identical conditions).

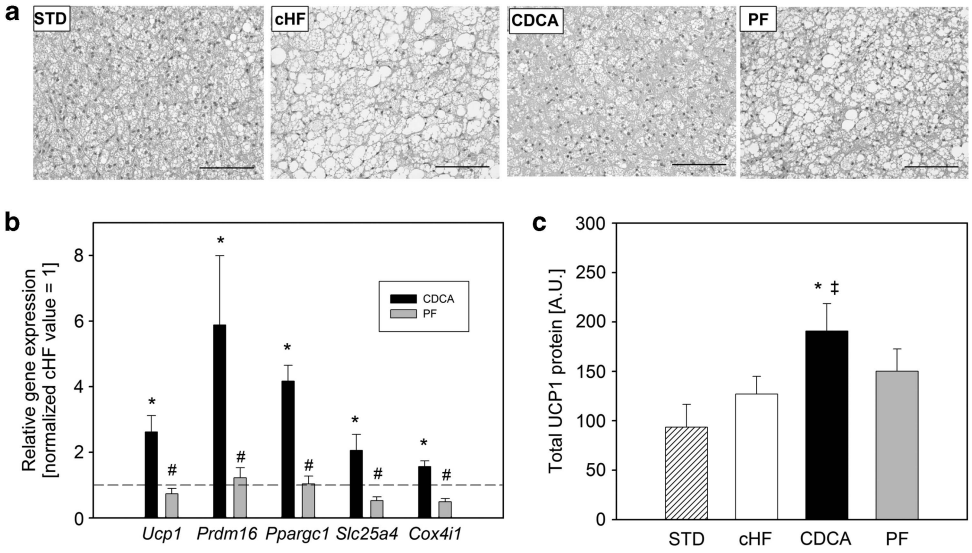

Figure 2. Interscapular BAT parameters in the 3-week reversion experiment. (**a**) Representative images of BAT. (**b**) Relative gene expression (cHF = 1, dashed line); data were normalized using 18S RNA as a housekeeping gene. (**c**) Content of UCP1 protein in whole interscapular BAT. *Significantly different in comparison to the cHF group; #significantly different in comparison to the CDCA group; ‡significantly different in comparison to the STD group. Data are means ± s.e.m. ($n = 8$, except for STD, where $n = 4$). (**a**) Bar = 0.1 mm. CDCA, high-fat diet supplemented with 1% CDCA; cHF, high-fat diet; PF, pair-fed group; STD, standard chow diet.

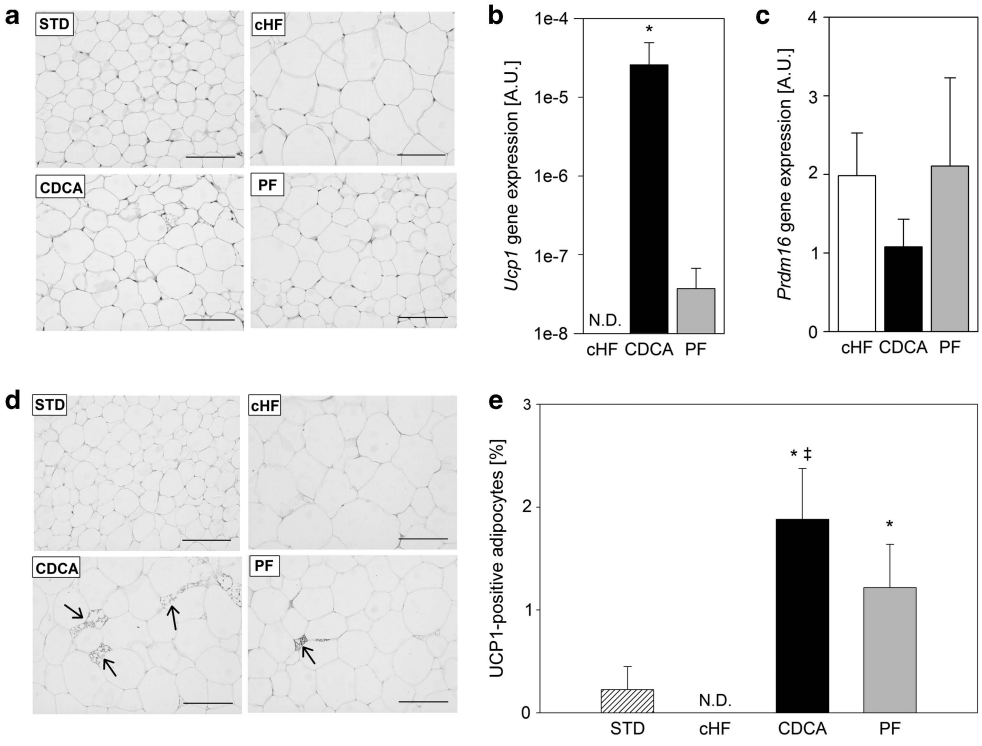

Figure 3. scWAT parameters in the 3-week reversion experiment. (**a**) Representative images of WAT. (**b** and **c**) *Ucp1* and *Prdm16* gene expression; data were normalized using 18S RNA as a housekeeping gene. (**d**) Representative images of immunostaining for UCP1; UCP1-positive cells are indicated by arrows. (**e**) Graphical representation of the percentage of UCP1-positive cells relative to all adipocytes visualized. *Significantly different in comparison to the cHF group; ‡significantly different in comparison to the STD group. Data are means ± s.e.m. ($n = 8$, except for STD, where $n = 4$). (**a** and **d**) Bar = 0.1 mm. CDCA, high-fat diet supplemented with 1% CDCA; cHF, high-fat diet; ND, not detected; PF, pair-fed group; STD, standard chow diet.

However, unlike in BAT, in scWAT, *Prdm16* gene expression did not reflect the activity of *Ucp1* gene, and expression of *Prdm16* gene in the cHF, CDCA and PF mice was similar (Figure 3c). In contrast to BAT, even in scWAT of the CDCA mice, we could not detect any UCP1 using western blots, indicating that in spite of the stimulation of *Ucp1* gene expression in WAT, UCP1 levels in this tissue were relatively low and that they were under the detection limit of the method (data not shown). Immunohistological analysis

revealed some UCP1-positive adipocytes (that is, 'brite' cells) in scWAT, especially in the CDCA mice (Figures 3d and e), but not in eWAT (data not shown).

Indirect calorimetry in the 3-week reversion experiment

To evaluate the effects of the CDCA intervention on EE and fuel partitioning, indirect calorimetry was performed during the third week of the 3-week reversion experiment. As expected, in all the groups, that is, the cHF, CDCA and PF mice, EE was relatively high during the dark phase of the day, when the mice are known to be active. However, except for a decline in EE during the dark phase in the PF mice, the expected effect of a limited food supply in the PF mice, no major differences in the time course of EE between the groups were observed (Figure 4a). Accordingly, analysis of mean EE over the whole day has not revealed any significant differences between the groups when the values are expressed per the whole animal even when evaluated by ANCOVA reflecting BW (Figure 4d). However, when EE was adjusted to BW, both the CDCA mice and the PF mice exhibited higher EE as compared with the control mice fed the cHF diet (Figure 4e). Whether this could suggest CDCA-induced increase in EE is a matter of debate (see Discussion). The evaluation of RQ, the marker of fuel partitioning, during the day revealed a decline in RQ during the dark phase in the PF mice (Figure 4b), suggesting a gradual shift from carbohydrate to lipid oxidation in response to the limited food supply (see above). Moreover, during the dark but not during the light phase of the day, the CDCA mice exhibited a lower RQ as compared with the cHF mice (Figure 4b). The robust PRCF analysis of the RQ data, which takes into account all the RQ values measured in each group (see Materials and methods), supported the shift from carbohydrate to lipid oxidation in response to pair-feeding, and, importantly, it also suggested a food consumption-independent shift to lipid oxidation in response to the CDCA intervention (Figure 4c). The PRCF data were evaluated for the whole day rather than separately for the light and the dark phase of day, to eliminate the influence of the shift in rhythmicity elicited in response to the pair-feeding. Also, the mean RQ during the whole day (Figure 4f) as well as the 50th percentile of the PRCF data (Figure 4g) tended to be the lowest in the CDCA mice, but these differences were not statistically significant. Taken together, these data suggest that CDCA increased lipid oxidation in expense of carbohydrate oxidation, especially during the dark phase of the day, independent of food intake.

DISCUSSION

In accordance with the previous studies using cholic acid in cHF-fed mice performed by the group of Auwerx,[10,15,20] we have demonstrated that supplementation of a cHF using BAs, namely CDCA, could reverse dietary obesity and associated metabolic disorders. Thus, in response to the 8-week intervention, a dose-dependent effect of CDCA was observed with respect to the reduction of obesity, amelioration of dyslipidaemia, normalization of glucose homeostasis and reduction of ectopic accumulation of lipids in the liver and skeletal muscle. No detrimental effects on hepatic markers were observed, and in accordance with the effect of cholic acid[15] used in several of the previous studies,[10,15,20] the CDCA intervention had no effect on lipid absorption.

Most of the above mentioned beneficial metabolic effects of CDCA could be related to a transient decrease in food consumption observed at the beginning of the intervention. This is not consistent with the outcomes of the previous studies in mice,[10,15,20] in which admixing of cholic acid to cHF was

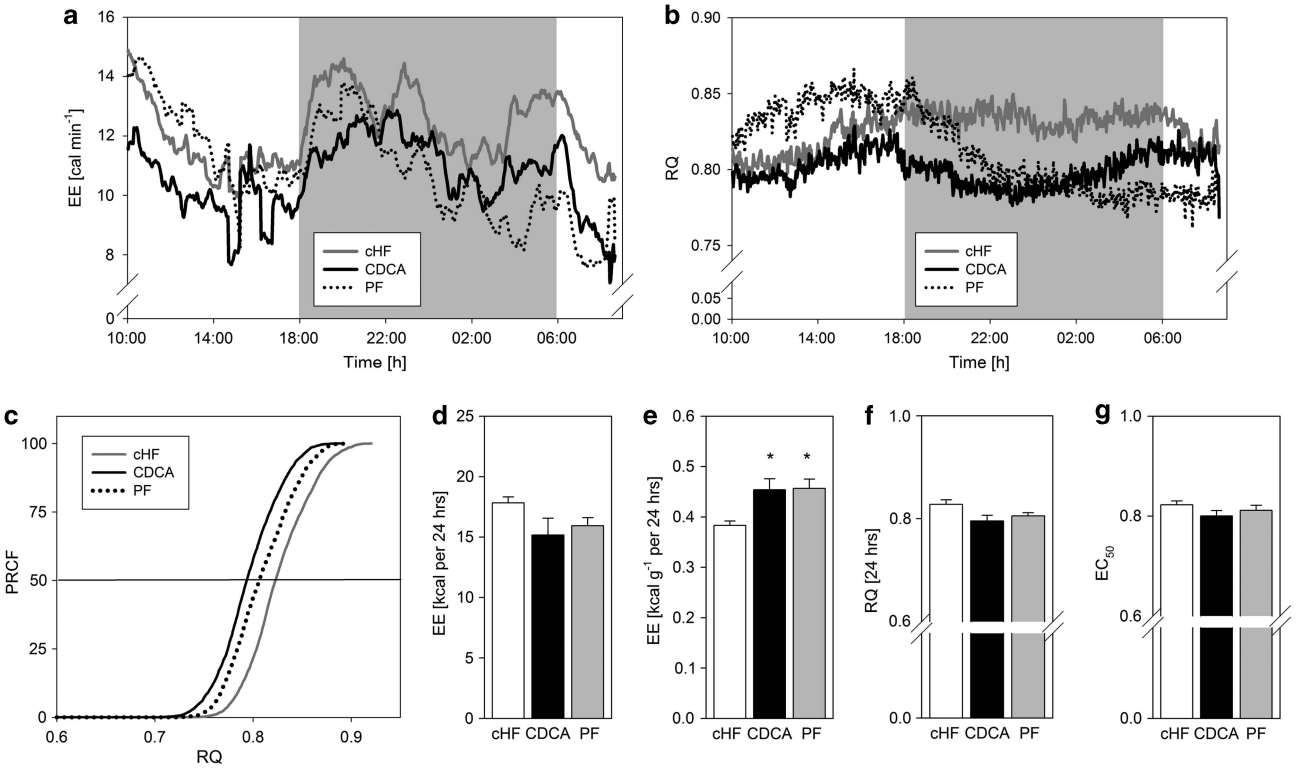

Figure 4. Indirect calorimetry performed between day 15 and day 17 of the 3-week reversion experiment. (**a**) Time course of the measurements of EE. (**b**) Time course of the RQ measurements; grey area in **a** and **b** represents the dark phase of the day. (**c**) Plot of PRCF of RQ values during the whole 24-h measurement period; each curve represents data pooled from all mice within a given group ($n = 7$–8; ~5 000 RQ measurements per curve). (**d**) Total EE per mouse (24 h). (**e**) Total EE per g BW (24 h). (**f**) Mean RQ (24 h). (**g**) 50th percentile value of PRCF (EC_{50}) derived from (**c**). *Significantly different in comparison to the cHF group. CDCA, high-fat diet supplemented with 1% CDCA; cHF, high-fat diet; PF, pair-fed group.

interpreted not to affect food consumption. However, in these previous studies, food intake was adjusted to BW of the animals (see Figure 1f in Watanabe *et al.*,[15] Figure 1a of Watanabe *et al.*,[20] Figure 1a of Watanabe *et al.*[10]), whereas in our study, food intake per mouse was considered. Therefore, in the previous studies, the decrease in absolute food intake could be masked when adjusted to BW, as BW was decreased in response to the cholic acid intervention. Owing to a relatively low specific metabolic rate of WAT, it is conceivable that non-adjusted (or lean body mass-adjusted) rather than total body mass-adjusted food intake should be considered when judging the impact of food intake on obesity.[40–42] However, neither lean body mass nor fat-free mass was evaluated in this study.

Therefore, in contrast with the previous studies, in which a potential effect of the decrease in food intake on obesity and associated disorders has been neglected,[10,15,20] we have attempted to dissect the roles of the decrease in food intake and the effect of CDCA *per se*, respectively, on obesity and energy metabolism by employing pair-feeding strategy. This approach revealed that the reduction of obesity could be mostly explained by the transient decrease in food intake during the initial phase of the intervention, whereas a relatively mild and food intake-independent reduction in adiposity (not detectable at the BW level) could also be observed.

The food intake-independent decrease in adiposity could result from the induction of UCP1-mediated thermogenesis, as suggested by upregulation of the *Ucp1* transcript and the increase in the total UCP1 protein in the interscapular BAT, as well as the upregulation of transcription of selected markers of mitochondrial biogenesis in BAT. This observation is in agreement with the previous study showing TGR5-mediated induction of the *Ucp1* transcript in response to cholic acid.[15] However, to our knowledge, our study demonstrates for the first time an elevation of UCP1 protein content in BAT in response to a BA. This is a critical observation, as UCP1 but not the UCP1 gene transcript is a relevant marker of the BAT thermogenic capacity.[28] The effect of the induction of UCP1-mediated thermogenesis of whole-body energy balance could be substantial for the stabilization of the lean phenotype in the long run, but it could not be detected using indirect calorimetry, reflecting the relatively low sensitivity of this technique and because lean BW data were not available in the present study (see above).

Concerning the inducible UCP1-mediated thermogenesis in brite cells located in WAT (see Introduction), our results document that brite cells could be induced in response to the CDCA intervention. However, in spite of a marked stimulation of the activity of the UCP1 gene at the transcript level observed in scWAT, the amount of UCP1 in the scWAT of the CDCA mice was very low as documented by both, undetectable UCP1 using western blots and a very small fraction of UCP1-positive adipocytes, as revealed using immunohistological analysis. Therefore, induction of UCP1 in interscapular BAT but not in brite cells interspersed in scWAT was probably involved in the induction of EE and lean phenotype in the CDCA mice. It remains to be established whether energy dissipation in other tissues, for example, TGR5-mediated thermogenesis in skeletal muscle,[15] could also be involved.

In spite of the induction of UCP1 in BAT as well the food intake-independent reduction in adiposity in the CDCA mice, indirect calorimetry could not reveal any difference in EE between the CDCA and PF mice, neither when EE per mice nor when EE adjusted to BW was considered. In accordance with the previous studies using cholic acid in cHF-fed mice,[15] also in our study, higher EE adjusted to BW was observed in the CDCA as compared with the cHF mice. However, this effect could be ascribed in full to the inappropriate normalization of EE to BW (see above, and Butler and Kozak[40]), as also documented by equal EE adjusted to BW in the CDCA and the PF mice. In accordance with the previous study using cholic acid,[15] a tendency to decrease RQ in response to the CDCA intervention was observed, which was independent on food intake, and suggested a shift from carbohydrate to lipid oxidation. Nevertheless, RQ changes during the day were affected by the shift in ingestion in the PF group.

Also, changes in gut microbiota can be possibly involved in the effects of CDCA on BAT, because some bacteria can convert CDCA to lithocholic acid, which is a more potent activator of TGR5 (reviewed in Greiner and Backhed [43]). However, this topic was out of the scope of this study.

In conclusion, our results document that CDCA could reduce obesity and associated metabolic disorders in the face of high lipid supply in mice and they suggest a major role of transient reduction in food intake in the anti-obesity effect. Moreover, our results indicate food intake-independent stimulation of UCP1-mediated thermogenesis in BAT in response to CDCA. Although the stimulation of EE in BAT was relatively low and could not be detected using indirect calorimetry, it could be important for the stabilization of the lean phenotype. In addition, the CDCA-induced increase in lipid catabolism could be beneficial with respect to reversal of obesity-associated metabolic disorders. Our results are consistent with the beneficial metabolic effects of BAs, which could be relevant in long-term treatments, but they also warn against overinterpretation of results of some of the previous studies using other BAs.

CONFLICT OF INTEREST

The authors declare no conflict of interest.

ACKNOWLEDGEMENTS

JST, FVD, APG and ATV were recipients of a Fundação para a Ciência e a Tecnologia PhD scholarship (SFRH/BD/38467/2007, SFRH/BD/38372/2007, SFRH/BD/44674/2008 and SFRH/BD/44796/2008, respectively). This project was supported by a FCT grant PTCD/SAU-OSM/72443/2006, PEst-C/SAU/LA0001/2011 and EU FP7 project DIABAT (HEALTH-F2—2011-278373) and by the Czech Science Foundation (13-00871S).

REFERENCES

1 Angelin B, Einarsson K, Hellstrom K, Leijd B. Effects of cholestyramine and chenodeoxycholic acid on the metabolism of endogenous triglyceride in hyperlipoproteinemia. *J Lipid Res* 1978; **19**: 1017–1024.
2 Teodoro JS, Rolo AP, Palmeira CM. Hepatic FXR: key regulator of whole-body energy metabolism. *Trends Endocrinol Metab* 2011; **22**: 458–466.
3 Watanabe M, Houten SM, Wang L, Moschetta A, Mangelsdorf DJ, Heyman RA *et al.* Bile acids lower triglyceride levels via a pathway involving FXR, SHP, and SREBP-1c. *J Clin Invest* 2004; **113**: 1408–1418.
4 Kast HR, Nguyen CM, Sinal CJ, Jones SA, Laffitte BA, Reue K *et al.* Farnesoid X-activated receptor induces apolipoprotein C-II transcription: a molecular mechanism linking plasma triglyceride levels to bile acids. *Mol Endocrinol* 2001; **15**: 1720–1728.
5 Sinal CJ, Tohkin M, Miyata M, Ward JM, Lambert G, Gonzalez FJ. Targeted disruption of the nuclear receptor FXR/BAR impairs bile acid and lipid homeostasis. *Cell* 2000; **102**: 731–744.
6 Stayrook KR, Bramlett KS, Savkur RS, Ficorilli J, Cook T, Christe ME *et al.* Regulation of carbohydrate metabolism by the farnesoid X receptor. *Endocrinology* 2005; **146**: 984–991.
7 Cariou B, van Harmelen K, Duran-Sandoval D, van Dijk TH, Grefhorst A, Abdelkarim M *et al.* The farnesoid X receptor modulates adiposity and peripheral insulin sensitivity in mice. *J Biol Chem* 2006; **281**: 11039–11049.
8 Duran-Sandoval D, Cariou B, Percevault F, Hennuyer N, Grefhorst A, van Dijk TH *et al.* The farnesoid X receptor modulates hepatic carbohydrate metabolism during the fasting-refeeding transition. *J Biol Chem* 2005; **280**: 29971–29979.
9 Abdelkarim M, Caron S, Duhem C, Prawitt J, Dumont J, Lucas A *et al.* The farnesoid X receptor regulates adipocyte differentiation and function by promoting peroxisome proliferator-activated receptor-gamma and interfering with the Wnt/beta-catenin pathways. *J Biol Chem* 2010; **285**: 36759–36767.
10 Watanabe M, Morimoto K, Houten SM, Kaneko-Iwasaki N, Sugizaki T, Horai Y *et al.* Bile acid binding resin improves metabolic control through the induction of energy expenditure. *PloS One* 2012; **7**: e38286.

11 Konikoff FM. Gallstones - approach to medical management. *MedGenMed* 2003; **5**: 8.
12 Prawitt J, Caron S, Staels B. Bile acid metabolism and the pathogenesis of type 2 diabetes. *Curr Diab Rep* 2011; **11**: 160–166.
13 Katona BW, Cummins CL, Ferguson AD, Li T, Schmidt DR, Mangelsdorf DJ *et al.* Synthesis, characterization, and receptor interaction profiles of enantiomeric bile acids. *J Med Chem* 2007; **50**: 6048–6058.
14 Neuschwander-Tetri BA. Farnesoid x receptor agonists: what they are and how they might be used in treating liver disease. *Curr Gastroenterol Rep* 2012; **14**: 55–62.
15 Watanabe M, Houten SM, Mataki C, Christoffolete MA, Kim BW, Sato H *et al.* Bile acids induce energy expenditure by promoting intracellular thyroid hormone activation. *Nature* 2006; **439**: 484–489.
16 Cannon B, Nedergaard J. Brown adipose tissue: function and physiological significance. *Physiol Rev* 2004; **84**: 277–359.
17 Wu J, Cohen P, Spiegelman BM. Adaptive thermogenesis in adipocytes: is beige the new brown? *Genes Dev* 2013; **27**: 234–250.
18 Rothwell NJ, Stock MJ. A role for brown adipose tissue in diet-induced thermogenesis. *Nature* 1979; **281**: 31–35.
19 da-Silva WS, Ribich S, Arrojo e Drigo R, Castillo M, Patti ME, Bianco AC. The chemical chaperones tauroursodeoxycholic and 4-phenylbutyric acid accelerate thyroid hormone activation and energy expenditure. *FEBS Lett* 2011; **585**: 539–544.
20 Watanabe M, Horai Y, Houten SM, Morimoto K, Sugizaki T, Arita E *et al.* Lowering bile acid pool size with a synthetic farnesoid X receptor (FXR) agonist induces obesity and diabetes through reduced energy expenditure. *J Biol Chem* 2011; **286**: 26913–26920.
21 Zingaretti MC, Crosta F, Vitali A, Guerrieri M, Frontini A, Cannon B *et al.* The presence of UCP1 demonstrates that metabolically active adipose tissue in the neck of adult humans truly represents brown adipose tissue. *FASEB J* 2009; **23**: 3113–3120.
22 Young P, Arch JR, Ashwell M. Brown adipose tissue in the parametrial fat pad of the mouse. *FEBS Lett* 1984; **167**: 10–14.
23 Loncar D. Convertible adipose tissue in mice. *Cell Tissue Res* 1991; **266**: 149–161.
24 Cousin B, Cinti S, Morroni M, Raimbault S, Ricquier D, Penicaud L *et al.* Occurrence of brown adipocytes in rat white adipose tissue: molecular and morphological characterization. *J Cell Sci* 1992; **103**: 931–942.
25 Petrovic N, Walden TB, Shabalina IG, Timmons JA, Cannon B, Nedergaard J. Chronic peroxisome proliferator-activated receptor gamma (PPARgamma) activation of epididymally derived white adipocyte cultures reveals a population of thermogenically competent, UCP1-containing adipocytes molecularly distinct from classic brown adipocytes. *J Biol Chem* 2010; **285**: 7153–7164.
26 Frontini A, Vitali A, Perugini J, Murano I, Romiti C, Ricquier D *et al.* White-to-brown transdifferentiation of omental adipocytes in patients affected by pheochromocytoma. *Biochim Biophys Acta* 2013; **1831**: 950–959.
27 Jespersen NZ, Larsen TJ, Peijs L, Daugaard S, Homoe P, Loft A *et al.* A classical brown adipose tissue mRNA signature partly overlaps with brite in the supraclavicular region of adult humans. *Cell Metab* 2013; **17**: 798–805.
28 Nedergaard J, Cannon B. UCP1 mRNA does not produce heat. *Biochim Biophys Acta* 2013; **1831**: 943–949.
29 Kuda O, Jelenik T, Jilkova Z, Flachs P, Rossmeisl M, Hensler M *et al.* n-3 fatty acids and rosiglitazone improve insulin sensitivity through additive stimulatory effects on muscle glycogen synthesis in mice fed a high-fat diet. *Diabetologia* 2009; **52**: 941–951.
30 Medrikova D, Jilkova ZM, Bardova K, Janovska P, Rossmeisl M, Kopecky J. Sex differences during the course of diet-induced obesity in mice: adipose tissue expandability and glycemic control. *Int J Obes* 2012; **36**: 262–272.
31 Rossmeisl M, Jelenik T, Jilkova Z, Slamova K, Kus V, Hensler M *et al.* Prevention and reversal of obesity and glucose intolerance in mice by DHA derivatives. *Obesity* 2009; **17**: 1023–1031.
32 Salmon DM, Flatt JP. Effect of dietary fat content on the incidence of obesity among ad libitum fed mice. *Int J Obes* 1985; **9**: 443–449.
33 Kopecky J, Rossmeisl M, Hodny Z, Syrovy I, Horakova M, Kolarova P. Reduction of dietary obesity in aP2-Ucp transgenic mice: mechanism and adipose tissue morphology. *Am J Physiol* 1996; **270**: E776–E786.
34 Smith PK, Krohn RI, Hermanson GT, Mallia AK, Gartner FH, Provenzano MD *et al.* Measurement of protein using bicinchoninic acid. *Anal Biochem* 1985; **150**: 76–85.
35 Kus V, Prazak T, Brauner P, Hensler M, Kuda O, Flachs P *et al.* Induction of muscle thermogenesis by high-fat diet in mice: association with obesity-resistance. *Am J Physiol Endocrinol Metab* 2008; **295**: E356–E367.
36 Flachs P, Ruhl R, Hensler M, Janovska P, Zouhar P, Kus V *et al.* Synergistic induction of lipid catabolism and anti-inflammatory lipids in white fat of dietary obese mice in response to calorie restriction and n-3 fatty acids. *Diabetologia* 2011; **54**: 2626–2638.
37 Weir JB. New methods for calculating metabolic rate with special reference to protein metabolism. *J Physiol* 1949; **109**: 1–9.
38 Even PC, Nadkarni NA. Indirect calorimetry in laboratory mice and rats: principles, practical considerations, interpretation and perspectives. *Am J Physiol Regul Integr Comp Physiol* 2012; **303**: R459–R476.
39 Seale P, Conroe HM, Estall J, Kajimura S, Frontini A, Ishibashi J *et al.* Prdm16 determines the thermogenic program of subcutaneous white adipose tissue in mice. *J Clin Invest* 2011; **121**: 96–105.
40 Butler AA, Kozak LP. A recurring problem with the analysis of energy expenditure in genetic models expressing lean and obese phenotypes. *Diabetes* 2010; **59**: 323–329.
41 Himms-Hagen J. On raising energy expenditure in ob/ob mice. *Science* 1997; **276**: 1132–1133.
42 Kaiyala KJ, Schwartz MW. Toward a more complete (and less controversial) understanding of energy expenditure and its role in obesity pathogenesis. *Diabetes* 2011; **60**: 17–23.
43 Greiner T, Backhed F. Effects of the gut microbiota on obesity and glucose homeostasis. *Trends Endocrinol Metab* 2011; **22**: 117–123.

Supplementary Information accompanies this paper on International Journal of Obesity website (http://www.nature.com/ijo)

Biochimie 124 (2016) 163–170

Contents lists available at ScienceDirect

Biochimie

journal homepage: www.elsevier.com/locate/biochi

Research paper

Early differences in metabolic flexibility between obesity-resistant and obesity-prone mice

Kristina Bardova [a], Olga Horakova [a], Petra Janovska [a], Jana Hansikova [a], Vladimir Kus [a], Evert M. van Schothorst [b], Femke P.M. Hoevenaars [b], Melissa Uil [b], Michal Hensler [a], Jaap Keijer [b], Jan Kopecky [a, *]

[a] Department of Adipose Tissue Biology, Institute of Physiology of the Czech Academy of Sciences, Videnska 1083, 142 20 Prague, Czech Republic
[b] Human and Animal Physiology, Wageningen University, De Elst 1, 6708 WD Wageningen, The Netherlands

ARTICLE INFO

Article history:
Received 13 August 2015
Accepted 15 November 2015
Available online 27 November 2015

Keywords:
Indirect calorimetry
Glucose tolerance
Weaning
C57BL/6J mice
A/J mice
Metabolic flexibility

ABSTRACT

Decreased metabolic flexibility, i.e. a compromised ability to adjust fuel oxidation to fuel availability supports development of adverse consequences of obesity. The aims of this study were (i) to learn whether obesity-resistant A/J and obesity-prone C57BL/6J mice differ in their metabolic flexibility right after weaning; and (ii) to characterize possible differences in control of glucose homeostasis in these animals using glucose tolerance tests (GTT). A/J and C57BL/6J mice of both genders were maintained at 20 °C and weaned to standard low-fat diet at 30 days of age. During the first day after weaning, using several separate animal cohorts, (i) GTT was performed using 1 or 3 mg glucose/g body weight (BW), while glucose was administered either orally (OGTT) or intraperitoneally (IPGTT) at 20 °C; and (ii) indirect calorimetry (INCA) was performed, either in a combination with oral gavage of 1 or 7.5 mg glucose/g BW, or during a fasting/re-feeding transition. INCA was conducted either at 20 °C or 34 °C. Results of both OGTT and IPGTT using 1 mg glucose/g BW at 20 °C, and INCA using 7.5 mg glucose/g BW at 34 °C, indicated higher glucose tolerance and higher metabolic flexibility to glucose, respectively, and lower fasting glycemia in A/J mice as compared with C57BL/6J mice. Thus, control of whole body glucose metabolism between A/J and C57BL/6J mice represents a phenotypic feature differentiating between the strains right after weaning.

1. Introduction

Type 2 diabetes is often associated with obesity and related metabolic disorders. It reflects systemic metabolic changes resulting from excessive accumulation of body fat [1]. Thus, while lean and insulin-sensitive subjects are metabolically flexible, in obese and particularly in type 2 diabetic subjects the capacity to adapt fuel oxidation to fuel availability is compromised, reflecting in large the resistance of muscle metabolism to insulin [2]. Fatty acid oxidation in the fasted state is decreased as is the ability to efficiently switch to glucose oxidation in the post-prandial state [2]. However, some obese individuals remain metabolically healthy and even obese monozygotic twins can differ in their metabolic health [3]. Therefore, deterioration of metabolic flexibility represents one of the key self-standing markers of the development of type 2 diabetes, which could precede the outbreak of the disease by several years [4]. Metabolic flexibility is typically assessed using indirect calorimetry (**INCA**) as the response in respiratory quotient (**RQ**) to change in energy fuel [2]. In human studies, INCA is often used to assess metabolic flexibility either during an euglycemic-hyperinsulinemic clamp or during a meal test [2]. In laboratory

Abbreviations: AMPK, AMP-activated protein kinase; AU, arbitrary units; AUC, area under the curve; BW, body weight; B6, C57BL/6J mice; EE, energy expenditure; GTT, glucose tolerance test; HMW, high molecular weight; INCA, indirect calorimetry; IPGTT, intraperitoneal glucose tolerance test; LMW, low molecular weight; MMW, medium molecular weight; NEFA, non-esterified fatty acid(s); OGTT, oral glucose tolerance test; RQ, respiratory quotient; TAG, triacylglycerol(s); VO_2, oxygen consumption; VCO_2, carbon dioxide production.

* Corresponding author.
E-mail addresses: kristina.bardova@fgu.cas.cz (K. Bardova), olga.horakova@fgu.cas.cz (O. Horakova), petra.janovska@fgu.cas.cz (P. Janovska), jana.hansikova@fgu.cas.cz (J. Hansikova), vladimir.kus1@gmail.com (V. Kus), evert.vanschothorst@wur.nl (E.M. van Schothorst), hoevenaars@vumc.nl (F.P.M. Hoevenaars), melissa.uil@gmail.com (M. Uil), hensler.michal@gmail.com (M. Hensler), jaap.keijer@wur.nl (J. Keijer), kopecky@biomed.cas.cz (J. Kopecky).

http://dx.doi.org/10.1016/j.biochi.2015.11.014
0300-9084/

rodents, metabolic flexibility is typically evaluated using INCA during fasting/re-feeding transition [5,6] rather than in conjunction with the technically demanding clamp. Recently, an alternative approach was introduced in our group, to measure metabolic flexibility in mice as a response in RQ to a glucose bolus during INCA [7]. The information obtained using INCA could be complemented using glucose tolerance test (**GTT**), which monitors the homeostatic blood glucose clearance in response to a glucose challenge and reflects multiple mechanisms [8].

Inbred strains of mice are frequently used to characterize the mechanisms underlying development of obesity and associated metabolic disorders, with the obesity-resistant A/J mice and obesity-prone C57BL/6J (**B6**) mice [9,10], as two important models for the respective conditions. Body weight (**BW**) of mice of the A/J strain is lower than that of the B6 mice when fed standard low-fat diet and the A/J mice exhibit a relatively fast and strong induction of leptin by high-fat diet. In contrast, B6 mice increase their leptin levels only in association with increase in BW in response to high-fat diet, and the leptin levels in B6 mice exceed those in A/J only after B6 mice develop massive obesity [9,11]. Leptin supplementation of B6 mice does not prevent high-fat diet-induced obesity [12]. Thus, resistance of tissue metabolism to leptin, together with a relatively weak sensitivity to adrenergic stimulation [13], could contribute to the susceptibility of B6 to diet-induced obesity. It has also been shown that in adulthood and with free access to the standard diet, A/J mice exhibited (i) higher energy expenditure in the resting conditions reflecting liver β-oxidation, (ii) lower running endurance capacity reflecting muscle β-oxidation, and (iii) preferential activation of carbohydrate over lipid oxidative metabolism during exercise, as compared with B6 mice [14]. Whether all these differences contribute to the differential susceptibility to obesity remains to be clarified. In fact, the low obesogenic effect of high-fat diet in adult A/J mice has been ascribed to inducibility of liver lipid metabolism, including both mitochondria [15] and peroxisomes [16,17]. During a 2-week-period after weaning, whole-body lipid oxidation as well as muscle β-oxidation could be induced by high-fat diet in A/J mice but not in B6 mice, in association with a rescue of cold-tolerance of the A/J mice [6]. These results support the role of metabolic flexibility to lipids, the major fuel for non-shivering thermogenesis in brown fat and possibly also in other tissues, in the differential induction of non-shivering thermogenesis by high-fat diet in mice of the two strains early after weaning. However, possible differences in the control of carbohydrate metabolism between post-weaning mice of the two strains need to be further characterized.

To assess metabolic flexibility to glucose, mice of both A/J and B6 strains were studied right after weaning using different INCA protocols. These measurements were complemented by GTT. Using both approaches, profound differences in the control of glucose metabolism were found, with A/J mice showing relatively high metabolic flexibility and glucose tolerance.

2. Material and methods

2.1. Animals and diets

Experiments were performed using B6 and A/J mice of both genders (mice from the breeding colonies established at the Institute of Physiology in 1993 and 1997, respectively; both strains were imported from the Jackson Laboratories, Bar Harbor, ME). Mice were housed at 20 °C, with a 12-h light cycle, with a free access to water and breeding diet (Ssniff M-Z; proteins 36%, carbohydrates 53%, lipids 11% of energy content; 13.9 kJ/g). At 30 days of age, between 7:00 and 9:00 a.m., pups were removed from their breeding nests and they were single-caged, their BW was evaluated and they were offered pre-weighted standard low-fat diet (Ssniff R/M-H; proteins 33%, carbohydrates 58%, lipids 9% of energy content; 13 kJ/g; both diets from Ssniff Spezialdieten GmbH, Soest, Germany). At 6:00 a.m. the following day (i.e., one day after weaning), diet was removed, food intake was recorded and mice remained with free access to water, but without food, until GTT or INCA was performed (starting at 12:00 p.m.; except for INCA performed using a fasting/re-feeding protocol see below). All experiments were conducted in accordance with the guidelines for the use and care of laboratory animals of the Institute of Physiology (Approval Number: 172/2009), the directive of the European Communities Council (2010/63/EU), and the *Principles of Laboratory Animal Care* (NIH publication no. 85-23, revised 1985).

2.2. Glucose tolerance

At 12:00 a.m., after 6-h-fasting, GTT was performed at 20 °C, using either 1 mg or 3 mg glucose/g BW. Glucose was either injected intraperitonealy (**IPGTT**) using water solution of 10% D-glucose, wt/vol, or administered orally (**OGTT**) as intragastric gavage of water solution of 10% (1 mg glucose/g BW) or 50% (3 mg glucose/g BW) D-glucose, wt/vol, respectively. Tail blood was sampled at 0 (fasting blood glucose, just before glucose administration), 15, 30, 60, and 120 min; glycemia was measured using a glucometer (LifeScan, USA). To avoid the confounding effect of different baseline glucose levels, incremental rather than total AUC was evaluated. To reveal possible effects of mice handling, injection and gavage on glycemia, additional tests were conducted using 0.9% NaCl solution instead of glucose using separate groups of mice.

2.3. Energy metabolism

Two different INCA protols were applied while whole-body metabolic response to either intragastric glucose bolus or re-feeding the standard low-fat diet was characterized. In both protocols, animals were fasted for 5 h before glucose administration, or re-feeding, respectively.

INCA with a glucose bolus: INCA was conducted either at 20 °C or 34 °C after 3-h-fasting, for 2 h between 9:00 a.m. and 11:00 a.m. in a fasting state, then the measurement was interrupted and a bolus of either 1 mg or 7.5 mg glucose/g of BW was administered by intragastric gavage using water solution of 10% (1 mg glucose/g BW) or 50% (7.5 mg glucose/g BW) D-glucose, wt/vol, and the measurement continued for 4 h until 3:00 p.m.

INCA during fasting/re-feeding: INCA was conducted at 34 °C, starting at 1:00 p.m., when diet was removed. At 6:00 p.m, blood samples were collected using tail bleeding (fasted state) and pre-weighted ratio of the standard low-fat diet was administered, and INCA continued until 8:00 a.m. the following day when blood samples were collected again (re-fed state). Overnight food consumption was determined by weighting the diet remaining in the cage; no spillage of diet was detected.

INCA was performed similarly as before [6] using an 8-chamber system (Somedic, Horby, Sweden) and individually caged mice (Eurostandard type II mouse plastic cages; ~6000 ml; Techniplast, Milan, Italy). The cages were placed in sealed measuring chambers equipped with thermostatically controlled heat exchangers. Oxygen consumption (***VO*$_2$**; ml O_2/min) and carbon dioxide production (***VCO*$_2$**; ml CO_2/min) were recorded every 2 min under a constant airflow (1000 ml/min) in each chamber simultaneously. To assess fuel partitioning, RQ was calculated (RQ = VCO_2/VO_2). Energy expenditure (**EE**; cal) was calculated using the equation $3.9*VO_2$ (ml) + $1.1*VCO_2$ (ml) [18,19].

2.4. Plasma assays

Non-esterified fatty acids (**NEFA**) and triacylglycerols (**TAG**) levels were determined in EDTA-plasma using the NEFA-C kit (Wako Chemicals, Neuss, Germany) and Triacylglycerol's Liquid kit (Pliva-Lachema Diagnostika, Brno, Czech Republic). Total adiponectin levels and adiponectin multimeric complexes in plasma were determined using Western blotting as described before [20]. Serum levels of leptin were measured using the mouse serum Milliplex Multiplex Assay kit (Millipore Corporation, Billerica, MA, USA) according to the manufacturer's protocol and analyzed using the BioPlex200 system (Bio-Rad, Veenendaal, The Netherlands). Plasma insulin levels were determined by the Sensitive Rat Insulin RIA Kit (Millipore, Billerica, MA, USA).

2.5. Corticosterone levels

Corticosterone levels were measured either in plasma or in extracts [21] from feces collected during 24 h of INCA using ImmuChem double antibody corticosterone 125I RIA kit (MP Biomedicals, California, NY, USA) and 1:200 dilution of the samples.

2.6. Statistical analysis

All values are presented as means ± standard error (SEM). Differences among groups (gender, strain, and nutritional status) were analyzed either by two-way or three-way ANOVA with the use of post-hoc Holm-Sidak method, carried out using SigmaStat (SSI, San Jose, CA, USA). Analysis of log-transformed data was performed when variances were heterogeneous. Analysis of Covariance (ANCOVA) was performed using NCSS (NCSS, Kaysville, Utah, USA) using post-hoc Bonferroni (All-Pairwise) Multiple Comparison Test. Difference between groups was evaluated using t-test. An increase in RQ values caused by intragastric gavage was quantified as Hill-Slope parameter of curve fitted into individual RQ data from each mouse using SifmaStat (SSI, San Jose, CA, USA). While evaluating RQ data from fasting/re-feeding protocol, RQ was corrected by the level of consumed diet with using residuals of the linear regression of the RQ and the real consumption of the diet. Threshold of significance was defined at $p < 0.05$.

3. Results

3.1. Body weight at weaning

Average weaning body weight (day 30, weaning) in all mice of the study document marginally higher BW of (i) B6 as compared with A/J mice (6% and 7% in female and male mice, respectively), and (ii) male as compared with female mice (9% and 11% in A/J and B6 mice, respectively; Table 1). Similar differences could be observed in all the animal cohorts used for the individual experiments (Suppl. Table 1).

3.2. Glucose tolerance test

Average fasting glycemia (day 30) as measured in all mice in the GTT cohorts (Fig. 1A–F; male, $n = 37–39$; female, $n = 30–37$) indicated lower glycemia in A/J mice as compared with B6 mice (male 140 ± 4 mg/dl vs 180 ± 6 mg/dl, $p < 0.01$; female 123 ± 3 mg/dl vs 160 ± 6 mg/dl, $p < 0.01$), while no effect of the gender could be observed. When IPGTT was performed using 1 mg of glucose/g BW (Fig. 1A, B), B6 mice increased their blood glucose levels more than A/J mice (Fig. 1A). Only the effect of strain, but not of the gender, on incremental AUC was statistically significant ($p < 0.01$; Fig. 1B, two-way ANOVA). Also when OGTT was performed using 1 mg glucose/g BW (Fig. 1C, D), B6 mice increased their blood glucose levels more than A/J mice (Fig. 1C) and only the effect of strain on incremental AUC was statistically significant (Fig. 1D; $p = 0.04$). However, the scatter of the experimental data obtained during OGTT (Fig. 1C, D) was lower as compared with the scatter during IPGTT (Fig. 1A vs Fig. 1C; and Fig. 1B vs Fig. 1D). When OGTT was performed using 3 mg glucose/g BW (Fig. 1E, F), the difference in the time course of glycemia between the strains became smaller (Fig. 1E) and it was not different when expressed as incremental AUC (Fig. 1F). When saline solution was either injected or administered as oral gavage instead of glucose under the conditions corresponding to the above tests, only a negligible change in glycemia was observed (Suppl. Fig. 1).

In a separate experiment, insulin plasma levels were evaluated in the fasting state and 30 min after the glucose load (Suppl. Table 2). No differences dependent either on the strain or on the gender were found in the fasting state. In response to glucose during IPGTT, insulin levels increased ($p = 0.03$), irrespective neither on the strain nor on the gender. After the oral application of glucose, insulin levels increased only in B6 mice.

3.3. Indirect calorimetry

The difference in glucose tolerance between the strains observed using both IPGTT and OGTT prompted us to investigate whether the inter-strain difference could be also observed using INCA. Therefore, INCA was performed at 20 °C in conjunction with intragastric gavage of 1 mg glucose/g BW (Fig. 2A), i.e., under the conditions similar to OGTT using this particular glucose bolus (see above, Fig. 1C, D). In addition, in a separate experiment, the response to a gavage of 7.5 mg glucose/g BW was evaluated (Fig. 2B), i.e., the highest dose of glucose tested (using up to 0.27 ml 50% D-glucose glucose/mice; i.e. close to the gastric volume of the mice). EE evaluated in fasted state before the glucose bolus was not affected by the strain, but it was higher in male as compared with female mice (A/J: 6.18 ± 0.21 vs 5.63 ± 0.19 cal/min, $p = 0.03$; B6: 6.19 ± 0.16 vs 5.72 ± 0.13 cal/min; $p = 0.02$, pooled data from both experiments, $n = 35–59$) reflecting higher BW of male mice (see Table 1). Based on ANCOVA analysis, no difference was observed in EE between groups using BW as a covariate. Fasting RQ was not affected by the gender, while it was higher in A/J mice than in B6 mice (male: 0.85 ± 0.01 vs 0.82 ± 0.01, $p = 0.01$; female: 0.86 ± 0.01 vs 0.82 ± 0.01; $p < 0.01$, pooled data from both experiments, $n = 35–59$). In response to the glucose bolus, a transient increase in RQ was observed documenting an increase of carbohydrate oxidation. The increase in RQ was only subtle with the lower glucose bolus (Fig. 2A) and it was much higher with 7.5 mg glucose/g BW (Fig. 2B), reaching values between 1.00 and 1.05, which suggested stimulation of both carbohydrate oxidation and

Table 1
Body weight of mice at weaning.

	A/J male	A/J female	C57BL/6J male	C57BL/6J female	Strain	Gender
n	104	87	132	135		
BW (g)	14.6 ± 0.2	13.1 ± 0.4	15.6 ± 0.2	14.2 ± 0.2	<0.01	<0.01

Pooled data from various experiments in this study. Data are evaluated using two-way ANOVA for influence of strain and gender, respectively. Data are mean ± SEM.

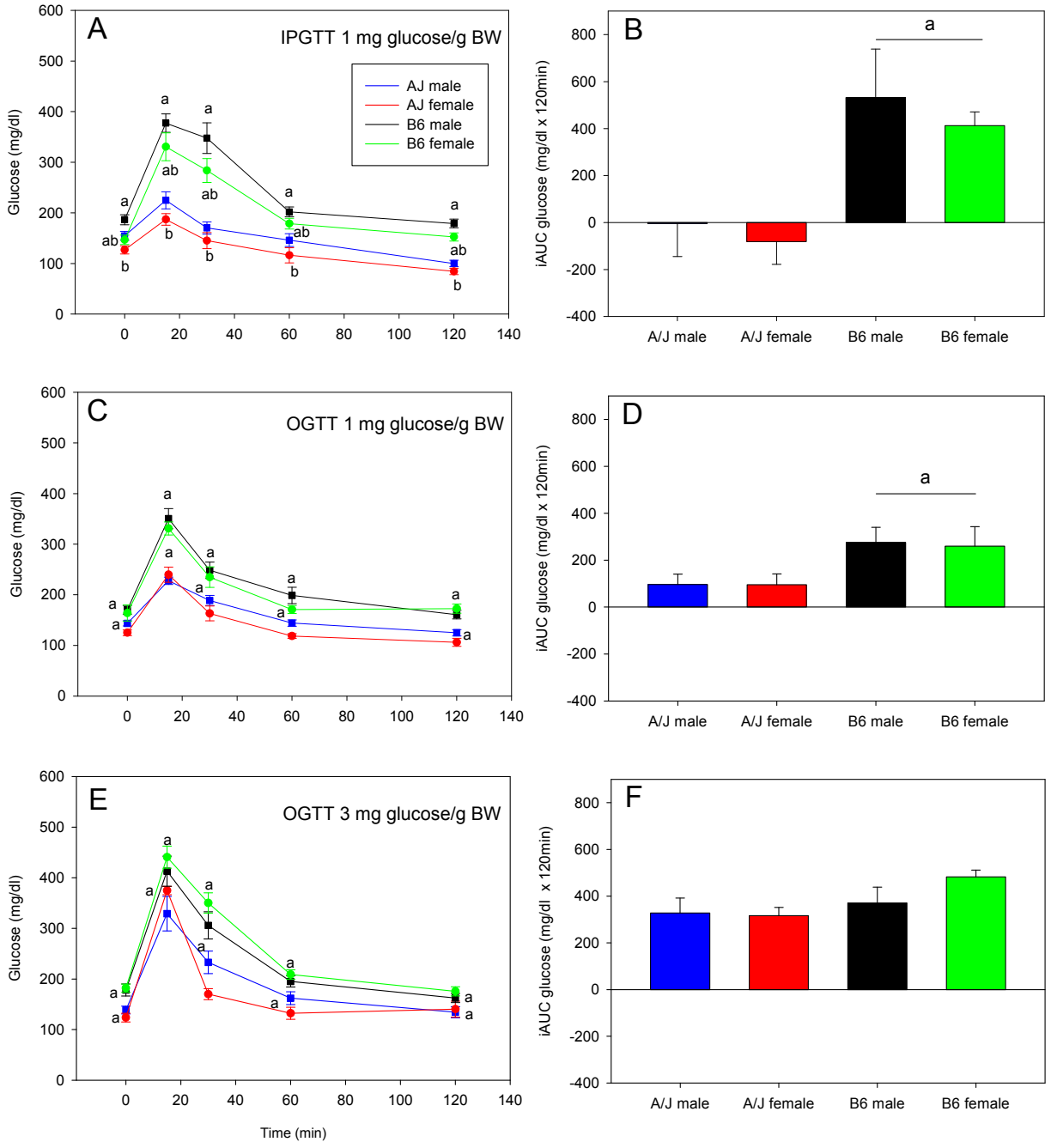

Fig. 1. IPGTT (**A, B**) or OGTT (**C**–**F**) performed using either 1 mg glucose/g BW (**A-D**) or 3 mg glucose/g BW (**E, F**) at 20 °C. Left panels, the time course glycemia during the test; right panels, incremental AUC. The effects of strain and gender on plasma glucose levels were determined using two-way ANOVA. Data are mean ± SEM; $n = 5–11$. a, different from A/J strain; b, different from male mice.

lipogenesis [22]. However, except for a relatively slow decline of RQ in A/J mice in the case of the higher glucose bolus, no other differences between the strains were observed.

Next, we sought to learn whether possible inter-strain difference in metabolic flexibility could be detected when conducting INCA at a thermoneutral temperature, i.e., while avoiding the confounding stimulation of non-shivering thermogenesis by cold. Cold-induced thermogenesis depends in large on activation of lipid catabolism and this strong metabolic response could counteract glucose-induced metabolic response. The measurement was performed at 34 °C, within the previously defined thermoneutral zone for mice pups of this age (data not shown), using an intragastric gavage of 7.5 mg glucose/g BW (Fig. 2C). As expected, EE in fasted state at 34 °C was lower than at 20 °C (Suppl. Fig. 2) and it tended to be higher in male as compared with female mice (A/J: 3.08 ± 0.11 vs 2.88 ± 0.12 cal/min, $p = 0.26$; B6: 3.52 ± 0.12 vs 2.86 ± 0.11 cal/min, $p < 0.01$), while it was not different between the strains (Suppl. Fig. 2). Fasting RQ was not affected neither by the gender, nor by the strain (Fig. 2C). The transient increase in RQ elicited by the gavage of glucose peaked faster and at higher values in A/J as compared with B6 mice, independent of the gender. An increase in RQ values caused by intragastric gavage was quantified as HillSlope parameter of curve fitted into individual RQ data from each mouse. This parameter was significantly higher in A/J mice ($p = 0.01$),

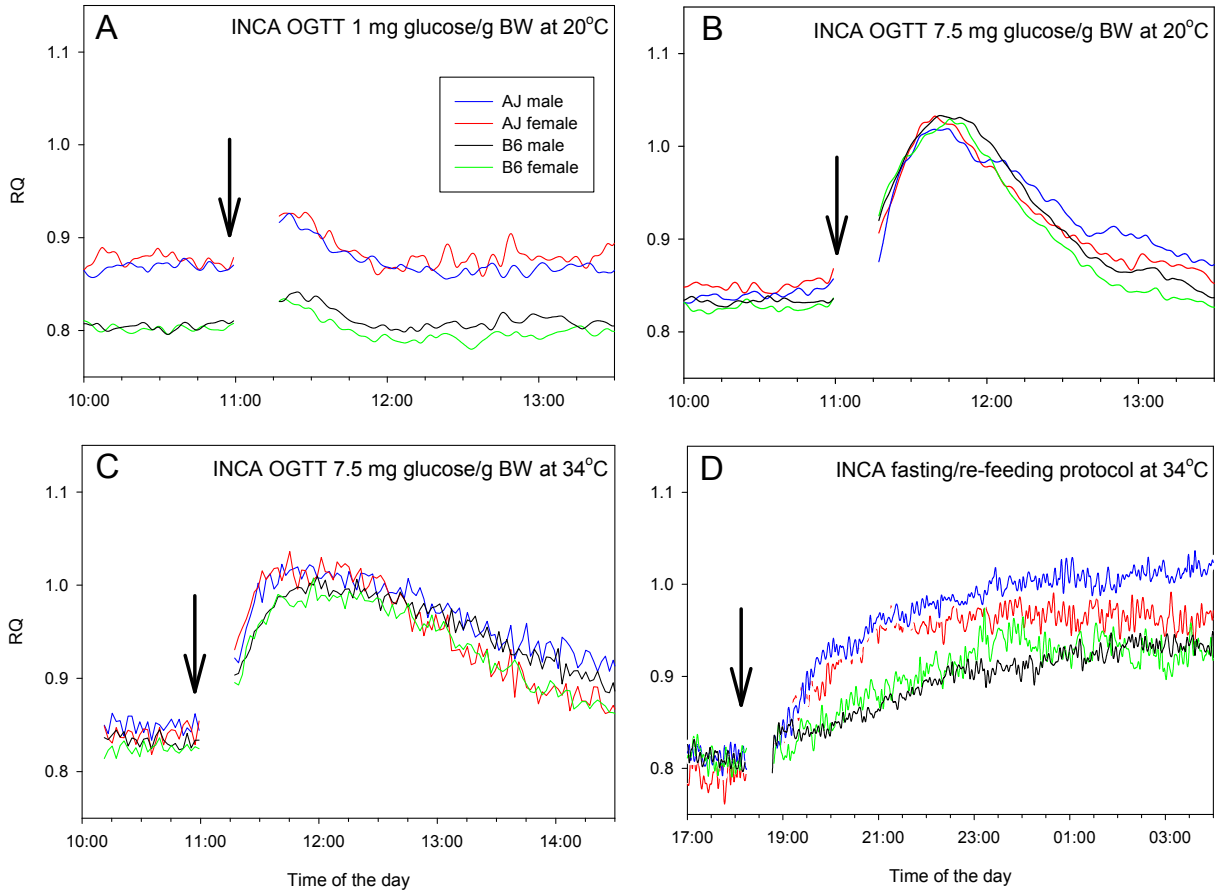

Fig. 2. INCA performed using either an intragastric gavage of glucose (arrow; **A-C**) in mice fasted for 5 h before the bolus or during fasting/re-feeding transition (**D;** food was removed for 5 h before it was offered again at 6:00 p.m.; arrow). Measurements were performed either at 20 °C (**A, B**) or 34 °C (**C, D**). (**A**) 1 mg glucose/g BW; (**B, C**) 7.5 mg glucose/g BW. Each line represents an averaged signal from several mice: (**A**) $n = 12–22$; (**B**) $n = 18–41$; (**C**) $n = 14–22$; (**D**) $n = 13–18$.

indicating higher metabolic flexibility. Similarly as when using this particular dose of glucose at 20 °C, peak RQ values were close to 1.00, but, at variance with INCA at 20 °C, the decline in RQ values was faster in female as compared with male mice, independent of the strain.

Eventually, INCA was performed at 34 °C during a transition from fasted to re-fed state (Fig. 2D and Table 2) while respecting the circadian rhythm of feeding in mice. Thus, instead of stimulating glucose metabolism before the middle of the light phase of the day, as performed in all the experiments described above, fasted mice were allowed free access to food at 6:00 p.m., just before the dark phase of the day, during which mice are relatively active and consume most of their daily food intake. The overnight caloric intake was higher in A/J mice as compared with B6 mice (Table 2). At variance with the evaluation of EE at 34 °C in previous experiment between 9:00 a.m. and 11:00 a.m. in a fasted state (Fig. 2C), EE measured between 4:30 p.m. and 6:00 p.m. in a fasted state was lower in A/J as compared with B6 mice, independent of the gender, and RQ was not affected neither by the strain nor by the gender (Table 2 and Suppl. Fig. 2). In response to re-feeding, EE increased by a factor of 1.3–1.8 ($p < 0.01$) independent of the gender and this effect was higher in A/J as compared with B6 mice (Table 2 and Suppl. Fig. 2). In response to re-feeding, RQ increased in both strains ($p < 0.01$), with a faster response in A/J as compared with B6 mice, independent of the gender. In about 3–4 h, RQ reached values corresponding to metabolic switch to oxidation of carbohydrates. When evaluated between 0:00 a.m. and 2:00 a.m., RQ values were higher in A/J mice than in B6 mice (Fig. 2D and Table 2). This difference remained apparent even after adjustment to the caloric intake (residuals of RQ values corrected for caloric intake; A/J male 0.004 ± 0.001, A/J female 0.005 ± 0.001, B6 male 0.009 ± 0.001, B6 female 0.008 ± 0.001; two-way ANOVA $p < 0.01$ for strain; expressed as RQ increase/kJ of consumed standard low-fat diet). In A/J mice, male mice showed higher RQ values (around 1.0) than female mice, while gender had no effect in B6 mice (Fig. 2D and Table 2).

In the fasted state, levels of glucose, NEFA and TAG were similar in all the groups (Table 2). In response to re-feeding, glucose reached higher levels in B6 mice, independent of the gender (Table 2). The effect of time was highly significant ($p < 0.01$; three-way ANOVA). While NEFA levels decreased in B6, they increased in A/J mice, independent of the gender (Table 2). TAG levels increased to a similar extent (1.6- to 2.2-fold) in all the groups ($p < 0.01$), and in the re-fed state, they were similar in all the groups (Table 2). Cholesterol levels were similar in all the groups, independent of the nutritional status (not shown).

Leptin levels were higher in A/J mice as compared with B6 mice, in both fasted and in re-fed state, and they were higher in re-fed than fasted state, irrespective of gender (Fig. 3A). Total adiponectin (Fig. 3B, C)) as well as high molecular weight (HMW) adiponectin (Fig. 3 B, C) levels in plasma were higher in B6 as compared with A/J mice, both in the fasted and in the re-fed state (Fig. 3B, C). Levels of both leptin and adiponectin were higher in female as compared with male mice, irrespective of either the

Table 2
Re-feeding during INCA at 34 °C.

	A/J male	A/J female	C57BL/6J male	C57BL/6J female	Strain	Gender
Caloric intake (kcal)	7.04 ± 0.78	5.85 ± 1.13	5.22 ± 0.28	4.74 ± 0.67	0.04	0.22
Indirect calorimetry parameters						
EE (cal/min)						
Fasted	2.77 ± 0.12	2.74 ± 0.18	3.13 ± 0.11	3.21 ± 0.15	<0.01	0.87
Re-fed	4.84 ± 0.26	4.91 ± 0.39	4.48 ± 0.20	4.29 ± 0.19	0.06	0.81
Delta EE	2.07 ± 0.24	2.17 ± 0.27	1.35 ± 0.17	1.00 ± 0.23	<0.01	0.59
RQ						
Fasted	0.81 ± 0.01	0.79 ± 0.01	0.81 ± 0.02	0.82 ± 0.01	0.34	0.71
Re-fed	1.00 ± 0.03	0.97 ± 0.02	0.92 ± 0.02	0.93 ± 0.02	0.01	0.51
Delta RQ	0.20 ± 0.03	0.18 ± 0.02	0.13 ± 0.02	0.13 ± 0.03	0.02	0.85
Plasma parameters						
Glucose (mg/dl)						
Fasted	119 ± 8	102 ± 17	103 ± 10	106 ± 6	0.55	0.48
Re-fed	135 ± 9	138 ± 18	195 ± 11	187 ± 17	<0.01	0.85
Delta glucose	16 ± 12	36 ± 21	92 ± 8	82 ± 17	<0.01	0.73
NEFA (mmol/l)						
Fasted	0.62 ± 0.04	0.61 ± 0.07	0.53 ± 0.03	0.65 ± 0.04	0.67	0.26
Re-fed	0.75 ± 0.13	0.69 ± 0.14	0.39 ± 0.03	0.53 ± 0.09	<0.01	0.70
Delta NEFA	0.14 ± 0.12	0.08 ± 0.15	−0.14 ± 0.04	−0.18 ± 0.10	0.01	0.63
TAG (mg/dl)						
Fasted	46 ± 5	48 ± 3	56 ± 9	52 ± 6	0.33	0.91
Re-fed	103 ± 12	105 ± 14	90 ± 9	104 ± 19	0.38	0.36
Delta TAG	57 ± 12	56 ± 11	30 ± 10	53 ± 16	0.25	0.42

Re-feeding during INCA at 34 °C: Caloric intake was assessed between 6:00 p.m. and 8:00 a.m. the following morning in INCA; fasted EE and RQ were evaluated during 90 min before re-feeding (between 4:30 p.m. and 6:00 p.m.), while RQ in re-fed state was evaluated 6–8 h after re-feeding (between 0:00 a.m. and 2:00 a.m.), EE was measured between 6:00 p.m. and 8:00 a.m. Delta was calculated as the difference between fasted and re-fed state. Plasma parameters: fasted, at 6:00 p.m.; re-fed, at 8:00 a.m. the next day after re-feeding, respectively, using tail-blood samples. See Fig. 2D for INCA time-courses and Fig. 3 for leptin. Data are evaluated using two-way ANOVA for influence of strain and gender, respectively; *p* values are indicated. Data are mean ± SEM, n = 13–18.

strain or the nutritional status (Fig. 3).

While plasma corticosterone levels reflect immediate stress level, corticosterone in feces represents stress levels during the last 6–8 h [23]. After INCA, corticosterone levels were measured in plasma in the re-fed state, as well as in feces collected during 24 h of the measurement. No significant differences in corticosterone levels were found between A/J and B6 male mice neither in plasma (84 ± 24 and 89 ± 27 ng/ml) nor in feces (15 ± 7 and 21 ± 11 ng/24 h). Thus, the differences in glucose homeostasis observed between the strains could not be explained by different stress levels during INCA.

4. Discussion

The principal finding of this study is that, right after weaning, A/J mice exhibit a higher glucose tolerance, evaluated using classical GTT, and lower glycemia in fasted state, as well as lower insulinemia after oral glucose application, as compared with B6 mice. This difference in glucose homeostasis could be explained, at least in part, by higher induction of whole-body glucose oxidation in A/J mice, i.e. higher metabolic flexibility to glucose. As documented by INCA at thermoneutral temperature in combination with both, intragastric gavage and fasting/re-feeding, the switch to glucose oxidation was faster and more extensive in A/J mice. In addition, similarly to situation in human diabetic patients, cellular glucose uptake could be also involved [2].

The above results on the early differences in glucose metabolism between A/J and B6 mice are reminiscent of our previous results demonstrating higher inducibility of muscle fatty acid oxidation in A/J mice in response to a 2-week-feeding high-fat diet right after weaning [6], as well as higher activation of carbohydrate oxidation during exercise in adult A/J mice [14]; see Introduction). In accordance with the results of the previous study in adult mice [14], lower energy expenditure was found in this study in A/J mice as compared with B6 mice in fasted state. In contrast, in the re-fed mice, such inter-strain difference could not be observed here (Table 2). It should be stressed that in the post-weaning mice studied here, mice of the two strains only marginally differed in their BW. Therefore, the pronounced differences in the regulation of fuel utilization observed between the strains were not secondary to body fat accumulation. The mechanisms behind these differences remain to be characterized. Our previous results in the postweaning mice suggest that AMP-activated protein kinase (**AMPK**) could be involved ([6]; see also below).

Both strains of mice differed in plasma levels of adipokines when studied shortly after weaning. In agreement with the results of Surwit et al. [12] but not those of Watson and colleagues [9], with both studies performed under similar conditions as in our experiments, leptin levels were higher in A/J as compared with B6 mice. All these results could be affected by some differences in the composition of the maternal diet during the second half of lactation [24] and namely just before weaning when the pups consume a mixture of relatively low-fat breeding diet and high-fat mother's milk. We have also found gender-dependent and strain-independent differences in leptin levels in these mice, with the higher levels observed in the female mice, in spite of lower body weight of these mice as compared to the male animals. In our knowledge, such gender-dependent difference in leptin levels in postweaning mice was not described before. It is conceivable that relatively high leptin levels in A/J mice could contribute, through stimulation of the leptin-AMPK axis, to the higher metabolic flexibility of these animals. On the other hand, stimulation of the activity of this regulatory pathway in itself would have no impact on energy dissipation (reviewed in Ref. [25]), also in accordance with the relatively low energy expenditure of A/J mice. Moreover, leptin can be also involved in counteracting metabolic preference for glucose in A/J mice by increasing TAG hydrolysis and FA oxidation [26].

Similarly to leptin, also adiponectin is assumed to stimulate AMPK axis, and hence fatty acid oxidation, and it could also augment insulin sensitivity and glucose metabolism [27]. However, also in accordance with the results of others [28], adiponectin levels

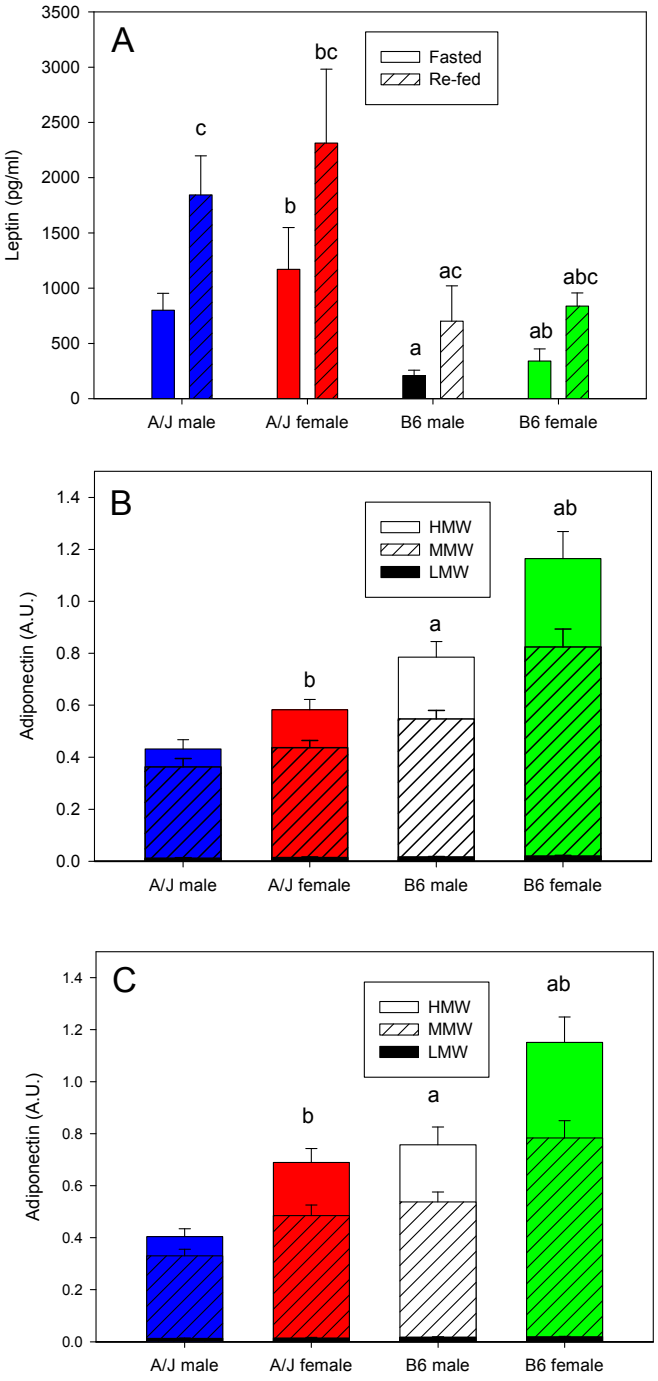

Fig. 3. Leptin and adiponectin plasma levels during INCA at 34 °C. The re-feeding protocol was used. Plasma adipokines levels were measured in fasted (at 6:00 p.m.) and re-fed (at 8:00 a.m., the next day after re-feeding) state, respectively, using tail-blood samples. (**A**) leptin plasma levels in the fasted and re-fed state, respectively. The effect of strain, gender, and nutritional status on leptin levels were determined using three-way ANOVA. Adiponectin plasma levels in the fasted (**B**) and re-fed (**C**) state. Low molecular weight (LMW), medium molecular weight (MMW) and high molecular weight (HMW) adiponectin complexes were evaluated separately. The effects of strain and gender on total adiponectin were determined using two-way ANOVA. See also Fig. 2D and Table 2. Data are mean ± SEM; $n = 13–18$. a, different from A/J strain; b, different from male mice; c, different from fasted state.

in A/J mice were relatively low, and they were also lower in male as compared with female mice (see Ref. [20]; see Fig. 3B, C). Thus, adiponectin is not likely to explain the beneficial metabolic phenotype of A/J mice, but it could explain in part the difference in RQ between the strains in the re-fed state suggesting a higher lipid oxidation (lower RQ) in B6 mice (Table 2).

Our study introduced the use of both GTT and INCA for assessment of glucose tolerance and metabolic flexibility to glucose, respectively, in postweaning mice. By comparing various experimental protocols, we have defined optimum conditions for the application of both approaches, while getting conclusive and compatible results. However, it should be stressed that GTT and INCA should be regarded as two independent approaches, reflecting only a partial overlap of the basic mechanisms involved (see also ref. [8]). Moreover, even when GTT and INCA were conducted using the same glucose bolus (i.e., 1 mg glucose/g BW), it was not possible to use the INCA data for interpretation of the GTT data, due to only a negligible effect on RQ under these conditions.

Regarding GTT, the well-established approach to study glucose tolerance in mice, our results suggest that glucose administration using oral gavage rather than intraperitoneal injection could bring more reproducible results, as documented by the relatively low scatter of the experimental data obtained during OGTT (Fig. 1C, D). Moreover, the former approach also reflects, among the other factors contributing to glucose homeostasis under these conditions, possible involvement of the incretin system [29]. It should be also stressed that, in accordance with the effect of incretins on pancreatic insulin secretion and glucose homeostasis, transient increase in blood glucose levels was lower during OGTT as compared with IPGTT (see also ref [30]) and the main difference was observed at 30 min after glucose administration (Fig. 1).

Regarding INCA, we show here, using a system with simultaneous signal recording in the individual metabolic chambers, that reliable results could be obtained in measurements on individual mice pups with body weight close to 15 g. Especially, if the measurements are conducted at a thermoneutral temperature, the rate of the increase in RQ in response to glucose bolus or to re-feeding, as well as the RQ levels reached after the re-feeding, the difference in metabolic flexibility to glucose between the two strains could be reproducibly depicted (Fig. 2 C, D). However, interpretation of the INCA data is complicated by different RQ fasting levels in experiments using 1 and 7.5 mg glucose/g BW at 20 °C. This discrepancy remains unexplained; the basal RQ levels could be affected by the time of the year when the measurement was conducted, since individual experiments differed in this respect. E.g., blood concentration of corticosterone are seasonally dependent [31], while corticosterone could influence glucose metabolism and RQ. However, in this study corticosterone was measured only in connection with a single INCA experiment, while characterization of seasonal changes in corticosterone levels was out of scope of this study.

Since animals from in-house colonies were used, an effect of genetic drift could complicate the applicability of our findings to mice of the parental strains, which are commercially available. However, this possibility is relatively small, as documented by various experiments conducted at our laboratory using the animals of the parental strains along with the animals used in this study, which always gave similar results (not shown).

In conclusion, our results demonstrated that differences in glucose tolerance, as well as metabolic flexibility to glucose, assessed by GTT and INCA, respectively, could be detected in mice pups with different genetic background right after weaning. They suggest that glucose metabolism represents one of the key features underlying the vast differences in whole-body phenotype between A/J and B6 mice.

Acknowledgments

Supported by the European Union's Seventh Framework

Program under grant agreement no. 244995 (BIOCLAIMS Project) and by the Czech Science Foundation (14-36804G).

Appendix A. Supplementary data

Supplementary data related to this article can be found at http://dx.doi.org/10.1016/j.biochi.2015.11.014.

References

[1] P.G. Kopelman, Obesity as a medical problem, Nature 404 (2000) 635–643.
[2] J.E. Galgani, C. Moro, E. Ravussin, Metabolic flexibility and insulin resistance, Am. J. Physiol. Endocrinol. Metab. 295 (2008) E1009–E1017.
[3] J. Naukkarinen, S. Heinonen, A. Hakkarainen, J. Lundbom, K. Vuolteenaho, L. Saarinen, S. Hautaniemi, A. Rodriguez, G. Fruhbeck, P. Pajunen, T. Hyotylainen, M. Oresic, E. Moilanen, A. Suomalainen, N. Lundbom, J. Kaprio, A. Rissanen, K.H. Pietilainen, Characterising metabolically healthy obesity in weight-discordant monozygotic twins, Diabetologia 57 (2014) 167–176.
[4] E. Corpeleijn, M. Mensink, M.E. Kooi, P.M. Roekaerts, W.H. Saris, E.E. Blaak, Impaired skeletal muscle substrate oxidation in glucose-intolerant men improves after weight loss, Obesity (Silver Spring) 16 (2008) 1025–1032.
[5] F.P. Hoevenaars, J. Keijer, H.J. Swarts, S. Snaas-Alders, M. Bekkenkamp-Grovenstein, E.M. van Schothorst, Effects of dietary history on energy metabolism and physiological parameters in C57BL/6J mice, Exp. Physiol. 98 (2013) 1053–1062.
[6] V. Kus, T. Prazak, P. Brauner, M. Hensler, O. Kuda, P. Flachs, P. Janovska, D. Medrikova, M. Rossmeisl, Z. Jilkova, B. Stefl, E. Pastalkova, Z. Drahota, J. Houstek, J. Kopecky, Induction of muscle thermogenesis by high-fat diet in mice: association with obesity-resistance, Am. J. Physiol. Endocrinol. Metab. 295 (2008) E356–E367.
[7] L.P. Duivenvoorde, E.M. van Schothorst, H.J. Swarts, J. Keijer, Assessment of metabolic flexibility of old and adult mice using three noninvasive, indirect calorimetry-based treatments, J. Gerontol. A Biol. Sci. Med. Sci. 70 (2015) 282–293.
[8] L.P. Duivenvoorde, E.M. van Schothorst, H.M. Swarts, O. Kuda, E. Steenbergh, S. Termeulen, J. Kopecky, J. Keijer, A difference in fatty acid composition of isocaloric high-fat diets alters metabolic flexibility in male C57BL/6JOlaHsd mice, PLoS One 10 (2015) e0128515.
[9] P.M. Watson, S.P. Commins, R.J. Beiler, H.C. Hatcher, T.W. Gettys, Differential regulation of leptin expression and function in A/J vs. C57BL/6J mice during diet-induced obesity, Am. J. Physiol. Endocrinol. Metab. 279 (2000) E356–E365.
[10] R.S. Surwit, M.N. Feinglos, J. Rodin, A. Sutherland, A.E. Petro, E.C. Opara, C.M. Kuhn, M. Rebuffe-Scrive, Differential effects of fat and sucrose on the development of obesity and diabetes in C57BL/6J and A/J mice, Metabolism 44 (1995) 645–651.
[11] R.S. Surwit, A.E. Petro, P. Parekh, S. Collins, Low plasma leptin in response to dietary fat in diabetes- and obesity-prone mice, Diabetes 46 (1997) 1516–1520.
[12] R.S. Surwit, C.L. Edwards, S. Murthy, A.E. Petro, Transient effects of long-term leptin supplementation in the prevention of diet-induced obesity in mice, Diabetes 49 (2000) 1203–1208.
[13] S. Collins, K.W. Daniel, A.E. Petro, R.S. Surwit, Strain-specific response to beta3-adrenergic receptor agonist treatment of diet-induced obesity in mice, Endocrinology 138 (1997) 405–413.
[14] S. Haramizu, A. Nagasawa, N. Ota, T. Hase, I. Tokimitsu, T. Murase, Different contribution of muscle and liver lipid metabolism to endurance capacity and obesity susceptibility of mice, J. Appl. Physiol. 106 (2009) 871–879.
[15] C. Poussin, M. Ibberson, D. Hall, J. Ding, J. Soto, E.D. Abel, B. Thorens, Oxidative phosphorylation flexibility in the liver of mice resistant to high-fat diet-induced hepatic steatosis, Diabetes 60 (2011) 2216–2224.
[16] D. Hall, C. Poussin, V.R. Velagapudi, C. Empsen, M. Joffraud, J.S. Beckmann, A.E. Geerts, Y. Ravussin, M. Ibberson, M. Oresic, B. Thorens, Peroxisomal and microsomal lipid pathways associated with resistance to hepatic steatosis and reduced pro-inflammatory state, J. Biol. Chem. 285 (2010) 31011–31023.
[17] J. Fiamoncini, N. Turner, S.M. Hirabara, T.M. Salgado, A.C. Marcal, S. Leslie, S.M. da Silva, F.C. Deschamps, J. Luz, G.J. Cooney, R. Curi, Enhanced peroxisomal beta-oxidation is associated with prevention of obesity and glucose intolerance by fish oil-enriched diets, Obesity (Silver Spring) 21 (2013) 1200–1207.
[18] J.B. Weir, New methods for calculating metabolic rate with special reference to protein metabolism, J. Physiol. 109 (1949) 1–9.
[19] K.J. Kaiyala, D.S. Ramsay, Direct animal calorimetry, the underused gold standard for quantifying the fire of life, Comp. Biochem. Physiol. A Physiol. 158 (2011) 252–264.
[20] D. Medrikova, Z.M. Jilkova, K. Bardova, P. Janovska, M. Rossmeisl, J. Kopecky, Sex differences during the course of diet-induced obesity in mice: adipose tissue expandability and glycemic control, Int. J. Obes. (Lond.) 36 (2012) 262–272.
[21] S.K. Wasser, S.L. Monfort, J. Southers, D.E. Wildt, Excretion rates and metabolites of oestradiol and progesterone in baboon (Papio cynocephalus cynocephalus) faeces, J. Reprod. Fertil. 101 (1994) 213–220.
[22] Y. Schutz, The basis of direct and indirect calorimetry and their potentials, Diabetes Metab. Res. Rev. 11 (1995) 383–408.
[23] P.V. Turner, E. Vaughn, J. Sunohara-Neilson, J. Ovari, F. Leri, Oral gavage in rats: animal welfare evaluation, J. Am. Assoc. Lab. Anim. Sci. JAALAS 51 (2012) 25–30.
[24] E. Herrera, E. Amusquivar, Lipid metabolism in the fetus and the newborn, Diabetes Metab. Res. Rev. 16 (2000) 202–210.
[25] S. Klaus, S. Keipert, M. Rossmeisl, J. Kopecky, Augmenting energy expenditure by mitochondrial uncoupling: a role of AMP-activated protein kinase, Genes Nutr. 7 (2011) 369–386.
[26] R.B. Harris, Direct and indirect effects of leptin on adipocyte metabolism, Biochim. Biophys. Acta 1842 (2014) 414–423.
[27] T. Yamauchi, J. Kamon, Y. Minokoshi, Y. Ito, H. Waki, S. Uchida, S. Yamashita, M. Noda, S. Kita, K. Ueki, K. Eto, Y. Akanuma, P. Froguel, F. Foufelle, P. Ferre, D. Carling, S. Kimura, R. Nagai, B.B. Kahn, T. Kadowaki, Adiponectin stimulates glucose utilization and fatty-acid oxidation by activating AMP-activated protein kinase1, Nat. Med. 8 (2002) 1288–1295.
[28] J.W. Bullen Jr., S. Bluher, T. Kelesidis, C.S. Mantzoros, Regulation of adiponectin and its receptors in response to development of diet-induced obesity in mice, Am. J. Physiol. Endocrinol. Metab. 292 (2007) E1079–E1086.
[29] L.L. Baggio, D.J. Drucker, Biology of incretins: GLP-1 and GIP, Gastroenterology 132 (2007) 2131–2157.
[30] S. Andrikopoulos, A.R. Blair, N. Deluca, B.C. Fam, J. Proietto, Evaluating the glucose tolerance test in mice, Am. J. Physiol. Endocrinol. Metab. 295 (2008) E1323–E1332.
[31] L. Meyer, J. Caston, A.G. Mensah-Nyagan, Seasonal variation of the impact of a stressful procedure on open field behaviour and blood corticosterone in laboratory mice, Behav. Brain Res. 167 (2006) 342–348.